UNIVERSITY OF LIVERPOOL

A STUDY OF THE ELECTRICAL PROPERTIES OF POLYCRYSTALLINE BASED ORGANIC DEVICES

Thesis submitted in accordance with the requirements
of the University of Liverpool for the degree of Doctor
in Philosophy

by

SIDRA AFZAL

JUNE 2012

ABSTRACT

A study of the Electrical Properties of Polycrystalline based Organic Devices

Sidra Afzal

In this thesis, examination of polycrystalline organic based devices such as the Schottky diode and MOS capacitor is carried out. The data is interpreted in terms of a polycrystalline model based mainly on a conventional polysilicon model with slight modifications to fit the organic properties. A brief introduction to the existing charge transport models for organic materials is presented. The most dominant being the variable range hopping model for disordered materials. The disorder analysis is appropriate in the grain boundaries of a polycrystalline material. The distribution of the traps of density of states (DOS) is commonly described by the Gaussian distribution and the associated exponential approximate at low energies. This is a valid assumption for organic semiconductors with low carrier mobility values [N. Sedghi et al., J. Non Crys. Solids 352, 1641, 2006].

Detailed investigation on the temperature effects of the polycrystalline Schottky diode leads to determination of important electrical parameters. Such studies are essential in understanding the conduction processes of the organic device, particularly in terms of trapping effects, which is essential in the development of device models for organic circuitry. Several parameters such as dopant (N_D) and carrier concentrations (p), effective mobility (μ_{eff}), depletion width (W_{dep}), effective Debye length (L_{De}), Meyer Neldel energy (MNE) and the characteristic temperature of the carriers (T_0) are extracted from the current-voltage characteristics of the diode. For a soluble derivative of pentacene, 6, 13-triisopropylsilyethynyl pentacene (TIPS) blended with Polytriarylamine (PTAA), the respective values extracted at room temperature are found to be approximately 10^{17} cm^{-3}, $1.8x10^{-2}$ $cm^2V^{-1}s^{-1}$, 185 nm, 11 nm, 31.5 meV and 780 K, respectively. As the temperature falls, the values of most parameters remain constant until a critical temperature. The activation energy also remains constant at approximately 0.3 eV for various applied voltages in saturation. Below this critical temperature, W_{dep}, L_{De} and T_0 increase whilst μ_{eff}, N_D/p and characteristic

temperature of the states (T_C) decrease. Similar analysis is carried out on doped layers of TIPS with a different insulating binder Poly-alpha methylstyrene (PAMS). The value of W_{dep}, L_{De}, T_0, μ_{eff}, N_D/p, *MNE* and T_C obtained from such doped Schottky diode are approximately 100 nm, 5 nm, 1200 K, $1x10^{-2}$ $cm^2V^{-1}s^{-1}$, $2x10^{17}$ cm^{-3}, 35 meV and 400 K, respectively. The Capacitance-Voltage (C-V) analysis on polycrystalline Schottky diodes provides N_D of approximately 7.6 x 10^{16} cm^{-3}, 5.2 x 10^{14} cm^{-3} and 2.98 x $10^{14}cm^{-3}$ at 500 Hz, 1 kHz and 2 kHz respectively. These N_D values are lower than those extracted from current-voltage characteristics and decrease with increasing frequency. This is thought to be due to the low mobility of holes, unable to respond to the signal at higher frequencies.

The conduction in polycrystalline organic Schottky diode is proposed using a 2-dimensional (2D) model, which focuses on both the lateral and vertical conduction paths. The organic semiconductor layer is assumed to be relatively thin so that only a single layer of the grain exists between adjacent grain boundaries for the vertical conduction. A two dimensional situation is treated as two separate one dimensional problems that are positioned at right angles to each other. The grain and grain boundaries in the polycrystalline material are explained in terms of two boundary conditions. The variation of potential in grain boundary is the basis in defining the variation of potential in the grains. Conduction under forward bias in the grain and grain boundary is thus established assuming two distributions for the DOS, namely the Gaussian and Laplace. In comparison, Laplace DOS is believed to be a better representation of the distribution of states, where a large number of energy levels are being scanned with applied voltage.

The ac properties of a polycrystalline based MOS capacitor are investigated. The frequency and temperature effects on the C-V characteristics of MOS capacitor based on another soluble derivative of pentacene, refered here as S1150, are studied. Equivalent circuits which include the effects of bulk and series resistance due to contact effects are analysed. The bulk resistance (R_b), bulk capacitance (C_b) and series resistance (R_S) are found to be approximately

13 kΩ, 760 pF and less than 309 Ω respectively, for an organic film thickness (t_{OSC}) of 27nm. For $N_D \approx 3.6 \times 10^{17} cm^{-3}$ at 1 kHz, the hole mobility is found to be approximately $4.6 \times 10^{-7} cm^2 V^{-1} s^{-1}$. As expected the mobility decreases with increase in frequency. Furthermore, the temperature study of inverse square space charge capacitance ($1/C_S^2$) against absolute temperature (T) provides an intercept close to T (~ 330K) instead of T_C. A low intercept value indicates a decrease in disorder which suggests that the large grains may be dominating the capacitance.

CONTENTS

Dedicated

to

My Loving Parents

ACKNOWLEDGEMENTS

I am eternally grateful to almighty Allah (s.w.t) for giving me all that I have ever asked for. Without His wish I would not be close to where I am now and wish to be. I am eternally thankful.

I wish to express my sincere appreciation to my supervisors, Dr. M. Raja and Professor W. Eccleston for their continuous guidance, knowledgeable conversations and time throughout my research. I would like to show gratitude to Dr. D. Donaghy and Dr. R. Myers for their educated discussions, assistance in the clean rooms and willingness to help. I am a part of a truly wonderful group. I would also like to thank the European Commission through Fp6 'PolyNet' project and Northwest Development Agency through 'Northern Way' project for their financial support.

My greatest recognition extends towards my parents for without their full confidence, support, guidance, prayers and immense love, I would not have been able to succeed. I also extend my special thanks to my caring sister, Mehak, for always being there to help me and uplift my mood. I am thankful for their presence even though they are so far away. I love them all forever dearly. Moreover, significant credit goes to my husband, Shiraz, for his continuous encouragement, support, thoughtfulness and love throughout my degrees. His constant dedication towards me has been my motivation through the hardest of my times. In addition, I am forever grateful to my grandma, Aunt Ruby, Uncle Liaqat and my cousins for their regular prayers and immense affection. Furthermore, I am highly appreciative of my new family for tolerating my absence and continuously supporting me in my studies and other activities.

Special thanks to: Cathy, my housemate and a very good friend, for being a motivation and a lovely person; Farnoush, Kat, Pramodh, Samrita, Shaima, Hassan, Neda, Moin, Umar, Carol and Suniya for being my invaluable friends. Thanks to all my other friends I have not mentioned here, you all mean a lot to me. I consider myself very lucky to have such amazing family and friends.

ABBREVIATIONS

DDQ	2, 3-Dichloro-5, 6-dicyano-1, 4-benzoquinone
DOS	Density of states
HOMO	Highest occupied molecular orbital
L1	Laplace first distribution law
LUMO	Lowest unoccupied molecular orbital
MNE	Meyer Neldel Energy
MOS	Metal- Oxide- Semiconductor
MTR	Multiple trap and release
OFET	Organic field effect transistors
OLED	Organic light emitting diode
OTFT	Organic Thin film transistors
P3HT	Poly3-hexylthiophene
PTAA	Polytriarylamine
RFID	Radio frequency Identification Tags
SAM	Self aligned monolayer
SCLC	Space charge limited currents
TIPS-pentacene	6, 13-triisopropylsilyethynyl pentacene
UML	Universal mobility law
VRH	Variable range hopping

SYMBOLS

T	Absolute Temperature		of states (DOS)
N_a	Acceptor ion concentration	Q_{dep}	Charge in depletion region
E_a	Activation energy	n_t	Concentration of trapped charge
v_0	Attempt-to-hop frequency	σ	Conductivity
k	Boltzmann's Constant	R_C	Contact resistance
qV_{bi}	Built- in potential	J	Current Density
Y_b	Bulk admittance	L_D	Debye Length
C_b	Bulk Capacitance	$N(0)$	Density of states per unit volume at the Fermi level
R_b	Bulk Resistance		
C_{dep}	Capacitance of the Depletion Region	N_{sn}	Density of states that can be part of the percolating sub-network
$n(E)$	Carrier concentration at energy level E		
n_0	Carrier concentration at Fermi level	W_{dep}	Depletion Region Width
p_S	Carrier concentration at the surface	ε_i	Dielectric constant of the insulator
n_{bulk}	Carrier concentration in semiconductor bulk	ε_{ox}	Dielectric constant of the oxide (~10 for Al_2O_3)
T_0	Characteristic temperature describing the width of the carrier distribution	ε_S	Dielectric constant of the semiconductor
T_C	Characteristic temperature of density	d	Distance between two electrodes

D_{ij}	Distance between two hopping states	E_F	Fermi Level Energy
λ	Distribution width of Laplace distribution function/ Gaussian distribution function	Q_{fixed}	Fixed oxide charge
		C_{fb}	Flat-band Capacitance
		V_{fb}	Flat-band voltage
μ_D	Drift mobility	φ	Flux
L_{De}	Effective Debye Length	ψ	Force
μ_{eff}	Effective mobility	δ	Fraction of localized states occupied by the carrier
F	Electic field		
F_{ox}	Electric Field across the oxide layer	δ	Fraction of states occupied
F_S	Electric Field at the oxide-semiconductor interface	n_f	Free carrier concentration
		ε_∞	High-frequency permittivity of the semiconductor
$\emptyset$	Electric Potential (V)		
$q\chi$	Electron affinity	Q_i	Interface charge
E_C	Energy at Conduction band	Q_{it}	Interface trap charges
E_i	Energy at Intrinsic Level	E_r	Intra-molecular reorganization energy
E_{vac}	Energy at vacuum level	n_i	Intrinsic carrier concentration
E_V	Energy at Valence band	α	Inverse localization length
E_g	Energy band gap		
ΔE ‘	Energy barrier	C_{max}	Maximum Capacitance
E_t	Energy of the trap states	W_{max}	Maximum Depletion Region Width
m	Exponent dependent on T_C and the material	D_{max}	Maximum distance between two hopping

	states	t_{OSC}	Thickness of the organic semiconductor
E_{max}	Maximum energy that any initial or final state can have.	t_{ox}	Thickness of the oxide layer
C_{min}	Minimum Capacitance	V_T	Threshold Voltage
$\emptyset_{Xmin}$	Minimum potential at grain centre	τ	Time taken for a hop to take place
Q_{mobile}	Mobile ion content	Y_t	Total admittance
μ_0, K	Mobility prefactor	C_t	Total Capacitance
C_{oxide}	Oxide Capacitance	Z_t	Total impedance
Q_{ot}	Oxide trapped charges	C_{MOS}	Total MOS capacitance
ε_0	Permittivity of free space	R_t	Total Resistance
ε_0	Permittivity of free space	E_{tr}	Transport energy in a disordered material
$\emptyset_X$	Potential at full grain curve	E_T	Transport energy in an crystalline material
$\emptyset_z$	Potential at the edge of the grain	$2\lambda^2$	Variance of Laplace distribution function
α	Ratio between the effective density of states at the transport band edge and the density of trap	V_G	Voltage applied at the gate contact
b	Size of the localized states	$q\phi_{ms}$	Work function difference between the metal and the semiconductor
θ	The ratio of free carrier concentration to the total carrier concentration	$q\phi_m$	Work function of the Metal
		$q\phi_{sc}$	Work function of the Semiconductor

CHAPTER 1- INTRODUCTION

This chapter briefly introduces organic materials, the related technology and applications. It covers the organisation of the thesis and the main contributions made in the thesis.

1.1 INTRODUCTION TO ORGANIC MATERIALS AND TECHNOLOGY

Considerable research and effort is undertaken to understand semiconducting, conducting and light emitting properties of the organic materials for the improvement of organic electronics. This is done so by the use of different synthesis and self-assembly techniques. Unique opportunities exist for the improvements in the performance of these organic materials for the use in large area, low temperature devices made on substrates such as a paper or plastic. These materials are capable of generating new applications for the use in technologies as computing and connectivity devices.

The possibility to optimise the properties of the organic materials by synthetic chemists has provided much success and development in the organic electronics industry. Research work throughout the past four decades has led to a dramatic improvement in the performance by the use of innovative chemistry, processing, ability to grow, control over the self assembly and subsequently the ordering of the material. Development of materials such as longer-chain conjugated polymers, organic–inorganic composites, conjugated organic small molecules, and short-chain oligomers is under progress. These materials possess the ability to emit light, conduct current, and act as semiconductors. Their conducting and semiconducting properties are present due to the ability to transport charge by the overlap of p-orbital between neighbouring molecules.

The organic materials can be made to self-assemble in order to improve the p-orbital overlap, consequently improving the carrier mobility. Some of these materials also possess the ability to be flexible and tough such that they can be used in processes at low temperatures with techniques such as solution casting, vacuum evaporation, stamping and ink-jet printing. New products can thus be produced using methods such as roll to roll manufacturing. Products include radio frequency identification (RFID) tags, logic for smart cards and low cost information displays on flexible plastic materials.

Essential device characteristics are recognised by obtaining parameters such as the mobility values. Substantial investigation has been conducted on various organic materials such as small molecule pentacene [1-4] showing mobility improvements of about five orders of magnitude in last two decades. The chemical structures and reported mobilities of organic materials compared to the inorganic silicon materials are shown in Table 1.1. The table shows that pentacene evaporated films have achieved mobilities like that of amorphous silicon used in thin-film transistors (TFTs), for the use in active matrix liquid crystal displays (AMLCD). Single crystal

organic p-type pentacene has shown mobilities of ~3 orders of magnitude lower than single crystal silicon [4].

Table 1.1. Comparison between mobility values of various organic materials and Silicon.

Semiconductor		Mobility ($cm^2V^{-1}s^{-1}$)
Silicon	Single crystal	300-900
	Polycrystalline	50-100
	Amorphous	~1
P3HT		$< 2 \times 10^{-1}$ [5, 6]
PTAA		4×10^{-2} - 4×10^{-3} [7]
Pentacene		~1
TIPS-pentacene		~1.2 [8]

The performance and commercialization of organic semiconductors used as inorganic materials have already been reported in literature. However, there are still a number of challenges posed by organic semiconductors. To compete with the existing standards and keep a strong market presence, organic semiconductors must perform better than the inorganic ones. New organic manufacturing processes must be cost effective offering electrical devices that are not only cheaper than inorganic devices but novel at the same time. Moreover, semiconductor lifetimes and charge transport properties are affected by surroundings such as air and water. Change in the chemical structure of semiconductor and hence the electrical properties are observed with time resulting in a decline in performance [9]. Thus a reliable method to improve semiconductor lifetime for organic devices such as optoelectronics devices is by encapsulation so that air and water have a no or limited effect on the device performance [10].

A credible approach for the improvement in the film formation properties of small molecule semiconductors is the addition of insulating or semiconducting materials. This allows high performance small molecules to segregate and crystallise into large grains. Solution processing of small molecules provides the high performance of vapour deposited films with the benefit of low cost fabrication. Solution processed 6, 13-triisopropylsilyethynyl pentacene (TIPS-pentacene), a derivative of pentacene, has acclaimed better mobility values than the former with mobilities larger than 1.2 $cm^2V^{-1}s^{-1}$ and rectification ratios of more than eight orders of magnitude in TIPS-pentacene based TFTs [8]. In spite of their non uniform morphology, solution cast TIPS-pentacene films are said to produce better molecular ordering and show better TFT characteristics as compared to spin or dip coated counterparts [11].

1.2 THESIS ORGANISATION

The aim of this thesis is to present an insight into the electrical properties of organic polycrystalline semiconductors, with ultimate interest in developing models for organic semiconductor devices. Fabrication and measurements of fundamental devices such as the Schottky diode and MOS capacitor are presented in detail. The data obtained is interpreted in terms of a polycrystalline model based on existing conventional poly-silicon and disordered models. Electrical characteristics of the Schottky diode and small signal analysis of MOS capacitors provide vital information for modelling. Furthermore, an attempt is made on modelling polycrystalline organic Schottky diode under forward bias. It is believed that simple models for organic devices can eventually be incorporated together for the modelling of both dc and ac organic circuits. The section below briefly introduces the chapters in this thesis.

The charge transport in crystalline inorganic semiconductors is through well ordered energy levels that overlap to form energy bands. The resulting valence and the conduction bands are for electron and hole transport. The electrons can exist in *s*-, *p*-, *d*- and *f*- orbitals. However, the atoms in a typical organic system have their electrons in the *s*- and *p*- orbital which form molecules with σ- and π- bonds respectively. The overlapping of two π- π bonds in between the molecules and other bonds such as the van der Waal bonds causes the formation of two different energy bands namely the Highest Occupied Molecular Orbital (HOMO) and the Lowest Unoccupied Molecular Orbital (LUMO) band. These are akin to the valence and conduction bands in inorganic semiconductor respectively.

Carrier conduction is possible with the application of an externally applied voltage in the organic material, just as in inorganic materials. Externally applied bias causes injection of holes into the HOMO level or electrons in the LUMO band, and subsequently the organic material behaves either as a p-type or an n- semiconductor. Nevertheless, subtle differences exist between organic and inorganic materials that must be analysed with caution.

Chapter Two is an introduction to polycrystalline organic materials with overview of various charge transport models in organics. The charge transport mechanisms are a much debated subject with different proposed models. For disordered organic materials, it is assumed that the carrier conduction is based on hopping between different sites, which subsequently defines the mobility of the charge carriers. Disordered materials are characterized as the distribution of localised states where the states lying above the Fermi level are characterized as *donor-like* whereas the states below are *acceptor-like*. We assume that the localised states to be defined by a Gaussian

distribution which can be likely approximated to an exponential distribution for the density of states (DOS) in the band tail. The Meyer Neldel Energy (MNE), related to the width of the Gaussian distribution or the slope of the exponential can be consequently defined. This is also attributed to disorder nature in the material.

Chapter Three describes the electrical characterization of polycrystalline based Schottky diodes. The active material used is polycrystalline TIPS-pentacene in various blended forms; with plastic binders such as Polystyrene (PS) and Poly-alpha methylstyrene (PAMS), disordered organic semiconductor Polytriarylamine (PTAA) and dopant such as 2, 3-Dichloro-5, 6-dicyano-1, 4-benzoquinone (DDQ). Firstly, the fundamental behaviour of a Schottky diode is discussed followed by an introduction to space charge limited currents. Furthermore, detailed fabrication techniques and their effect on the results are discussed. A simplified expression for the current density in the exponential region of the forward characteristic is shown to determine the characteristic temperature of the intrinsic distribution of carriers. An extension of space charge limited current expression incorporating the universal mobility law is developed to determine the value of the charge carrier mobility. Consequently, various other parameters are obtained from the current-voltage (I-V) characteristics. Furthermore, the variation of I-V characteristics with temperature for two different blends of TIPS-pentacene such as TIPS/PTAA and doped TIPS/PAMS is conducted. Various parameters extracted in the forward and reverse characteristics show a strong dependent on the measurement temperature. The activation energy for both blends are found by plotting Arrhenius plots of bulk limited current density in saturation and conductivity against temperature. The small signal analysis of the capacitance voltage characteristics (C-V) is also conducted to find the dopant concentration in depletion from the plot of inverse squared capacitance against voltage.

Chapter Four focuses on the development of a 2-Dimensional (2D) model for the polycrystalline organic material. Lateral conduction in devices such as the OTFT based on polycrystalline material is represented, to consist of various grains separated by thin grain boundaries. Here carriers have to move through a number of grain and grain boundaries between the source and drain contacts. For a vertical conduction as in Schottky diodes, the conduction is assumed to occur mainly within a single grain aligned between the Schottky and back contacts, and separated by the grain boundaries. The 2D situation is taken as two, one dimensional problems at right angles to one another. Universal mobility law is applied at the edge of the grain and grain boundary, which are considered as ordered and disordered materials respectively. To develop the 2D model, the grain is constructed using the change of field in the grain due to grain boundary.

Assuming an exponential distribution of states, the current in the forward direction in the grains is established. Finally, Laplace distribution of states is proposed to explain the density of states in an organic disordered material. The carrier concentration is subsequently explained in terms of Maxwell-Boltzmann statistics and Laplace DOS.

Chapter Five is primarily concerned with the analysis of C-V characteristics of a Metal-Oxide-Semiconductor capacitor. The discussion of conventional MOS capacitor physics is followed by the fabrication process involved in producing the organic MOS capacitors. The effect of frequency and voltage are considered to obtain parameters such as the doping concentration, insulator thickness and threshold voltage from the respective characteristics. Hysteresis is discussed to be due to oxide and interface charges. The effects of photo-oxidation are also briefly considered. An equivalent RC circuit to model frequency-dependent capacitance of MOS capacitor is considered and examined. In addition, an equivalent circuit model is also proposed to find the bulk components. Furthermore, experimentally obtained temperature dependence of the capacitance-voltage characteristics are used to explain the variation in charge transport in polycrystalline organic S1150 based MOS capacitors.

Chapter Six concludes the whole thesis in terms of all the work undertaken and the experimental results obtained. Further prospects for research are also proposed.

1.3 CONTRIBUTIONS

The list below comprises the contributions made in this thesis:

- Space charge limited currents (SCLC) is defined in the forward characteristics of the Schottky diode where the mobility values are expected to be quite low.
- A model demonstrating the universal dependency of mobility on carrier density is presented for space charge limited currents. Hence, space charge limited current expression including Universal Mobility Law (UML) is developed for disordered organic semiconductors.
- Disordered materials are compared with the conventional crystalline solids to define the UML in polycrystalline organic semiconductors.
- Analysis of the dc characteristics of polycrystalline organic Schottky diodes is carried out. From the obtained results, the characteristic temperature of the intrinsic distribution of carriers T_0 is obtained from the exponential region for various different TIPS-pentacene blends. Various other parameters such as characteristic temperature of DOS,

T_C, the ratio of free charge carriers to the total charge carriers in the intrinsic DOS, θ, MNE, ideality factor and other parameters are extracted.

- A large value for ideality factor is consistent with previous experiments on disordered materials. The high value in the range of 3-5 proves that the material is not intrinsic and some trapping effects are taking place. High values of T_C and hence MNE are indicative of both the extrinsic and intrinsic traps at room temperature.
- A good linear fit to the experimental plot of natural log of the reverse characteristics against quarter powered voltage is observed at room temperature indicative of the barrier lowering due to an external field and the image force. The gradient provides the dopant density which is taken to be numerically equal to the carrier concentration for conduction. The ratio of depletion region width and Debye length is high, suggesting that an abrupt depletion region approximation can be applied.
- Temperature effects on the electrical characteristics of two different blends of polycrystalline organic Schottky diodes is conducted, namely TIPS/PTAA and doped TIPS/PAMS. For TIPS/PTAA Schottky diode, as the temperature falls, the values of most parameters remain constant until a critical temperature. The activation energy also remains constant at approximately 0.3eV for various applied voltages in saturation. Below this critical temperature, most parameters are observed to decrease.
- For doped TIPS/PAMS Schottky diode, parameters such as effective mobility, carrier concentration, MNE decrease with decreasing temperature. From the Arrhenius analysis, two different activation energies are obtained in the range of temperatures observed. At lower temperature range, the activation energy is seen to be twice that of the one obtained in the higher temperature range.
- Dopant concentration is found from the slope of inverse square capacitance against voltage plot.
- A two dimensional model for a polycrystalline organic semiconductor based Schottky diode is proposed based on simple two one dimensional cases using Gauss's law. The grains and the grain boundaries are identified in terms of simple equations and the current density classified for both.
- A new model is proposed for the charge conduction mechanism in disordered organic semiconductors based on Laplace's first law- Laplace L1 DOS. A term for the carrier concentration is finally devised.

- Organic polycrystalline based MOS capacitors show a decrease in the maximum capacitance with the change in frequency of the ac signal and temperature, unlike the conventional inorganic MOS capacitors.
- Small signal behaviour for an ideal MOS capacitor is discussed in terms of various equivalent circuits. Parameters such as the thickness of the oxide layer, thickness of the organic semiconducting layer, the series resistance, bulk capacitance and bulk resistance are found from the C-f analysis.
- Temperature dependence of the C-V characteristics is also observed for organic MOS capacitors. Either the grain or the grain boundary of the polycrystalline material is expected to dominate. The results provide a temperature value very close to the absolute temperature T instead of the T_C. Thus, contrary to what is believed, the ordered grains are seen to dominate.

1.4 REFERENCES

[1] Y. Lin, D. J. Gundlach, S. Nelson, and T. N. Jackson, IEEE Device Lett. 18, (1997) 606.

[2] A. Dodabalapur, L. Torsi, and H. E. Katz, Science 268, (1995) 270.

[3] C. D. Dimitrakopoulos, S. Purushothaman, J. Kymissis, A. Callegari, J. M. Shaw, Science 283, (1999) 822.

[4] J. H. Schoon, S. Berg, C. Kloc, B. Batlogg, Science 287, (2000) 1022.

[5] D. H. Kim, Y. D. Park, Y. Jang, H. Yang, Y. H. Kim, J. I. Han, D. G. Moon, S. Park, T. Chang, M. Joo, C. Y. Ryu, K. Cho, Adv. Mater. (Weinheim, Ger.) 15 (2005) 77.

[6] H. Sirringhaus, P. J. Brown, R. H. Friend, M. M. Nielsen, K. Bechgaard, B. M. W. Langeveld Voss, A. J. H. Spiering, A. J. Janssen, E. W. Meijer, P. Herwig, D. M. de Leeuw, Nature, London 401 (1999) 685.

[7] W. Zhang, J. Smith, R. Hamilton, M. Heeney, J. Kirkpatrick, K. Song, S. E. Watkins, T. Anthopoulos, I. Mc Culloch, J. Am. Chem. Soc. 131, (2009) 10814-10815.

[8] S. K. Park, T.N. Jackson, J.E. Anthony, D.A. Mourey, Appl. Phys. Lett. 91, (2007) 63514.

[9] F.C. Krebs, K. Norreman, Prog. Photovol. Res. Appl. 15, 8 (2007) 697.

[10] J. Meyer, P. Görrn, F. Bertram, S. Hamwi, T. Winkler, H-H. Johannes, T. Weimann, P. Hinze, T. Riedl, W. Kowalsky, 21, 18 (2009) 1845.

[11] S. K. Park, T. N. Jackson, J. E. Anthony, IEEE Electron Dev. Lett. 28, (2007) 877.

CHAPTER 2- CHARGE TRANSPORT MECHANISMS IN ORGANIC MATERIALS

Disordered and polycrystalline organic semiconductors used in the thesis are introduced. The existent distribution of states models and the distribution functions are defined. Also, charge transport mechanisms in various organic materials are discussed.

2.1 INTRODUCTION

Organic semiconductors are promising materials for electronics and opto-electronic devices as they provide opportunities for low cost, large area applications. The charge transport mechanisms in organic materials are under constant debate. Various charge transport models have been developed to describe the conduction in disordered organic materials for example, with good agreement to experimental data. Some of such fundamental models are discussed in this chapter.

Interest in disordered organic semiconductors is vital in understanding the conduction mechanisms in polycrystalline organic materials. The majority of this thesis is based on understanding polycrystalline materials, which is believed to consist of grains that are ordered and grain boundaries that are similar to disordered materials. Although the conduction is expected to dominate in the ordered grains, the grain boundaries however limit the flow of the charge carries. Thus, understanding charge transport in terms of disordered organic semiconductors is important for defining charge transport in polycrystalline materials.

2.2 ORGANIC MATERIALS

The interest in organic materials for use in various electronic applications stemmed from the limitations of commonly used inorganic materials such as silicon. Although silicon has good characteristics, the applications are normally based on rigid substrates such as glass and are expensive to produce. Unlike organic semiconductors, its fundamental properties render it unsuitable for the majority of opto-electronics applications such as the lasers used in optical communications. Although cheap information-storing devices like smart cards and inventory control tags can be made, amorphous silicon requires a glass substrate and is not practical in use.

In 1950s work on crystalline organics materials started as an alternative to silicon [1]. Although plastic is a very poor conductor of electricity, joint Nobel prize winners Heeger, MacDiarmid, and Shirakawa, in 1970s, demonstrated that polyacetylene backbone can be tweaked to enhance its conductivity. Consequently, later in 1980s, results on first efficient organic LEDs (OLEDs) were published by Kodak and independently results on the first organic transistors (OTFTs) were also made public. Friend et al. at Cambridge University further published the first results on polymer light emitting diodes in 1990s [1].

Ever since then, substantial research has been invested in organic electronics and opto-electronics to improve the conducting, illuminating and semiconducting properties of conjugated polymers

and small molecules. This has been immensely focused on the development of innovative synthesis and fabrication techniques. The advantage of using organic materials in integrated circuits is that plastic devices are lighter, cheaper than conventional semiconductors, and can be used in optoelectronics. It can also be used for storage and displays as organic materials consume less power. Displays, using OLEDs, are of particular interest in organic electronics as they can be developed on large areas and flexible substrates. Fully flexible displays can be developed where the active matrix is designed of OTFTs instead of amorphous silicon TFTs and the pixel elements are made of OLEDs instead of devices such as LCDs.

OTFTs are another field of innovative research for their application in displays, radio frequency information (RFID) tags and smart cards. A large number of researches continue to advance in order to improve the operational speed of plastic transistors, which is attributed to the charge carrier mobility of the organic semiconductor. Recently, OTFTs based on small molecules have demonstrated high performance with charge mobilities comparable to amorphous silicon transistors existent in display industry. Organic materials offer attractive attributes at a fraction of the cost of silicon.

Organic solar cells with efficiencies of more than 5% have been demonstrated and are attractive due to their compatibility with large area and low temperature processes, thus resulting in lower processing cost than that of silicon. The main advantage of using organic semiconductors is that molecules and polymers can be tailored to include specific electronic or optical properties. Despite such attractive features, organic materials face a constant challenge in terms of electrical and optical stability. They are also attributed to low carrier–mobility even with the addition of dopant ions. Furthermore, the processing steps required for developing organic devices are somewhat different from the classical processes in semiconductor industry.

In this thesis, two main organic semiconductors namely Polytriarylamine and TIPS-pentacene are studied. In the following section, their respective chemical structures and electronic properties are briefly discussed, and used in the subsequent chapters.

2.2.1 Disordered Organic Semiconductor

Polytriarylamine (PTAA) is a p-type disordered organic semiconductor with a structure shown in Fig.2.1. It has been publicized to have reasonable charge carrier mobilities especially when the molecular weight is low [2], with reasonably good operational and environmental stability due to its high ionization potential [3]. Vast amount of research has been carried out on PTAA in order

to understand and define its basic electrical properties, operating conditions and conduction mechanisms.

In the time-of-flight experiments conducted by Newman [4], bulk mobilities of more than 10^{-2} $cm^2V^{-1}s^{-1}$ have been observed for PTAA. The basis for high mobility was regarded to be due to low concentrations of bulk or interface traps. Moreover as PTAA forms a smooth layer, no effects of crystal interfaces are observed [5]. Experimental work on PTAA-based field-effect transistors (OFET) reported hole mobilities of $10^{-3}cm^2V^{-1}s^{-1}$ in ambient conditions [6]. The bulk mobility value, usually lower, is observed to be higher than the field-effect mobility in PTAA-based experiments mentioned above.

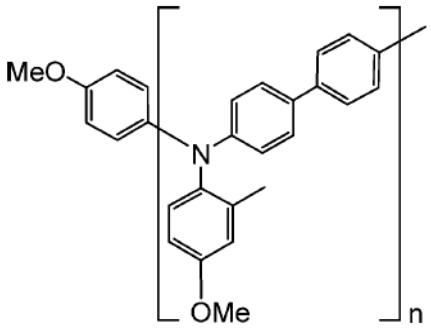

Figure 2.1. Chemical structure of Polytriarylamine PTAA.

2.2.2 Polycrystalline Organic Semiconductor

Pentacene is a p-type semiconductor related to the groups of small molecules. It has a herringbone structure with a combination of edge-to-face and face-to-face molecular interactions which limits the bulk mobility. The performance of pentacene based device can be improved by altering the molecule to form molecular crystals with increased p-orbital overlap.

6, 13-triisopropylsilyethynyl pentacene (TIPS-pentacene) is a derivative of pentacene that is soluble in most of organic solvents. The functionalized groups added to pentacene are permanent and do not need high temperature steps for removal. Enhanced carrier transport and improved molecular ordering properties are attributed to TIPS-pentacene as the bulky functional groups help to disrupt the herringbone structure of unmodified pentacene. Adding a functionalized group to pentacene reduces edge-to-face molecular interactions [7] and results in more face-to-face

molecular interactions. TIPS-pentacene has enhanced p-orbital overlap and a reduced inter-planar spacing compared to unmodified pentacene (Fig.2.2).

Like most polycrystalline organic semiconductors, TIP-pentacene [8, 9] is acclaimed to have higher mobility, compared to the disordered organic semiconductors such as polytriarylamine (PTAA) and poly3-hexylthiophene (P3HT) [10, 11]. Nonetheless, the mobility of the disordered counterparts can be enhanced by extrinsically introducing controlled amount of dopants such as 2, 3-Dichloro-5, 6-dicyano-1, 4-benzoquinone (DDQ) as previously reported by Brown et al. [12] and Raja et al. [13]. In this thesis, experimental analysis on TIPS-pentacene will be carried out to highlight that an increase in conductivity is associated with the addition of dopants. Furthermore, additional experimental work is carried out on TIPS-pentacene and PTAA blend.

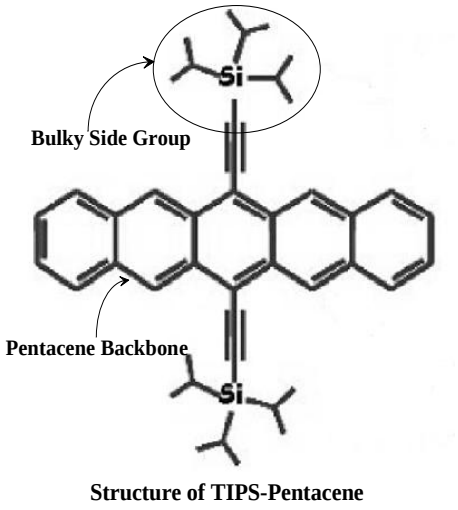

Figure 2.2. Chemical structure of 6, 13-triisopropylsilyethynyl pentacene (TIPS-pentacene)

2.3 DISTRIBUTION FUNCTIONS FOR OCCUPANCY OF THE CARRIERS

The probability of particles occupying available energy levels in a certain system can be described in terms of the probability distribution functions. Such functions include the Fermi-Dirac (F-D) probability, the Bose-Einstein (B-E) and the Maxwell Boltzmann (M-B) distributions as described further in this section [14-16]. The probability of occupancy of energy levels by Fermions is defined by the Fermi-Dirac function. Fermions such as electrons are particles with half-integer spin obeying Fermi-Dirac statistics opposed to bosons which have an integer spin. These particles

are named after Enrico Fermi and Paul Dirac whereas Bosons obey the Bose-Einstein statistics and are named after Satyendra Nath Bose. A quantum mechanical principle called the Pauli Exclusion Principle states that no two identical fermions may occupy the same quantum state at a given time. For more than one Fermion occupying the same place in space, the properties of each Fermion, such as the spin, must be different from the rest. Therefore, fermions are usually associated with matter while bosons are often force carrier particles.

Addition of Fermions such as the electrons to the energy levels will fill the vacant states in the energy levels. The states in the higher energy levels are filled after the lower energy levels are filled completely. Increase in temperature causes the shift between completely empty states and completely filled states to be gradual instead of being abrupt as demonstrated in Fig.2.3. In thermal equilibrium, the F-D function is the probability that an electron at energy, *E*, occupies an energy level. The F-D function f_{F-D} at temperature *T = 0K* is given by

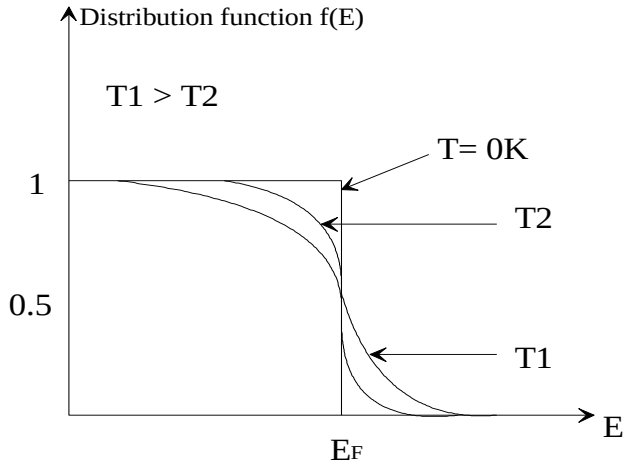

Figure 2.3. The Fermi distribution functions at various temperatures. At T= 0K, the Fermi function has a step like behaviour. Increasing temperature smears the function out and causes the function to develop an exponential tail.

$$f_{F-D}(E) = \frac{1}{1 + exp\left(\frac{E - E_F}{kT}\right)} \begin{cases} 1 & if\ E \geq E_F \\ 0 & if\ E < E_F \end{cases} \qquad 2.1$$

where *T* is the temperature of the system and E_F is the Fermi level energy. For energies that are a few *kT*s above the Fermi level, the F-D function has a value of unity and at Fermi Level (*T = 0K*), it has a value of half, thus resembling a step function. For energies a few *kT*s larger than the Fermi

level, the value decreases exponentially with energy. The other distribution functions, such as B-E function $f_{B\text{-}E}$(E) and M-B distribution function $f_{M\text{-}B}$(E) can be defined as follows and are compared to F-D function.

B-E function is

$$f_{B-E}(E) = \frac{1}{\exp\left(\frac{E}{kT}\right) - 1} \qquad 2.2$$

M-B function is also called the classic distribution function since it provides the probability of occupancy for particles that are non-interacting at lower densities. These non-interacting particles are distinguishable from each other

$$f_{M-B}(E) = \exp\left[-\left(\frac{E - E_F}{kT}\right)\right] \qquad 2.3$$

where E_F is the Fermi energy (i.e. the chemical potential) which is known only when the density of states and the electron density are known. This is when $f(E_F)$ is halved. The distribution function for Bosons show that $f(E)$ can be much larger than 1 in principle.

For small systems in thermal equilibrium with a single energy level, the distribution function is dependent on the density of states. The Fermi level energy E_F can be determined if the carrier concentration n is known. At finite temperatures, n is hard to determine in terms of E_F. If the electron density is small such that $f(E)$ is small, Fermi function can be represented by overlooking the 1 in the denominator. This gives the M-B function, only when $f(E)$ values are miniscule (i.e. non-degenerate statistics).

2.4 MODELS FOR DENSITY OF STATES (DOS)

2.4.1 Gaussian Distribution

As the polymer chain length varies and the interactions cannot be generalized as having delocalized energy bands such as the conduction and the valence band separated by an energy gap, the charge transport sites are energetically spread. This energetic DOS can be described in terms of Gaussian distribution, N_g, as supported by the examination on the absorption spectra of polymer materials resulting in the Gaussian shaped distribution by Bassler [17]. In addition, Gaussian distribution is maintained since the polymeric material response varies only a little with the application of an electric field. The shape reveals the disorder and therefore is essential to

define the charge transport. In 1993, Bassler defined charge transport of a disordered organic semiconductor within the Gaussian DOS [17]. The transport was described by a hopping mechanism of the carriers between discrete energy states within the Gaussian distribution as in Fig.2.4. The hopping rates were given by Miller- Abraham model [18] and the hypothesis of weak electron-phonon coupling was assumed to disregard polaronic effects. Detailed discussion on Miller- Abraham and polaronic model is presented later in this chapter. Positional and energetic disorder is thought to be introduced when the charge hops in a standard arrangement of hopping sites. Gaussian DOS in terms of energy can be explained by [17]

$$N_g(E) = \frac{1}{\left(\frac{E_\sigma}{E_0}\right)\sqrt{2\pi}} \exp\left(-\frac{(E-E_\mu)^2}{2{E_\sigma}^2}\right) \qquad 2.4$$

where E_σ is the standard deviation of Energy, $E_0$is equal to 1 and has the dimensions of E_σ, ${E_\sigma}^2$ is the variance and E_μ is where the energy deviation is maximum.

Hartenstein et al. [19] presented another approach for describing the positional disorder employing the Gaussian distribution model for the DOS but without verifying a distribution function for the electronic coupling between different sites. The hopping sites, in this case, were grouped in clusters with their closest neighbouring sites and the cluster sizes are dependent on the random inter-cluster distances. Limitations include the use of the model at lower dopant concentrations, for which the inter-site distances are very instable.

2.4.2 Exponential Distribution of States

In disordered organic semiconductors, the DOS is distributed across a wide range of energies and is given by a Gaussian distribution as defined in Section 2.4.1. At low carrier concentrations, the Gaussian distribution can be approximated to an exponential function [20]. The transport within such discrete states is related to a variable range hopping mechanism. Variable range hopping mechanism, extension of the hopping model proposed by Miller and Abrahams [18], assumes that the localized states are spread over the entire energy gap [21]. In Variable Range Hopping (VRH) [22], the charge carriers may either hop over a small distance with a high activation energy or hop over a long distance with a low activation energy. In 1985, the concept was further extended by Monroe with his theory for the transport of photo-excited carriers within an exponential density of states (DOS) [23]. The transport of charges was described to be in the band tail with both hoping and thermal excitation of carriers to the band edge.

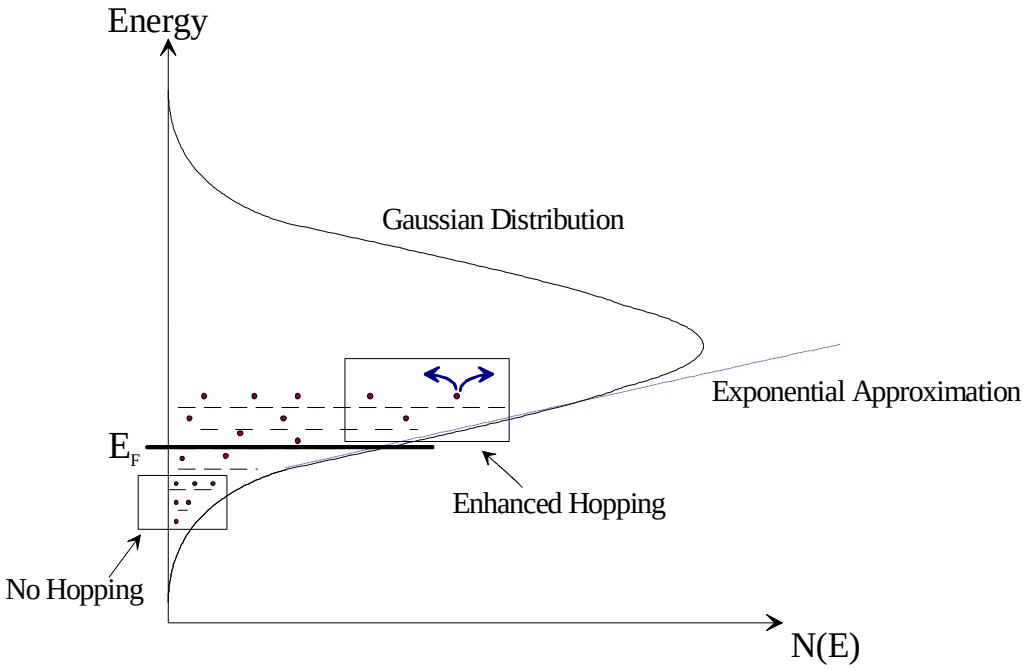

Figure 2.4. Demonstration of Gaussian Distribution of states (GDOS). GDOS can be approximated to follow exponential distribution at low energy levels as discussed in Section 2.4.2. Hopping, represented by the blue arrows, is thought to follow variable range hopping (Section 2.5.4). The filled circles represent the charges introduced by both the electrical field and doping of semiconductor.

Vissenberg and Matters [22], in addition, developed VRH to take into account the filling of localized states with charge carriers in contrast to the one developed by Bassler which is a one particle model. At low carrier densities and low temperatures, the transport properties are said to be in the tail states of Gaussian DOS, approximated as an exponential DOS (Fig.2.4) [24]:

$$N_{exp}(E) = \frac{N_{to}}{kT_0} \exp\left(\frac{E}{kT_0}\right) \qquad 2.5$$

where N_{exp} is the exponential distribution of the localized states, N_{to} is the number of states per volume unit, T_0 is the characteristic temperature describing the width of the carrier distribution, k is the Boltzmann's constant and E the energy level. The energy distribution of the carriers at equilibrium is given by Maxwell Boltzmann's distribution. If the system is filled with a charge carrier density, δN_t, which occupies a small fraction $0 < \delta < 1$ of the states, the position of the

Fermi level is fixed by the condition that $E_F >> kT_0$. This means that most carriers occupy the sites with energy E <<0 and the condition $T < T_0$ is fulfilled. When $T_0 < T$, the assumption that charge transport is only in the tail of the DOS is invalid.

2.4.3 Laplace Distribution

A widely accepted model for the distribution of states is the Gaussian disorder model through which the carriers hop to produce current as in Section 2.4.1. The efficiency of hopping defines the mobility of the carriers and hence the charge transport as previously discussed in this chapter, Chapter 3 and in Chapter 5. Recently, Eccleston [25] proposed using Laplace distribution of states (L1 DOS) to define the density of states in an organic disordered material. Laplace L1 has also found different variations in electronics, material sciences and physics and can be seen in statistics such as Fermi Dirac and Maxwell Boltzmann statistics.

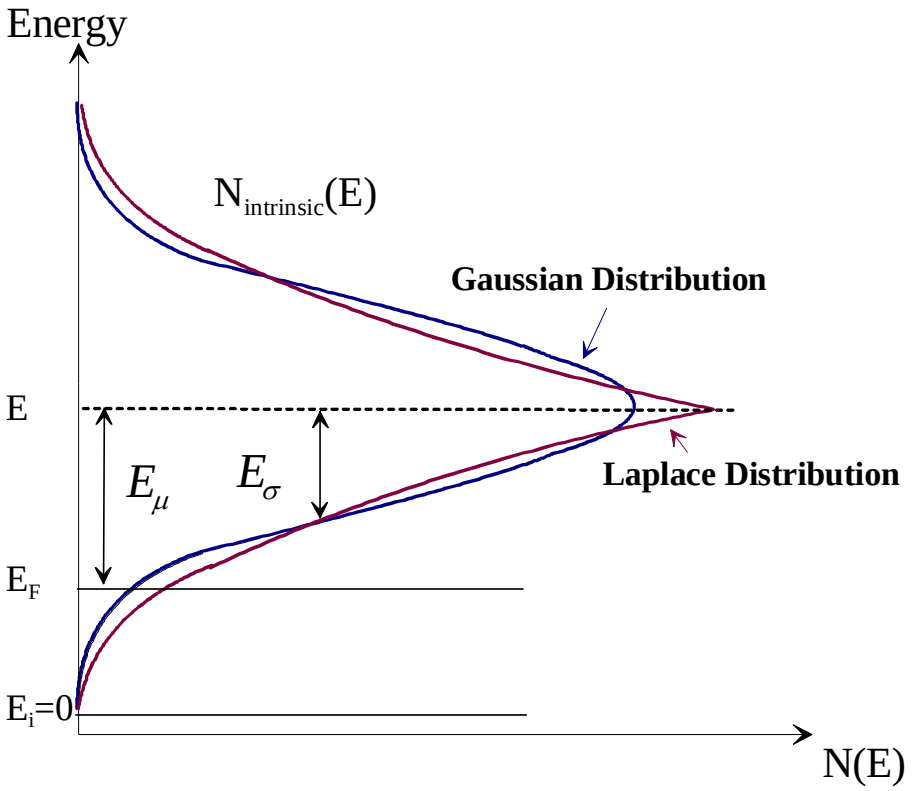

Figure 2.5. A comparison between Laplace and Gaussian distribution. Laplace distribution has a thicker tail and a longer pointed peak. E_μ is the energy deviation of the maximum from Fermi level to the centre of the Laplace or Gaussian distribution. E_σ is the standard deviation of the Laplace or Gaussian distribution and is used to explain the Meyer Neldel Energy in

Section 2.4.4.

In 1774 Pierre-Simon Laplace introduced a continuous probability distribution that has a probability density function called the Laplace distribution. It is a double exponential function as it can be assumed to be two exponential distributions attached back to back. It is the distribution of the difference of two independent exponential random variables with the same mean. The distribution is essentially symmetric about the centre and therefore uni-modal as seen in Fig.2.5. It can be defined in a dimensionless form with a distribution width λ, location θ and variance $2\lambda^2$ [26]

$$g(x|\theta,\lambda) = \frac{1}{2\lambda}\exp\left(-\frac{|x-\theta|}{\lambda}\right) \qquad 2.6$$

and in terms of energy as

$$N_{L1}(E) = \frac{1}{2\left(\frac{E_\sigma}{E_0}\right)}\exp\left(-\frac{E-E_\mu}{E_\sigma}\right) \qquad 2.7$$

where E_σ is the standard deviation or the width of the Laplace DOS, E_0 is the reference energy equal to 1 with units corresponding to E_σ such that E_σ/E_0 is dimensionless, E_μ is the energy deviation of the maximum and $2{E_\sigma}^2$ is the variance. $E=0$ is assumed to be the Fermi level of the intrinsic material. Figure 2.5 demonstrates subtle differences between a Gaussian and Laplace DOS.

2.4.4 Significance of Meyer Neldel Energy in DOS

The Meyer Neldel rule (MNR) is an experimental relation observed in very many different electronically, polaronically and ionically conducting semiconductors such as single-crystal and polycrystalline semiconductors, amorphous semiconductors, organic semiconductors, and ionically conducting crystals and glasses [27-29]. Although it is a commonly observed phenomenon, the origin of MNR in inorganic and organic semiconductors is still under constant debate. Several processes, with a thermally activated behaviour, coexisting simultaneously can lead to the MN rule. It is due to the processes for which several excitations provide the entire energy required for the system [30, 31]. A number of theories exist to explain the origin of MNR and have been discussed in the following text.

The MN rule is defined as a constituent of disorder [32, 33] and the shift in the quasi Fermi level with temperature [34]. Meijer et al. [35] and Yelon et al. [31, 36] defined MNR due to characteristic transport mechanism in disordered materials. Theoretical studies proposed by Fishchuk et al. suggest that the width of DOS in the disordered energy band is said to be proportional to Meyer Neldel energy (MNE) [37]. Fig.2.5 shows the width of the distribution as the energy E_σ corresponding for MNE for both Gaussian and Laplace DOS. Furthermore, MNE is further defined in terms of the characteristic temperature attributed to the disordered DOS in Eq. (3.14), Chapter 3.

In organic electronics, this prediction provides a method for evaluation of the amount of energetic disorder in the material as these materials are said to have a large density of localised states with high activation energy [38]. Moreover, MNE can also be applied to polycrystalline organic materials having ordered grains and disordered grain boundaries. Previously, Roberts [39] followed by Cohen et al. [40] defined the MN rule for polycrystalline or amorphous semiconductors derived from an exponential tailing of the majority band states. This theory has been applied in the upcoming chapters.

Conversely, polaron concept has also been used to theoretically justify MNE in different systems. Polarons are defined as an introduction of lattice deformation around a charge carrier. Kemeny and Rosenberg [41] proposed a model for organic semiconductors where electrons or polarons tunnel past intermolecular barriers from activated energy states of the organic molecules. Polaron model is discussed in detail in Section 2.5.3. However, the polaronic effects in a disorder based transport model are neglected because disorder is considered the main reason for localisation of charge in organic semiconductors. In organic semiconductors, the application of this theory is dependent on validating the use of multi-phonon model to explain hopping of carriers in localised states. Higher activation energy is evident in experiments involving multi-phonons. Increase in the activation energy is indicative of the involvement of a number of phonon that creates various conduction paths for charge transport. Furthermore, the activation energy observed in organic disordered materials is in the range of single phonon energy. This is in contrary to the theory that the transport is due to a multi-phonon process.

The existence of MNE can be explained by fundamental parameters such as the electrical current, conductivity, diffusion and other physical parameters. Elementary quantities like the charge carrier mobility are used to understand the mechanisms of MNE. However, justification of MNE for the charge carrier mobility is debatable. Sample fabrication methods such as the oxygen

partial pressure at annealing, the extent of non-stoichiometry, dopant concentration and other techniques all have an effect on the MNE [42].

In conclusion, MNR is a frequent occurrence in disordered organic materials with a pervasive value. However, there is no universal agreement on the basis of MNR as it is argued to be a result of either the charge carriers having a polaronic nature or due to a common DOS in the disordered material.

2.5 CHARGE TRANSPORT MECHANISMS IN ORGANICS

For pure crystal materials with organized molecular crystals, the charge transport is assumed to occur via charge carriers in delocalized states such as that seen in inorganic conventional semiconductors. The model assumes that the mobility in these materials follows an inverse power law with temperature. That is, that the mobility decreases with the increase in temperature like in highly pure crystalline materials observed in the time-of-flight experiments [43]. Although this is true for very low temperatures, the assumption does not withstand the analytical results. Except at low temperatures, the intermolecular distance is always more than the corresponding mean free path which renders it incompatible with diffusion-limited processes. In inorganic semiconductor crystals as in the case of silicon or germanium, the constituting atoms have strong coupling between each other and the delocalization of the electronic states is possible due to long-range ordering. The valence and conduction bands are thus possible with the distance between referred to as the band gap. The conduction band in inorganic crystals can be thermally activated to generate free carriers. These in turn leave positively charged holes in the valence band. The assumptions such as the one-electron limit for inorganic materials [44, 45] are impossible to consider in organic materials due to the large numbers of atoms and molecules.

In organic semiconductors, there exist a number of defects mainly structural and chemical. For this reason, it is not possible to regard their transport as of inorganic semiconductors and the use of conduction mechanism such as hopping is required. Hopping from one site to another is due to phonon assisted tunnelling mechanism and many models defined for organic semiconductors include the use of four-dimensional Miller- Abraham equation [18]. Covalent interactions occur with weaker van der Waals and London forces dominating intermolecular interactions. Unlike inorganic semiconductors, the energy bands are narrower and a slight introduction of disorder can disrupt the highest occupied molecular orbital (HOMO) and the lowest unoccupied molecular orbital (LUMO) bands. Therefore, interactions localized on individual molecules play a major

role. Charge carriers that are localised can either move by charge hopping with temperature or due to an externally applied electric field. However, thin organic semiconductor films have complicated charge transport behaviour due to the spatial and energetic disorder. The conductivity and hence the mobility is dependent on the density of charge carriers, temperature and the electric field.

Charge transport in organic materials has remained a highly controversial topic over the years. Although huge efforts have been dedicated to charge transport in organics [46-49], issues such as the mobility and temperature dependence, have not been adequately determined. The lack of an analytical model has complicated the organic semiconductor device design. The prediction of device models is complex due to an unclear understanding of the physical origin of many parameters and the difficulty to reproduce results.

The charge transport is based on Gaussian distribution of the density of states with energies, as observed by an optical spectrum from the research of Bassler [17], where the charge transport sites are localized [50]. The analysis of hopping mechanism in organic semiconductors is supported by the introduction of transport energy defined as the energy required for maximizing the hopping probability. Transport energy for a carrier is independent on the initial energy of the carrier and helps in deciding mobility edge [51]. Theories for inorganic disorder materials such as the percolation theory [52] and the concept of charge transport defined by transport energy, E_{tr} already exist [23, 51, 53]. In organic semiconductors with low carrier concentrations, the activation of charge carriers to E_{tr} happens from the Fermi level instead of the equilibrium energy as E_{tr} is temperature dependent [23, 52, 54]. A number of charge transport models are considered for organic semiconductors in the following text which include the Miller-Abraham hopping model, percolation model, variable range hopping model and the multiple trap and release model.

2.5.1 Miller Abraham Hopping Model

In disordered organic semiconductors, the lack of an ideal three dimensional periodic lattice makes the charge transport process harder to understand. Unlike conventional semiconductors, the spatial and energetic disorder has no symmetry and the conduction process in terms of valence and conduction band does not necessarily apply. Instead, HOMO and LUMO terms are used to describe the highest occupied and the lowest unoccupied levels respectively. In disordered semiconductors, very low mobility exists due to the existence of localized states *N*, referred to as *N(E)* for energetically distributed states at a particular energy, *E*. The charge carriers are required to hop between these localized states producing low carrier mobility values. These carriers must

overcome the energy difference between the two localized states by either absorbing or emitting phonons.

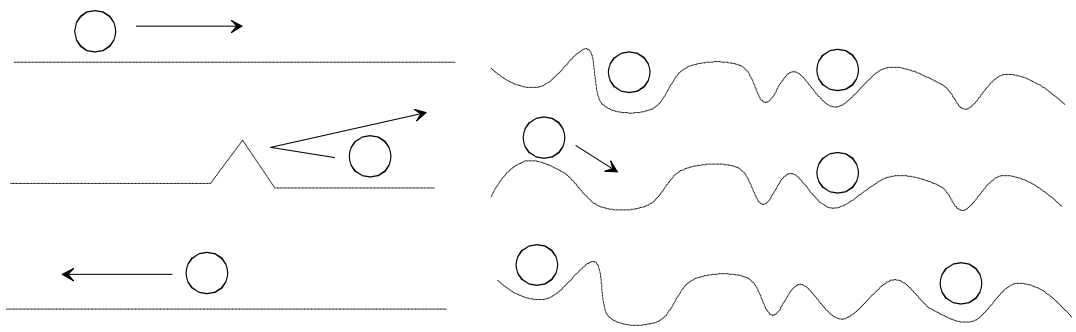

(a) (b)

Figure 2.6.Charge transport mechanism for an inorganic crystal; (a) with band transport and delocalized free carriers. Disruption in crystal symmetry is given by a bump. (b) with hopping transport. The lattice vibrations are necessary for a localized carrier, localized due to defects, disorder or self-localization, to move from one site to another [50].

A number of different hopping models were predicted. Conwell [24] and Mott [55] suggested the process of phonon-induced hopping in regards to metallic conduction in inorganic semiconductors and later, Pines, Abrahams and Anderson [56] suggested the electron relaxation processes. Mott described the hopping transport in a constant density of states (DOS) where the concept of hopping to higher energies and over long distances had equal significance. He linked the conductivity σ to vary with temperature according to the relation

$$\sigma \, \alpha \exp\left(-\frac{T_1}{T}\right)^{1/4} \qquad 2.8$$

where $T_1 = {}^{128}/_{9\pi k b^3 N(0)}$, *N(0)* is the density of states at the Fermi level and b is the size of the localized states [21].

Shortly, a single-phonon hopping model for lightly doped semiconductor at a very low temperature was proposed by Miller and Abrahams based on a single-phonon jump rate description [18]. This model was supported on the fact that the localized states were shallow

impurity levels with narrow range energy levels. This meant that a higher probability existed for electron to jump to the nearest empty site (Fig.2.6).

The hopping rate of carriers from occupied *i* to unoccupied *j* localized donor states depends on the height of the energetic barrier $E_j - E_i$ and the distance D_{ij} between the states *i* and *j*

$$v_{i\to j} = v_0 \exp(-2\alpha D_{ij}) \begin{cases} \exp\left[-\frac{(E_j - E_i)}{kT}\right] & \text{for } E_j > E_i \\ 1 & \text{for } E_j < E_i \end{cases} \qquad 2.9$$

where the pre-factor v_0 is the attempt-to-hop frequency, α is the inverse localization length, and *k* is the Boltzmann constant. $\exp(-2\alpha D_{ij})$ represents the tunnelling probability and $\exp\left[-\frac{(E_j - E_i)}{kT}\right]$ represents temperature dependence of the phonon density.

For disordered organic semiconductors, the disordered sections of the material act as isolated states making Eq. (2.9) valid at high temperatures [21]. In inorganic semiconductors at higher temperatures, hopping transport is overcome by band-like transport. This is owing to the inversion of carriers such that they shift from donor states into a higher number of energy levels at the conduction/valence band edge.

Multi-phonon processes have been ignored in this model. These are said to control the charge transport in organic semiconductors if the charge carriers are localised polarons. Charge transport based on polaron model has been discussed in detail in Section 2.5.3. Ignoring multi-phonon processes would lead to an erroneous value from the temperature dependent mobility. However, in disordered materials, considering that weak electron-phonon interactions exist. The polaronic effects can be ignored [17]. A hopping model similar to the Miller-Abraham model was proposed by Bleibaum et al. where they introduced a prefactor dependent on the electron-phonon coupling strength, the phonon DOS and other properties of an organic semiconductor [57].

2.5.2 Percolation Model

In organic thin film transistors, percolation models without the presence of electric field have been applied. The electrical field applied laterally can be ignored due to large size of the channel [22]. This is nevertheless untrue in the case of vertical conduction where the electrical field through the semiconductor is much larger and the charge carrier distribution is hard to model.

Percolation models were first introduced to explain the charge transport in disordered inorganic semiconductors [58]. However, it has also been used to explain charge conduction in organic semiconductors [22, 59]. Charge conduction in organic semiconductors is mainly due to the application of externally applied electric field or hopping between localised states due to thermal activation. The polaronic effects, mentioned in Section 2.5.3, are ignored as they are considered small with regards to energetic disorder. The activation energy required for hopping is not reliant on the molecular conformation energies used to form activated complexes before transfer of charge. It is only dependent on the site energy differences [60] and can be written in terms of Miller-Abraham model, Eq. (2.9). In thermal equilibrium, the hopping rate can be explained to obtain conductance G_{max} [61]. Eventually, every hop between localised states in an organic semiconductor can be explained in terms of a unique conductance. This conductance is described by the quasi Fermi energy, the respective site energy and the intermolecular spacing.

Considering an exponential DOS and ignoring the spatial disorder, the conductance network can be determined. Conductance due to every hop, in an organic semiconductor especially a disordered material, is likely to fluctuate by several orders of magnitude [60]. The organic semiconductor is distributed into a number of conducting clusters. These are defined relative to a reference conductance, G. Conduction pathways between sites $G_{max} \leq G$ are removed from the network. In this manner, only a group of spatially detached clusters of high conductivity are left behind, $G_{max} > G$. Decreasing the reference conductance G, increases the size of the isolated clusters. Percolation first occurs at a critical conductance where the maximum reference conductance $G = G_C$. This is where a continuous, infinite cluster spanning the whole system is formed. It contains a number of clusters that are all connected by critical conductance G_C. The conductivity of the cluster is explained by the most resistive link due to the possibility that the infinite cluster varies by several orders of magnitude. G_C then determines the total conductance of the system. Ambegaokar and co-workers [58] used a three-part network to define critical percolation conductance G_C in terms of clusters. The first part of the network was a set of isolated clusters of high conductivity; second was a subset of high conductance clusters forming a critical sub-network essentially the sample-spanning cluster; and the third part consisted of the remaining resistors. In this network, the second part dominates the overall conductance of the network.

Decrease in the reference conductance G causes an increase in approximate number of bonds per site B. A large sized cluster, with sites $G_{max} > G$, indicates a large B. When B reaches some critical bond value of B_C, the cluster size must be adequately large to be in contact the neighbouring clusters. Thus making an uninterrupted path that covers the whole of the disordered

organic semiconductor. For a disordered three dimensional system B_C~*2.8* [62] and is obtained by numerical simulations.

Using Miller-Abraham's model for conductance introduced in 1960s, the maximum distance, D_{max}, between two hopping sites between which a hop can occur is given by

$$D_{max} = \frac{1}{2\alpha} \ln\left(\frac{G_C kT}{q v_0}\right) \qquad 2.10$$

and the maximum energy, E_{max}, that any initial or final state can have is given by

$$E_{max} = kT \ln\left(\frac{G_C kT}{q v_0}\right) \qquad 2.11$$

where v_0 being the attempt-to-hop frequency. Thus the density of states that can be part of the percolating sub-network, N_{sn}, is presented by

$$N_{sn} = 2\rho E_{max} \qquad 2.12$$

where ρ is the site density function.

As only the sites within a range D_{max} are linked together in a sub-network, this criterion can be written in terms of a dimensionless quantity, v_c and can be linked to Mott's law [63].

$$v_c = {D_{max}}^3 N_{sn} \qquad 2.13$$

2.5.3 Polaron Model

The polaron model is based on the quasi-particles called polarons composed of a charge and its accompanying polarization field. It was first introduced in 1958 for inorganic crystals [65], and soon after it in 1959 for molecular crystals [66]. In disordered organic materials such as conjugated polymers, the charge transport can be explained in terms of polaronic motion due to strong electron-phonon interactions [67]. An example of an introduction of polaron is shown in Fig.2.7 in a heterocyclic polymer. These interactions are associated with the ability of conjugated

polymers to change their geometry upon charging. The origin of localisation is therefore due to the formation of polarons.

An individual charge carrier has a coulomb field that first polarises its surrounding and then couples itself to it. The charge therefore has an accompanying deformation which acts like a quasi-particle, also known as a polaron. The charge carrier carries the lattice deformation it induces and the polaron is considered to be self-trapped.

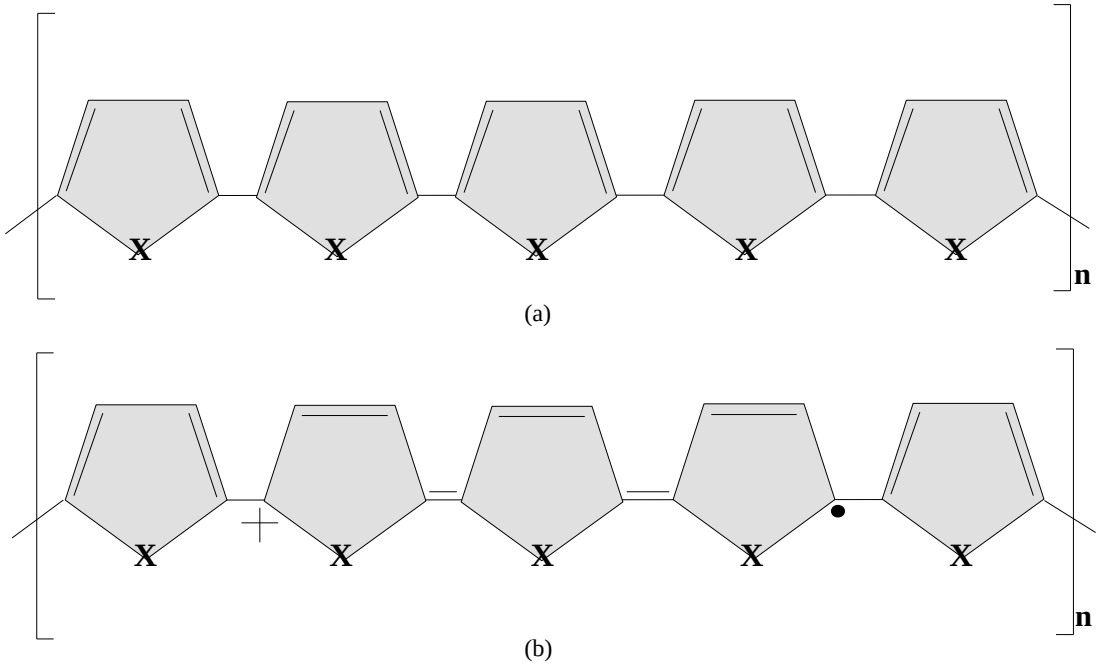

Figure. 2.7. (a) A heterocyclic polymer where X can be Sulphur (S), Nitrogen (N) or Oxygen (O). (b) A polaron lattice deformation is established into the conjugated backbone of heterocyclic polymer. This can be caused by p-type doping causing the loss of an electron [64].

Moreover, polaron charge transport can also be explained for crystalline semiconductors which produce polaronic mobilities of orders of magnitude higher than the disordered semiconductors. This is due to the difference in strength of electron-phonon interactions in the disordered semiconductor which changes the physical properties of a polaron [68, 69]. Inorganic crystalline semiconductors undergo weak electron-phonon coupling because of their long range crystallinity. The charge carriers are thought to interact with the lattice simply by momentum varying collisions and are thought to be almost free. This type of conduction is named Druke-like charge conduction model.

In disordered semiconductors, the extent of interactions is usually constrained by the huge amounts of structural defects. The lattice deformation, unlike in crystalline semiconductors, can therefore be compared with the inter-atomic distances. These lead to strong short range electron-lattice interactions due to the self-trapping of carriers at a single position and are explained as 'small polarons'. Yamashita and Kurosawa [65] and Holstein [66] were the first to develop the model based on small polaron transport.

Polaron movement is thought to be by a succession of random jumps between neighbouring sites. Marcus [69] defined the transition (hopping) rate, $v_{i\to j}$, for polarons in terms of E_r, the intra-molecular reorganization energy,

$$v_{i\to j} \propto \frac{1}{\sqrt{E_r T}} \exp\left[-\frac{(E_j - E_i + E_r)^2}{4E_r kT}\right]. \qquad 2.14$$

The charge mobility μ, with field F and temperature dependence T, is defined by the thermally activated hops between adjacent sites i and j [70, 71].

$$\mu = \mu_0 \exp\left[-\frac{E_r}{4kT} - \frac{(bF)^2}{4kTE_r}\right] \frac{\sinh\left({bF}/{2kT}\right)}{{bF}/{2kT}} \qquad 2.15$$

where μ_0 is slightly temperature dependent and b is the average lattice difference. Eq. (2.15) expects a thermally activated behaviour for mobility. This is in concurrence with the information that polaronic tansport occurs via thermally induced deformations of the lattice.

Su-Schrieffer-Heeger (SSH) also determined a charge transport model in terms of polarons for conjugated polymers [72]. The theory was derived from bond alteration along an ideal conjugated polymer chain with weak inter-chain coupling. The geometrical structure of the polymer was said to change immensely by the addition of a charge due to bond alteration over a certain number of monomeric units (3-5). Main concerns with using SSH model include the disregard of electron-electron and electron-hole interactions which play an important role in the transport and recombination of charge carriers.

2.5.4 Variable Range Hopping Model

For disordered materials such as conjugated polymers, the charge transport is thought to be through hopping mechanisms. Variable range hopping (VRH) is thought to occur in systems where the thermal energy, *kT*, is less than the energy variation between successive states. The concept of VRH was first introduced by Mott [55] as discussed in Section 2.5.1 in Eq. (2.8). He assumed that the probability of hopping to higher energies or over far distances was equivalent. The density of states, in this case, is expected to be spread consistently about the Fermi level.

VRH mechanism is commonly acknowledged charge transport model applied to organic systems as the energy and positional disorder of localized states in the organic material dominates the charge transport. Vissenberg and Matters defined disordered materials to have VRH in states which vary in energy exponentially [22]. VRH implies that a carrier may either hop over a small distance with high activation energy or hop over a long distance with a low activation energy. This is unlike the idea of hopping where the thermally activated tunnelling of carriers between localized states governs the charge transport instead of carrier activation to a transport level. The mobility is said to increase with carrier concentration by either field effect or doping as an introduction of acceptors in a p-type semiconductor causes a small number of unoccupied states to be filled. Increasing in doping causes more levels of unoccupied states to be filled such that hopping is easier at higher energies when an external voltage is applied and therefore mobilities are higher.

The model then assumed that the mobility in these materials can be thermally activated and depends on the gate voltage according to a power law. As the gate voltage increases, the injected charge carriers fill up the traps such that as a result, the trapping becomes less and the charge transport is seen to improve. This dependence is noticed in disordered materials and is of great importance as it is similar to the one observed from our experimental results on polycrystalline material. It is essential in the analysis of electrical characteristics of organic devices such as the OTFTs, OLEDs and Metal-Oxide-Semiconductor field effect transistors (MOSFETs).

In combination with percolation theory [58, 70] and VRH theory first suggested by Grunewald and Thomas [53], Vissenberg [22] studied the influence of temperature and the influence of the filled states on the conductivity based on the variable range hopping theory in an exponential DOS. The model was based for lower temperatures and for materials with low carrier densities. The expression for the density of states as a function of the temperature and carrier concentration is given in terms of exponential distribution in thermal equilibrium, Eq. (2.5). VRH is demonstrated in Fig.2.4 as the hopping between states.

2.5.5 Multiple Trap and Release Model

For organic materials such as the polycrystalline organic semiconductors, model based on multiple trapping and release (MTR) [71-73] with a temperature dependent transport exists [74, 75]. For this model, two separate types of conducting mediums exist; crystalline ordered grains which are separated from each other by disordered amorphous grain boundaries. The grains incorporate delocalized carriers while the grain boundaries contain carriers trapped in localized states. It assumes that delocalised transport is limited near the band gap due to the existence of a distribution of traps. The trapped carriers in the grain boundaries can be thermally activated to a transport level where charge conduction is easier. This charge transport is very similar to the one described above as hopping mechanism. For grain boundaries, the model predicts mobility dependent on temperature which decreases with the improvement in the quality of the devices. The gate bias dependence decreases with increasing quality as well confirming that the defects decrease such as seen in single crystal devices.

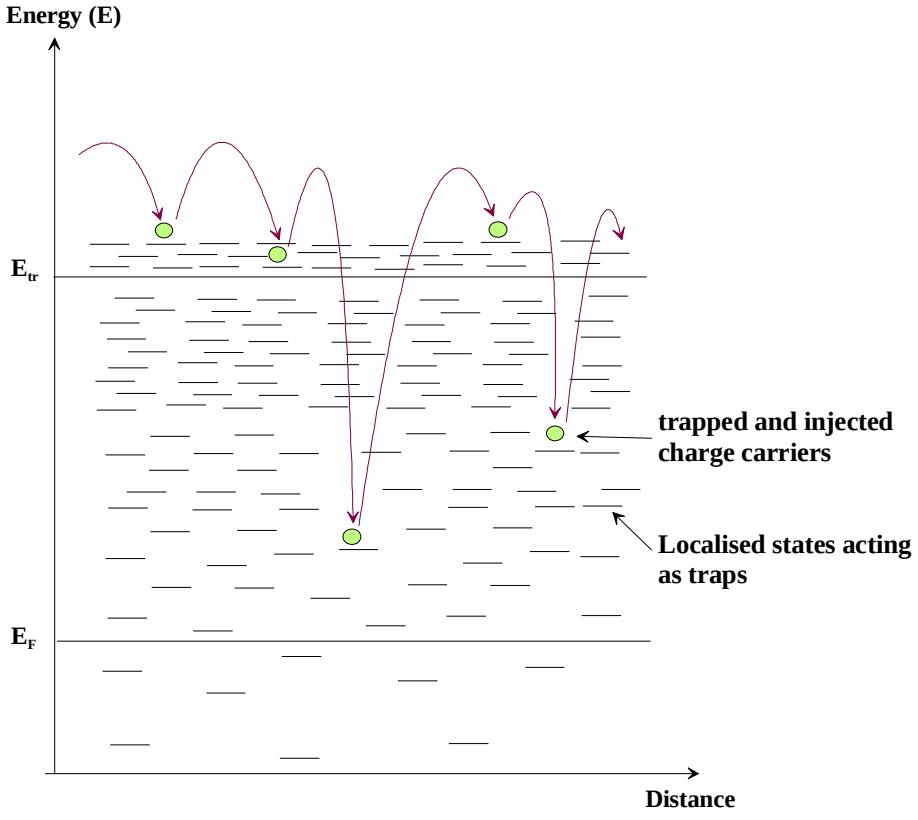

Figure 2.8. Demonstration of multiple trap and release model (MTR). The deep lying localised states briefly trap the carriers. These carriers can be thermally released to states around the transport level E_{tr}.

Horowitz et al. [74] have recently used the MTR model to establish charge transport in organic semiconductors, namely sexithiophenes and dihexylsexithiphenes, based OTFTs with an exponential distribution of gap states, initially derived from MTR model applied to an inorganic material by Le Comber and Spear [71]. The MTR model accounts for the low mobility in amorphous organic materials. Hopping of charge carriers between localised states is dominated over a critical level known as the transport energy, E_{tr} which defines the mobility edge as shown in Fig.2.8. Trapping is associated with lattice defects and impurities in which the charge carriers are immobilized and confirms a narrow band gap with high trapping. Traps can either be shallow or deep; shallow traps related with the conduction or valence bands and deep traps situated near the centre of the band gap.

The existent organic semiconductor charges or the injected charges are all trapped and then released by thermal activation process. Ignoring the diffusion processes, the drift mobility μ_D can be defined in terms of the energy of the trap states E_t, the mobility at band edge μ_0 and the ratio between the effective density of states at the transport band edge and the density of traps, α.

$$\mu_D = \mu_0 \alpha \exp\left(-\frac{E_t}{kT}\right) \qquad 2.16$$

Eq. (2.16) predicts an Arrhenius- like temperature dependence on the carrier mobility, like the VRH model. The transport of carriers is, therefore, seen to be greatly dependent on the level of energy of the trap states, the externally applied voltage and the temperature [74].

2.5.6 Charge Transport in Polycrystalline Organic Semiconductors

Charge transport in disordered materials is assumed to be due to hopping between the localised states. However, charge transport in polycrystalline organic semiconductors is significantly different due to the two distinct regions; the grains and the grain boundaries. The charge transport is dependent on the grain size but is said to be limited by the grain boundaries due the existence of trap states. The crystalline-like grains are much more conductive such that the Fermi level is able to move somewhat freely compared to the grain boundaries. The barrier, in the grain boundary, is believed to be controlled by the density of states in the disordered grain boundary irrespective of the position of the potential barrier within the material. Therefore, Fermi level pinning is expected in disordered grain boundaries. A small change in the external field at the grain boundary can cause a significant change in the energy levels in the grains. Gaussian shaped

distribution of states (DOS) is expected in organic semiconductors with disorder [76, 77]. This can be precisely approximated to an exponential function for DOS when the carrier concentrations are expected to be small in the band tail of the Gaussian distribution, Fig.2.4 [20, 78-80]. A polycrystalline semiconductor can also be expected to follow the Gaussian DOS as the grain boundaries limit the carrier flow due to discontinuities in the bonding. In this case, the equations already developed for a disorder model seem to be applicable to polycrystalline organic materials. Furthermore, the value of the Meyer Neldel Energy associated with disorder in the system is obtained in polycrystalline organic materials even though the basic concept relates only to truly disordered semiconductors [35]. As a result, the charge transport in a polycrystalline material can be approximated as of disordered nature.

The section that follows defines the Universal Mobility Law in terms of disordered organic materials to demonstrate the significance of effective mobility in polycrystalline organic semiconductors.

I. Universal Mobility Law in Disordered Organic Semiconductors and its Significance in Polycrystalline Materials.

A single mobility term can be used to describe carrier mobility in organic crystalline semiconductors. However, as disordered materials follow exponential DOS, the mobility term is not constant and described in terms of effective mobility [81].

The transport of carriers in an exponential DOS is governed by the thermally activated hopping between the states. According to Variable range hopping mechanism, the movement of carriers is dependent on the distance between the states in DOS and the energetic distribution of states. In an exponential DOS, the analytical model discussed can be developed without taking into account the precise mechanism by which the carriers move [82].

Increasing the number of states per unit area causes an immense increase in the hopping between the states hence leading to an increase in carrier density which is proportional to mobility. For disordered materials, the effective mobility and the carrier density can be written in terms the characteristic temperature of the exponential DOS, T_C where $T_C > T$ and is valid for small carrier concentrations. Brown et al. were one of the first to investigate the UML with measurements carried out on field effect transistors (FETs) doped with poly (B'-dodecyloxy- α, α', -α',

α''terthienyl) (polyDOT$_3$) [81]. The relation can also be applied on organic disordered materials such as P3HT and PTAA.

$$\mu_{eff} = \mu_0 \, n^m = K \, n^m \qquad 2.17$$

$$m = {}^{T_C}/_{T} - 1 \qquad 2.18$$

K is the mobility prefactor, μ_0 is the mobility prefactor, μ_{eff} is the effective mobility of the material, n is the carrier concentration and m is the exponent dependent on T_C and the material. The carriers in a disordered material do not possess a constant mobility as they are distributed in energy so that Mott-Gurney law for space charge limited currents does not apply (Section 3.3.2). The carriers occupy a range of energy levels and behave differently than carriers in conventional semiconductors. This means that a more generalized expression with dependence of mobility on the carrier concentration has to be considered.

The carrier concentration (taken equivalent to the dopant concentration), obtained for these materials was extracted from the reverse current characteristics using the quarter power law by applying the Mott-Schottky relationship [83]. The extracted dopant concentrations in reverse bias assume that the dopant concentration in the depletion region is uniform and that the dopant ions are stationary. The assumption of the carrier concentration equivalent to the dopant concentration is made as the electrical conductivity in the organic material is dominated by these dopant related carriers. This is except when the carrier concentration n is enhanced by field effect such that in a thin film transistor or by optical excitation. It is therefore extremely important that the existing concepts developed for inorganic disordered semiconductors are used with caution when defining conduction in organic disordered materials.

In disordered organic semiconductors, the carrier occupancy of the states is dependent on the position of the Fermi level which lies in the band tail of the Gaussian DOS. At energies below the Fermi level, the states are almost full with the location of localised states further apart from each other such that they can be considered immobile with the occupancy probability close to one (Fig.2.4). For energies above the Fermi level, the density of states is considerably more with many unoccupied states so it is easier for the charge carriers to hop around from state to state. The carriers above and below the Fermi level can thus be evaluated with relative ease. Carriers above the Fermi level being free where as the carriers below being trapped and not contributing to

current, under external bias. Below the Fermi level, the energy levels are *Donor-like* whereas the energy levels above the Fermi level are *Acceptor-like*. *Donor-like* traps are positive if unoccupied or neutral if occupied whereas *Acceptor-like* traps are either negative if occupied or neutral if unoccupied [14].

The integration from the Fermi level to infinity is chosen to include all the charge carriers contributing to current flow. The combined effect of decreasing charge occupancy and increasing energy states indicates that the charge transport is dominated by the hopping events close to the Fermi level. At the peak of the DOS, the carrier concentration is insignificant such that integrating to infinity does not add any excess charge which is not taking part in conduction. For n-type disordered semiconductors, this is given by (Appendix A)

$$n(E) = \frac{T_0 N(0)}{T_C} \exp\left(\frac{E_F}{kT_C}\right) \qquad 2.19$$

where E is the energy of the localised states, T_C is the characteristic temperature of density of states (DOS) and $N(0)$ is the number of states per unit volume at $E=0$. In this case, only hopping of carriers, observed above the Fermi level, contribute to current conduction. However, this limits the application of the model to low carrier concentrations and temperatures so that the charge transport can be dominated by the band tail of the exponential DOS.

Ignoring diffusion currents and assuming that drift currents are most dominant in disordered materials leads to

$$J_{gb} = q\mu_{eff}\left[\frac{T_0 N(0)}{T_C} \exp\left(\frac{E_F}{kT_C}\right)\right] F \qquad 2.20$$

A direct comparison to the ordered crystalline grains is made to understand μ_{eff}, the effective mobility. Comparison can be made at the edge of the grain where the disordered boundary meets the crystalline grain for which the equation was initially developed. Ignoring the band bending at the interface as well as in the absence of current flow, the flux to and fro the grain boundary and the grain must be equal in thermal equilibrium (Fig.2.9). This causes an effective transport level to be formed in the grain boundary much like the E_T level in the grain such that it appears to be a

single energy level. Existence of an effective transport level must apply for all currents including the current at zero bias. At the edge of the grain, the carrier concentration for an ordered material is given by

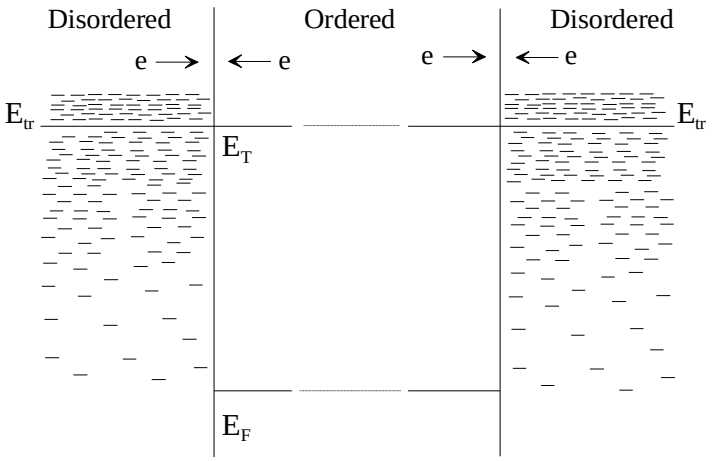

Figure 2.9 Ordered organic semiconducting material in contact with a disordered organic material to explain universal mobility law in organic polycrystalline semiconductors. The transport level in the grains E_T is assumed equivalent to the transport energy level in the grain boundaries E_{tr}.

$$n = N_T \exp\left(-\frac{E_T}{kT}\right) exp\left(\frac{E_F}{kT}\right) \qquad 2.21$$

$$\exp\left(\frac{E_F}{KT}\right) = \left(\frac{n(E)T_C}{N(0)T_0}\right)^{T_C/T} \qquad 2.22$$

where N_T is the hypothetical carrier density at the transport level at the grain edge, and E_T is the energy corresponding to the transport energy level in the grain. It should be noted that E_T in the grain and E_{tr} at the edge of the boundary are assumed to be similar. Combining Eq. (2.21) and Eq. (2.22) and assuming that the drift currents dominate gives

$$J = q\left[\mu_T N_T \exp\left(-\frac{E_T}{kT}\right)\left(\frac{T_C}{N(0)T_0}\right)^{T_C/T} n^{\left(T_C/T\right)-1}\right] n(E)F \qquad 2.23$$

The effective mobility can then be written in terms of carrier concentration as in Eq. (2.17) and refers to as the universal mobility law (UML). μ_0 is the mobility prefactor explained in terms of

$$\mu_0 = \mu_T N_T \exp\left(-\frac{E_T}{kT}\right)\left(\frac{T_C}{N(0)T_0}\right)^{T_C/T} \quad 2.24$$

The use of a single mobility prefactor for the exponential DOS in a disordered material is not typical. Although μ_0 can be defined experimentally, the physical significance of the mobility prefactor is hard to understand. A higher transport energy level means an increase in mobility value because of the increase in hopping probability. Although the interpretation of disordered organic materials in terms of standard inorganic semiconductors is unconventional, it is a useful tool to understand motion of carriers in disordered materials (Appendix B). The exponent in Eq. (2.17) is seen to be dependent on the characteristic temperature of the DOS, T_C as seen in Eq. (2.18) [84].

2.6 SUMMARY

The charge transport mechanism in organic semiconductor devices is dependent on the charge carrier mobility which is generally much lower than the inorganic semiconductors. It is thus essential to understand the charge transport mechanisms in organic semiconductors. Despite years of research, there is no absolute rationalization available to characterize conduction in one particular fashion due to the complexity and diversity of the materials and devices available. In this chapter efforts were made to introduce various charge transport mechanisms in organic semiconductors. These include the percolation model, polaron model, MTR and VRH. It is generally agreed that thermal assisted tunnelling, also known as hopping, is the basis of transport in most disordered organic semiconductors. Field and temperature dependence of the carrier mobility is explained in terms of hopping in Gaussian DOS in LEDs whereas the hopping in an exponential DOS explains the gate voltage and temperature dependence in FETs. Although this is the case, one description must be used to explain the electrical characteristics of these organic devices as the polymers described in these devices fit in with the same class of disordered π-conjugated systems.

The Gaussian function and the associated exponential approximate at low energies were used to describe the distribution of states (DOS) in disordered organic semiconductors. It is widely believed that the charge transport model in organic materials co-exist within the discrete energy states defined by the Gaussian distribution. In this thesis, we assume the distribution to follow the exponential DOS as the Fermi level lies in the band tail of the Gaussian DOS. For disordered

organic materials, it is hard to explain the mobility to be constant as the charge carriers on different energy levels in the exponential distribution experience different hopping rates. For this reason, the concept of transport energy is used to describe a position in energy over which it is easier to demonstrate mobility of carriers also known as the mobility edge. Hence effective mobility for organic disordered materials can be described using the universal mobility law in inorganic semiconductors. Moreover to understand effective mobility in polycrystalline organic semiconductors, comparison between ordered grains and disordered grain boundaries is made at the edge of the grain where the grain meets the grain boundary.

2.7 REFERENCES

[1] D. Knipp, *Introduction to organic electronics*, 2006, website: *http://www.faculty.iu-bremen.de*, viewed: 28/09/2011

[2] S. Barard, M. Heeney, L. Chen, M. Cölle, M. Shkunov, I. McCulloch, N. Stingelin, M. Philips, and T. Kreouzis, J. Appl. Phys. 105, (2009) 013701.

[3] H. Sirringhaus, Adv. Mater. 17, (2005) 2411.

[4]C. R. Newman, H. Sirringhaus, J. C. Blakesley, and R. Speller, Appl. Phys. Lett. 91, (2007) 14210.

[5] T. Yamamoto, T. Ito, and K. Kubota, Chem. Lett. 17, (1988) 153.

[6] J. Veres, S. Ogier, and G. Lloyd, Chem. Mater. 16, (2004) 4543.

[7] K. Nomoto, N. Hirai, N. Yoneya, N. Kawashima, M. Noda, M. Wada, J. Kasahara, IEEE Trans. Electron Devices 52, (2005) 1519.

[8] P. Sung Kyu, K. Chung Chen, J. E. Anthony, T. N. Jackson, Elec. Dev. Meet., IEDM Tech. Digest, IEEE Inter. (2005) 4.

[9] P. Sung Kyu, P. Sung Kyu, J. E. Anthony, and T. N. Jackson, Elec. Dev. Let., IEEE, 28, (2007) 877.

[10] H. Sirringhaus, P. J. Brown, R. H. Friend, M. M. Nielsen, K. Bechgaard, B. M. W. Langeveld-Voss, A. J. H. Spiering, A. J. Janssen, E. W. Meijer, P. Herwig, and D. M. de Leeuw, Nature, London 401, (1999) 685.

[11] D. H. Kim, Y. D. Park, Y. Jang, H. Yang, Y. H. Kim, J. I. Han, D. G. Moon, S. Park, T. Chang, M. Joo, C. Y. Ryu, K. Cho, Adv. Mater. 15, (2005) 77.

[12] A.R. Brown, D.M. de Leeuw, E.E. Havinga, A. Pomp, Syn. Metals, 68, (1994) 65.

[13] M. Raja, G. Lloyd, N. Sedghi, R. Di Lucrezia, S. J. Higgins, W. Eccleston, Mat. Res. Soc. Symp.,708, (2002) 423.

[14] S. M. Sze, *Physics of Semiconductor Devices*, Second Ed., John Wiley and Sons, New York, 1981.

[15] B. G. Streetman, S. Banerjee, *Solid state electronic devices*, Prentice Hall, fifth edition, New Jersey, 2000.

[16] B. V. Zeghbroeck, *Principles of Semiconductor Devices*, website*: http://ece-www.colorado.edu/~bart/book/*, viewed: 30/09/2011.

[17] H. Bassler, Phys. Stat. Sol. (b), 175, (1993) 15.

[18] A. Miller, E. Abrahams, Phys. Rev. 120, 3, (1960) 745.

[19] B. Hartenstein, H. Bassler, Chem. Phys., 191, (1995) 321.

[20] N. Sedghi, D. Donaghy, M. Raja, S. Badriya, S.J. Higgins, W. Eccleston, J. Non-Crys. Solids 352 (2006) 1641.

[21] N. F. Mott, E. A. Davis, *Electronic processes in non-crystalline materials*, Second Ed., Oxford University Press, London, 1979.

[22] M. C. J. M. Vissenberg, M. Matters, Phys. Rev. B, 57, (1998) 12964.

[23] D. Monroe, Phys. Rev. Lett. 54, (1985) 146.

[24] E. M. Conwell, Phys. Rev. 103, (1956) 51.

[25] W. Eccleston, *Private Communication*, 2011.

[26] R. Stockute, P. Johnson, website: *www.pj.freefaculty.org/stat/Distributions/Laplace-03.pdf*, viewed: 11/02/2011, 2006.

[27] B. Rosenberg, B. B. Bhowmik,H. C. Harder, E. Postow, J. Chem. Phys. 49 (1968) 4108.

[28] D. E. Carlson, C. R. Wronski, *Amorphous Semiconductors*, Appl. Phys. 36. Ed, M. H. Brodsky, NY, Springer, (1979) 287.

[29] T. Dosdale and R. J. Brook, Solid State Ionics, 8, (1983) 297.

[30] G. Boisvert, L.J. Lewis, A. Yelon, Phys. Rev. Lett. 75 (1995) 469.

[31] A. Yelon, B. Movaghar, Phys. Rev. Lett. 65 (1990) 618.

[32] P. Irsigler, D. Wagner, D. J. Dunstan, J.Phys. C: Solid State Phys. 16, (1983) 6605.

[33] R. J. Dewsberry, Phys.D Appl. 8, (1975) 1797.

[34] H. Overhof, P. Thomas, *Electronic Transport in Hydrogenated Amorphous Semiconductors*, Springer, Berlin, 1989.

[35] E. J. Meijer, M. Matters, P. T. Herwig, D. M. De Leeuw, T. M. Klapwijk, Appl. Phys. Lett. 76, (2000) 3433.

[36] A. Yelon, B. Movaghar, H. M. Branz, Phys. Rev. B 46, (1992) 12244.

[37] I.I. Fishchuk, A.K. Kadashchuk, J. Genoe, Mujeeb Ullah, H. Sitter, Th.B. Singh, N.S. Sariciftci, H. Bässler, Phys. Rev. B 81 (2010) 045202.

[38] P. Stallinga, *Electrical characterization of organic electronic materials and devices*, Wiley, 2009.

[39] G. G. Roberts, J. Phys. C. Solid State Phys.4, (1971) 3167.

[40] M. H. Cohen, E. N. Economou, C. M. Soukoulis, Non-Crys. Solids 66, (1984) 285.

[41] G. Kemeny, B. Rosenberg, J. Chem. Phys. 53, (1970) 3549.

[42] J. C. Dyre, J. Phys. C: Solid State Phys. (1986) 195655.

[43] N. Karl, J. Marktanner, R. Stehle, W. Warta, Synth. Metal. 42, (1991) 2473.

[44] E. A. Silinsh, V. Capek, *Organic molecular crystals: interactions, localization and transport phenomenon*, AIP Press, New York, 1994.

[45] V. M. Kenkre, J. D. Andersen, D. H. Dunlap, C. B. Duke, Phys. Rev. Lett. 62, (1989) 1165.

[46] J. L Bredas, D. Beljonne, J. Cornil, J. P. Calbert, Z. Shuai, R. Silbey, Synth. Metal. 125, (2002) 107.

[47] R. C. Haddon, X. Chi, M. E. Itkis, J. E. Anthony, D. L. Eaton, T. Siegrist, C. C. Mattheus, T. T. M. Palstra, J. Phys. Chem. B 106, (2002) 8288.

[48] Y. C. Cheng, R. J. Silbey, D. A. Da Silva, J. P. Calbert, J. Cornil, J. L. Brdas, J. Chem, Phys. 118, (2003) 3764.

[49] L. Giuggioli, J. D. Andersen, V. M. Kenkre, Phys. Rev. B. 67, (2003) 045110.

[50] M. Pope, C. E. Swenberg, *Electronic processes in organic crystals and polymers*. UK, Oxford University Press, 1999.

[51] S. D. Baranovskii, P. Thoms, G. J. Adriaenssens, J. Non-Cryst. Solids, 190, 3, (1995) 283.

[52] B. I. Shklovskii, A. L. Efros, *Electronic Properties of Doped Semiconductors*, Springer, New York, 1984.

[53] M. Grunewald, P. Thomas, Phys. Stat. Solidi B 94, (1979) 125.

[54] S. Baranovskii, I. Zvyagin, H. Cordes, S. Yamasaki, and P. Thomas, Phys. Status Solidi B 230, (2002) 281.

[55] N. F. Mott, Can. J. Phys. 34, (1956) 1356.

[56] D. Pines, Can. J. Phys. 34, (1956) 1367.

[57] O. Bleibaum, H. Bottger, V.V. Bryksin, Phys. Rev. B 66, (2002) 104203.

[58] V. Ambegaokar, B. I. Halperlin, J. S. Langer, Phys. Rev. B, 4, 8, (1971) 2612.

[59] B. N. Limketkai, P. Jadhav, M. A. Baldo, Phys. Rev. B 75 (2007) 113203.

[60] G. Meller, T. Grasser, *Organic Electronics*, Springer, 2010.

[61] M. C. J. M. Vissenberg, *Opto -Electronic properties of disordered organic semiconductors*, University of Leiden, The Netherlands, 1999.

[62] G. E. Pike, C. H. Seager, Phys. Rev. B 10, (1974) 1421.

[63] N. F. Mott, E. A. Davis, *Electronics processes in noncrystalline materials*. UK, Clarendon, 1971.

[64] N. K. Guimard**,** N. Gomez**,** C. E. Schmidt, Prog. Polym. Sci. 32, (2007) 876

[65] J. Yamashita, T. Kurosawa, J. Phys. Chem. Solids 5, (1958) 34.

[66] T. Holstein, Ann. Phys 8, (1959) 325.

[67] K. Fesser, A. R. Bishop, D. K. Campbell, Phys. Rev. B 27, (1983) 4804.

[68] D. Emin, Phys. Rev. B 48, (1993) 13691.

[69] T. Holstein, Ann. Phys. 281, (2000) 706.

[70] B. I. Shlovskii, A. L. Efros, *Electronic Properties of Doped Semiconductors*, Springer, Heidelberg, (1984).

[71] P. G Le Comber, W. E. Spear, Phys. Rev. Lett. 25, (1970) 509.

[72] G. Horowitz, M. E. Hajlaoui, and R. Hajlaoui, J. Appl. Phys. 87, (2000) 4456.

[73] V. Podzorov, E. Menard, A. Borissov, V. Kiryukhin, J. A. Rogers, and M.E. Gershenson, Phys. Rev. Lett. 93, (2004) 086602.

[74] G. Horowitz, R. Hajlaoui, and P. Delannoy, J. Phys. III, 5, (1995) 355.

[75] J. Noolandi, Phys. Rev. B, 16, 10 (1977) 4466.

[76] V. I. Arkhipov, P Heremans, E. V. Emelianova, G. J. Adriaenssens, H. Bassler, J. Phys.: Condens. Matter 14 (2002) 9899.

[77] W. L. Kalb, S. Haas, C. Krellner, T. Mathis, B. Batlogg, Phys. Rev. B 81 (2010) 155315.

[78] M. Matters, D. M. de Leeuw, M. J. C. M. Vissenberg, C. M. Hart, P. T. Herwig, T. Geuns, C. M. J. Mutsaers, C. J. Drurt, Opt. Mater. 12 (1999) 189.

[79] T. Okachi, T. Nagase, T. Kobayashi, H. Naito, Apply. Phys. Lett. 94 (2009) 043301.

[80] P. Stagllinga, H. L Gomes, F. Biscarini, M. Murgia, D. M. De Leeuw, J. Appl. Phys. 96 (2004) 9.

[81] A. R. Brown, C. P. Jarrett, D. M. De Leeuw, M. Matters, synth. Met. 88, (1997) 37.

[82] M. Mahadhavan, PhD Thesis, University of Liverpool, 2008.

[83] Chih-Tang Sah, *Fundamentals of Solid State Electronics*, World Scientific, 2006.

[84] Y. Roichman, Y. Preezant, N. Tessler, Phys. Stat. Solidi A, 201, (2004) 1246.

CHAPTER 3- ANALYSIS OF POLYCRYSTALLINE ORGANIC SCHOTTKY DIODES

Electrical characteristics of polycrystalline organic semiconductor, 6, 13-triisopropylsilyethynyl pentacene (TIPS-pentacene) are interpreted. Different blends of TIPS-pentacene with an organic binder are also analysed. The effects of changing fabrication conditions are discussed. Furthermore, the effect of temperature variance on the electrical characteristics is examined for two blends of TIPS-pentacene. Capacitance-Voltage measurements on Schottky diodes are conducted to obtain the dopant concentration and built-in potential.

3.1 INTRODUCTION

Organic Schottky barrier diodes have been under scrutiny for decades with initial experiments producing poor performance and irreproducible results mainly due to the poor conducting organic semiconductors available at the time [1]. The introduction of solution processable organic materials brought advancement in organic electronics [2- 5]. This was not simply due to the betterment in performance but also ease of deposition techniques and consequently low cost processes. Organic Schottky diodes are important in understanding the fundamental characteristics of the material bulk. Schottky diodes are fast switching devices which can be used in rectifying circuits such as in RFID tags [6]. In RFID tags, the diodes are required to rectify fast ac signals from the RFID reader to dc signals for the tag chip to interpret.

Organic Schottky diodes consist of an ohmic contact which is used as a reference and a Schottky contact which makes a rectifying contact with the organic semiconductor. Through the ohmic contact, large voltages may be applied thereby allowing free flow of carriers into the semiconducting material. This consequently allows the study of a much wider distribution of carriers within the semiconductor, unlike in MOS capacitors and OTFTs. For these devices only a small voltage is used to vary the carriers on the surface whilst majority of the voltage is across the oxide layer.

The study of contact resistance in organic is of significant importance due to the barrier formation at ohmic-semiconductor interfaces in real devices. The use of techniques such as the Ultra-Violet photoelectron spectroscopy (UPS) and inverse UPS have been utilized for the accurate determination of energy levels in both metals and semiconductors in order to determine the range of the potential barriers [7]. Various chemical treatments have been reported to reduce such potential barriers and thus improve the ohmic conduction causing low resistance to carrier flow [8] and consequently equal access to electrons and holes. On the other end, a rectifying contact forms a large potential barrier at the metal/semiconductor interface due to mismatch in work functions. Application of an external voltage modifies this potential barrier depending on its polarity.

The main focus of this chapter is the fabrication and electrical characteristics of the Schottky diode based on small molecule polycrystalline organic semiconductor, 6, 13-triisopropylsilyethynyl pentacene (TIPS-pentacene). The chapter proceeds from the fundamental

theory of Schottky diodes for inorganic semiconductor to application of the theory to organic diodes. The theory is modified with respect to changes in semiconducting materials. The chapter deals with TIPS-pentacene comprising of ordered grains and disordered grain boundaries which is further elaborated in detail in the following chapters. Different blends of TIPS-pentacene with an organic binder are analysed. The effects of using organic insulating and semiconducting binders are discussed. Two types of ohmic contacts are also discussed and consequently surface treatments for the ohmic contact are investigated.

From the electrical characteristics, forward saturation characteristics are interpreted in terms of space charge limited currents (SCLC). SCLC is associated with low dopant density and very low carrier mobility in disordered type structures. In the chapter, a modified SCLC for organic material including a dependence of material thickness and power of voltage is discussed. The main difference between SCLC equation derived for conventional semiconductors and organics is the dependence of the material thickness and applied voltage on temperature. The effects of temperature variance on the electrical characteristics are also discussed for two different blends of TIPS-pentacene and consequently the activation energy for both is found. Small signal measurements are also conducted to determine the dopant/carrier concentrations and compared to those extracted from DC measurements.

3.2 FUNDAMENTAL THEORY OF SCHOTTKY DIODES

Over nine hundred articles are listed under metal- semiconductor literature [9] highlighting the extensive research and development work carried on Schottky diodes over the past decades [10-12].

3.2.1 Contact Barrier Height in Ordered Inorganic Semiconductors

Figure 3.1 shows the band profiles of a metal and semiconductor under thermal equilibrium. The work function qϕ_m is the energy required to take an electron out to the vacuum state. When an n-type semiconductor is in contact with the metal, assuming $\phi_m > \phi_{sc}$, a rectifying contact is formed. When in contact, the Fermi level lines up and remains flat once thermal equilibrium is reached. Although this is said for ideal cases, a small difference in energy levels causes a potential drop when in thermal equilibrium [13]. As the Fermi level remains flat, the electrons from the semiconductor flow to the metal. A deficiency of electrons in the semiconductor introduces

positive charged centres and causes edge of the valence and conduction bands to bend downwards at the interface.

The height of the barrier produced at the semiconductor metal interface is the difference between the semiconductor conduction band and the metal Fermi level and expressed as [13]

$$q\phi_m - q\phi_{sc} + (E_C - E_F) = q\phi_m - q\chi_s \qquad 3.1$$

where $q\phi_{sc}$ is the semiconductor work function and $q\chi_s$ is the electron affinity (the least amount of energy required to free an electron from the conduction band of a semiconductor).

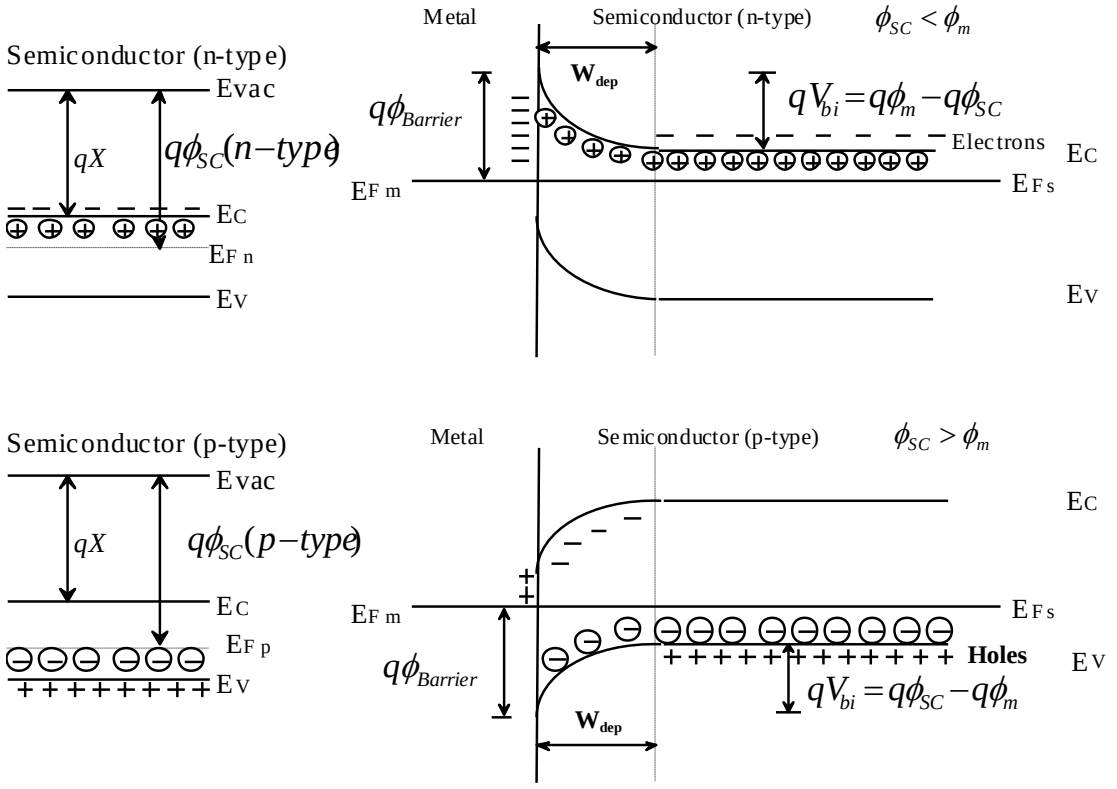

Figure 3.1. The band profile for both an n-type and a p-type semiconductor in equilibrium with the metal. Fermi level is flat in absence of current flow.

The electrons travelling from the semiconductor to metal see a barrier. This barrier in terms of potential is given by qV_{bi} known as the built in potential.

$$qV_{bi} = q\phi_m - q\phi_{sc} \qquad 3.2$$

For a p-type semiconductor in contact with a metal with $\phi_{sc} > \phi_m$, the electron travel from the metal to the semiconductor causing a build up of negative charge on the semiconductor side. The band bends upwards such that the electrons entering the p-type semiconductor face a barrier at the interface which needs to be overcome for electron transport, Fig.3.1. The semiconductor side of the contact contains the space charge region with depletion layer thickness depending on the concentration of the ionized acceptor atoms.

For non ideal surfaces, a model with interface states is considered. Interfacial states are formed from the presence of chemical defects, broken bonds, oxide formation and impure semiconductors at the metal semiconductor interface. Electronic levels are formed in the interfacial bandgap. A neutral level, n_0, at mid bandgap defines the centre below which any electronic level distribution is neutral if filled. Above n_0, any electronic level distribution is neutral if empty.

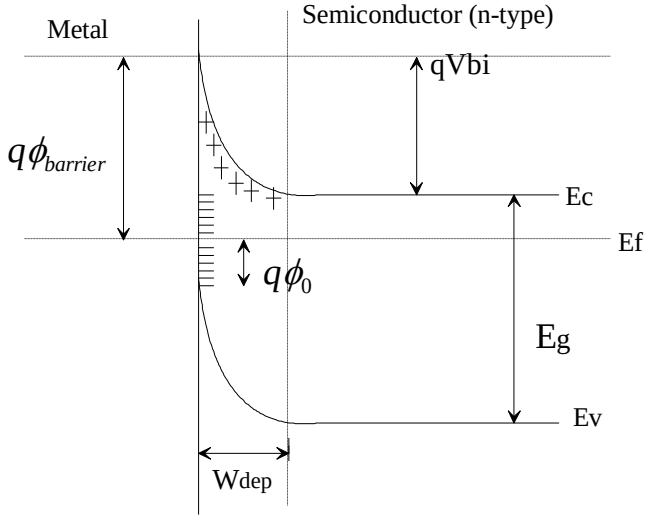

Figure 3.2. Fermi level pinning at the Fermi level due to interface states in an n-type semiconductor. E_g is the energy difference between the conduction and valence band, ϕ_0 is the potential due to trapping and $\phi_{barrier}$ is the potential related to the barrier.

The Fermi level is said to be pinned if the density of the interface states near the neutral level is assumed to be very large. In this case, any addition or reduction of electrons from the semiconductor would have no effect on the shape of the Fermi level E_F [13] (Fig.3.2).

$$q\phi_{Barrier} = \frac{1}{2}E_g - q\phi_0 \qquad 3.3$$

where E_g is the energy difference between the conduction and valence bands.

Fermi level is independent of the metal used and hence the barrier height is independent of the change in external applied voltage. The barrier height strictly depends on the interface properties of the metal and semiconductor. Reduction in the barrier height for electron flow is dependent on the image force in real devices and is discussed below. However, the built in potential is able to fluctuate depending on the magnitude and polarity of the external applied voltage.

3.2.2 Schottky Effect

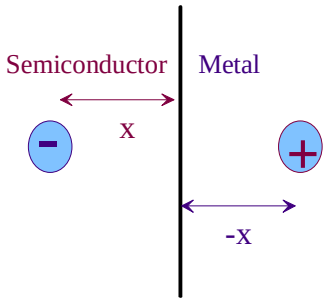

Figure 3.3.Image charge present in the metal due to an equal opposite charge in the semiconductor.

Schottky effect is defined as the lowering of potential energy with the application of an electric field because of the induction of image-force so that the charge carriers can be discharged [13]. The barrier height seen by the charge carriers at the metal semiconductor interface is dependent on the electric field in the depletion region and the image force lowering effect. Image Force lowering in due to a positive charge induced in the metal to compensate for a negative charge (electron) existing in an n-type semiconductor (Fig.3.3). The force of attraction between the electron and induced positive charge is equivalent to the force that would exist between an

electron and any positive charge. The distance of both of these charges from the interface is said to be equal. Hence image charge can be said to be equal and opposite.

This image charge exerts a force on the barrier causing it to decrease in height. Image Force, ψ, can be written as:

$$\psi = -\frac{q^2}{4\pi\varepsilon_0\varepsilon_\infty(2x)^2} = -\frac{q^2}{16\pi\varepsilon_0\varepsilon_\infty x^2} \quad 3.4$$

$\varepsilon_0, \varepsilon_\infty$ is the permittivity of free space and high frequency permittivity of the semiconductor respectively, and x is the distance from the interface.

The work done by an electron in the course of its transfer from infinity to a point x gives the potential energy.

$$E(x) = \int_\infty^x \psi\,(x)\,dx = \frac{q^2}{16\pi\varepsilon_0\varepsilon_\infty}\int_\infty^x \frac{1}{x^2}\,dx \quad 3.5$$

$$E(x) = \frac{q^2}{16\pi\varepsilon_0\varepsilon_\infty x} \quad 3.6$$

The potential energy equation obtained shows us that the potential energy decreases with increasing distance such that it is negligible as x goes to infinity.

Barrier height lowering due to external field can be written in terms of potential energy as

$$E(x) = q\int F(x)\,dx = qFx \quad 3.7$$

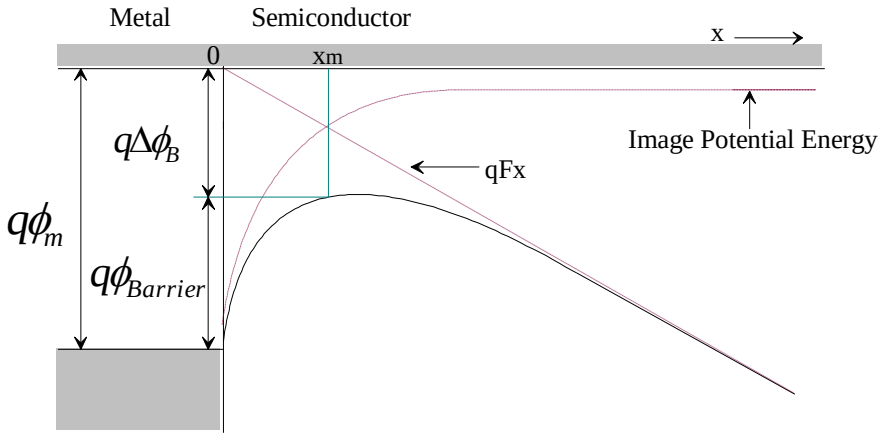

Figure 3.4.Energy band diagram of metal in contact with a semiconductor with image force and an external field causing the barrier lowering.

where *F(x)* is the applied field. Applying an external force causes the potential energy of the charge carrier to increase linearly with distance.

The total energy w.r.t x is given by

$$E_{total}(x) = \frac{q^2}{16\pi\varepsilon_0\varepsilon_\infty x} + qFx \qquad 3.8$$

When the potential energy due to image force is equal and opposite of that of the applied field,

$$\frac{q^2}{16\pi\varepsilon_0\varepsilon_\infty x} = qFx \qquad 3.9$$

$$x_m = \left(\frac{q}{16\pi\varepsilon_0\varepsilon_\infty F}\right)^{1/2} \qquad 3.10$$

where x_m is the maximum distance from the interface. Therefore, the barrier height (Fig. 3.4) can be written as

$$\Delta\emptyset_B = \frac{q}{16\pi\varepsilon_0\varepsilon_\infty x_m} + Fx_m = 2Fx_m \qquad 3.11$$

The image force lowering is dependent on the field produced by the electron. If there is no movement of electron, there is no image force and hence the barrier height does not change. Assuming that the field due to image force lowering is equal to the external field applied.

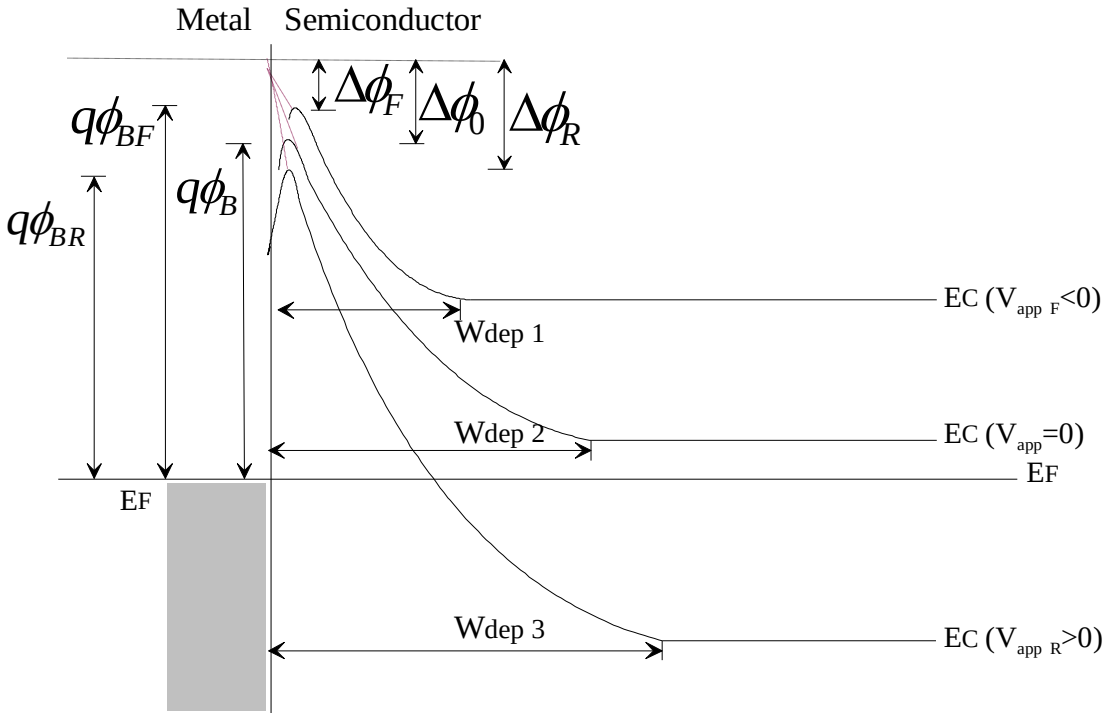

Figure 3.5. Energy band diagram of a metal in contact with an n type semiconductor under different bias condition. $\emptyset_R$, $\emptyset_F$ and $\emptyset_0$ are the barrier height lowering in reverse, forward and equilibrium respectively. Voltage (V_{app}) in this case is applied to the Ohmic contact.

$$\Delta\emptyset_B = \left(\frac{qF}{4\pi\varepsilon_0\varepsilon_\infty}\right)^{1/2} \qquad 3.12$$

Taking Schottky Effect into consideration for an n-type semiconductor in contact with metal under different bias conditions as in Fig.3.5, the depletion region width $x = W_{dep}$ and the built in potential varies. Forward bias causes the depletion region width to contract causing the built in

potential to decrease with the peak of the barrier moving away from the metal semiconductor interface. Applying a reverse bias causes an opposite effect. It widens the depletion region and causes the built in potential to current flow to increase whereas the barrier peak moves slightly closer to the interface. Energy diagram of a metal with an n-type semiconductor at different bias conditions is given in Fig.3.5 [13] for a single energy level. W_{dep1}, W_{dep2} and W_{dep3} are the space charge region widths for different biasing conditions in forward bias, equilibrium and reverse bias respectively.

3.3 TIPS-PENTACENE BASED SCHOTTKY DIODES

3.3.1 Fabrication of TIPS-Pentacene Schottky Diodes

The cross-section of the TIPS-pentacene based Schottky diode is shown in Fig.3.6. A number of samples were produced with different fabrication steps. The process commenced with the deposition of an ohmic electrode, either gold or copper, with a typical thickness of 50 nm. The contact, in some samples, was then pre-treated with pentafluorobenzenethiol (PFBT) prior to drop casting the TIPS-pentacene from solution.

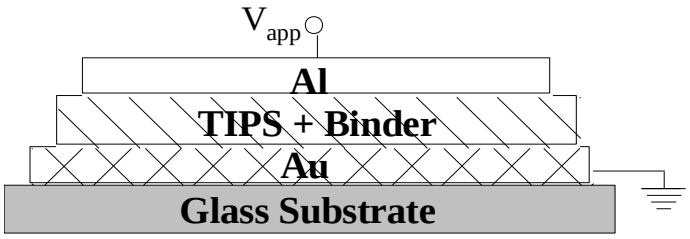

Figure 3.6. Structure of a two-terminal vertical organic Schottky diode. The blocking contact consists of aluminium and gold acts as the reference ohmic contact. Controlled amounts of TIPS: Binder was mixed in solution and drop cast onto the substrate. Typical film thicknesses were about 10 μm with visibly large grain size. The morphology was greatly dependent on the fabrication techniques involved.

PFBT is said to form a self-assembled monolayer on the gold contact which enhances the ohmic behaviour with the semiconductor. The PFBT layer acts as an electron acceptor [14] and increases the metal work function by almost 1eV thus reducing the potential barrier seen by the majority carriers (holes). The gold coated glass samples were immersed in the PFBT solution for about 10 minutes then the residue was rinsed off using propanol for further 10-15 minutes. As the PFBT

layer did not seem to improve the ohmic behaviour in our samples, the step was ignored in latter fabrications of organic Schottky diodes.

After the chemical treatment, the gold surface was treated under oxygen plasma so as to enhance the adhesion with the organic material upon drop casting. The samples were placed in a chamber consisting of oxygen plasma for approximately 5 minutes. This treatment was also carried out on the glass substrate prior to the gold evaporation so as to roughen the surface and thus improve the adhesion of gold to the glass.

Next step included the deposition of the semiconductor. At the interface between the ohmic gold contact and the organic material, width of the depletion layer formed due to work function difference can be written as

$$W_{ohmic\_d} = \left[\frac{2\varepsilon_0\varepsilon_S V_{bi}}{qN_D}\right]^{1/2} \qquad 3.13$$

where V_{bi} is the built-in potential, ε_0 is the permittivity of free space, ε_S is the semiconductor dielectric constant, q is the charge and $N_D \sim N_a$ is the dopant (or acceptor ion) concentration. If the semiconductor is heavily doped, the depletion width can be made extremely narrow such that electrons can tunnel through to the metal side even with a potential barrier. The quality of an ohmic contact, determined by the contact resistance R_C, is dependent on built-in potential and field and can be reduced by increasing the dopant levels or using a low barrier height. A buffer layer placed at gold/organic semiconductor is likely to reduce contact resistance and other unwanted effects [15].

Major injection of charges is through the gold layer where there is thought to be no energy barrier between the gold and TIPS-pentacene. However, this is contradicted [16, 17] with the existence of energy barrier of the order of 0.5-1eV between pentacene and gold due to the formation of interfacial dipoles [18] causing charge transfer, screening or hybridization effects [16, 17].

The inclusion of an organic insulating binder in a solution blend of organic semiconductor is said to improve the stability and integrity in the devices [19]. They are also seen to improve the morphology of the film. The charge mobility values are thought to decrease as the binder essentially dilutes the material as well as disrupts the molecular order. However, binders are

chosen for their low permittivity dielectric constants which limit the decline in mobility occurring due to dipole disorder [19-21]. Polymer binders such as Poly-alpha methylstyrene (PAMS, mass 1.2k), Polystyrene (PS, mass 350k) can dissolve in organic solvents such as Toluene and Xylene [22] with TIPS-pentacene to form a solution demonstrating strong molecular ordering and stability [19]. Amorphous polytriarylamine (PTAA) is also used as an organic binder to provide a good compromise between satisfactory morphology and acceptable mobility.

Table 3.1. (a) A list of steps involved in producing an organic Schottky diode, and (b) A list of the number of samples fabricated and analysed in this chapter.

Fabrication Steps	
Substrate	Glass Flexible Substrate
Treatment	Oxygen Plasma
Ohmic Contact	Gold Copper
Treatment	PFBT Oxygen Plasma
Active Layer	TIPS-pentacene
Binder	Poly-alpha methylstyrene (PAMS) Polystyrene (PS) Polytriarylamine (PTAA)
Schottky Contact	Aluminium

(a)

Sample No.	**Ohmic Contact**	**Blend**	**Schottky Contact**
1	Copper	TIPS/PAMS	Aluminium
2	Copper	TIPS/PS	Aluminium
3	Gold	TIPS/PAMS	Aluminium
4	Gold	TIPS/PS	Aluminium
5	Gold	TIPS/PTAA	Aluminium
6	Gold	TIPS/PAMS/0.3% DDQ	Aluminium
7	Gold	TIPS/PAMS/0.5% DDQ	Aluminium
8	Gold	TIPS/PAMS + DDQ	Aluminium

(b)

For the purpose of the experiment, either a readymade TIPS/binder solution was used or a solution was prepared by dissolving TIPS and binder in the ratio of 1:1 in 1ml of toluene or xylene. The binder used was essentially either PAMS or PS in order of increasing molecular weight. PTAA was also used as a binder in an attempt to enhance the crystalline morphology of

the film formed in 1:1 ratio. Toluene, with a boiling point of 111°C, was used in most of the conducted experiments unless stated otherwise.

After drop casting, the TIPS/binder solution was dried by heating the sample on a hot plate. The temperature was set such that the drying took place at an optimum speed reducing the chances of the solution getting too concentrated, too quickly. The drop cast samples were covered with a container while on the hot plate so that the polymer could stay in the atmosphere and dry in a solvent rich environment. Furthermore, the semiconductor layer was allowed to dry in a box at room temperature, preferably overnight. Although the samples took longer to dry, the film morphology demonstrated visual evidence of polycrystalline grain structure with tall, long, thin grains especially for TIPS with PAMS. Conversely, ripples were observed on the semiconductor surface if the temperature chosen was too high. They were also noticed whilst the gold samples were heated on a hot plate at high temperatures and a readymade TIPS in Toluene solution was drop cast onto them. The film morphology, in these cases, was more amorphous-like with smaller grain size compared to the former method.

Although the deposition of the active layer by drop casting gives reasonably continuous films, they are less uniform than spin coating. However as increasing thickness of the active layer (~10μm for drop cast films) in the diode produces better results and eliminates the possibility of short circuiting during measurements, the former deposition method is adopted. Drop cast films seem to show molecular terracing, large grains and the best ordering when compared to equally thick spun films [23]. The improved molecular ordering and device performance can be related to the speed at which the films are formed and varies widely for different boiling point organic solvents [24, 25]. Growth of highly ordered films is obtained when a high boiling point solvent is evaporated slowly at a low formation speed [24]. Optimum results were obtained when the drop cast film was dried at a temperature of about 60°C in a solvent-rich environment and left to dry overnight in ambient air for the film to dry completely. The difference in morphology seen in both cases may be due to the function of the solvent, solution concentration, film formation, speed, drying temperature and other reasons during fabrication.

As stated by M H. Choi et al. [26], a thicker active layer has a self-passivation effect by intrinsic organic semiconductor even when the surface is affected by moisture or oxygen. Protection against oxygen and moisture is of necessity for an extended life of the organic semiconductor devices [27]. The use of non-aromatic solvents with TIPS-pentacene causes the solvent molecules

to solvate non-conjugated segments of the semiconductor which leads to films with lower electrical conduction abilities [26, 28] and hence lower device performance even with superior uniformity.

The next step of the fabrication process involved the shadow mask evaporation of the Schottky metal, Aluminium of approximate thickness of 200nm. Two kinds of diodes were obtained; the circular diodes with a diameter of either 1mm or 2mm and square diodes of 2mm width.

Finally, all the dc characteristics of the Schottky diodes were performed in air on Hewlett Packard 4145B semiconductor parameter analyser taking 50mV voltage steps. New trapping sites for carriers are created in ambient air by the absorption of water in the organic semiconductor, decreasing the electrical conduction properties of the device whereas doping due to oxygen is more prominent in dry air [29].

3.3.2 Electrical Characteristics of TIPS-Pentacene Schottky

Polycrystalline semiconductors are thought to consist of highly conductive ordered regions known as grains (G) and disordered regions known as grain boundaries (GB). The charge transport depends immensely on the size of the grains [30-33], however it is also limited by the grain boundaries due to the presence of traps, which results in the pinning of the Fermi level E_F. Consequently, the ingrain mobility of a TIPS based device is found to be 5-6 orders of magnitude higher than in the grain boundary [15].

In our polycrystalline Schottky diode model as represented by a 2D schematic and corresponding energy diagrams in Fig.3.7, we assume the grain boundaries to be much smaller in size compared to the grains, such that any potential drop across the boundaries are negligible. The flux in the boundaries is restricted by a potential barrier however the electron concentration (assuming an *n*-type semiconductor) at the grain centre still resembles that of an organic semiconductor. Also if a constant flux is assumed, then the gradient of E_F depends on the carrier concentration, and any change in the gradient contributes to a change in barrier height $q\emptyset_S$, seen by the carriers at the edge of the grains.

Upon application of an external field, the potential at the grain boundary varies which in turn changes the effective barrier seen by the carriers involved in the current flow at the grain edge. Although the barrier seen by the carriers is changed by the external field, it is essentially

controlled by the density of states (DOS) in the grain boundary. The variation of such DOS with energy is commonly defined by a Gaussian distribution [34, 35], which may be approximated to an exponential function [36-39] at low energies, as assumed in our analysis. Such a distribution of states is associated with a characteristic temperature T_C which is related to the width of the Gaussian distribution of density of localised states due to disorder and the slope of the exponential approximate. It also defines the so-called Meyer-Neldel Energy (MNE) given as

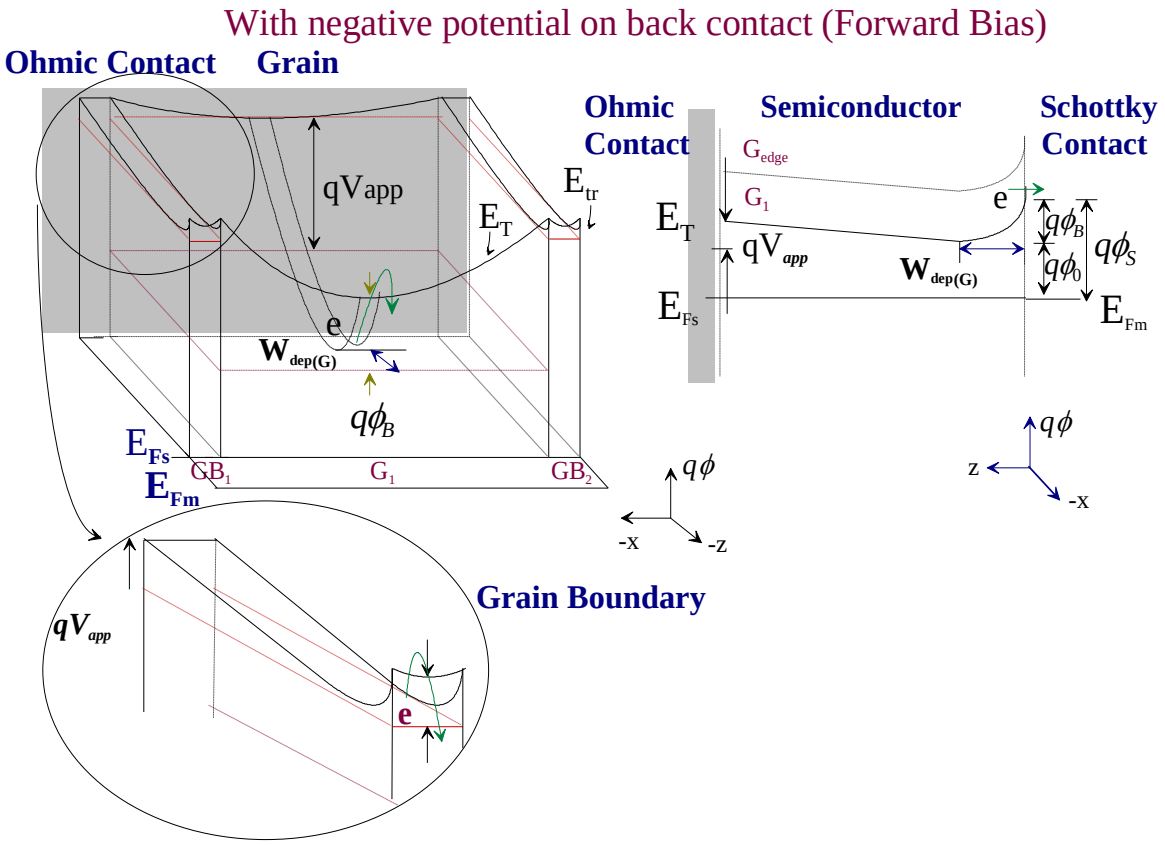

Figure 3.7. A proposed 2-Dimensional model of a polycrystalline n-type semiconductor with a single grain (G) enclosed between two grain boundaries (GB). The grain boundaries are elaborated for the ease of understanding. Ohmic metal is connected at the back while the front makes a Schottky contact with the Schottky metal. Application of external voltage V_{app} at the ohmic contact causes a rise or decline in the transport energy E_{tr} and E_T level in the grain boundary and grain respectively. $q\emptyset_S$ is the surface energy w.r.t the Fermi Level, E_F. The rest of the parameters shown in the model will be discussed in Chapter 4.

$$MNE = \frac{kT_C}{q}, \qquad 3.14$$

which is an essential parameter of merit for most disordered organic semiconductors of value 35meV [37, 38]. The corresponding value of T_C is approximately 400K. Since the energy barrier at the grain boundary is a function of the charge distribution at such boundaries, many factors such as gate bias, dangling-bond density, grain sizes, disorientation angle, and temperature play important roles [41, 42].

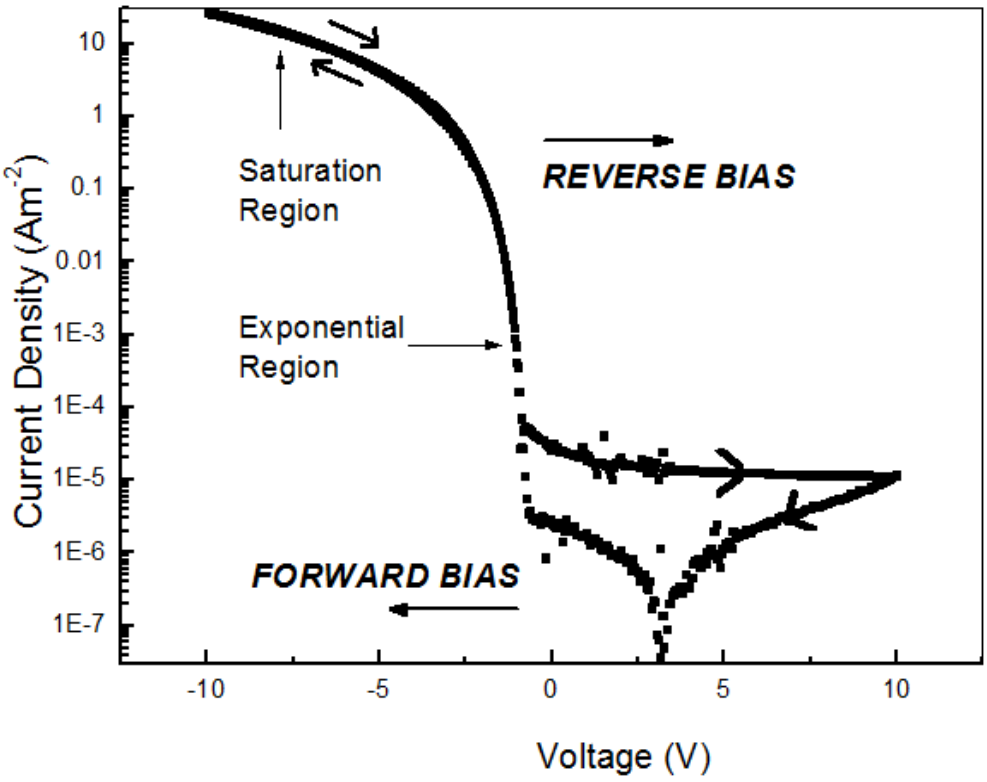

Figure 3.8. The best obtained current density against voltage plot of an organic Schottky diode with TIPS/PAMS as the active layer (Table 3.1(b)). Gold is used as the ohmic contact, aluminium is used as the Schottky contact and the device area is $7.85 \times 10^{-7} m^2$. The terms saturation region and exponential region are marked on the plot. The arrows on the characteristics define the direction of the applied voltage.

Figure 3.8 shows a general semi-log of the current density against voltage (J-V) plot illustrating the forward and reverse bias currents for a TIPS-pentacene based Schottky diode. Under the forward bias the current increases as the barrier is reduced and subsequently increases the carrier

concentration. In this case, two regions can be identified and categorised here as the exponential and saturation regions. Saturation region is essentially due to the slowing down of current due to bulk effects. Under the reverse bias, the drop in clockwise direction is due to the trapping effects constituent of organic materials. In the reverse characteristics, the current is low due to the expansion of the depletion region and are simply used to obtain the dopant concentration. The forward characteristics, however, are discussed in detail in the next section.

I. Forward Bias

A. Exponential Region

Application of an external forward bias raises the barrier and all the energy levels in the neutral semiconductor. The E_F and transport level, E_T in the grain, rises resulting in an increase in carriers entering the neutral region with sufficient energy to cross over the Schottky barrier (Fig.3.9c). The carrier concentration overcoming such a barrier increases exponentially with the increase in applied voltage as given by Eq. (3.15) [39] (Appendix A).

A flat quasi Fermi level E_F is used to determine the carrier density at the peak of the barrier and is similar to assuming that the carriers reach their steady state Maxwell-Boltzmann Distribution.

$$p = N'(0)kT_0\, exp\left(-\frac{E_F}{kT_C}\right) \qquad 3.15$$

where p is the hole concentration, $N'(0)$ is the rate of change of energetic distribution of carriers at reference energy $E = 0$, E_F is the Fermi level energy, k is the Boltzmann's constant and T_C is the characteristic temperature. Eq. (3.15) is obtained by integrating the product of the DOS and Maxwell-Boltzmann statistics, both of which are given by exponential functions. In the forward direction, the exponential rise in the current obtained at low voltages from the current voltage characteristics is associated with the exponential fall in the carrier occupancy with energy as dictated by the Maxwell Boltzmann approximation of the Fermi Dirac statistics in the tail of the Fermi Dirac distribution.

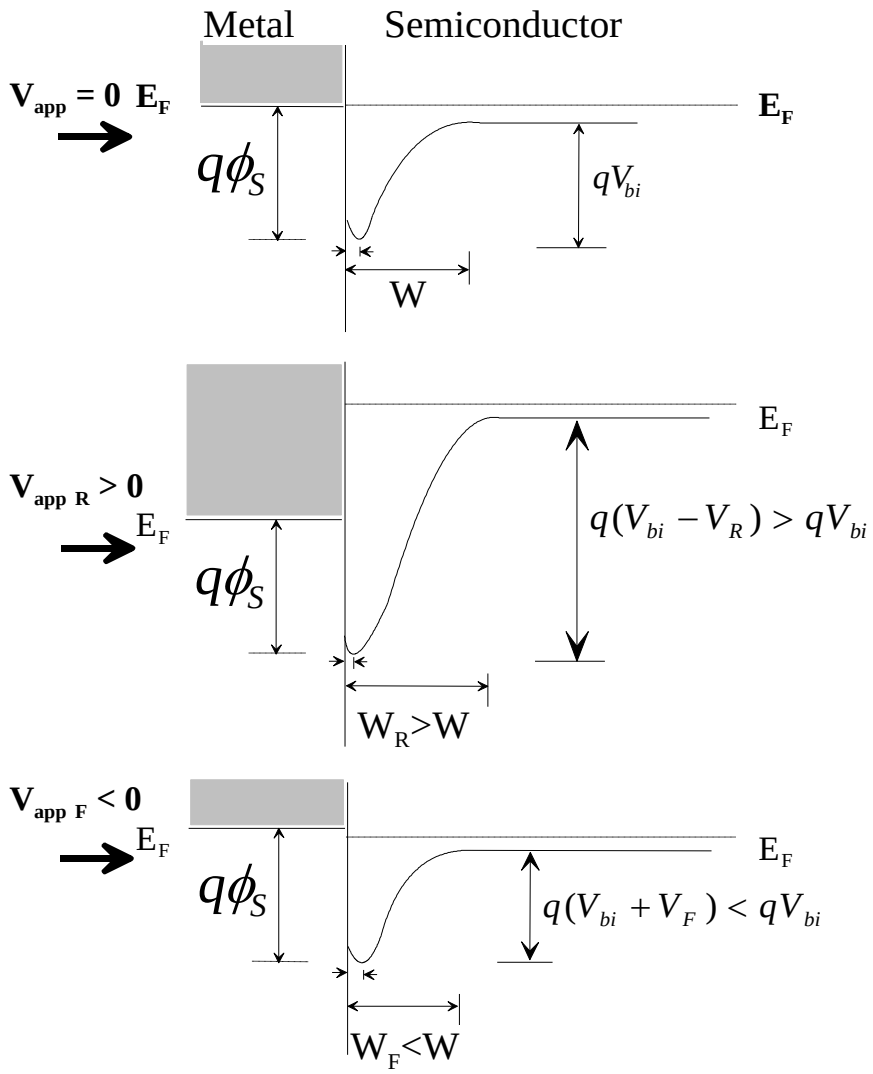

Figure 3.9. Band diagram of a p-type Schottky diode with application of an external bias. (a) at zero bias, $V_{app} = 0$, (b) in reverse bias, $V_{app\ R} > 0$ and (c) in forward bias, $V_{app\ F} < 0$.

Variable range hopping is expected in the disordered grain boundaries. In a semiconductor two distinct charge transport mechanism appear; drift and diffusion. Diffusion is due to the existence of concentration gradient whereas drift is due to the application of an external field. The Fermi level is assumed flat across the thickness of the semiconductor in thermal equilibrium and diffusion currents are expected to be very low compared to the drift currents. This allows the diffusion currents to be ignored. Assumption of only drift currents driving carriers in the exponential region of the J-V characteristics gives current density. The total carrier concentration

contributing to current flow in the forward direction of the Schottky diode has an exponential dependency with energy as in Eq. (3.15). The current density J_F of the Schottky diode under forward bias is thus given as,

$$J_F \propto \exp\left(\frac{qV_{app}}{\eta kT}\right) \quad 3.16$$

where q is the electronic charge, η is the ideality factor, V_{app} is the applied voltage and T is the absolute temperature. For ideal diodes such as in silicon, the value of the ideality factor is about 1 however in organics it is found to be as high as 3 [43, 44]. The ideality factor observed for Fig.3.8 is 2.42. Such high values are associated with the presence of extrinsic trapping sites in the material depending on material purity and interface defects introduced during processing. It is thus useful to represent the carrier distribution in terms of the effective temperature T_o which relates to both spatial disorder due to thermal vibrations and also energetic disorder due to the distribution of states T_c as given by Eq. (3.17) [39],

$$\frac{1}{T_0} = \frac{1}{T} - \frac{1}{T_C} \quad 3.17$$

Consequently, the current density under forward bias for an organic device can be given as,

$$J_F \propto \exp\left(\frac{qV_{app}}{kT_o}\right) \quad 3.18$$

The value of T_0 obtained for TIPS-pentacene from J-V plot in Fig.3.8 is 725K, thus resulting in T_C of 512K, which corresponds to Meyer Neldel Energy of 44.1meV using Eq. (3.14).

B. Space Charge Limited Currents in Saturation Region

The dominion of space charge limited currents (SCLC) signify the departure of ohmic conduction. To apply one-carrier SCLC, the properties of the injecting contact must be ignored. This is because an introduction of a potential barrier at the contact will cause the characteristics of the contact to dominate. Thus, two assumptions are made. One, that an infinite number of charge

carriers can enter through the anode/cathode with ease and second, that the diffusion currents can be ignored as they are only important in areas in close proximity of the injecting contact.

At low voltages, assuming that there is no voltage drop due to the injecting contact, the current follows ohmic conduction. Increasing the applied voltage causes a space charge region to be formed in the semiconductor close to the metal/semiconductor interface and causes the SCLC to dominate.

The theory of SCLC between two electrodes with a constant mobility value and without the presence of trapping effects was introduced by Mott-Gurney [45].

$$J = \frac{9}{8}\mu\varepsilon_0\varepsilon_i\left(\frac{{V_{app}}^2}{x^3}\right) \qquad 3.19$$

where ε_0 is the permittivity of free space and ε_i is the dielectric constant of the insulator, n_f is the free carrier concentration, V_{app} is the applied voltage and μ is the mobility. As the distance increases between the contacts, the free carrier concentration falls as in Fig. 3.10.

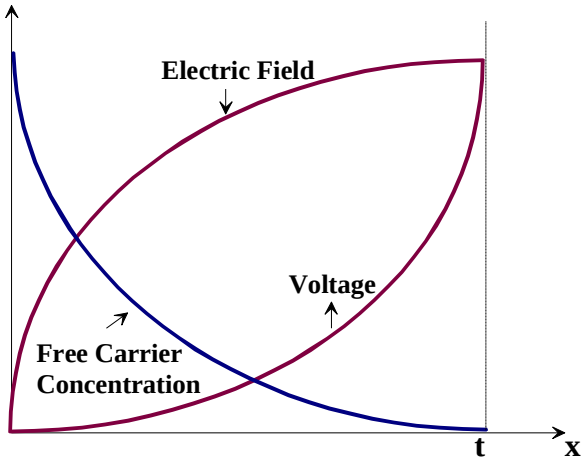

Figure 3.10. An ideal insulator with no trap charge shows a variation of free carrier concentration, voltage and electric field with distance, x. The distance, measured across the two electrodes, is given by the term t.

Mott and Davis [46] extended the theory to account for SCLC controlled by shallow traps with exponential energy distribution. For organic semiconductors however, the density of states is generally energetically distributed in a Gaussian and the states in the tail act as trapped states [47]. Rose [48] was the first to develop the theory of SCLC followed by extensive research by Lampert and Mark [49, 50]. The space charge limited currents, in this case, is thought to dominate when the carrier concentration injected in the organic semiconductor is comparable to the thermal free carriers. Ohmic conduction, for this reason, is not valid and the conduction is controlled by the high density of traps or low carrier mobilities. The electric field, in this instance, is no longer linear to the carrier concentration but has a strong dependence upon applied voltage.

Grain boundaries are assumed to have a low carrier effective mobility and hence space charge limited currents (SCLC) are expected to dominate in the saturation region of the current density against applied voltage plot in Fig.3.8. On the contrary, the grain is ordered where the material is single crystal and thus the mobility is much higher in comparison. The grain boundary follows the exponential distribution function for the variation of trapped charge. The theory of SCLC applies for charge transport only if a small injection barrier exists between the metal and the semiconductor and carriers can be efficiently injected into the device. SCL currents can be used for estimating parameters such as mobility and trap concentration in organic semiconductors [51, 52].

The effective mobility in a disordered grain boundary has a thermal dependence due to the energetic DOS and thus a thermally activated behaviour. At higher energies in exponentially distributed states, there is a better possibility for the carriers to hop around as more number of empty states exists. In inorganic semiconductors, the shallow traps correspond to the extrinsic energy levels located a few *kT*s away from the conduction band. In organic semiconductors, the definition of free and trapped charge carriers has to be a little altered and the intrinsic localised states contain both the trapped, n_t and free charge carriers, n_f. The ratio of free charge carriers to the total charge carriers in the intrinsic DOS can thus be defined in terms of θ (Appendix B). θ is the barrier electrons have to surpass.

$$\theta = \frac{n_f}{n_f + n_t} \approx \frac{T}{T_C} \qquad 3.20$$

For disordered organic semiconductors, θ is limited to unity as according to UML, T_C must be more than T. θ does not comply if T_C is lower than T and the carrier densities are very high. At low temperatures, the free carrier concentration is much less than the trapped carrier concentration making θ negligible. Increase in temperature causes the Fermi level to rise and the charge carriers to gain sufficient energy to occupy higher energy levels so that the free carrier density increases. θ from the J-V characteristics plotted in Fig.3.8 is 0.59.

In disordered semiconductors if diffusion currents are ignored, the current density J due to drift of free carriers can be written as

$$J = q\mu n_f F \qquad 3.21$$

where μ is the effective mobility, n_f is the concentration of free injected carriers and F is the electric field. Current density taking UML, as in Eq. (2.17), in accord gives

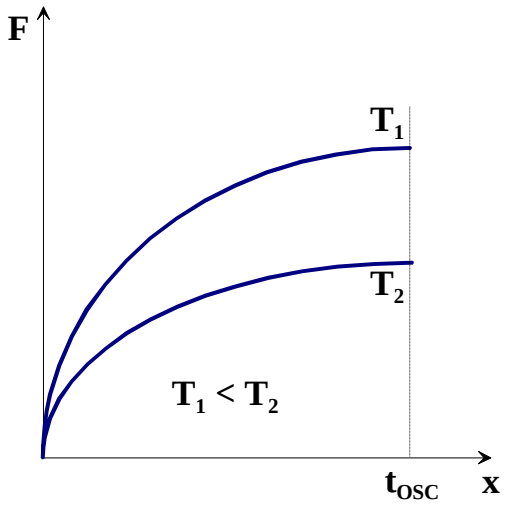

Figure 3.11. The change in electric field, F with variation of temperature, T. The distance is measured across the thickness of the disordered organic material from the injecting contact, t_{OSC}. The component m is a material dependent term that changes the electric field with change in temperature.

$$J = q(K\, n^{m+1})F \qquad 3.22$$

Current transport above the Fermi level is caused by free carriers and any change in the amount of carriers determines the field across the semiconductor. Poisson's equation can be used to link the change in electric field with thickness of the active layer

$$\frac{dF}{dx} = -\frac{q}{\theta\varepsilon_0\varepsilon_S}n \qquad 3.23$$

$$\frac{dF}{dx} = -\frac{q}{\theta\varepsilon_0\varepsilon_S}\left(\frac{J}{qKF}\right)^{\frac{1}{m+1}} \qquad 3.24$$

Integrating the electric field with respect to the thickness of the active layer is given by

$$F = \left(\left(\frac{m+2}{m+1}\right)\frac{q}{\theta\varepsilon_0\varepsilon_S}\right)^{\frac{m+1}{m+2}}\left(\frac{J}{qK}\right)^{\frac{1}{m+2}}x^{\frac{m+1}{m+2}} \qquad 3.25$$

where *x* is the thickness of the semiconducting layer. Integrating the voltage applied with respect to the thickness of the semiconductor gives the space charge limited current for a disordered organic semiconductor (Fig.3.11). The effective mobility is linked with electric field and thus the existence of *m* in Eq. (3.25) indicates strong temperature dependence. In saturation region of a disordered organic semiconductor, the current density in the neutral region is given by

$$J = \frac{K}{q^m}\left(\frac{\theta\varepsilon_0\varepsilon_S(m+1)}{m+2}\right)^{m+1}\left(\frac{2m+3}{m+2}\right)^{m+2}\frac{{V_{app}}^{m+2}}{x^{2m+3}} \qquad 3.26$$

This gives the value of *K* from the slope of the plot of *J* against V^{m+2} as T_C and *m* are known from the exponential characteristics of *J* against *V* plot, using Eq. (2.18).

Substituting *m=0* in Eq. (3.26) gives the Mott-Gurney law Eq. (3.19) thus indicating that Eq. (3.26) is correct. At higher biases the current starts to increase more rapidly with voltage and Child's law is no longer valid indicating that the mobility increases with the applied voltage. The mobility is seen to be dependent on the temperature.

Another effect to consider is the width of the space charge region compared to the neutral region. In forward bias, the increase in potential causes the barrier height to reduce considerably and hence the space charge region reduces causing the neutral region to increase. This increase in the neutral region is important to be considered in SCL current model for disordered organic materials. However to stay uncomplicated, we assume that the width of the neutral region is constant. The voltage rise is comparable to the exponential rise in the currents seen across the Schottky barrier until the current is limited by the resistance of the neutral region R_b.

$$R_b = \frac{t_n}{qn\mu A} \qquad 3.27$$

where t_n is the thickness of the neutral region, n is equivalent to the dopant concentration N_D , A is the area and μ is the mobility.

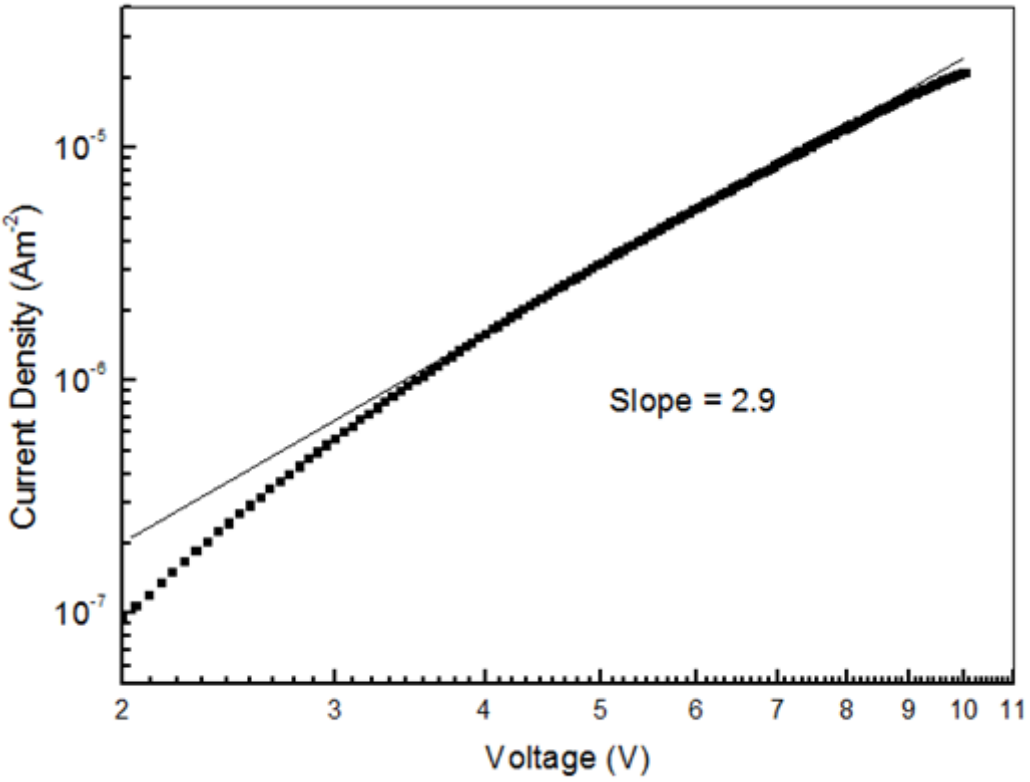

Figure 3.12. Current density against bulk voltage gives a slope of 2.9 in the saturation region indicating the Space charge limited currents to be dominating. This is believed to be due to the disordered grain boundaries trapping a large amount of holes.

Figure 3.12 shows the logaritmic plot of the forward current density against voltage in the saturation region as highlighted in Fig.3.8. Assuming that there is no potential drop across the gold electrode, the neutral region shows either ohmic or space charge limited behaviour, as demonstrated by the value extracted from the slope in Fig.3.12. Here the slope is found to be greater than one and of the value of 2.9. This thus suggests that the space charge limited currents rather dominate. The grain boundaries are said to be responsible for the trapping of large amounts of charge as they are amorphous in nature. The concept of UML in developing the SCLC equation is not simply restricted to disordered materials but also applicable to polycrystalline such as TIPS-pentacene, which consists of ordered grains and more particularly grain boundaries which are disordered in nature. This has been discussed in detail in Section 2.5.6.

II. Reverse Bias

In reverse bias, the depletion region widens restricting the path for current flow. The barrier seen by the carriers is due to the combined effect of the built in potential and the applied bias (Fig.3.9b). The field in terms of Poisson's equation is written as

$$\frac{dF}{dx} = \frac{d^2V}{dx^2} = \frac{qN_D}{\varepsilon_0\varepsilon_S} \tag{3.28}$$

N_D is the dopant concentration. Integrating gives Field in terms of dopant ion concentration

$$\int dF = \int \frac{qN_D}{\varepsilon_0\varepsilon_S}\, dx \tag{3.29}$$

$$F = \frac{qN_D x}{\varepsilon_0\varepsilon_S} \tag{3.30}$$

where x here is the depletion region width, W_{dep},

$$W_{dep} = \left(\frac{2\varepsilon_0\varepsilon_S}{qN_D}\,(V_{app} - V_{bi} - \frac{kT}{q})\right)^{1/2} \tag{3.31}$$

V_{bi} is the built in potential, V_{app} is the applied voltage and kT/q is due to the majority carriers distribution tail. $kT/q << V_{app}$ and V_{bi} so can be ignored. Applied field is therefore

$$F = \left(\frac{2qN_D}{\varepsilon_0\varepsilon_S}\,(V_{app} - V_{bi})\right)^{1/2} \quad 3.32$$

And the barrier height, from Section 3.2.2, described solely in terms of the applied field can be written as

$$\Delta\emptyset_B = 2Fx_m \quad 3.33$$

$$\Delta\emptyset_B = 2.\left(\frac{q}{16\pi\varepsilon_0\varepsilon_\infty}\right)^{1/2}(F)^{1/2} \quad 3.34$$

$$\Delta\emptyset_B = \left(\frac{q^3N_D}{8\pi^2{\varepsilon_0}^3{\varepsilon_\infty}^2\varepsilon_S}.(V_{app} - V_{bi})\right)^{1/4} \quad 3.35$$

Under reverse bias, the barrier at the interface changes due to the image force effect at the metal/ semiconductor interface (Section 3.2.2). The current density, J_R in this case is given as in Eq. (3.36) [13],

$$J_R \propto \exp\left[\frac{q}{kT}\left(\frac{q^3N_D\left(V_{app} - V_{bi} - kT/q\right)}{8\pi^2\varepsilon_0^3\varepsilon_S^3}\right)^{1/4}\right] \quad 3.36$$

where N_D is the dopant concentration, V_{bi} is the built in potential, ε_0 permittivity of free space and ε_S dielectric constant of the semiconductor.

As the reverse bias increases, the depletion width expands towards the back ohmic contact. In order to determine whether the abrupt depletion region approximation is applicable, plots of the logarithmic of the reverse current density against the reverse voltages to $V^{0.25}$ at room temperature were obtained as in Fig.3.13. The value for N_D obtained from the slope is approximately $4.85\text{x}10^{17}\text{cm}^{-3}$. It is noticed that $V^{0.25}$ varies linearly with the reverse current

density which implies the possibility of a uniform doping profile of acceptor ions. It is essential to also establish whether the abrupt depletion region approximation is valid in organics. Generally, the interface at the edge of the depletion and neutral regions are assumed to be abrupt. In practice this is not the case however the assumption is valid if the depletion region width is much larger than the Debye length Eq. (3.37).

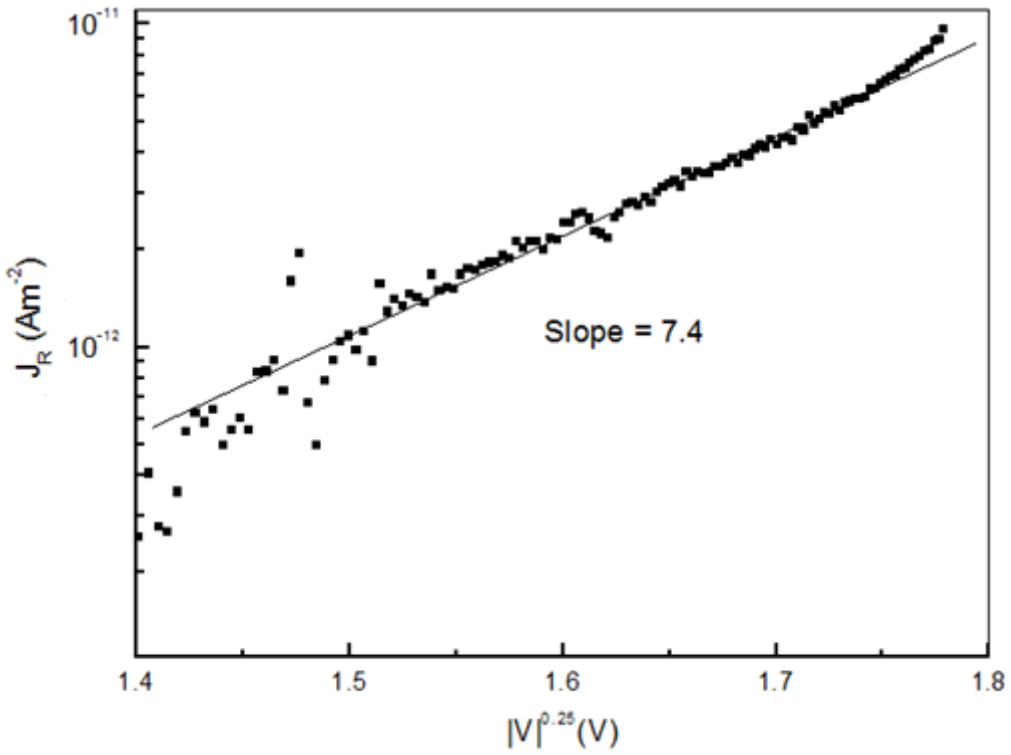

Figure 3.13. Log J_R against $V^{0.25}$ plot for TIPS/PAMS Schottky diode in reverse bias. The dopant density calculated by this method is 4.85 x $10^{17}cm^{-3}$.

Effective Debye length is the distance over which the charge carriers increase such that it gets close to the intrinsic value and the semiconductor becomes effectively neutral. It is defined as the length over which a charge imbalance is neutralized by the majority carriers under equilibrium conditions and is inversely proportional to the dopant concentration [21]. The expression for a p-type disordered semiconductor, derived from [13], is written as Eq. (3.37) and the value is found to be approximately 3.9 nm [53].

$$L_{De} = \left(\frac{kT_C \varepsilon_0 \varepsilon_S}{q^2 N_D}\right)^{1/2} \quad 3.37$$

where $\varepsilon_0$is the permittivity of free space, ε_s is the dielectric constant of the semiconductor, $T_c$is the characteristic temperature of the exponential DOS and N_D is the dopant concentration.

The depletion width W_{dep} is also estimated for TIPS-pentacene and found to be approximately 16 times more than L_{De} as defined in Eq. (3.38).

$$\frac{W_{dep}}{L_{De}} \approx \left(\frac{2qV_{app}}{kT_C}\right)^{1/2} \quad 3.38$$

All the above equations will be utilised further in the analysis of the experimental data in the next sections, and to consequently extract essential material and device parameters.

III. Effects of Changing Device Fabrication on the Electrical Characteristics

Schottky diodes with two different ohmic contacts i.e. Gold or Copper and Aluminium Schottky contact were fabricated. The effect of using different binders such as PS and PAMS with TIPS-pentacene, and drying conditions were also explored. Figure 3.14 shows the current-voltage characteristics of the various diodes with different ohmic contacts, binders and drying temperature. The results demonstrate that the choice for the ohmic contact is essential as the on-current and subsequently rectification ratios depend on it. This is simply because the current flow at high voltages is limited by the properties of the back metal-organic interface. Introduction of a series resistance due to an imperfect ohmic contact results in a restriction to the free flow of carriers.

The theoretical work function of gold is higher than that of copper but the practical work function change drastically with the deposition method used. It also depends on the chemical nature of the resulting metal- organic interface. TIPS-pentacene, like most other organic semiconductors, is intrinsically p-type and therefore requires a high work function metal to make good ohmic back contacts with it. The LUMO band of TIPS-pentacene is far from the Fermi level of the gold, thus electron injection is very unlikely as there is a significant barrier between their energies. This

means that there is no current passing through the TIPS-pentacene layer. Nevertheless, a small current is observed even when care is taken during fabrication.

The difference between pentacene and gold interface is shown in Fig.3.15 showing a clear deviation from the model by Mott-Schottky [58]. Interface issues can be improved by a method suggested by Li et al. [59] where a region in the organic material is made with low mobility and placed at the interface with the metal. The rest of the organic semiconductor layer is of higher quality.

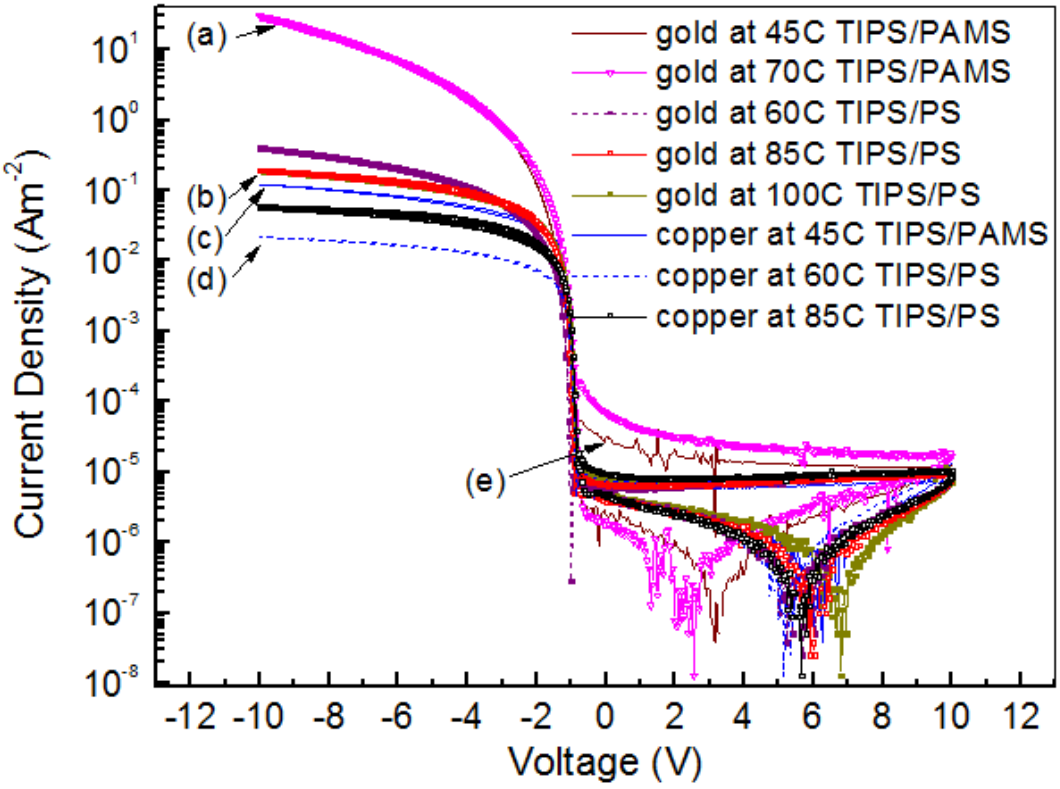

Figure 3.14.Current Density (J) against Voltage (V) plot of the best obtained TIPS/ PAMS and TIPS/ PS 1mm diameter diodes at different drying temperatures with two different ohmic contacts from Table 3.1(b). Gold is observed to be a better ohmic contact than copper, giving better rectification measured in orders of magnitude at -10V and 10V. Table 3.2 lists the results obtained.

Figure 3.14 shows Schottky diodes with both TIPS/ PAMS and TIPS/ PS as the active layer at different drying temperatures and with two different ohmic contacts. Changing ohmic contacts from copper as in Fig.3.14 (c) to gold in (e) in a TIPS/PAMS diode changes the saturation

currents from ohmic conduction to space charge limited conduction respectively. Nevertheless, gold electrode provides better rectification than copper.

From Fig.3.14, the rectification with copper as ohmic contact provides better results with PAMS binder in Fig.3.14 (c) than PS (d). Fig.3.14 (c) has an approximate rectification of 10^4 whereas (d) has an approximate rectification of 10^3. The rectification ratios are measured at -10V and 10V in forward and reverse bias respectively. The reason for the increase in rectification of Fig.3.14 (c) compared to (d) may be due to the effective mass of the binders (PAMS < PS). Moreover, the conduction mechanism in saturation is neither ohmic nor space charge as the slope found is less than one. Ideality factor obtained for (c) is 1.83 whereas for (d) it is 1.28, close to the ideality factor of ideal silicon.

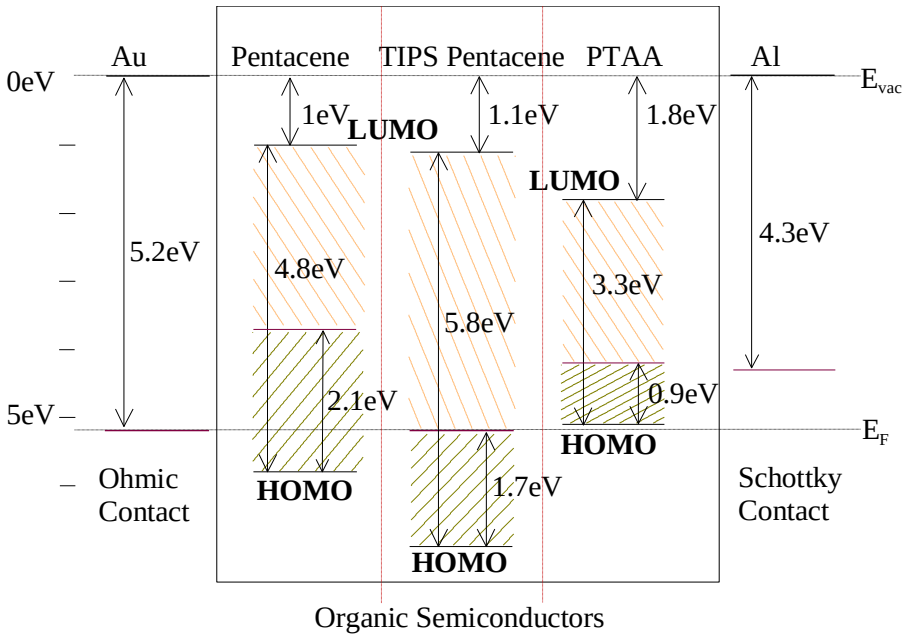

Figure 3.15. Energy diagram of a Schottky diode with an organic semiconductor; pentacene, TIPS-pentacene [54, 55] or PTAA [56, 57]. Gold forms an ohmic contact whereas aluminium forms a Schottky contact with the organic semiconductor.

Experiments with TIPS-pentacene films carried out without a binder provided rough surfaces with a layer that was easy to peel off indicating limited adhesion between the active layer and contact. The measurements of such layered Schottky diodes formed short circuits. Increasing the thickness

of the drop cast TIPS-pentacene film still resulted in short circuits and layer flaking. Hence, to improve the morphology both TIPS/PAMS and TIPS/PS layers were drop cast to produce uniform and smooth films. The effects of change in binder in Fig.3.14 show that PAMS binder produces improved characteristics with high rectification than the PS binder. The values obtained for T_0 and T_C from Fig.3.14 (b) are 441K and 937K approximately. Values obtained from Fig.3.14 (a) give T_0 and T_C as 558K and 648K respectively. The MNE obtained from Eq. (3.14) for both (b) and (a) are 81meV and 56meV respectively. In both the cases, the value of T_C found is more than the value of T_0 indicating MNE due to disorder to be significant. *m*, the material dependent parameter therefore becomes considerable. The ideality factor found for (b) and (a) in the exponential region of the plot is 1.47 and 1.83 respectively.

Moreover, TIPS-pentacene with organic semiconductor PTAA produced better morphology compared to PAMS and PS blends. PTAA showed best film uniformity followed by PAMS and PS respectively. However, improved morphology in PTAA blend did not improve the performance of the Schottky diode. This is because insulating materials such as PTAA introduced more molecular disorder and hence decreased the mobility values.

Drying organic semiconductors films after their deposition is favourable to the device characteristics [60] and for this reason, TIPS/PAMS and TIPS/PS samples were dried at different temperatures. The drying times differed with temperature, decreasing with increasing temperature.

TIPS/PAMS on gold produced similar layers at temperatures of 45 °C and 70 °C as in Fig.3.14 (e) and (a) respectively. Drying temperature of 70 °C produced a better rectification current ratio of 10^6 approximately. The ideality factor obtained for Fig.3.14 (e) and (a) were 2.42 and 1.86 respectively. The results indicate that the change in drying temperature changes the crystalline properties and hence morphology of the material. An efficient removal of organic solvent must have some dependence on the drying temperature. For the 70 °C sample, as in Fig.3.14 (a), the parameters obtained were T_0= 558K, T_C= 648K, *m*= 1.16, effective mobility= 7.28×10^{-2} cm^2/Vs and carrier concentration of $2 \times 10^{17} cm^{-3}$. The slope obtained in the saturation region is more than 2 indicating that the conduction is space charge limited. The value of T_0, extracted from the exponential region, is much lower than expected in polycrystalline materials and can be an indication of the distribution of carriers to be narrower than other organic semiconductors such as PTAA [61].

TIPS/PS on gold at drying temperatures of 60 °C, 85 °C and 100 °C produced best rectification current ratio of around 4.5 orders of magnitude (~$10^{4.5}$) measured at -10V and 10V (Fig.3.14). The ideality factor obtained from the I-V characteristics of the sample dried at 85 °C was around 1.4 which is around the inorganic semiconductor range with some added impurities. The corresponding parameters obtained were T_0= 441K, T_C= 937K, m= 2.12 and carrier concentration of 5 x10^{18}cm^{-3}. The slope obtained from the space charge region is less than unity for all TIPS/PS samples thus rendering the concept of space charge limited currents in saturation invalid. Ohmic conduction is thus responsible in saturation region. In this case, the disorder in the material must not be affecting the conduction. Grain boundaries are generally responsible for disorder in a polycrystalline material but as ohmic conduction dominates, the grains must be large enough to allow the flow of carriers without the boundaries affecting the charge. The drying temperature of 85 °C must then be an optimum temperature to produce better morphology of the TIPS/PS layer with large grain size. Such high drying temperatures are effective in such a blend due to the high boiling point of PS when compared to PAMS.

Table 3.2. List of blends and the parameters obtained from their current-voltage characteristics in Fig.3.14.

	(a)	(b)	(c)	(d)	(e)
Ohmic contact	Gold	Gold	Copper	Copper	Gold
Blend	TIPS/ PAMS	TIPS/ PS	TIPS/ PAMS	TIPS/ PS	TIPS/ PAMS
Drying Temperature (^{o}C)	70	85	45	60	45
Conduction in Saturation Region	Space Charge Limited	Ohmic	Ohmic	Ohmic	Space Charge Limited
Area (m^2)	7.85 x 10^{-7}	7.85 x 10^{-7}	7.85 x 10^{-7}	7.85 x 10^{-7}	7.85 x 10^{-7}
Rectification	~10^6	~10^4	~10^4	~10^3	~10^6
Dopant Concentration (cm^{-3})	2 x 10^{17}	5 x 10^{18}	7.5 x 10^{18}	3 x 10^{18}	4.85 x 10^{17}
T_0 (K)	558	441	548	383	725
T_C (K)	648	937	662	1386	511
Meyer Neldel Energy (meV)	56	81	57	120	44
m	1.16	2.12	1.21	3.62	0.7
θ	0.46	0.32	0.45	0.22	0.59
Ideality factor	1.83	1.47	1.83	1.28	2.42

The relationship between conductivity and doping in organic semiconductors has been under extensive research and debate for decades [62, 63]. Quantitative analysis of organic semiconductors shows that doping of organic semiconductors can increase their conductivity by many orders of magnitude. Molecular doping of thin organic films has been used to improve their photovoltaic behaviour [64, 65]. A general doping process model for organic semiconductors because of their weak intermolecular forces is a challenge. Therefore although doping of organic semiconductors is different to those in inorganic semiconductors, crystalline inorganic semiconductor can be used to explain the doping process in organic semiconductors [66]. The model based on inorganic crystalline semiconductor assumes that the increase in doping improves the conductivity and causes a smooth shift of the Fermi level to the valence states.

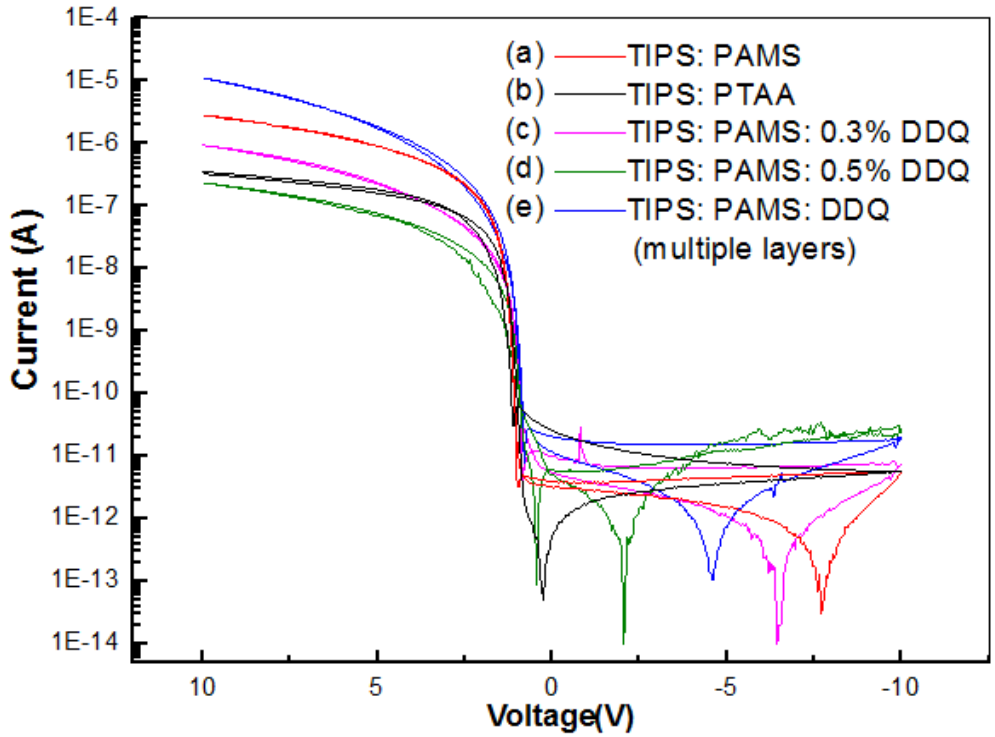

Figure 3.16. The best obtained Current-Voltage (I-V) characteristics of TIPS: PTAA and TIPS: PAMS with different percentages of doping. Addition of extra dopant ions does not have any significant effect on the I-V characteristics. All devices are 1mm circular diodes except TIPS/PTAA which is a 2mm circular diode. Results are listed briefly in Table 3.3.

Doping in inorganic semiconductors is easily done due to their strong covalent or covalent-ionic bonds [67]. Organic semiconductors, alternatively, are held together by van der Waal forces. Therefore only an insufficient number of free carriers are produced from the bending or breaking

of these low energy intermolecular bonds, or introduction of molecules such as DDQ into the lattice. Also, it is highly likely for the mobile charges to become trapped in the deep traps of an organic disordered semiconductor.

Table 3.3. A list of various blends with addition of extrinsic dopants and their corresponding dopant concentrations extracted from the reverse characteristics from Fig.3.16.

	(a)	(b)	(c)	(d)	(e)
Blend	TIPS/ PAMS	TIPS/ PTAA	TIPS/ PAMS/ DDQ	TIPS/ PAMS/ DDQ	TIPS/ PAMS + DDQ
Ratio	1:1	1:1	1:1:0.3%	1:1:0.5%	Multiple layers
Rectification	~10^6	~10^5	~10^5	~10^4	~10^6
Area (m^2)	7.85 x10^{-7}	3.14x10^{-6}	7.85 x10^{-7}	7.85 x10^{-7}	7.85 x10^{-7}
Dopant concentration(cm^{-3})	7x10^{17}	1x10^{15}	9x10^{18}	2x10^{19}	8x10^{17}

Rectification for multiple doping levels can be found from the plot in Fig.3.16 and are listed in Table 3.3, measured at -10V and 10V in forward and reverse bias respectively. The best rectification is seen to be achieved by TIPS-pentacene with a separate drop cast layer of highly concentrated DDQ solution. It is likely that a separate DDQ layer improves the connection between TIPS-pentacene and the gold electrode. Although the rectification ratio observed in Fig.3.16 (e) is not as good as the ones achieved in Fig.3.16, it is better than a single layer doped TIPS-pentacene on a gold ohmic contact (Fig.3.16 (a)). The dopant concentrations observed from Fig.3.16 for (a) to (e) are approximately 7x$10^{17}$$cm^{-3}$, 1x$10^{15}$$cm^{-3}$, 9x$10^{18}$$cm^{-3}$, 2x$10^{19}$$cm^{-3}$ and 8x$10^{17}$$cm^{-3}$ respectively. The dopant concentration obtained from the characteristics of (e) is not much different from (a) indicating that a separate DDQ layer does not help improve the charge carrier concentration in the device. TIPS: PTAA combination in (b) shows much lower dopant concentration than any other combination due to the increase in disorder in the organic layer. Comparison between Fig.3.16 (c) and (d) demonstrates a slight increase in dopant concentration due to the increase in dopant ions in the organic layer.

3.4 TEMPERATURE EFFECTS ON THE ELECTRICAL CHARACTERISTICS OF TIPS-PENTACENE SCHOTTKY DIODES

The temperature effects on the current-voltage characteristics were studied for two polycrystalline organic blends, TIPS/PTAA and doped TIPS/PAMS. The fabrication of the diodes and detailed analysis of the characteristics are discussed below. Both the forward and the reverse regions of the characteristics are investigated. The exponential current region is evaluated in terms of the conventional diode theory and the proposed theory existent for the organic disordered semiconductors. For both TIPS/PTAA and doped TIPS/PAMS, the saturation region is analysed to follow space charge limited currents (SCLC) and thus the SCLC expression is used to find the effective mobility in saturation.

Essential parameters are extracted from the electrical characteristics for the various temperature ranges. Limits on the validity of the theory such as the conduction mechanism, particularly at low temperatures are also discussed.

3.4.1 Experimental Details

Controlled amounts of TIPS-pentacene and binder (PTAA or PAMS/DDQ) were mixed together in solution so as to form the active layer, sandwiched between an Ohmic gold contact and Schottky aluminium contact (as in Fig.3.6). The functionalized TIPS-pentacene was drop cast to form the active layer as discussed in Section 3.3.1. The temperature of the substrate was kept higher than room temperature and at a constant level at the time of drop casting. The sample was covered with a glass lid to dry slowly in a solvent-rich environment to promote ordered molecular arrangements.

The dc measurements were then carried out using a HP4145 analyser connected to a Keithley voltage source and electrometer. For the temperature measurements, the device was connected onto a liquid nitrogen cryostat under 0.1 mbar vacuum and the temperature was lowered from room temperature to 160K for TIPS/PTAA diode and to 140K for TIPS/PAMS diode. For experimental setup, the sample had to be connected to a holder to keep it in place in the cryostat which was then connected to the measurement rig.

3.4.2 Temperature Effects on TIPS/PTAA Schottky Diode

Figure 3.17 shows the I-V characteristics of the TIPS/PTAA Schottky diode measured at various temperatures. The rectification ratios are seen to fall by orders of magnitude from 10^4 at room temperature to 10^2 at 161K (from -10V to 10V). Similar findings have also been observed in thermally evaporated pentacene-based thin-film transistors [68]. In order to determine the temperature effects on important parameters, we hereafter analyse the different regions of the characteristics respectively.

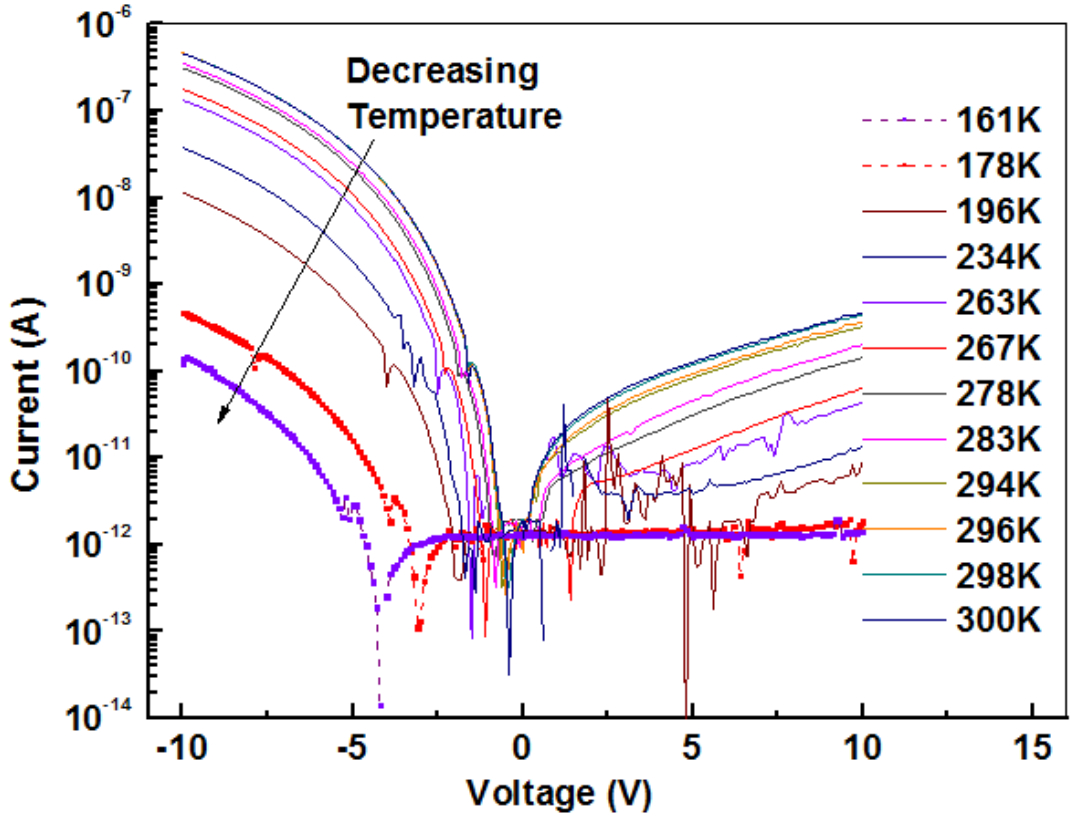

Figure 3.17. Temperature variance on the current against voltage (I-V) characteristics of TIPS/PTAA, 2mm diameter Schottky diode from Table 3.1(b).

Under reverse bias, the currents decrease possibly due to the change in barrier with the movement of the Fermi level downwards into lower energies with decreasing temperatures. This could possibly be due to the degradation of the semiconductor surface in vacuum with the reduction in the photo-oxidation effect. Interestingly, however, at the lowest temperatures i.e. 161K and 178K,

the reverse currents remain constant with increase in reverse bias. As discussed in Section 3.2, the reverse currents depend on two factors, the image force lowering effect and the applied field. The results from Fig.3.17 indicate that there is a net current which does not change with applied field. The field in this case is not changing rapidly at the peak of the barrier and thus the depletion charge is not increasing quickly. Therefore, the net current seen at lower temperatures is expected to be due to the applied field, staying constant throughout the voltage range measured. The reverse current, at lower temperatures, is therefore expected to be dependent on $V^{0.5}$ due to the applied field instead of $V^{0.25}$ assumed earlier at higher temperatures. Also, the plots are seen to be non-linear at lower voltages in the reverse characteristics and are supposed to be the contribution of a variety of current conduction mechanisms. Using Eq. (3.36), the dopant concentration is found to be around $1x10^{17}cm^{-3}$ at room temperature from the plot of reverse current density against $V^{0.25}$ in Fig.3.18. Such high dopant concentrations may possibly be due to the presence of residual ions incorporated during synthesis and/or due to photo-oxidation effects as a result of exposing the device in ambient conditions.

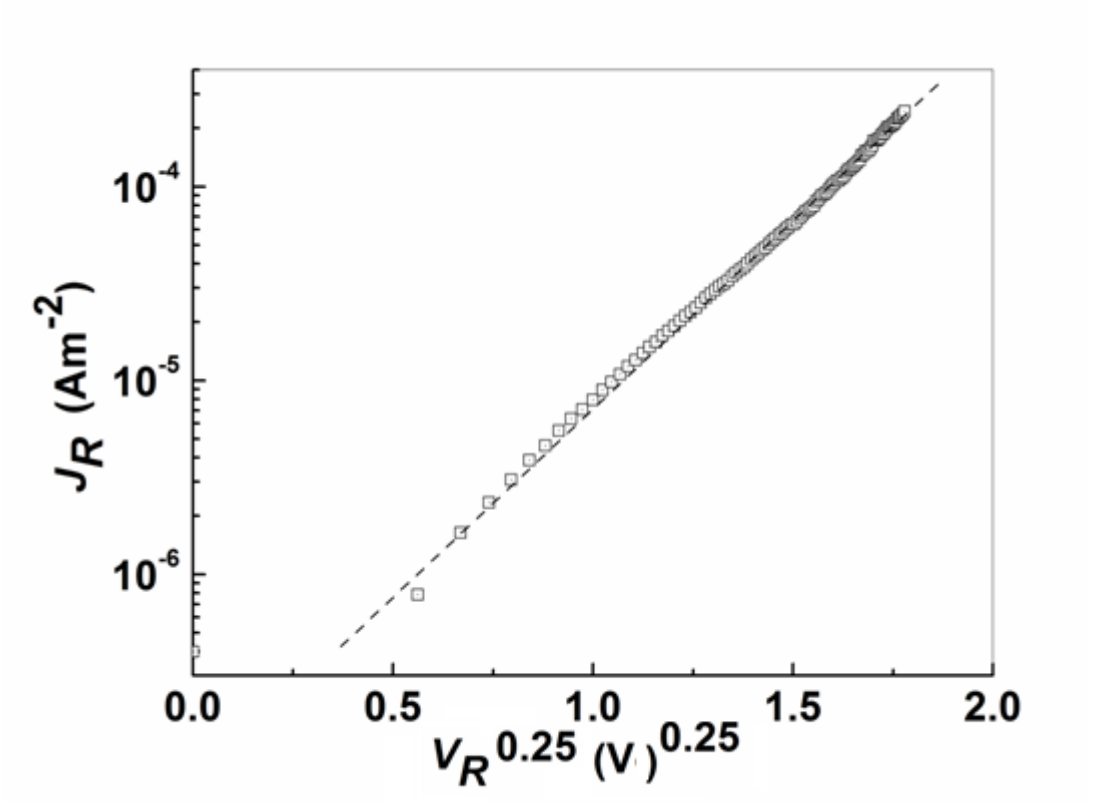

Figure 3.18. Logarithmic plot of the variation of J_R against $V_R^{0.25}$ measured at room temperature. A good linear fit to ¼ power law suggests the abrupt depletion edge approximation to be applicable in organics. Divergence at low voltages is due to work-function difference between the Schottky contact and semiconductor.

Further analysis of the effect of temperature was carried out on the depletion width W_{dep} and the effective Debye length L_{De}. At room temperature, W_{dep} (Eq. (3.31)) and L_{De} (Eq. (3.37)) are found to be approximately 185nm and 11nm respectively. As L_{De} is only 6% of W_{dep} from Eq. (3.38), this further emphasises the validity of using the abrupt depletion approximation in organics. Similar ratio between the depletion width and the Debye length is observed in TIPS/PAMS Schottky diodes measured at room temperature in Section 3.3.2. As the temperature falls from room temperature, both parameters remain nearly constant until 200K as in Fig.3.19. Below this temperature, the values are found to increase linearly which may be due to errors in obtaining the slope in Fig.3.17 since the reverse currents measured at the lowest temperatures were nearly constant as the applied voltages increased (Fig.3.17). Nevertheless, generally an increase in L_{De}

causes the resulting field across it to be smaller and thus the carriers move at a smaller diffusion rate, thereby limiting the current flow in the neutral region.

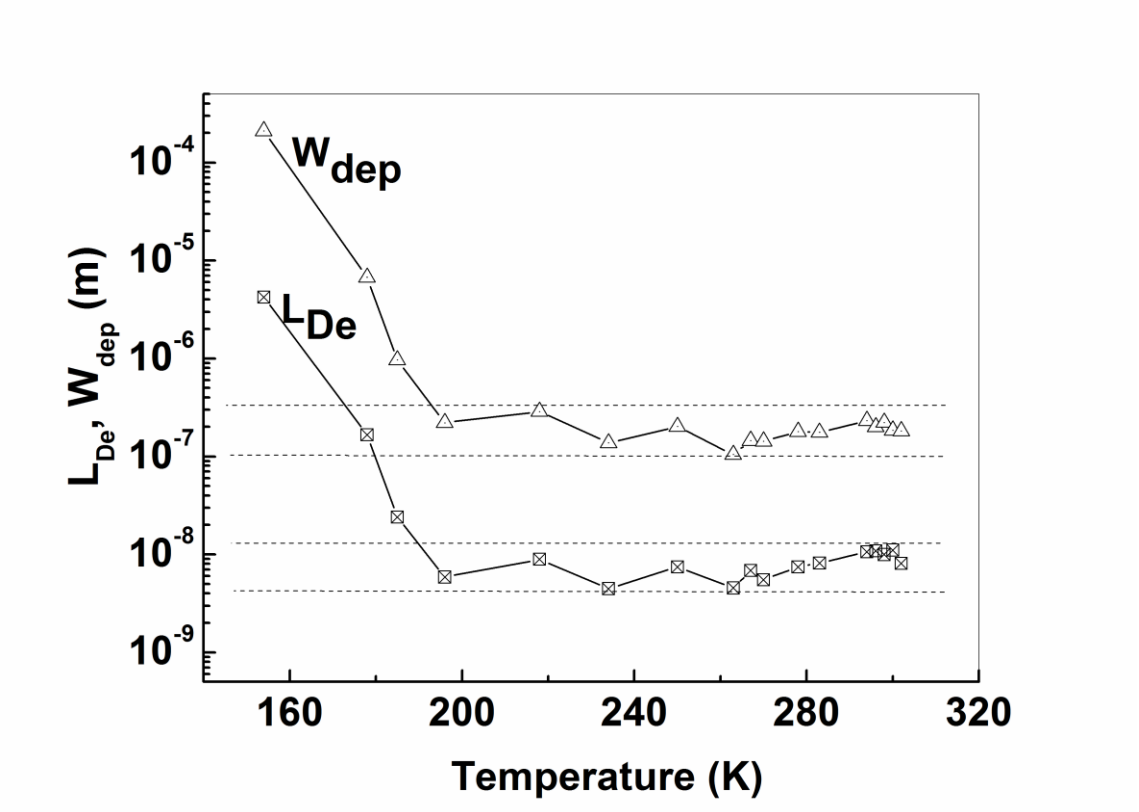

Figure 3.19. Logarithmic plots of the variations in the depletion region width W_{dep} and effective Debye length L_{De} with change in temperature. Both parameters remain constant at approximately 185nm and 11nm respectively above 200K.

Under forward bias in Fig.3.17, as the temperature falls, the forward current decreases and the threshold voltages shift towards more negative voltages, as demonstrated in Fig.3.19. This is thought to be possibly due to the shift in the quasi-Fermi level to lower energies as shown in Fig.3.20 (considering that the material is p-type). At lower energies and in the band tail, the Gaussian distribution is approximated to an exponential function indicating that the density of states increases rapidly at low energies. This behaviour can also be accounted for by the decrease in effective mobility with lowering temperature, as described later in the discussion. Furthermore, a thin layer of accumulated space charge between the Schottky metal and the active layer, at the interface may also be present. The movement of the threshold voltage to more negative voltages may be explained if the Schottky junction is considered to behave like a battery with some

existent charge. This existent charge is accumulated due to the sudden reversal of voltage from one temperature to the other as the temperature changes. Externally applied voltage is therefore initially used to neutralize the existent charge and get the Fermi level to equilibrium. The current can then flow across the diode.

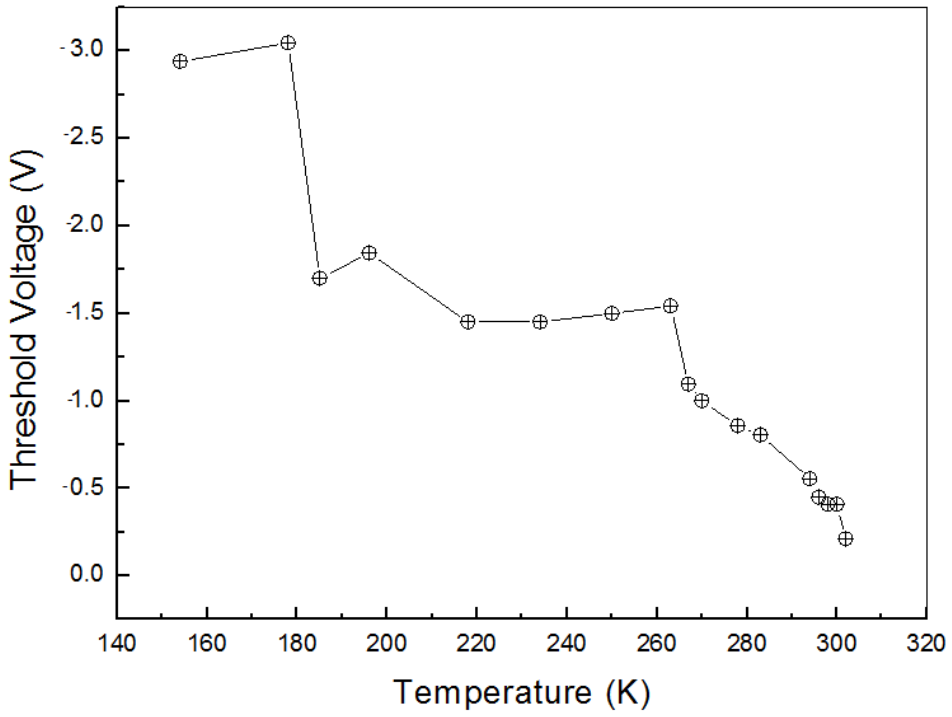

Figure 3.20. Threshold voltage, from the current density against voltage plot in Fig.3.17, is demonstrated with the variation in temperature. The plot shows an increase in threshold voltage with decreasing temperature most likely due to the accumulation of charge at the metal/semiconductor interface.

From the exponential region, the values for the characteristic temperature of exponential distribution of traps and the characteristic temperature of carriers can be obtained. In the exponential region, the substantial fall in the exponential current as the temperature reduces (in Fig.3.17), leads to extremely large values of the ideality factor, rising from about 3.57 at 300K to 15.6 at 154K. Such an increase in the ideality factor also results in larger values of T_0 obtained from using Eq. (3.18) as with decreasing temperature and increasing energy, the energetic distribution of holes becomes increasingly wider.

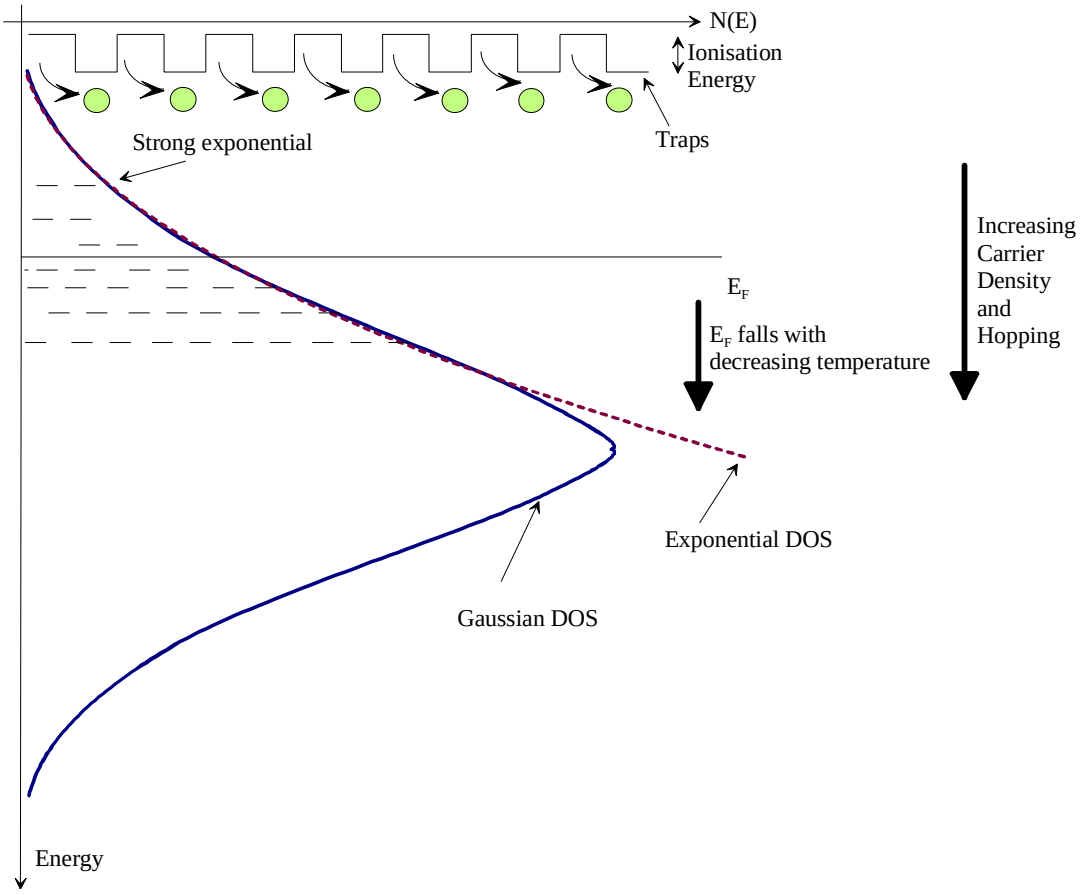

Figure 3.21. The shift in quasi Fermi level to lower energies with decrease in temperature for a p-type semiconductor. Movement of the Fermi level has an effect on the charge transport in the material. The peak of the extrinsic trap distribution is represented by regular boxes and the filled circles represent the charge carriers.

Having obtained T_0, the values of T_C were also determined using Eq. (3.17) [39]. The characteristic temperature of exponential distribution of traps, T_C, is expected to stay constant whilst T_0 changes due to the change in the ideality factor. Instead T_C varies in a range that can be described as experimental errors and hence we assume that the theory fits perfectly with the observed trend. Furthermore, Sedghi et al. [39] provide evidence of a constant T_C from the capacitance-voltage analysis of an organic MIS diode. Furthermore the Meyer-Neldel Energy (MNE), from Eq. (3.14), is found to remain within a range of 30-34 meV at temperatures above 270K as in Fig.3.22. Below this temperature, a linear decrease in MNE is observed, which may be attributed to the formation of a potential barrier at the interface between the ohmic contact and the active layer as described further in next section.

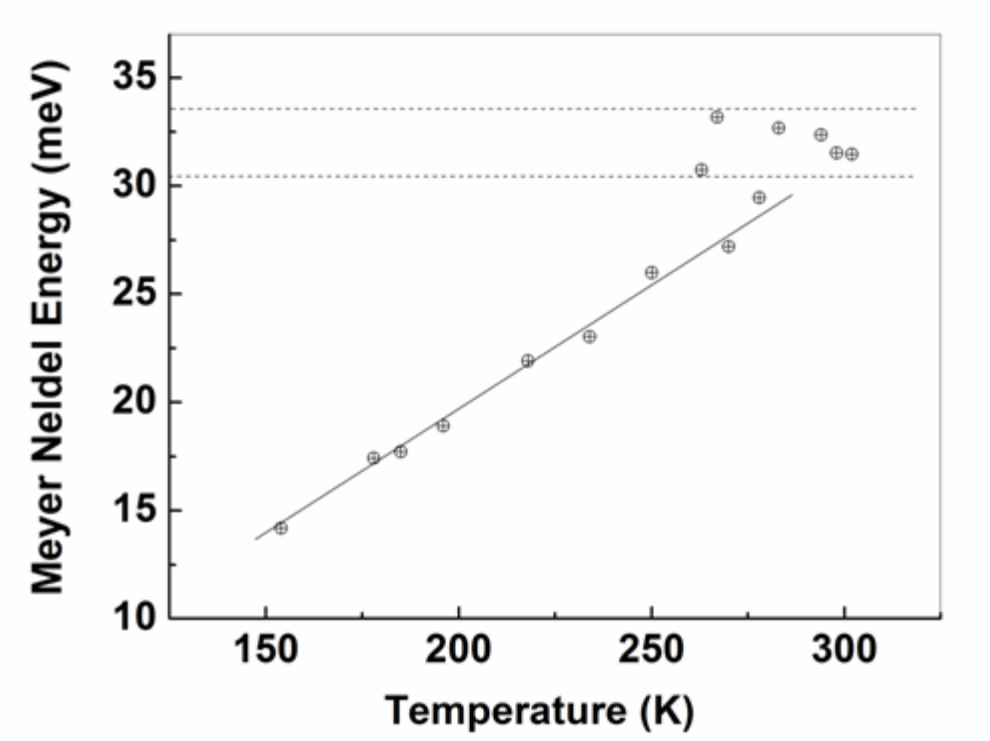

Figure 3.22. Variation of the Meyer-Neldel Energy (MNE) with temperature. The MNE lies within a range of 30 - 34meV, associated with the distribution of the states at temperatures above 270K.

In the saturation region in Fig.3.17, the current is thought to be dominated by the resistivity of the semiconductor bulk, which depends on the extrinsic hole concentration and the effective mobility μ_{eff}. We assume the current due to the extrinsic carriers contributed by the dopant states to be larger than that due to the intrinsic carriers. Consequently, the extrinsic concentration is obtained assuming every dopant in the depletion region constitutes to a free carrier in the neutral region i.e. $N_D \sim p$. Figure 3.23 shows the variation of the carrier concentrations with change in temperature. At high temperatures i.e. in the range of 200-300K, the carrier concentration is nearly constant with an average value of $10^{17}cm^{-3}$.

Below 200K, a drop in the concentration is possibly due to errors in extracting the dopant concentration which is associated with poor linear fits to the J_R against $V_R^{0.25}$ plots (as in Fig.3.18 at 300K). The current density might vary with $V_R^{0.5}$ instead as discussed above. However this drop is also likely to be due to the shift in the quasi-Fermi level of the semiconductor to lower energies

as the temperature falls, accordingly resulting in a potential barrier between the ohmic contact and the active layer.

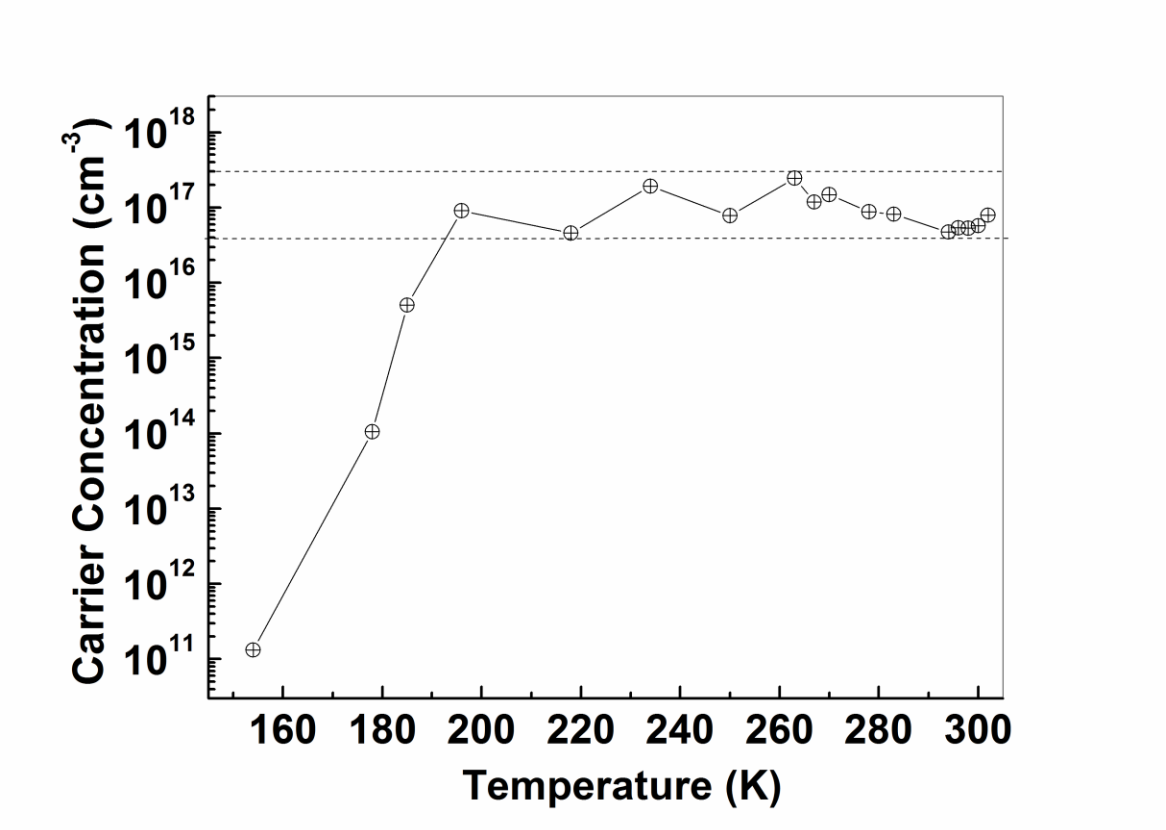

Figure 3.23. Logarithmic plot of the variation of carrier concentration with change in temperature. The carrier concentration is nearly constant at an average 10^{17}cm-3 above 200K. Below 200K, the assumption that the dopant concentration is similar to carrier concentration becomes doubtful and hence, the carrier concentration obtained at lower temperatures is uncertain.

The values for the μ_{eff} were found to decrease as the temperature dropped (Fig.3.24). A decrease in μ_{eff} is commonly associated with the thermally activated behaviour of the carriers in disordered materials. The mobilities for polycrystalline pentacene TFTs however were also seen to decrease with temperature [68]. The inability of the Fermi level to reach the mobile trap states is due to the disorder-promoted trap states near the edge of the grain [69]. It is also possible that the model used at higher temperatures is inappropriate at lower temperatures. One reason could be the derivation of carrier concentration from the dopant concentration in reverse. Although the assumption might be true at high temperatures, however at lower temperatures the decrease in dopant concentration and hence carrier concentration is uncertain. At temperatures in the range

measured for the purpose of study, dopant concentration is highly unlikely to vary. Hence the value of the carrier concentration can be expected to be erroneous.

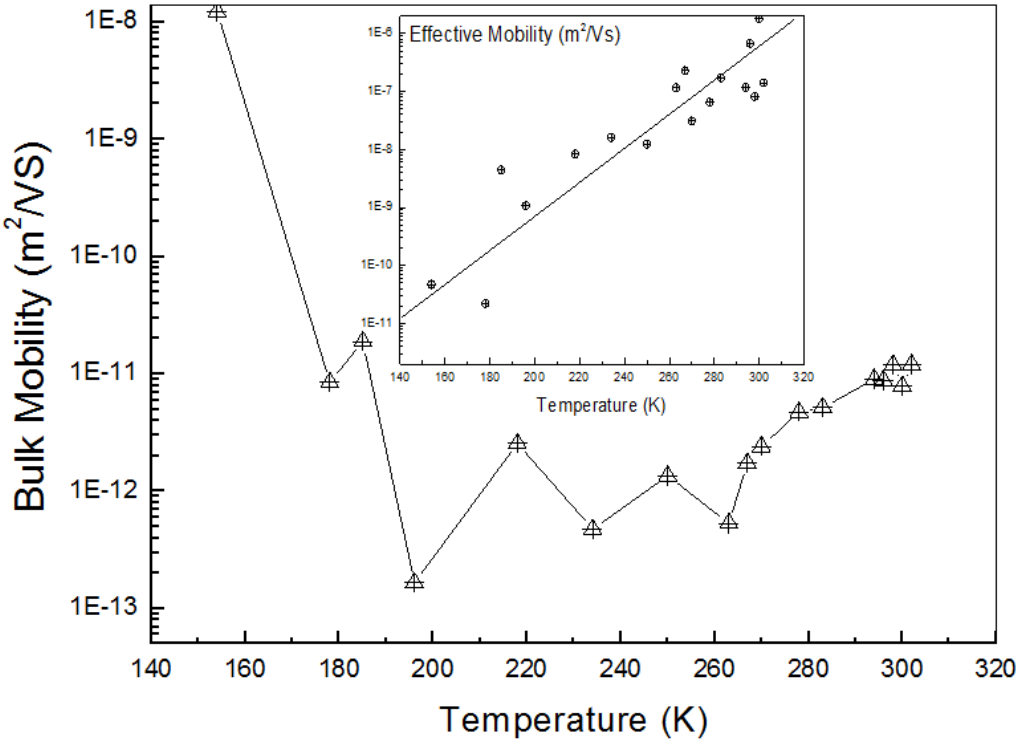

Figure 3.24. The variation of effective mobilty and bulk mobility with temperature for TIPS/PTAA based Schottky diode. The bulk mobility is seen to increase whereas the effective mobility is seen to decrease with a reduction in temperature.

Bulk mobility using Eq. (3.27), associated with the neutral region, is seen to decrease with decreasing temperature till a certain temperature after which it increases till about 150K as in Fig 3.24. In contrast, Eq. (2.17) shows that the effective mobility is directly dependent on the carrier concentration. It can be calculated by finding K from the gradient of the plot of J against V_{app}^{m+2} in the saturation region, n from Fig.3.31 and m using Eq. (2.18).

As the temperature lowers, the Fermi level moves closer to the HOMO level and hence deeper in the distribution of traps indicating an increase in the carriers available for conduction. However, the carriers injected at the metal electrode into various energy states have to penetrate down through the distribution of states until they reach quasi equilibrium. This process is difficult at

lower temperatures as the thermal energy of the holes is significantly reduced thus reducing the hopping rate. The Fermi level does not lie in the band tail of the Fermi-Dirac distribution anymore and therefore it is unlikely for a quasi level to exist at lower temperatures.

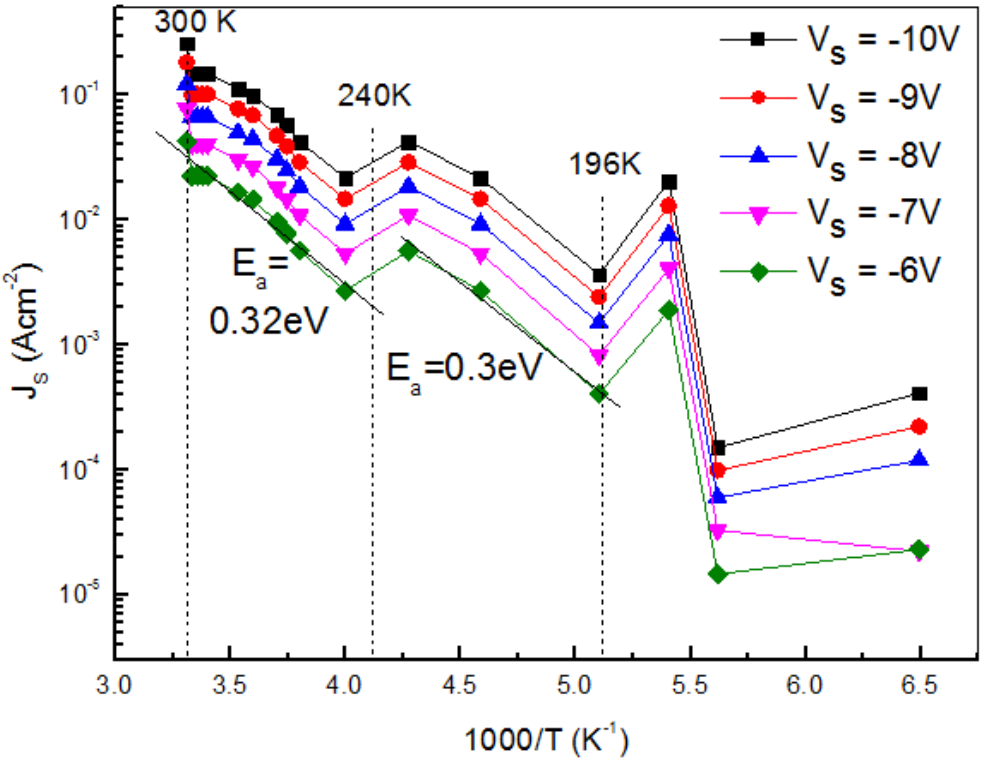

Figure 3.25. Logarithmic Arrhenius plot of the variation of the current density, Js, over a temperature range for various forward biases in the saturation region. The activation energy (Ea) obtained from the slope is found to be nearly constant a different voltages at approximately 0.3eV.

In order to further understand the transport properties and the effect of temperature on the transport energy, the activation energy E_a of the organic material at high temperatures is determined from the Arrhenius plot of current density J_s against *1000/T* in saturation as in Fig.3.25. The hopping of the carriers in an exponential DOS from E_F to a single transport level is usually explained in terms of their activation energy, E_a [70, 71]. At room temperature, the activation energy extracted from the slope is found to be 27meV, which corresponds to the thermal energy and a temperature of around 310K. The activation energy is found to be nearly constant at about 0.3eV, between temperatures of 196K and 240K and also 245K to 300K, for

different applied voltages in saturation. The small variation in E_a suggests that the energetic position of the transport energy remains almost constant within the examined temperature range. The fact that the activation energy does not change in most of the measured range indicates that the concentration of carriers is about constant as well, confirmed in Fig.3.23. And that the movement of quasi-Fermi level towards the HOMO level does not cause a major change in the amount of carrier concentration. The small change seen between 235K and 250K can be seen as a transition between two different conduction mechanisms with similar activation energies. These transport mechanisms are not totally distinguishable.

At lower temperatures, the activation energy must be reviewed with caution as the back ohmic contact forms a barrier to carrier flow into the semiconductor. This is because as the Fermi level lowers in the semiconductor with temperature, a work function difference between the ohmic metal and the semiconductor is introduced.

3.4.3 Temperature Effects on Doped TIPS/PAMS Schottky Diode

Figure 3.26 shows the I-V characteristics of a Schottky diode with doped TIPS/PAMS as the active layer measured at various temperatures from 138K to room temperature (RT). Decreasing the temperature causes the threshold voltage to shift towards more negative voltages most likely due to a thin layer of accumulated space charge between the metal and the interface. At each measured temperature, the voltage is swept from one direction to another. With sudden reversal of direction, not all accumulated charge from the previous cycle is discharged instantaneously. Thus, a thin layer of accumulated space charge is left to remain.

At room temperature a flat quasi-Fermi level is assumed across the thickness of the organic semiconductor under steady state conditions. To reach equilibrium and hence to achieve a flat quasi Fermi level, the injected carriers from the back metal need to penetrate through the distribution of localised states. Under both forward and reverse biases, a decrease in temperature causes the current to decline possibly due to the quasi Fermi level shifting to lower energies, as discussed previously and illustrated in Fig.3.21.

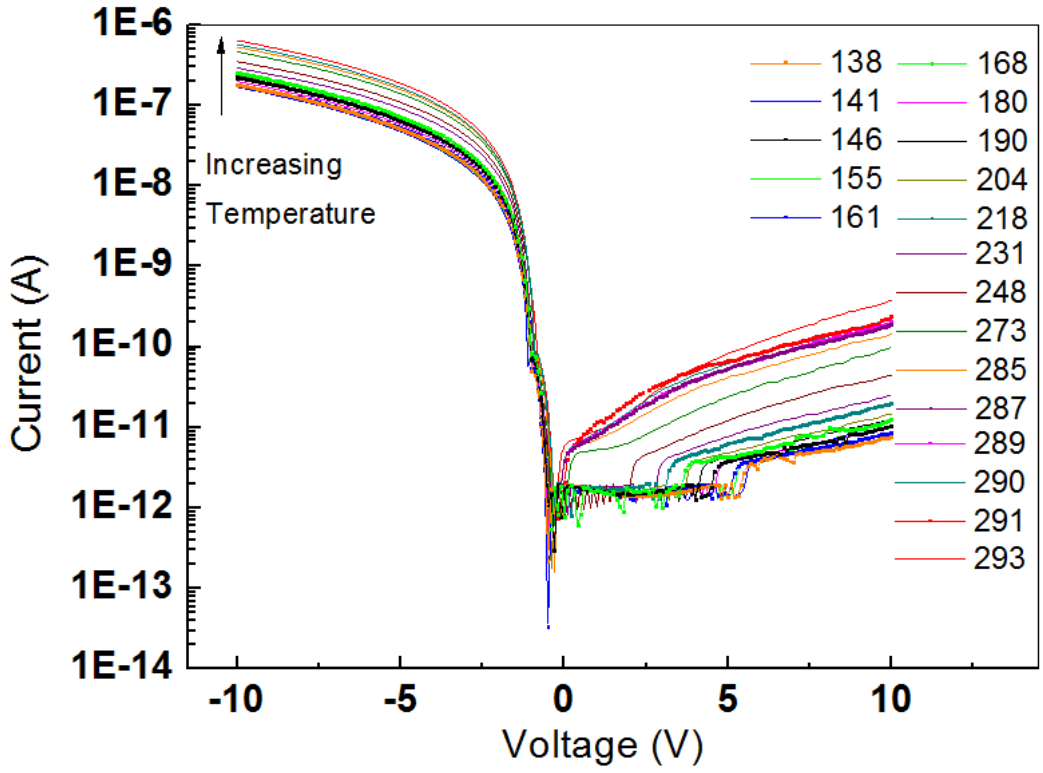

Figure 3.26. Current-Voltage (I-V) Characteristics of 0.3% DDQ doped TIPS/PAMS 1mm diameter Schottky diode at various temperatures from Table 3.1(b).

Interestingly the rectification ratios do not vary drastically with changes in temperature. The magnitude of the rectification ratio is approximately four orders of magnitude at room temperature, and four and half orders of magnitude at the lowest temperature of 138 K in the range -10 V to 10 V. These findings are in contrary to those obtained for TIPS/PTAA based Schottky diodes discussed previously. At lower temperatures, the thermal energy of the carriers is reduced and thus it becomes harder for the carriers to penetrate to the equilibrium level. Also, the hopping rate is reduced and it becomes harder for the carriers to obey the Fermi Dirac distribution function across the thickness of the organic layer. However, in the range of 248-138K, the reverse current in small reverse bias, appears to be independent of temperature variation. This effect can be associated to the conduction at an intrinsic level.

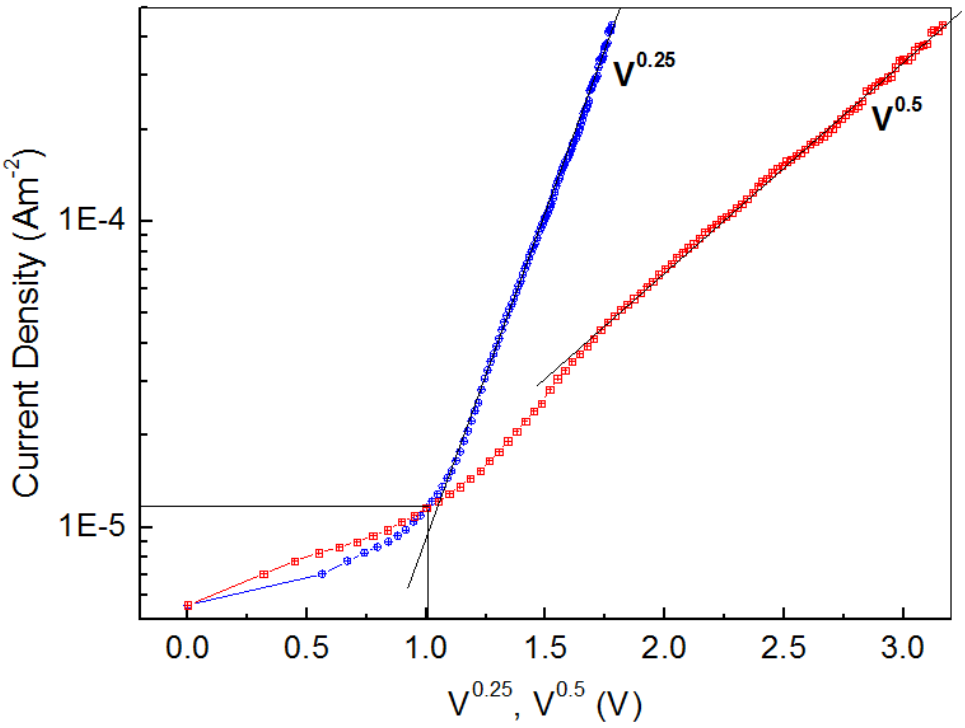

Figure 3.27. Plot of reverse current density, J against $V^{0.25}$ and $V^{0.5}$. A linear fit it obtained from the plot of J-$V^{0.25}$.

The plot of the logarithmic reverse current density against $V^{0.5}$ and $V^{0.25}$ at 305K is shown as in Fig.3.27. Quarter power law applies when barrier height lowering is due to both the image charge and externally applied field assuming the depletion region is abrupt. However if depletion region approximation does not apply, half power law dominates. The slope in Fig.3.27 determines the value of dopant concentration, using quarter power law in Eq. (3.36), which was approximately $2x10^{17}cm^{-3}$ for TIPS/PAMS Schottky diode. This value is in agreement to that obtained for TIPS/PTAA Schottky diode at room temperature. Such high dopant concentrations are most probably due to photo-oxidation effects and residual dopants included during synthesis.

The variations of the depletion region width and Debye length were further explored with change in temperature as in indicated in Fig.3.28. From the plot, both the depletion region width and the Debye length were found to increase as the temperature falls. At room temperature, L_{De} is approximately 5% of W_{dep}. Abrupt depletion region assumption can be applicable if the W_{dep}/L_{De} as in Eq.(3.15) is large, which stands true even at lower temperatures.

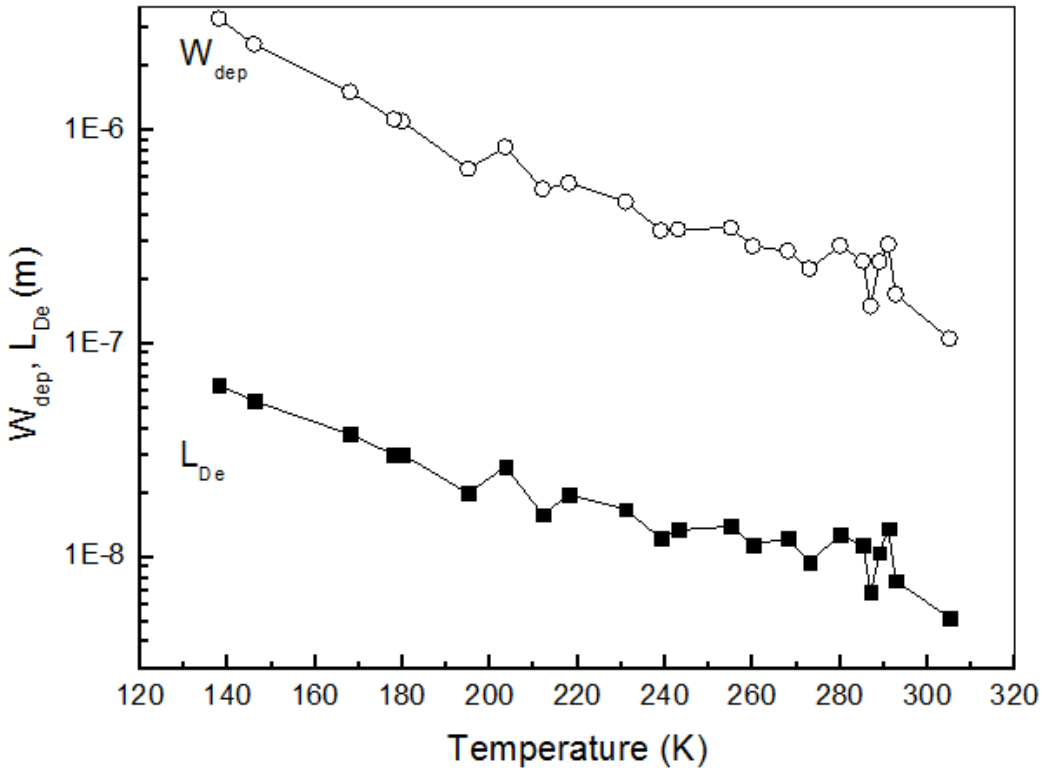

Figure 3.28. The depletion region width W_{dep} and the Debye length L_{De} plotted against temperature. Both parameters are seen to increase with decrease in temperature.

Under forward bias, the increase in the current levels is due to the decrease in Schottky barrier height and also the temperature dependence of the Fermi Dirac statistics. The latter provides energy to the holes to hop and redistribute into higher energy levels. For a p-type organic semiconductor with disorder, assumption of an exponential DOS means that as the energy moves downwards, the hopping transitions will rise exponentially. Therefore, although the free hole concentration is essentially unaffected, the hopping transition rate may be highly affected by the number of localised states available at higher energies.

In the forward characteristics of Fig.3.26, a small hump is visible at lower voltages in the exponential region, which is thought to be due to the oxidation of the aluminium contact. The current density, to explain the ideality factor, of Schottky barrier diode in exponential region can be given in terms of Eq. (3.18). In crystalline semiconductors, an ideal value of ideality factor is given by 1 (Eq. (3.16)). Thus assuming that the interface is free of extrinsic trap states and carriers

contributing to the current come from the energy range with width of ~kT. In the range 180-305K from the plot in Fig.3.29, the ideality factor of TIPS/PAMS blend increases between 3 and 5. Below 180K, the ideality factor gradually increases above 5. The value of ideality factor obtained at 138K is almost twice that of the ideality factor obtained at room temperature.

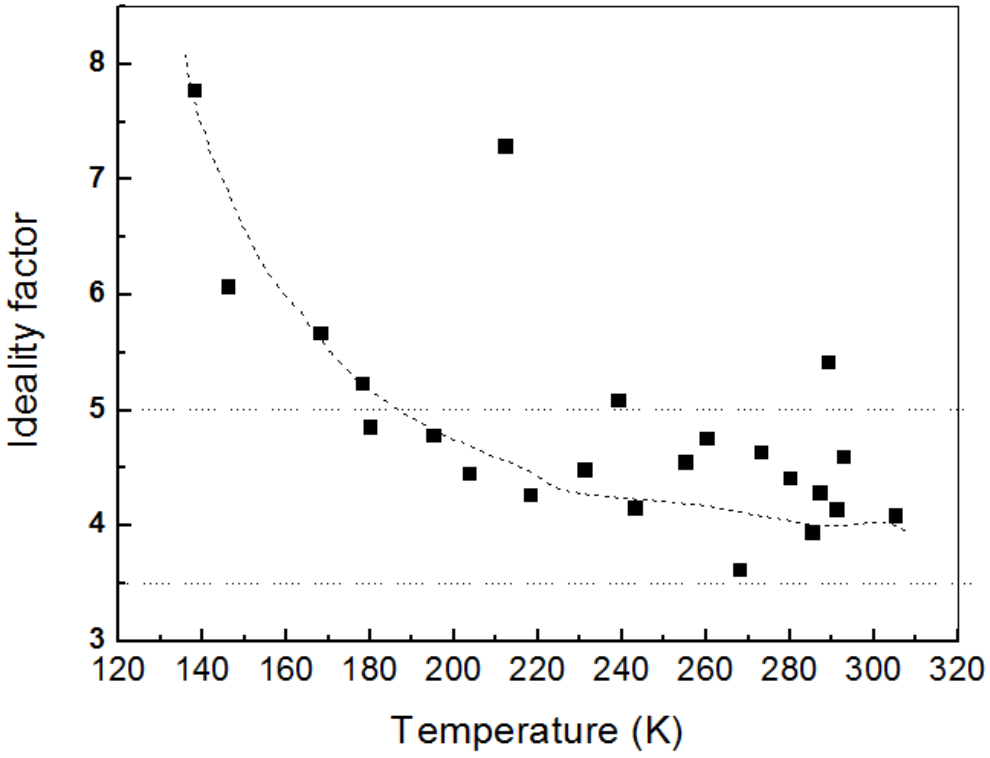

Figure 3.29. The change in ideality factor with temperature. Ideality factor increases slowly till about 180K in the range of 3 to 5. After 180K, ideality factor increases rapidly.

The change in ideality factor is indicative of the interface between the metal and the organic semiconductor changing with temperature. The interface at lower temperatures cannot be assumed to be free of extrinsic trapping states or other non-ideal behaviours. Although the value of ideality factor increase, T_0 is seen to decrease with decrease in temperature indicating that the Fermi Dirac statistics which governs the carrier distribution falls more sharply with a decrease in energy. T_0 obtained at room temperature is approximately 1250K and is less than the one obtained for TIPS/PTAA at room temperature (~1700K). kT_0 also decreases showing that the width of the energetic distribution of holes becomes narrower with decrease in temperature. The decrease in

the width of the energetic distribution of carriers at lower temperatures increases the possibility of holes crossing over at other potential barriers thus the assumption of ignoring carrier taking any alternate routes for conduction may not be wise. This limits the applicability of Eq. (3.18) at lower temperatures.

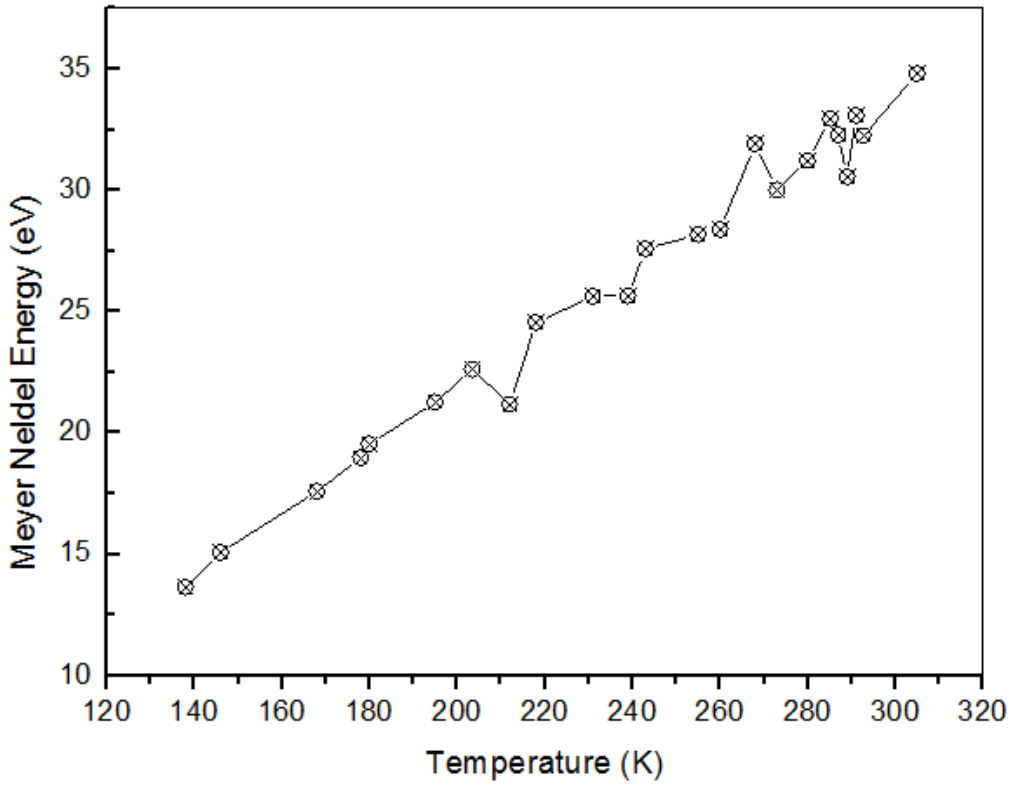

Figure 3.30. Meyer Neldel Energy (MNE) plotted against temperature associated with the disorder in the organic film.

As the temperature decreases, T_C falls and so does MN energy [72] (Fig.3.30). Hence, there must be a relationship between absolute temperature and the energetic distribution of DOS. In organic semiconductors, justification of the MN effect for the charge carrier mobility and the physical meaning of MNE are still heavily under debate. Even though numerous theoretical efforts based on a polaron model have been recommended to rationalize the MNR in different systems [73].

A significant assumption made by the suggested theory is that the MNE in disordered organic semiconductors is directly related to the width of the Gaussian DOS, thus providing a technique for evaluation of the degree of energetic disorder in the material. Furthermore, it is said that the

MNR effect for the temperature dependences of the charge carrier mobility is due to changing the carrier concentration and not because of change in the width of the DOS [74]. MNE obtained from Fig.3.30 at room temperature and the lowest temperature measured (138K) is approximately 35meV and 14meV respectively. Conversely, MNE obtained from TIPS/PTAA Schottky diodes at room temperature and 154K is approximately 31.5meV and 14meV respectively. The difference in MNE between doped TIPS/PAMS and TIPS/PTAA is thought to depend on energetic disorder in the individual blends. At room temperature, T_C acquired from Fig.3.30 using Eq. (3.14) and p from Fig.3.31 is roughly 400K and $2x10^{17}cm^{-3}$ respectively. At 138K, T_C and p are approximated to 159K and $5x10^{14}cm^{-3}$ respectively. This is confirmed with the increase in Debye length seen in Fig.3.28 when the temperature is decreased. Debye length at 138K from Fig.3.28 is nearly 0.6nm.

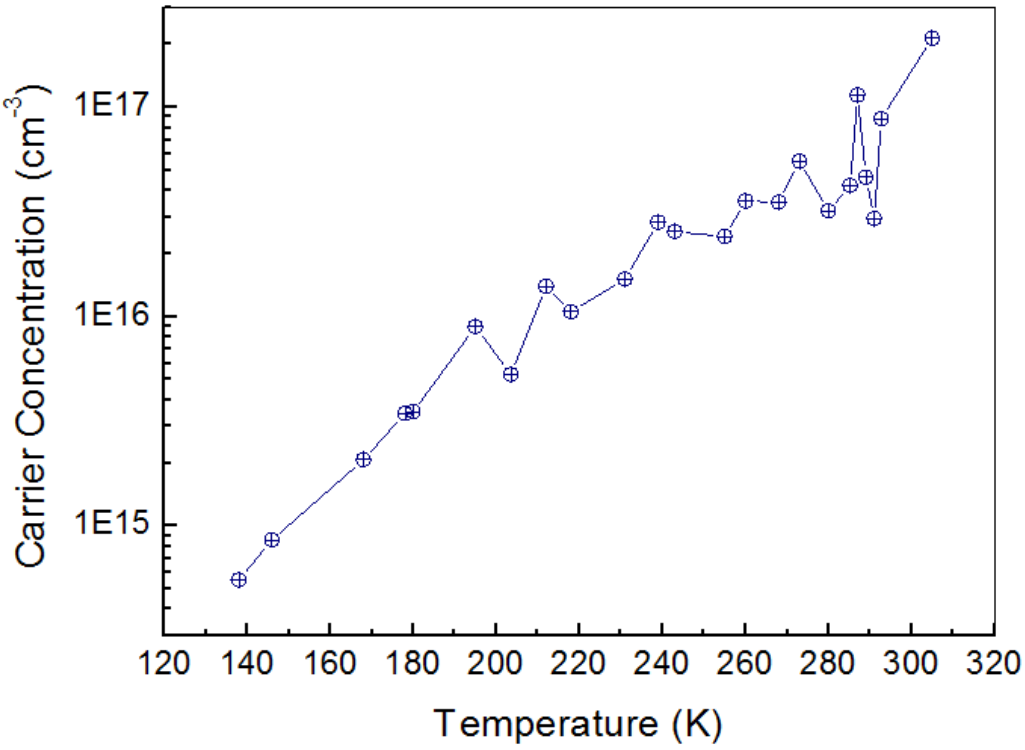

Figure 3.31. Carrier concentration against temperature. Carrier concentration decreases almost linearly with decrease in temperature.

The plot of carrier concentration and temperature is given in Fig.3.31. Intrinsic hole concentration is more than dopant concentration at higher temperatures for carrier conduction whereas the

opposite is true at lower temperatures. The material acts as an intrinsic semiconductor at higher temperatures as the quasi Fermi level moves to be closer to the intrinsic energy level. At lower temperatures, the intrinsic carriers are considered negligible.

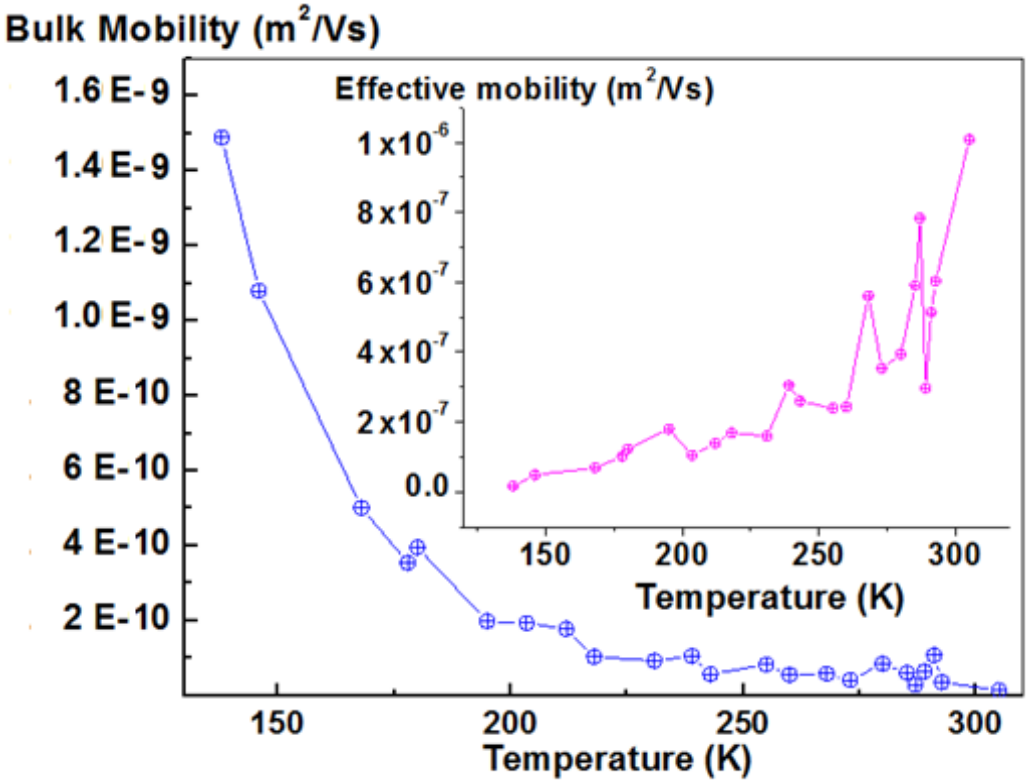

Figure 3.32. Plot of bulk mobility against temperature shows that bulk mobility is higher at lower temperatures. Inset is the plot of effective mobility with temperature. Effective mobility is seen to decrease with decrease in temperature as it is dependent on the carrier concentration.

In organic semiconductors, the effective mobility is directly dependent on the carrier concentration as demonstrated in Eq. (2.17). K is obtained from the gradient of the plot of J against V_{app}^{m+2} in the saturation region, n is obtained from Fig.3.31 and m is obtained using Eq. (2.18). Therefore, μ_{eff} at room temperature is approximately $10^{-2}cm^2V^{-1}s^{-1}$ for doped TIPS/PAMS blend as compared to about $5x10^{-3}cm^2V^{-1}s^{-1}$ for TIPS/PTAA from Section 3.4.2. The fall in carrier concentration with temperature causes the effective mobility to fall as well (Fig.3.32). The transport energy is greatly dependent on the carrier concentration and thus as the temperature

decreases, the transport energy might see a shift to lower energies. Transport energy, in organic semiconductors, is defined as a hypothetical energy level after which the carriers can jump between localised states as the states are closer together. The concept of transport energy is supported by the experimentally obtained T_0 values from the exponential region suggesting that most of the carriers following the current come from an energy $kT_0 \approx 4kT$.

Only a fraction of the exponential DOS distribution is occupied by charge carriers. Hence, the carriers hopping from the Fermi level govern charge transport. This can be confirmed by an Arrhenius-type plot of ln μ against $1000/T$ where the temperature dependence of mobility [75, 76] can be obtained. The plot provides the activation energy dependent on the carrier concentration giving the temperature independent position of the Fermi level position with respect to the centre of the DOS. At lower carrier concentrations, a non-Arrhenius type temperature dependence is expected from the plot of ln μ against $1000/T^2$. The charge transport in such a case is predominantly due to the hopping mechanism followed by the carriers to hop from a temperature dependent equilibrium DOS distribution [77, 78].

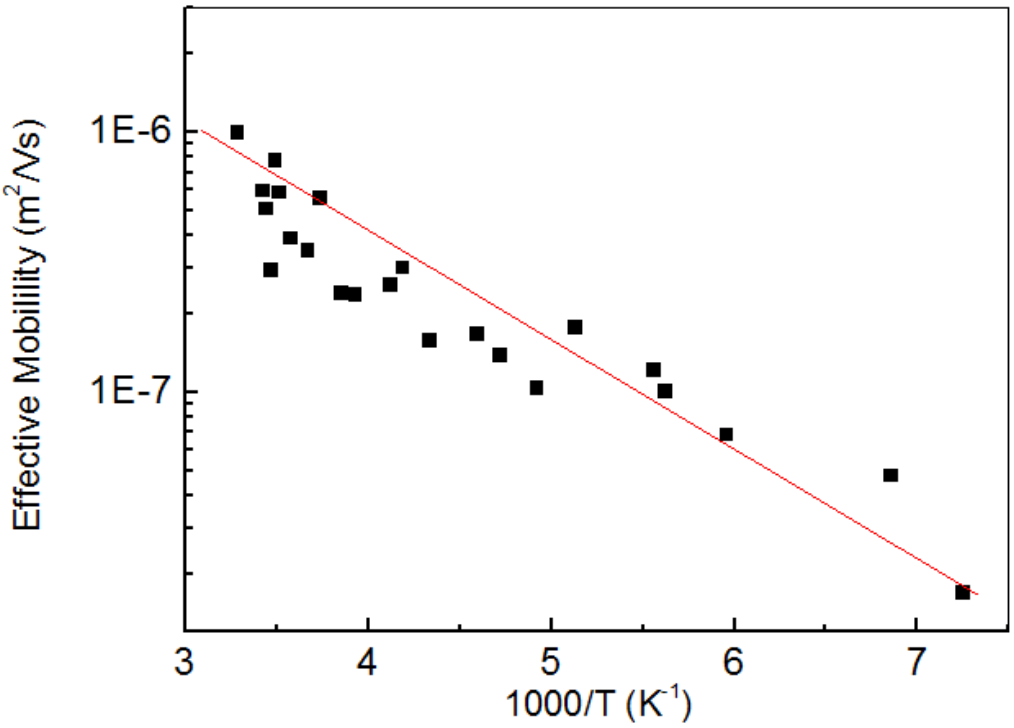

Figure 3.33. Arrhenius plot of effective mobility against 1000/T gives a straight line. The slope provides an estimate of the transport energy.

Figure 3.33 demonstrates an Arrhenius plot of ln μ against *1000/T* providing the transport energy from the slope. An increase in the transport energy E_{tr} is partially compensated by an increase in the prefactor so that the thermally activated effective mobility as in TIPS-pentacene semiconductor can be explained by

$$\mu_{eff} = \mu_0 \exp\left(-\frac{E_{tr}}{kT}\right) \qquad 3.39$$

where μ_0 is the prefactor and E_{tr} is the transport energy in a disordered grain boundary. The effective mobility is demonstrated experimentally by the use of Eq. (2.17). The prefactor μ_0 is associated with parameters associated with crystalline solids and can be avoided by plotting log μ_{eff} against log of carrier concentration (Fig.3.34).

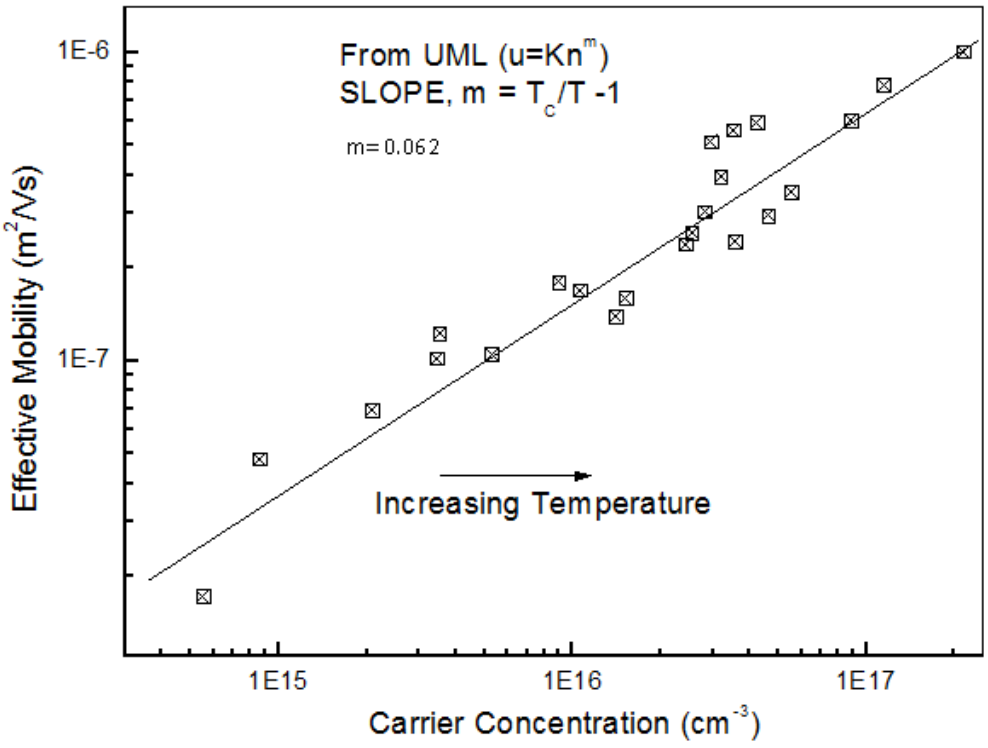

Figure 3.34. Effective mobility plotted against carrier concentration gives a straight line with both effective mobility and carrier concentration decreasing with decrease in temperature. The slope provides the value for m, a material and disorder dependent parameter.

MNE changes with disorder and is dependent on exponential DOS. The plot of effective mobility and carrier concentration gives a straight line whose intercept is *m*, a material dependent dimensionless parameter. The value of *m* in turn provides the ratio of T_C/T, a temperature dependent ratio. The values of T_C decreases as the temperature decreases. Figure 3.34 presents an agreement with the obtained ratio of exponential DOS to absolute temperature. It also indicates that the ratio of total injected carrier density to the free injected carrier concentration (defined in Appendix B) is constant for all temperatures in saturation region. T_C obtained from Fig.3.34 is approximately 320K. This is much less than expected and can be because both the effective mobility and carrier concentration are obtained experimentally with changing temperature.

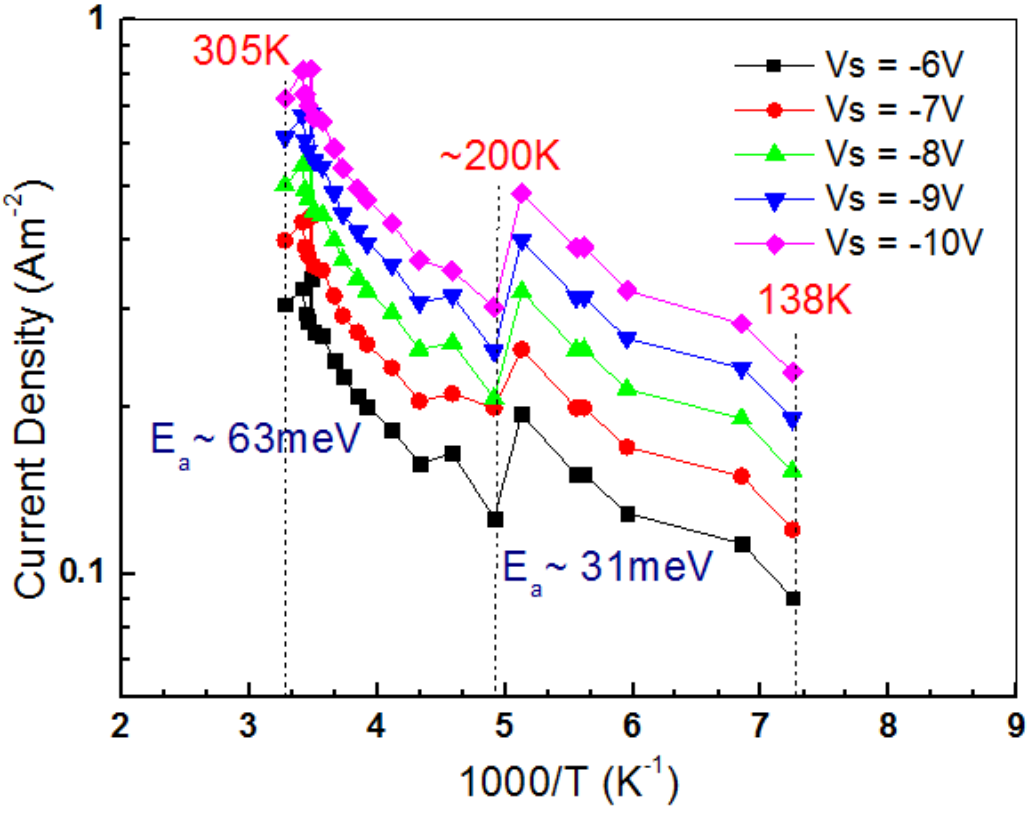

Figure 3.35. Arrhenius plot of saturation current density against 1000/T provides the activation energy from the slope. In the range 138 to about 210K, the activation energy E_a is 31meV. Above 210K to room temperature, E_a is approximately doubled.

Plotting the Arrhenius plot of current density, J or conductivity, σ against *1000/T* in saturation for different applied bias is another way to obtain the activation energies in the forward region.

Figure 3.35 shows two obtained activation energies. At high temperatures from about 210-305K, the obtained E_a is around 63meV whereas below 210K the activation energy is halved. E_a~0.3eV obtained from *J* against *1000/T* plot of TIPS/PTAA Schottky diode is higher in the temperature range analysed.

Another method to obtain activation energy is shown by plotting the Arrhenius plot of conductivity against *1000/T* (Fig.3.36). Conductivity is obtained by measuring the deviation of the voltage from exponential into the saturation regime in forward bias. The conductivity is given by

$$\sigma = \frac{Jt_{OSC}}{q\Delta V} \qquad 3.40$$

where *J* is the current density, t_{osc} is the thickness of the organic layer, q is the electronic charge and ΔV is the deviation in potential in the neutral region.

$$\sigma = \sigma_0 \exp\left(-\frac{E_a}{kT}\right) \qquad 3.41$$

$$\log \sigma \propto -\frac{E_a}{kT} \qquad 3.42$$

where σ_0 is the prefactor obtained from the experimental results. E_a obtained from conductivity against *1000/T* plot in Fig.3.36 is 69meV in a high temperature range of around 305-200K and is 32meV below 200K. These values are in agreement with the activation energies obtained by *J-1000/T* plot in Fig.3.35 for the same range of temperatures. At lower temperatures, the temperature dependence of the interface between back ohmic metal and the organic semiconductor becomes important. This is because at much lower temperatures the ohmic contact may not longer be ohmic but a barrier to current flow may possibly form. The transport energy obtained from the Arrhenius plot of effective mobility against *1000/T* gives a higher value of (~77.9meV) for the range 138-305K.

The two different activation energies obtained within the temperature range measured is thought to be due to two different conduction mechanisms present in the system. These activation energies are thought to be associated with Meyer Neldel energy and hence the distribution of states. A

model based on the statistical shift of E_F for inorganic materials is considered in terms of organic materials. This is dependent on the movement of the Fermi level with respect to the HOMO level with the change in temperature. The gap between the Fermi level E_F and the HOMO level E_{HOMO} increases with the increase in temperature and the rate of change of E_F is dependent on the gradient for the density of states. Two activation energies must then be due the dc conductivity in the extended extrinsic states. These extrinsic states also follow an exponential distribution and vary by Arrhenius dependence [79].

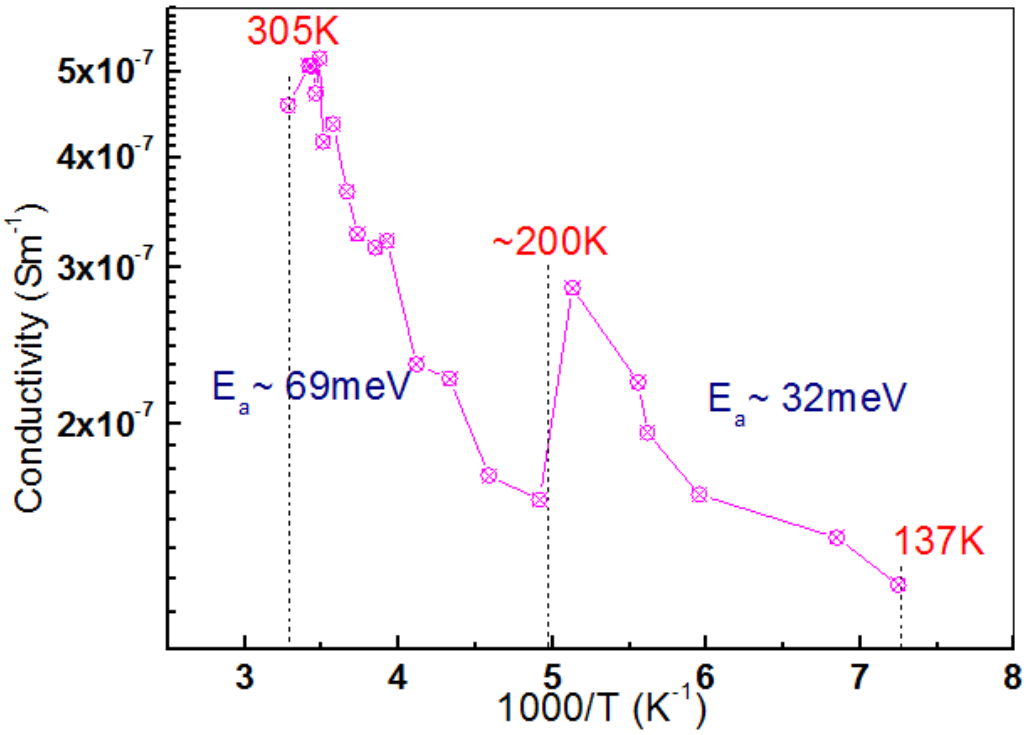

Figure 3.36. The variation of conductivity in the neutral region against 1000/T. Similar activation energy of 32meV is obtained in the range 137 to about 210K. Above 210K to room temperature, E_a is approximately doubled.

The temperature dependence of conductivity is very interesting as it provides similar results with the bulk limited currents. The change in activation energy is from ~69meV at higher temperature to ~32meV at lower temperatures corresponding to the 730K and 371K respectively. This transition is said to be because of the existence of two different temperature regions where two different transport mechanisms dominate individually. These are separated at around 200K due to

the charge transfer between two distributions with different occupancies and can coexist in the same device. The lower section of the temperature range in both Fig.3.35 and Fig.3.36 is indicative of one mechanism whereas the upper section is indicative of another transport mechanism. The existence and the dominance of these mechanisms are dependent on the structure of the sample and the temperature range being measured.

The high value of activation energy, corresponding to the characteristic temperature of 730K, observed is thought to be from the activated hopping in the band tail of the intrinsic distribution thus is consistent with the model proposed on the statistical shift. The lower value of activation energy is due to extended state transport as the Fermi level moves into lower energies with lower temperature and 371K is the characteristic temperature relating to ~32meV.

3.5 CAPACITANCE-VOLTAGE (C-V) CHARACTERISTICS OF TIPS-PENTACENE SCHOTTKY DIODE

Capacitance-Voltage (C-V) measurements are considered to be one of the most essential electrical measurements for devices. For organic Schottky diodes, they can be used to evaluate important device characteristics such as the impurity concentration [13, 82], interface, bulk and surface state characteristics [83-86]. A changing dc voltage and a constant small signal ac voltage is applied to the Schottky diode and can be defined in terms of both real and imaginary parts from the resulting admittance (as analysed in detail in chapter 5). The capacitance is taken to be the imaginary part whereas the conductance is considered as the real component.

The device can be illustrated as a small signal equivalent circuit model consisting of a capacitor and in parallel with a resistor, and the combined RC in series with a contact resistor. If deep trapping and series resistance effects are neglected, the equivalent circuit is just made up of a capacitor due to space charge in the organic semiconductor and the resistance due to residual conductance of the diode.

Figure 3.37 shows the C-V plot of a doped polycrystalline organic Schottky diode. The diode consists of a semiconducting layer of TIPS-pentacene doped with 0.5% of DDQ on top of evaporated gold. The depletion capacitance steadily increases with the application of a small reverse bias and is associated with the depletion region.

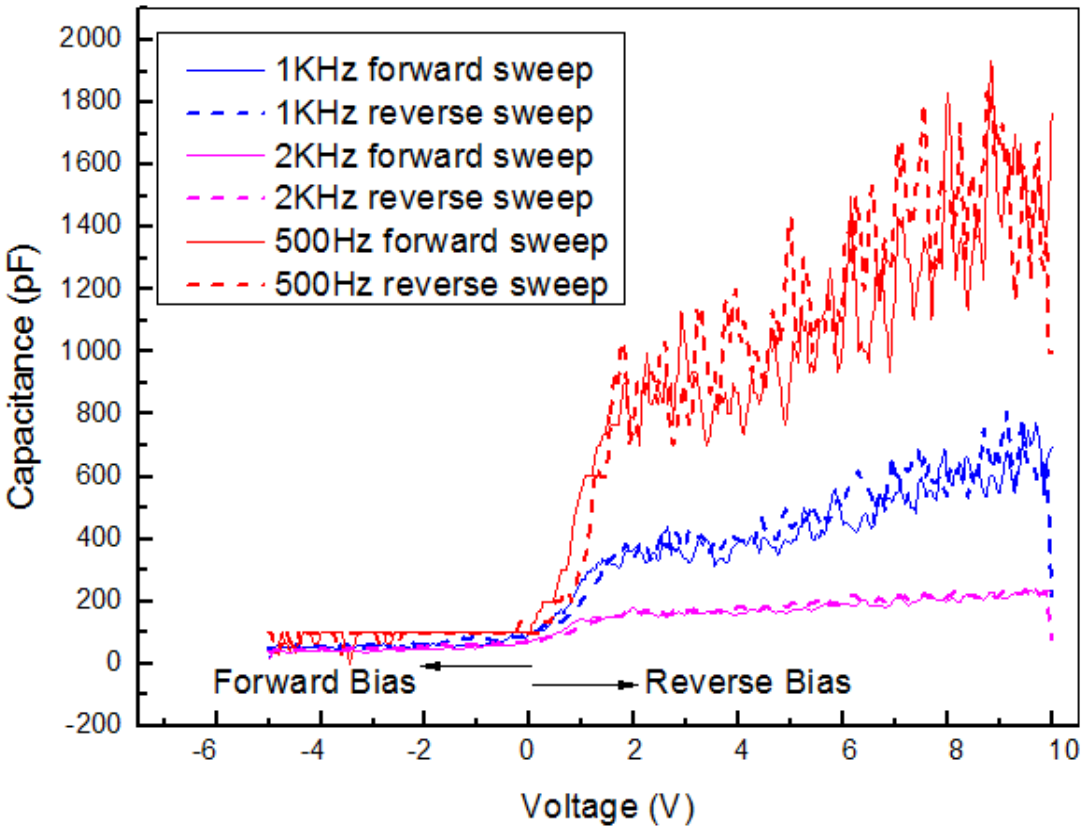

Figure 3.37. Capacitance Voltage characteristics of a 2mm diameter Schottky diode with active layer, TIPS doped with 0.5% of DDQ. The sample was dried on a hot plate before leaving it overnight in air. The small signal ac voltage applied is kept constant at 5mV whilst the dc voltage is varied.

Assuming that the Schottky diode is ideal with no interface layer, the slope of the inverse squared capacitance $1/C^2$ against voltage in depletion region provides information on the dopant (acceptor ion) concentration (Fig.3.38) [87] given by the term

$$N_D = \frac{-2}{q\varepsilon_0\varepsilon_S A^2} \frac{\Delta V}{\Delta\left(1/C^2\right)} \qquad 3.45$$

where N_D is the dopant concentration, A is the area of the Schottky diode, ε_S is the dielectric constant of the semiconductor, q is the electronic charge and ε_0 is the permittivity of free space.

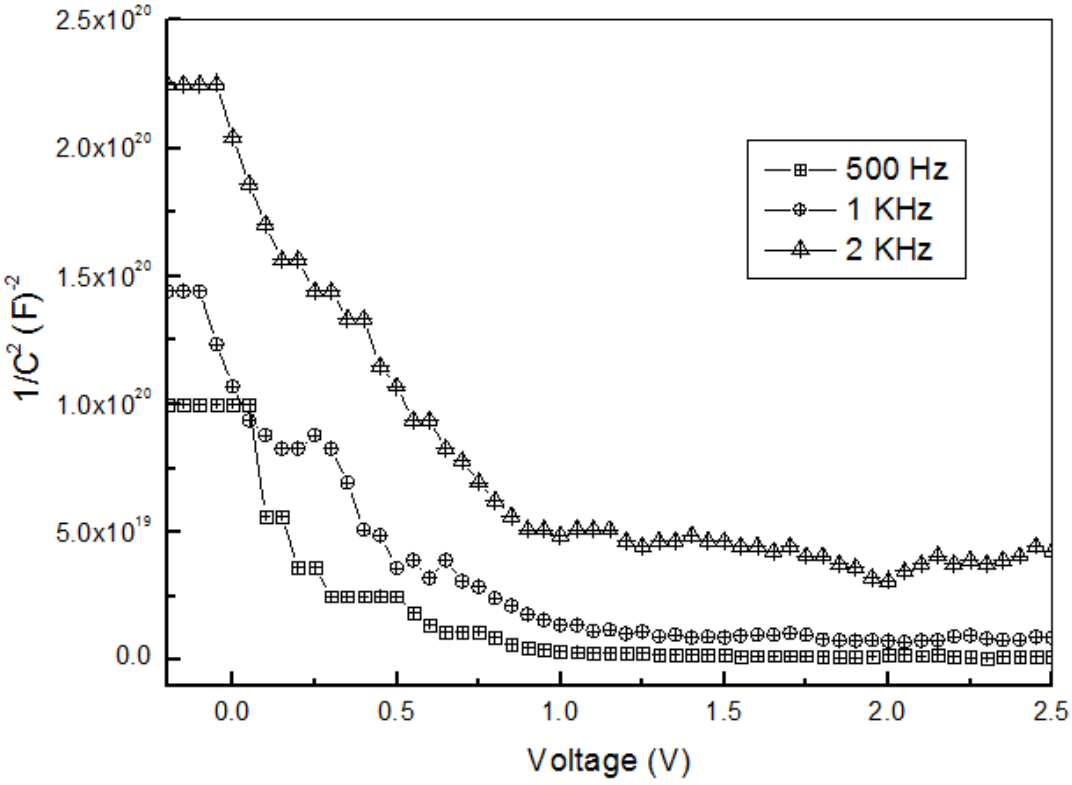

Figure 3.38. Plot of the inverse square capacitance against voltage at a frequency of 500 Hz and oscillating voltage of 5mV.

The dopant concentration N_D extracted at frequencies of 500Hz, 1kHz and 2kHz were approximately 7.6 x 10^{16} cm^{-3}, 5.2 x 10^{14} cm^{-3} and 2.98 x $10^{14}cm^{-3}$ respectively. The dopant concentrations obtained from such C-V measurements were lower than those extracted from current-voltage measurement of approximately $10^{17}cm^{-3}$ room temperature for both TIPS/PTAA and doped TIPS/PAMS blend. With C-V measurements, the dopant concentration is seen to decrease with increase frequency for the doped TIPS Schottky diode as in Fig.3.38. This is thought to be due to the low mobility of holes, which are unable to respond to the signal at higher frequencies. At such frequencies, the holes are only able to follow the dc signal which in turn decreases the contribution to capacitance. This means that the doping concentration obtained at the lowest measured frequency gives the best true estimation.

The built in potential V_{bi} observed from the intercept of $1/C^2$ against the applied voltage in Fig.3.38 varies with changes in the ac frequency. The high V_{bi} obtained maybe due to an interface layer formed between the metal and the organic layer.

3.7 DISCUSSION AND CONCLUSION

Detailed analysis of organic TIPS-pentacene based Schottky diodes is presented in this chapter. The rectification ratios achieved by using TIPS-pentacene produced better results than P3HT and PTAA [78, 81] indicating that TIPS-pentacene can be used in rectification circuits such as RFID tags. Various blends of TIPS-pentacene with organic materials are used to produce Schottky diodes. The use of TIPS solution alone as the active layer produced rough morphology and had poor adhesion with the gold electrode. Insulating organic binders such PAMS and PS with TIPS produced better morphology and improved connections with the ohmic contact.

Deposition of the drop cast layer on the ohmic contact is carried out on various temperatures. It is thought that varying the deposition temperature and drying in a solvent rich environment gives different nucleation rates and hence varied morphology. From the experimentation carried out, a lower temperature drying step help in the formation of larger grain sizes and introduces less disorder. It defines the intrinsic DOS and hence the width of the DOS. The width of the DOS is said to correspond to MNE and is believed to stay constant in the experiments involving the variation in temperature using a cryostat. This has been discussed in the text following Section 3.4. A number of chemical treatments are tried before and after the vacuum evaporation of the ohmic contact. Oxygen plasma treatment provides good adhesion. Treatment using PFBT did not provide any significant changes in the device structure and is not used in the fabrication of Schottky diodes. Addition of extrinsic dopants in the material such as DDQ did not have a major change in the current voltage characteristics and the dopant ions.

A new term for the SCLC in the saturation region of the forward characteristics is used in conjunction with UML to provide the dependence of current density on applied voltage. In reverse bias, the Schottky theory is used to find the dopant concentration. $ln\ J_R$ against $V^{0.25}$ gives good fits at room temperature. However, decreasing the temperature provides only a rough value for the dopant concentration. Therefore it is necessary to consider the exponential distribution of states with the Schottky theory.

A new blend using disordered organic semiconductor, PTAA, is also tested as a binder in combination with TIPS-pentacene and provided a good compromise between better morphology, adhesion quality and enhanced conductivity. The blend is believed to introduce molecular disorder in the layer. The fact that the active layer is made up of two organic semiconductors

instead of one semiconductor and one insulator means that the properties of the resulting layer are changed. It is believed that addition of a disordered material with the polycrystalline semiconductor increases the disorder in the system, making the disordered properties more dominant. Therefore, the effects of temperature on the electrical parameters of the polycrystalline TIPS-based Schottky diodes are investigated. Two TIPS-pentacene blends i.e. TIPS/PTAA and 0.3% doped TIPS/PAMS are examined in detail for comparison. Such studies are essential in understanding the conduction processes of the organic device particularly in terms of trapping effects, which is useful in the development of device models for organic circuitry.

Several parameters such as dopant and carrier concentrations (N_D/p), effective mobility (μ_{eff}), depletion width (W_{dep}), effective Debye length (L_{De}) and the characteristic temperature of the carriers (T_o) are extracted from the current-voltage characteristics of the diode. At room temperature, their respective values are found to be approximately $5.7\text{x}10^{16}\,\text{cm}^{-3}$, $1.8\text{x}10^{-2}\,\text{cm}^2/\text{Vs}$, 185nm, 11nm and 780K for the TIPS/PTAA diode. As the temperature is lowered from room temperature for TIPS/PTAA based Schottky diode, most parameters are found to remain constant until a critical temperature. Below this temperature, the depletion region width and effective Debye length are found to increase. This is probably due to the error in the fits to the J_R against $V_R^{0.25}$ plots at lower temperature. In contrast the carrier mobilities, carrier concentrations and MNE are found to decrease possibly due to the shift in the quasi Fermi level to lower energies, resulting in a potential barrier at the ohmic/semiconductor interface. At low temperatures, the thermal energies of the carriers are also reduced resulting in reduced mobility. The ideality factor and T_0 are found to increase with decrease in temperature which is probably due to the energetic distribution of holes becoming wider with increasing energy. Finally, the activation energy of TIPS is found to remain constant at various saturation voltages within a temperature range of 196K to 240K and 240K to 300K. This suggests that the transport level is independent of temperature and practically constant at energy of 0.3eV.

Doped TIPS/PAMS based Schottky diode is also analysed in depth. Lowering of temperature caused most of the parameters to change immediately below room temperature, unlike TIPS/PTAA diode. The carrier mobilities, carrier concentrations and MNE are found to decrease with decrease in temperature. Ideality factor and bulk mobility is seen to increase with decrease in temperature. For organic disordered materials with exponential DOS, the ideality factor is assumed in the range 3-5. Thus a rise in ideality factor above 5 at a much smaller temperature

range identifies the increase in extrinsic trapping states or other non-ideal behaviours. In conclusion, the activation energy of doped TIPS/PAMS is also found. The activation energy is extracted from the slope of the Arrhenius plot of effective mobility against 1000/T and is approximately 80meV. Activation energy is found from the saturation region, J_s in forward bias at various different applied biases and confirmed by the conductivity plots. The Arrhenius plots of ln J_s against *1000/T* and conductivity against *1000/T* provide two approximate activation energies in two temperature ranges. From 138-210K, the extracted activation energy is around 30meV. Above 210K to room temperature, the extracted activation energy is approximately 66meV. This suggests two different results. From the plot of effective mobility against *1000/T* plot, the transport energy level is independent of temperature as it is seen to be constant. From Arrhenius plots of conductivity and saturation currents, the transport energy level is seen to be dependent on temperature range.

In the model considered in this thesis, the current in the exponential DOS in the grain boundaries may be represented by a single hypothetical transport energy with an abrupt edge, just like the crystalline solids (or the adjacent grains). Transport energy in disordered materials is likely due to the exponential distribution of carriers strongly following the Fermi Dirac probability. In Schottky diodes, the minimum energy over which the hopping of carriers produces any current is defined as the transport energy. The existence of activation energy in both the blends indicates that the theory of transport energy defining the mobility edge stands strong in polycrystalline materials. The activation energy observed in TIPS/PTAA is larger than the activation energies obtained for TIPS/ PAMS. Higher activation energy is a property of disordered materials and may be because of the dominion of PTAA in TIPS/PTAA blend (Section 3.4.2). Regio-irregular P3HT is known to show the activation energy of 0.35eV [88]. PTAA, on the other hand, have shown activation energy of 0.6eV from experiments carried out by Mathijssen et al. on OFETs using PTAA as the organic semiconductor [89]. Depending on the fabrication processes, the activation energy of around 60-170meV is observed for TIPS-pentacene based OFETs from previous experiments carried out by Park et al. [90]. Therefore, the two activation energies obtained in TIPS/PAMS blend (Section 3.4.3) may be an evidence of both intrinsic and extrinsic DOS with two different transport energy levels. As this sample is doped, the extrinsic DOS may be owing to the DDQ dopant ions. More experimental and analytical work is required to fully comprehend this speculation.

In the approach employed, it is established that the UML applies without considering the conduction mechanism- variable range hopping. The effective mobility is thus found using the mobility prefactor and the carrier concentration. The mobility prefactor is obtained from the saturation region of the Schottky diode where SCL currents are expected to dominate. In this thesis, the effective mobilities obtained from the current voltage characteristics are in the order of 10^{-2} $cm^2V^{-1}s^{-1}$. However, mobilities obtained in existing experiments on OTFTs made with pentacene are in the orders of 10^{1} $cm^2V^{-1}s^{-1}$. The magnitude of mobilities obtained in TFTs is assumed to be two orders of magnitude higher that the mobilities obtained in Schottky diodes because of the field-effect. Furthermore, the ratio between the free and the trapped carriers is also obtained. From our results, the effective mobility is seen to decrease with decreasing temperature. This is owing to the disordered grain boundaries in the polycrystalline material. The results are a proof that the polycrystalline material can be modelled in terms of grains and grain boundaries.

Small signal capacitance-voltage measurements are conducted at a few different frequencies. The dopant concentration is found from the slope of the depletion region from the plot of $1/C^2$ against voltage. At frequencies of 500Hz, 1kHz and 2kHz, the dopant concentration is 7.6×10^{16} cm^{-3}, 5.2×10^{14} cm^{-3} and 2.98×10^{14} cm^{-3} respectively. These are much lower than the dopant concentration obtained from the IV characteristics in previous experiments. It is seen that dopant concentration decreases with increasing frequency for a polycrystalline Schottky diode as it is harder for the carriers to follow the ac signal.

3.8 REFERENCES

[1] P. M Grant, T. Tani, W. D. Gill, M. Grounbi , T. C. Clark,J. Appl. Phys. 52 (1981) 869.

[2] Y. Ohmori, Y. Manda, H. Takahashi, T. Kawai, K. Yoshino, Jpn. J. Appl. Phys.29 (1990) 837.

[3] H. Tomozawa, D. Braun, S. D. Phillips, R. Worland, A. J. Heeger, H.Kromer, Synth. Met. 28 (1989) 687.

[4] H. Tomozawa, D. Braun, S. D. Phillips, A. J. Heeger, H.Kromer, Synth. Met. 22 (1987) 63.

[5] N. Greenham, R. H. Friend, Sol. Stat. Phys. 49 (1995) 69.

[6] S. Steudel, K. Myny, V. Arkhipov, C. Deibel, S. De Vusser, J. Genoe, P. Heremans, Nature Materials, 4 (2005) 597.

[7] N. Koch, A. Kahn, J. Ghijsen, J-J. Pireaux, J. Schwartz, R. L. Johnson, A. Elschner, Appl. Surf. Sci. 82 (2003) 70.

[8] H. K. Henisch, *Semiconductor Contacts*, Oxford Science Series, 1984.

[9] A. H. Agajanian, V. L. Rideout, *A bibliography on metal- semiconductor (Schottky barrier) contacts*, IBM TechRep. TR22-1745, March 1974.

[10] E. H. Rhoderick and R. H. Williams, *Metal-Semiconductor Contacts*, Clarendon, Oxford, 1988.

[11] L. J. Brillson, *Handbook on Semiconductors*, edited by P. T. Landsberg, North Hollad, Amsterdam, 1992.

[12] G. Margaritondo, Rep. Prog. Phys. 62, (1999)765.

[13] S. M. Sze, *Physics of Semiconductor Devices*, Second Ed., John Wiley and Sons, New York, 1981.

[14] S. K. Park, J. E. Anthony, T. N. Jackson, IEEE Electron Dev. Lett. 28, 10 (2007) 877.

[15] J. Chen, C. K. Tee, M. Shtein, J. Anthony, D. C. Martin, J. Appl. Phys. 103 (2008) 114513.

[16] A. Kahn, N. Koch, W. Gao, J. Polym. Sci. Part B: Polym. Phys. 41 (2003) 2529.

[17] H. Ishii, K. Sugiyama, E. Ito, K. Seki, Adv. Mater. 11 (2009) 605.

[18] D. Gupta, N. Jeon, S. Yoo, Organ. Elec. 9 (2008) 1026.

[19] B. A. Brown, Veres J, Anemian. R. M , Williams R. , Ogier S. D. , Leeming S.W., *Organic semiconductor layers*, U. S. Merck Patent GmbH (Darmstadt, DE) 2009, 7576208.

[20] J. Veres, S. Ogier, S. W. Leeming, D. C. Cupertino, S. M. Khaffaf, Adv. Funct. Mater, 13, (2003) 199.

[21] A. Babel, S. A. Jenekhe, Macromolecules, 37, (2004) 9835.

[22] R. J. Myers, *Verbal Communication*, 2008.

[23] S. K. Park, T.N. Jackson, J.E. Anthony, D.A. Mourey, Appl. Phys. Lett. 91 (2007) 63514.

[24] S. K. Park, J. E. Anthony, T. N. Jackson, EMC Technical Digest, (2006) 64.

[25] J. F. Chang, B. Sun, D.W. Breiby, M.M. Nielsen, H. Sirringhaus, Chem. Mater. 16 (2006) 4772.

[26] M. H. Choi, S. H. Han, S. H. Lee, D. J. Choo, J. Jang, S. K. Kwon, Organ. Elec. 10 (2009) 421.

[27] S. H. Han, J.H. Kim, S.M. Cho, S.H. Lee, D.J. Choo, M.H. Oh, J. Jang, Appl. Phys. Lett. 88 (2006) 073519.

[28] S. H. Lee, M.H. Choi, S.H. Han, D.J. Choo, S.K. Kwon, J. Jang, Org. Elec. 9 (2008) 721.

[29] O. D. Jurchescu, J. Baas, T.M. Palstra, Appl. Phys. Lett. 87 (2005) 052102.

[30] G. Horowitz, M. E. Hajlaoui, R. Hajlaoui, J. Appl. Phys. 87 (2005) 4456.

[31] G. Horowitz, M. E. Hajlaoui, Synth. Met. 122 (2001) 185.

[32] R. Bourguiga, G. Horowitz, F. Garnier, R. Hajlaoui, S. Jemai, H. Bouchriha, Eur. Phys. J. Appl. Phys. 19 (2002) 117.

[33] G. Horowitz, M. E. Hajlaoui, Adv. Mater. (Weinheim, Ger.) 12 (2002) 1046.

[34] V. I. Arkhipov, P Heremans, E. V. Emelianova, G. J. Adriaenssens, H. Bassler, J. Phys. Condens. Matter 14 (2002) 9899.

[35] W. L. Kalb, S. Haas, C. Krellner, T. Mathis, B. Batlogg, Phys. Rev. B 81 (2010) 155315.

[36] M. Matters, D. M. de Leeuw, M. J. C. M. Vissenberg, C. M. Hart, P. T. Herwig, T. Geuns, C. M. J. Mutsaers, C. J. Drurt, Opt. Mater. 12 (1999) 189.

[37] T. Okachi, T. Nagase, T. Kobayashi, H. Naito, Apply. Phys. Lett. 94 (2009) 043301.

[38] P. Stagllinga, H. L Gomes, F. Biscarini, M. Murgia, D. M. De Leeuw, J. Appl. Phys. 96 (2004) 9.

[39] N. Sedghi, D. Donaghy, M. Raja, S. Badriya, S. J. Higgins, W. Eccleston, J. Non-Crys. Solids 352 (2006) 1641.

[40] M. Ullah, I. I. Fishchuk, A. Kadashchuk, P. Stadler, A. Pivrikas, C. Simbrunner, V. N. Poroshin, N. S. Sariciftci, H. Sitter, Appl. Phys. Lett. 96 (2010) 213306.

[41] S. Tsurekawa, K. Kido, T. Watanabe, Philos. Mag. Lett. 85 (2005) 41.

[42] H. S. Kong, C. Lee, J. Appl. Phys. 78 (1995) 6122.

[43] Z. Ahmad, M. Sayyad, Physica E. 41 (2009) 631.

[44] R. Gupta, K. Ghosh, P. Kahol, Physica E.41 (2009) 1832.

[45] N. F. Mott and R. W. Gurney, *Electron Processes in Ionic Crystals*, UK, Oxford University Press, 1948.

[46] S. Baranovskii, I. Zvyagin, H. Cordes, S. Yamasaki, and P. Thomas, Phys. Status Solidi B 230, (2002) 281.

[47] A. J. Campbell, D. D. C. Bradley, and D. G. Lidzey, J. Appl. Phys., 82, 12, (1997) 6326.

[48] A. Rose, Phys. Rev. 97, (1955) 1538.

[49] M. A. Lampert, P. Mark, Phys. Rev. 103, (1956) 1648.

[50] M. A. Lampert, P. Mark, *Current Injection in solids*, Academic Press, New York, 1970.

[51] C. W. Tang and S. A. VanSlyke, Appl. Phys. Lett., 51, 12, (1987) 913.

[52] O. D. Jurchescu, J. Baas, and T. T. M. Palstra, Appl. Phys. Lett., 84, 16, (2004) 3061.

[53] M. Raja, W. Eccleston, J. Appl. Phys. 110, (2011) 114524.

[54] 0. L. Griffith, J. E. Anthony, A. G. Jones, D. L. Lichtenberger, J. Am. Chem. Soc. 132, (2010) 580.

[55] Y. S. Lee, J. H. Park, J. S. Choi, Opt. Mater. 21 (2002) 433.

[56] T. Yamaue, T. Kawai, M. Onoda, K. Yoshino, J. Appl. Phys. 85, 3 (1999) 166.

[57] S. Schols, S. Verlaak, C. Rolin, D. Cheyns, J. Genoe, P. Heremans, Adv. Func. Mater. 18, (2008) 136.

[58] Chih-Tang Sah, *Fundamentals of Solid State Electronics*, World Scientific, 2006.

[59] T. Li, P. Ruden, I. H. Campbell, D. L. Smith, J. Appl. Phys. (2003) 93, 4017.

[60] M. Madec, *Private Communication*, University of Manchester, 2009.

[61] M. Mahadavan, PhD Thesis, University of Liverpool, 2008.

[62] C. P. Jarrett, R. H. Friend, A. R. Brown, and D. M. de Leeuw, J. Appl. Phys., 77 (1995) 6289.

[63] G. Ganzorig, M. Fujihira, Appl. Phys. Lett., 77, (2000) 4211.

[64] P. Leempoel, M. C. Acuna, F. F. Fan, and A. J. Bard, J. Phys. Chem., 86, (1982) 1396.

[65] D. R .Kearns, G. Tollin, and M. Calvin, J. Chem. Phys., 32, (1960) 1020.

[66] A. Nollau, M. Pfreiffer, T. Fritz, K. Leo, J. Appl. Phys., 87, (2000) 4340.

[67] B. A. Gregg, S. G. Chen, and H. M. Branz, Appl. Phys. Lett., 84, (2004) 1707.

[68] R. A. Street, D. Knipp, A. R. Volkel, Appl. Phys. Lett. 82 (2003) 3907.

[69] R. A. Street, D. Knipp, A. Volkel, Appl. Phys. Lett. 80, (2002) 1658.

[70] M. C. J. M. Vissenberg, M. Matters, Phys. Rev. B 57 (1998) 12964.

[71] S. D. Baranovskii, T. Faber, F. Hensel, P. Thomas, J. Phys., Condensed Matter 9 (1997) 2699.

[72] W. Meyer and H. Neldel, Z. Tech. Phys. Leipzig 18, (1937) 588.

[73] A. Yelon, B. Movaghar, Phys. Rev. Lett. 65 (1990) 618.

[74] I. I. Fishchuk, A. Kadachchuk, J. Genoe, M. Ullah, H. Sitter, T. B. Singh, N. S. Sariciftci, and H. Bässler, Phys. Rev. B, 81, (2010) 045202.

[75] I. I. Fishchuk, V. I. Arkhipov, A. Kadashchuk, P. Heremans, and H. Bässler, Phys. Rev. B 76,(2007) 045210.

[76] N. I. Craciun, J. Wildeman, and P. W. M. Blom, Phys. Rev. Lett. 100, (2008) 056601.

[77] H. Bässler, Phys. Status Solidi B 175, (1993) 15.

[78] V. I. Arkhipov, I. I. Fishchuk, A. Kadashchuk, and H. Bässler, *Semiconducting Polymers: Chemistry, Physics and Engineering*, Second Ed., edited by G. Hadziioannou and G. Malliaras Wiley, New York, 2007.

[79] H. Overhof and P. Thomas, *Electronic Transport in Hydrogenated Amorphous Semiconductors*, Springer-Verlag, Berlin, 1989.

[80] M. Kikuchi, J. Appl. Phys. 64, (1988) 4997.

[81] P. W. M. Blom and M. C. J. M. Vissenberg, Mater. Sci. Eng. 27 (2000) 53.

[82] E. H. Rhodrick, R. W. Williams, Metal Semiconductor Contacts, Second Ed., Oxford, Clarendon, 1988.

[83] J. J Shiau, R. H. Bube, Solid State Electron, 29, (1986) 1153.

[84] P. Muret, Semicond. Sci. Technol. 3, (1988) 321.

[85] J. Werner, K. Ploof, H. J. Queisser, Phys. Rev. Lett., 57, (1986) 1080.

[86] P. Muret, D. Elguennouni, M. Missous, E. H. Rhoderick, Appl. Phys. Lett., 58 (1991) 155.

[87] J. Bastien, A. Assadi, S. Sderholm, J. Hellberg, M. Moge, Synth. Metals, 82 (1996) 97.

[88] C. Tanase, E. J. Meijer, P. W. M. Blom, D. M. de Leeuw, Phys. Rev. Lett. 91, (2003) 216601.

[89] S. G. J. Mathijssen, M. Cölle, H. Gomes, E. C. P. Smits, B. de Boer, I. McCulloch, P. A. Bobbert, D. M. de Leeuw*, Adv. Mater. 19, (2007) 2785.

[90] J. G. Park, R. Vasic, J. S. Brooks, J. E. Anthony, *Functionalized pentacene field-effect transistors with logic circuit applications*, website: *arXiv:cond-mat/0510317v1*, viewed: 06/10/2011, 2005.

CHAPTER 4- TWO DIMENSIONAL MODEL FOR ORGANIC POLYCRYSTALLINE SEMICONDUCTOR MATERIALS

A two-dimensional model for polycrystalline organic semiconductor is proposed. Firstly, a lateral representation of a polycrystalline material is considered including a number of grains and grain boundaries in thermal equilibrium. Application of a bias causes drift and diffusion mechanisms to contribute to current flow. Furthermore, a vertical representation for a thin organic layer based Schottky diode is developed. In thermal equilibrium, detailed analysis is conducted to find two boundary conditions; at the edge of the grains and in the grain. Conduction under forward bias is eventually considered assuming an exponential approximate to the Gaussian distribution for the DOS. Finally, Laplace DOS is proposed as a better alternative to the Gaussian DOS.

4.1 CHARGE TRANSPORT IN POLYCRYSTALLINE ORGANIC MATERIALS

Pentacene and its derivatives are p-type polycrystalline semiconductors consisting of ordered grains and narrow disordered grain boundaries, as discussed briefly in the previous chapters. In order to comprehend the conduction behaviour in the two distinct regions, the grains and grain boundaries are considered separately. A two dimensional deliberation is significant in organic devices, particularly with the need to scale down channel lengths and increase grain lengths. Development of lateral and vertical conduction in a polycrystalline material is investigated. In this chapter, detailed analysis of the potential variation in the grains and the grain boundaries is provided. Two boundary conditions are developed in order to define the shape in grain and grain boundary due to the field; at the edge of the grain in the z- direction and in the grain in the x-direction, as illustrated in Fig. 4.1.

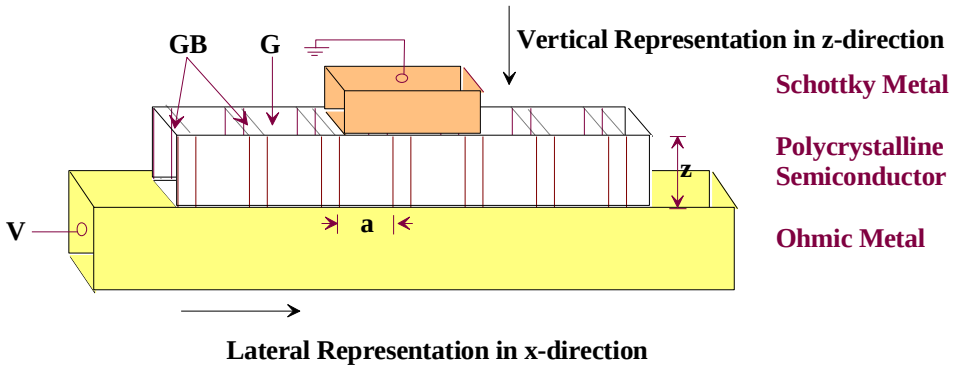

Figure 4.1. Schematics of a Schottky diode considering a thin organic polycrystalline layer sandwiched between an ohmic metal and a Schottky metal. A minimum number of grains and grain boundaries are assumed in the vertical direction. G and GB is representative of the grain and the grain boundary respectively, a is the distance between two grain boundaries and z is the thickness of the organic layer. The width of GB << G and is drawn wide for demonstration purposes only. x- and z- directions are illustrated above.

Lateral conduction in the case of a polycrystalline transistor, takes place across the channel length between the source and drain contacts, and at the interface between the dielectric and the organic layer. Upon application of an external bias, the conduction within the organic layer occurs

through movement of the carriers between the various aligned grains and grain boundaries present in the channel. This conduction is consequently dominated by either diffusion, drift or a combination of these mechanisms.

For the vertical conduction as in the Schottky diode, the carriers flow within the width of the active layer, from the bottom electrode to top or vice versa. For simplicity, we also assume that the Schottky diode comprise of a thin layer of organic semiconductor sandwiched in between the ohmic and Schottky metal (Fig.4.1). In such case, the grains and grain boundaries are parallel to the charge conduction. Consequently the vertical conduction is assumed to be across one layer of grain separated by grain boundaries (in z-direction), whilst the lateral conduction occurs across several grain and grain boundaries (in x direction). Grain size is important in vertical charge conduction analysis. In a Schottky diode, providing the grain size is large, the proposed vertical representation of a single layer of grains and grain boundaries is applicable. In printing processes, an OTFT has channel lengths of approximately 20μm whereas in organic diodes the thickness of the organic layer does not matter as long as the crystalline grain area is large. Subsequently, the approximation of a single layer of grains/grain boundaries across the thickness of the semiconducting layer is valid. However, this is an ideal scenario.

The model developed for a Schottky diode loosely fits for any polycrystalline based device having vertical conduction such as a MOS capacitor. An addition of an oxide layer between the Schottky metal (gate electrode) and the organic layer gives the structure of a MOS capacitor. However, the built in potential seen at the semiconductor/oxide interface is different than a semiconductor/metal interface. Without the application of an external bias, a vertical representation of the thin polycrystalline film is initially considered. In this chapter, an n-type organic semiconductor is assumed for the analysis.

4.2 CHARGE TRANSPORT IN LATERAL PATH

A model to analyse current flow in polycrystalline semiconductors has been proposed by Eccleston [1]. This is essentially the basis of polycrystalline theory discussed and illustrated in Fig.4.2. For the grain and grain boundary to be in equilibrium, the material is required to have the same ionisation potential. The transport level, in disordered material is defined as a subjective energy level, able of supporting a comparable current to that of an exponential density of states

under thermal equilibrium conditions. In such a case, the E_T and transport level at the adjacent edges of the grain and grain boundary are continuous. The inclusion of a transport level limits the model to small carrier concentrations. The concentration of electrons at the edge of the grains is dependent on the position of the Fermi level. The extent of the dip of the transport level in the grain is dependent on the size of the grain and the Debye length. For a grain reaching its intrinsic concentration at its centre, the Debye length can be defined as the distance over which the electron concentration increases to the intrinsic value such that the semiconductor becomes effectively neutral. The Debye length defined in the x-axis for the grains L_{Dx}, is dependent on the potential at the grain edge, is defined as in Eq.(4.1) [2]

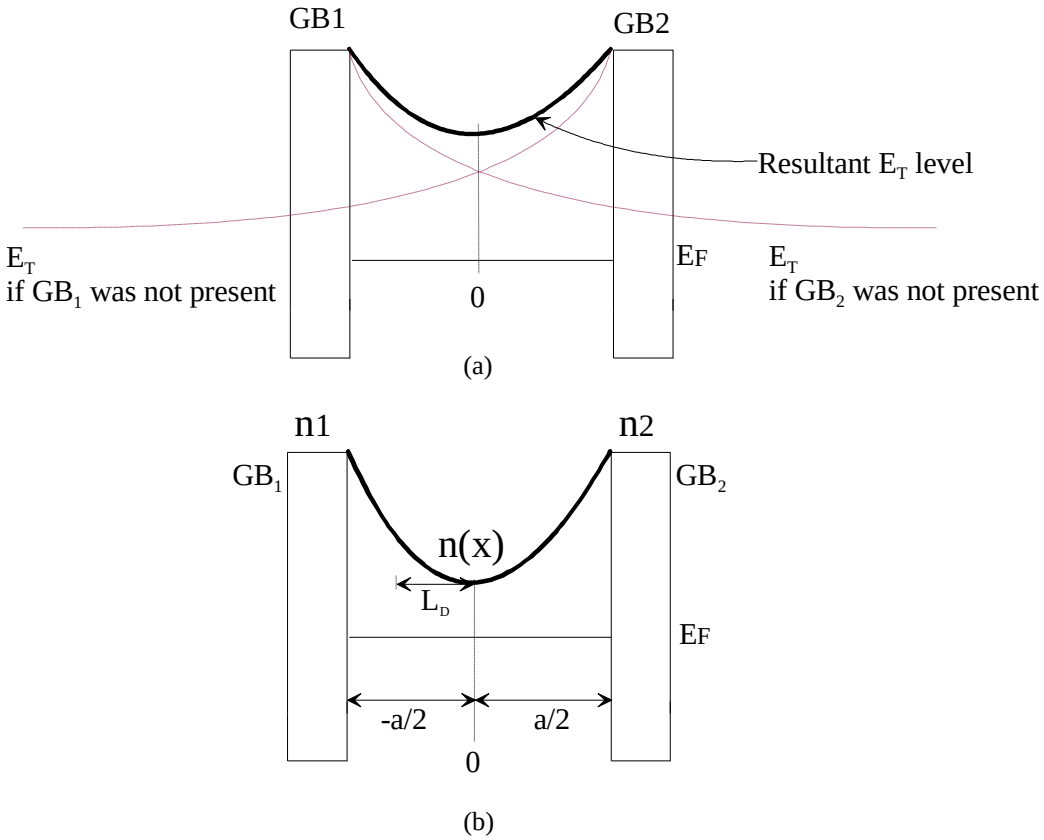

Figure 4.2. A flat quasi Fermi level is assumed indicating that the carriers in the grain are at thermal equilibrium without the application of a voltage. (a) The variation of transport energy, E_T, level with and without the presence of a second grain boundary in the x-direction. (b) The transport level reaches maximum n(x) at the centre of the grain. Debye Length, L_D, is taken from the centre of the grain. The carriers in the grain are considered to be in thermal equilibrium.

$$L_{Dx} = \left(\frac{2kT\varepsilon_0\varepsilon_g}{q^2 n} \right)^{1/2} \qquad 4.1$$

where n is the carrier density at the centre of the grain, T is the absolute temperature, ε_0 is the permittivity of free space and ε_g is the dielectric constant in the grains.

Figure 4.2a shows dotted curves extending from each grain boundary corresponding to a single crystal at infinity. In the case of the existence of grain boundary, an E_T level is formed for a semi-infinite grain as shown in the Fig.4.2b. The grain boundaries are assumed to be columnar and are much smaller than the grains. Also, the potential drop in the grain boundaries is taken to be negligible. Fig.4.2 shows that the grain boundaries are exaggerated in comparison to the grains and that the grain size is assumed to be equal to a. However, large potential barriers exist at the grain boundaries.

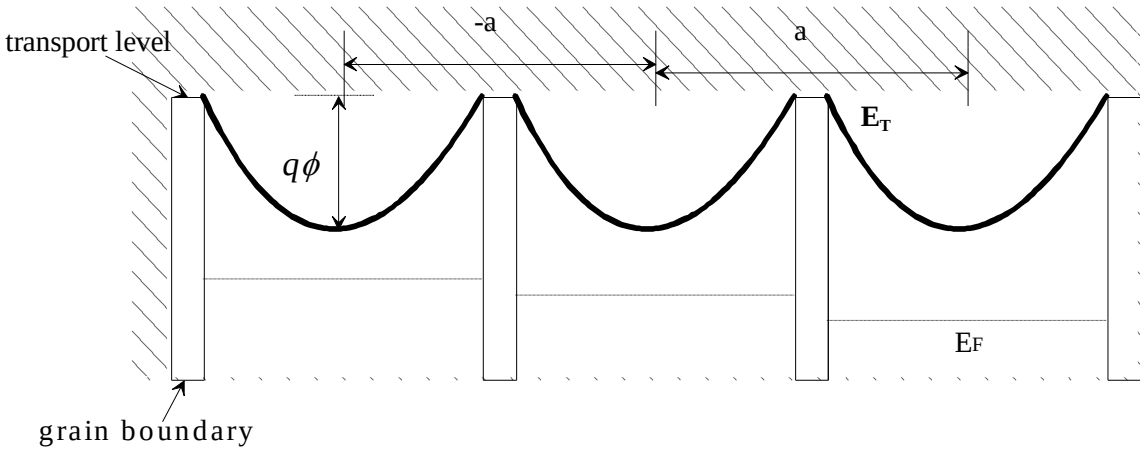

Figure 4.3. The Quasi-Diffusion Model for Polycrystalline organic material. The Fermi level is seen to change between neighbouring grains relative to the grain transport level, E_T.

The carrier conduction is dependent on mechanisms such a drift and diffusion. The quasi-diffusion model is presented in Fig.4.3. When low voltages are applied, there is no net potential drop between adjacent boundaries. However, there is a change in energy difference between the E_T level maximum and the Fermi levels between adjacent boundaries. The increase in distance between the E_T level maximum and the Fermi level at the grain centre corresponds to a decrease

in electron density. The gradient formed by such a mechanism is similar to classic diffusion without the linear variation with distance in this case.

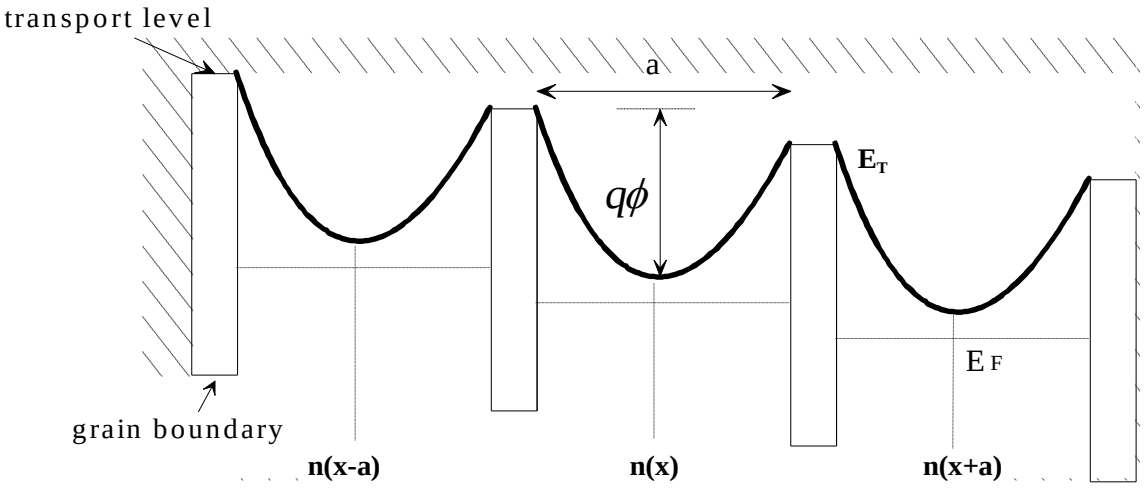

Figure 4.4. Quasi- drift model proposed for an organic polycrystalline material. The potential barrier at the grain boundary is gradually lowered. However, the electron concentration at the grain centres remains the same relative to the Fermi level.

Increasing the applied voltage will cause a net potential drop between adjacent grains. This does not have an effect on the Fermi level as it remains constant with respect to the E_T level maximum. This phenomenon is shown in Fig.4.4 and referred to as the quasi-drift since charge transfer occurs across a series of grain boundaries. An external field causes the potential barrier at the boundary to be lowered but the carrier density at the grain centres *n(x-a), n(x)* and *n(x+a)* remains constant. When both the quasi-drift and quasi-diffusion mechanisms contribute towards the current flow, the energy diagram looks like Fig.4.5.

The electric field F_{xmean} is obtained by dividing the voltage falling across the material by the thickness of the film. At each grain boundary, the potential barrier to the flow of carriers is therefore assumed to be reduced by aF_{xmean}.

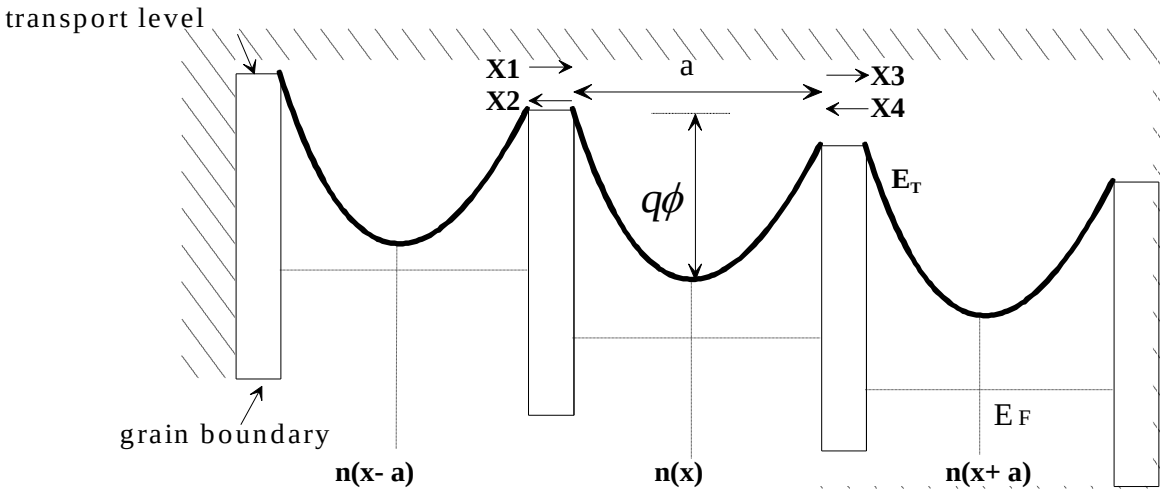

Figure 4.5. Flux seen at the boundary due to both quasi- drift and quasi- diffusion. X1, X2, X3 and X4 represent the position and direction of the carrier flux across the grain boundaries.

The flux of carriers across a certain grain boundary is thought to be proportional to the carrier density in the grain adjacent to the grain boundary/grain interface. The flux X at x is therefore written as [1]

$$X(x) = 4avn(x)\exp\left(\frac{q\emptyset}{kT}\right)\left[\sinh\frac{qaF_{xmean}}{kT}\right] - 2a^2v\frac{\partial n}{\partial x}\exp\left(\frac{q\emptyset}{kT}\right)\left[\cosh\frac{qaF_{xmean}}{kT}\right] \quad 4.2$$

where v is the frequency of electrons crossing the grain boundary, $n(x)$ is the density of carriers at the grain centre, $\emptyset$ is the potential barrier at the grain boundary relative to the centre of the grain in the absence of an applied field.

At a small electric field or for bigger grain sizes, $F_{xmean} \leq 2kT/qa$, $X(x)$ in Eq. (4.2) can be simplified to

$$X(x) = -D\left[\frac{dn(x)}{dx}\right] + n(x)\mu F_{xmean} \qquad 4.3$$

where $D = \frac{1}{4}a^2 v \exp\left(\frac{q\emptyset}{kT}\right)$ and $\mu = \frac{1}{4}\frac{a^2 v \exp\left(\frac{q\emptyset}{kT}\right)}{kT/q}$. D is defined as the quasi-diffusion coefficient whereas μ is the quasi-mobility of the carriers. The two terms defined in Eq. (4.3) can be regarded as diffusion and drift flux components respectively. The simplified X(x) indicates that although the flux at the grain centre is controlled by the potential barriers at the grain boundaries, the carrier conduction at the grain centre resembles that of inorganic crystalline materials.

Observation signifies that the quasi-diffusion coefficient, *D*, provides the Einstein's relationship as in Eq. (4.4) (Appendix C) [1, 2]. This is noteworthy as it indicates the use of concepts quasi-diffusion and quasi-drift for carrier conduction in the grains.

$$D = \mu kT/q \qquad 4.4$$

However, as both these conduction mechanisms are defined by the disordered grain boundaries there is an exponential dependence on the potential barrier. As the diffusion coefficient is dependent on the carrier concentration, the flux X(x) is approximately proportional to the gradient of the Fermi level. The increase in Fermi level gradient is observed with a decrease in the carrier concentration at the grain boundary contributing to the effective barrier lowering at the grain edge.

At a particular current level, under steady state conditions, there will be a small slope developed in the Fermi level or the carrier density would vary considerably (Appendix C) [1, 2]. Eq. (4.4) defines the single most important relationship used to understand the quasi Fermi level approximation in semiconductor devices under steady state conditions [2]. As the grain boundaries are small and the change in Fermi level gradient is smaller, the total effect is considered insignificant. In our analysis to follow, the Fermi level gradient is ignored and a flat quasi-Fermi level is considered throughout the grains and grain boundaries.

4.3 POTENTIAL VARIATION IN GRAINS AND GRAIN BOUNDARIES

Polycrystalline inorganic materials, such as silicon, give much lower mobility values than single crystal semiconductors. However, these mobility values are much greater than disordered/amorphous silicon. The extension of the existent polycrystalline theory is fundamental because polycrystalline organic materials such as pentacene and its derivatives are said to produce higher mobility values than the disordered organic materials [3]. Experimental results on disordered organic materials have shown mobility values of close to about $0.1cm^2V^{-1}s^{-1}$ [4, 5]. However, in the future, mobility value of more than $1cm^2V^{-1}s^{-1}$ is the target value in order to produce commercially viable circuits at 1μm minimum feature size [6]. A number of techniques are already being used to improve the feature size for the purpose of circuitry [7, 8]. Various researches, together with ongoing studies at Liverpool, are dedicated to unveil the potential of these polycrystalline organic materials despite their poor morphologies and other related difficulties [9-12].

Another reason for the extension of the polycrystalline model is for the purpose of computational modelling. Eventually, the models created for polycrystalline organic semiconductors in terms of the variation in potential in the grain and grain boundaries would provide a fundamental two dimension basis, not only for conduction in the vertical direction but also extend in the lateral direction. This could then be used as a building block to model conduction of a number of organic devices. The need to expand the dc theoretical models stems from the use of OTFTs as a fundamental component for many circuit applications. However primarily, it is essential that dc models for simple organic devices such an organic Schottky diode or MOS capacitor are understood. The aim is to look at diodes since an attempt to model devices in intrinsic polysilicon has already been published by the Organic Electronics group at Liverpool [1]. Development of dc theoretical models for such devices is crucial to ultimately develop compact models dealing with ac equivalent circuits. Software such as Cadence can be used as tools to consider dc models and to understand the more complicated ac models before fabrication is carried out. The aim is to have both a dc model and a transient model suitable for determining power-delay products for producing commercial applications in devices linked particularly to medical diagnosis. Building generic models will not only save the cost associated to fabrication but also avoid making complicated samples, save precious time and improve understanding of the structures. These models will be an immense help to design circuits for real applications.

The two dimensional situation, to explain charge transport, will be treated as two separate one dimensional problems at right angles to each other, as shown in Fig.3.7. The model consists of vertical columnar grains detached by vertical boundaries. In films that are compared with the lateral dimensions associated with devices, this is likely to be a good approximation. A number of assumptions are introduced for the development of this model making the model susceptible to errors. These errors, however, are constant throughout the model. There are two outlooks to such an approach. One is to solve Poisson's Equation for the grain boundary with the universal mobility law (UML) incorporated and the second is that the carrier density in the grain boundary determines the electrostatics in the grains. The latter is used for our analysis. The variation of potential is ultimately used for the calculation of carrier density.

To develop the model further, a few boundary conditions must be defined in thermal equilibrium. As no external voltage is being applied, the Fermi levels in the grain and the grain boundary are aligned such that lateral flux can be ignored. The flux due to the grain is in equilibrium with the flux due to the neighbouring grain boundary. Firstly, the variation of potential through the depth (z- direction) of the grain boundary has to be established. This enables the variation of potential in the grain to be found (x- direction). The two potential variations give an idea of the charge carriers at any point in the grains that are available for conduction. The main path of the current density J is through the grain centre and therefore a term for the potential at the centre of the grain is established. This is done so by assuming that each grain extending from the grain boundary is wide enough to meet in the centre of the grain. In this case, the variation of potential is such that the resulting grain reaches intrinsic concentration at the centre of the grain i.e. that the field due to grain boundary is zero at the centre. This needs to be checked against known parameters.

4.3.1 Field in Grain due to Grain Boundary

In vertical Schottky diodes, the work function difference defines a barrier at the interface between the metal and semiconductor [2]. For a polycrystalline organic semiconductor, this is equivalent to the potential barrier matching with the Fermi level within the grain or the grain boundary. As the Fermi level in the grain and the grain boundaries are aligned in thermal equilibrium, this potential barrier is greatest at the centre of the grain causing the maximum amount of interface bending.

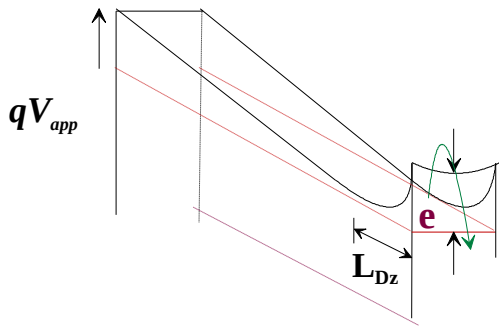

Figure 4.6. Potential Barrier observed by an electron at the Semiconductor Metal Schottky contact interface. L_{DZ} is the Debye length in the z-direction, V_{app} is the applied voltage at the ohmic contact, e is the electron.

The potential barrier in the grain boundary noticed over the top of the Schottky barrier limits the flow of charge due to trapping effects (Fig.4.6). The grains, on the other hand, dominate the charge transport from the ohmic contact to the Schottky interface with the application of an external bias. This is made possible by the lower energy barrier seen at the grain centre compared to the grain boundary. As the number of charge carriers in the grain boundary increases, the energy difference between the Fermi level and the grain edge reduces allowing more charge carriers to cross over into the adjacent grain. This in fact means that the grain boundaries define the variation of potential that eventually control the grain edge and hence the carrier concentration in adjacent grains. The variation of potential in the grain boundary is controlled by the states obeying the exponential distribution law.

In the grain boundary, an assumption that the current density alone determines the electrostatics across the thickness of the layer is required to make some calculations of the potential variations. The variation of potential across the thickness of the active layer (in the z direction) of the grain boundary has to be found to give the first boundary condition at the edge of the grain. The variation of potential across the grain (in the x direction) dependent on the potential at the grain edge can thus be found. This gives the second boundary condition in the grain. Furthermore, the main path to conduction through the region and the carrier concentration at a certain point can then be found. This leads to the carrier concentration at the peak of the barrier between the metal and the semiconductor to be determined.

Assuming that from the edge of the grain, the distance in the grain (in x-direction) over which the carrier density becomes intrinsic falls at the centre of the grain $x_D=a/2$, the maximum field strength in the grain can be defined by Gauss's law [2]

$$F_x = \frac{qN_D|x_D|}{\varepsilon_0\varepsilon_s} \quad 4.5$$

The potential drop across this region is given by the area under the graph of field against distance. The field declines linearly and is given as

$$F_x = \frac{2\emptyset}{x_D} \quad 4.6$$

Equating Eq. (4.5) and Eq. (4.6) together gives the width from the grain edge

$$|x_D| = \left(\frac{2\varepsilon_0\varepsilon_s\emptyset}{qN_D}\right)^{1/2} \quad 4.7$$

Imagine a polycrystalline material with the size of the grain x equal to a, between two adjacent grain boundaries. If for instance, the distance extending from each grain boundary into the grain reaches the intrinsic level after the centre of the grain ($x > a/2$), the resultant potential curve in the grain would be at a higher energy level (Fig.4.2). As a result, the number of carriers available for conduction is lower. This case is ignored for the analysis given below. At a grain boundary potential $\emptyset_z$, grain reaching its intrinsic level at the centre of the grain at distance $a/2$ from each of the grain boundary is the maximum width providing the best number of carriers for conduction. The grain boundaries on either side of the grain are on an equal potential and are at an equal distance away from the centre of the grain as discussed in Section 4.1. For simplification of analysis the grain size is approximated to be 1 μm in the x direction. Hence, the assumption that the carrier concentration reaches intrinsic levels at grain centre (~0.5μm) is valid. The potential drop across this region is 0.5eV with respect to the neutral level and is defined by the grain

boundary. The value for potential drop is chosen at random for simplification. Using Eq. (4.7), an estimate value for N_D (~5.5x10^{14} cm^{-3}) can be obtained. The dopant concentration observed from the current density against voltage plot for a TIPS-pentacene Schottky diode in Section 3.3 indicates a N_D of approximately 10^{17}cm^{-3}. These high dopant levels can be associated to the addition of impurities during fabrication or due to photo-oxidation effects. Moreover, N_D in the range of 10^{14}–10^{16} cm^{-3} is determined from the capacitance-voltage characteristics of the Schottky diodes for various frequencies in Section 3.5. These example parameters have been used to develop the curves such as shown in Fig.3.7 and Fig.4.7. Making these assumptions limits our model but is necessary for a basic analytical presentation.

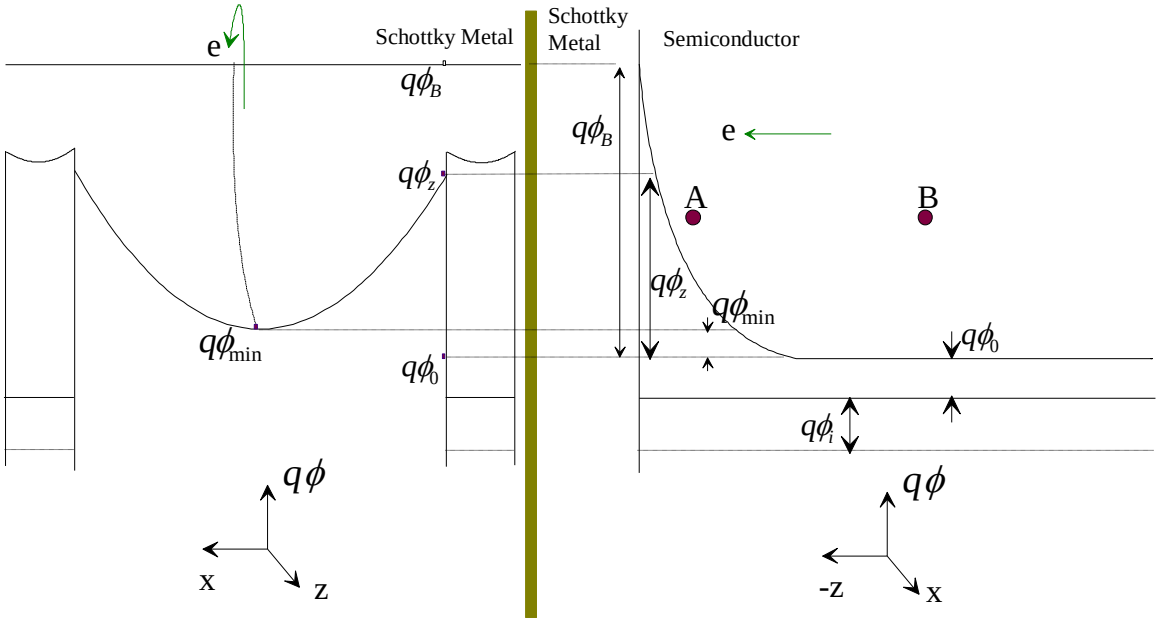

Figure 4.7. Energy Band diagram of an energy level in the grain (LHS) corresponding to the exponential decline in energy in the grain boundary (RHS). $q\emptyset_B$ is the energy at the Schottky barrier w.r.t the neutral level, $q\emptyset_0$ is the energy at the neutral level w.r.t the Fermi level, $q\emptyset_{min}$ is the energy at the centre of the grain w.r.t the neutral region, $q\emptyset_z$ is the energy at any point z in the z direction w.r.t to the neutral region, $q\emptyset_i$ is the energy at intrinsic level w.r.t the Fermi level.

In a polycrystalline material, the dopant ion concentration is uniform and somewhat stationary. Thus, indicating that any change in the energy of Fermi level will have little effect on the fraction of ionised dopant. The density of the intrinsic conducting states, into which the dopant carriers are

distributed, is a result of their being a much higher carrier density *N(E)* compared with the dopant levels. For organic materials, typically dopant related carriers dominate the electrical conduction unless the carrier concentration is improved by optical excitation or by field effect such as in the case of thin film transistors [13-15]. It is therefore essential to be cautious when applying the conduction mechanisms to the already existent inorganic disordered materials.

I. First Boundary Condition at the Edge of the Grain

In the z-direction, the potential variation in the grain boundary is affected by the trapping of electrons in the grain boundaries, subsequently allowing the carrier concentration in such region to be determined. Consequently, adjacent carrier concentration at the edge of the grain can also be determined. The distribution of trap density *N(E)* and the rate of change of density with energy *N′(E)* is determined by the exponential distribution given by

$$N'(E) = \frac{N(0)}{kT_C} \exp\left(\frac{E}{kT_C}\right) \qquad 4.8$$

Applying the Maxwell Boltzmann statistics, $f(E)$, the density of trapped electrons in the grain boundaries is given by (refer to Chapter 2)

$$n(E) = \int N'(E) f(E) dE \qquad 4.9$$

The density of traps above the Fermi level is larger than the one below the Fermi level. At lower energies, the fewer number of localised states are located further apart from each other limiting the hopping probability to almost zero. At higher frequencies, the hopping probability of electrons will rise due to the combined effect of exponential DOS and the Fermi Dirac statistics. At the peak of the exponential distribution, the density of traps is small. The minimum energy level over which the electrons are able to hop into empty states corresponds to the Fermi level. Integrating from the Fermi level to infinity provides a very good approximation of the carrier concentration at the Fermi level, n_0, playing a role in charge transfer.

$$n_0 = \frac{N(0)T_0}{T_C}\exp\left(\frac{E_F}{kT_C}\right) \quad 4.10$$

The denominator kT_C is dependent on the lower integration limit. It is indicative of the Fermi level lying in the band tail of the distribution where there is a slow rise in the DOS and the DOS is strongly exponential. Assuming Maxwell Boltzmann's statistics is unchanged with a quasi Fermi level, the intrinsic carrier concentration, n_i, can be written as

$$n_i = \frac{N(0)T_0}{T_C}\exp\left(\frac{E_i}{kT_C}\right) \quad 4.11$$

The ratio of carrier concentration at Fermi level, n_0, and at the intrinsic level, n_i, is therefore

$$\frac{n_0}{n_i} = \exp\left(\frac{E_F - E_i}{kT_C}\right) \quad 4.12$$

$$\frac{n_0}{n_i} = \exp\left(-\frac{q\emptyset_i}{kT_C}\right) \quad 4.13$$

The ratio of carrier concentration in the neutral region of the semiconductor, n_{bulk}, to the one at Fermi level is given by

$$\frac{n_{bulk}}{n_0} = \exp\left(\frac{E_{tr} - E_F}{kT_C}\right) \quad 4.14$$

$$\frac{n_{bulk}}{n_0} = \exp\left(\frac{q\emptyset_0}{kT_C}\right) \quad 4.15$$

where E_{tr} is the transport energy in the grain boundaries and $\emptyset_0$ is the potential between the bulk energy level and the Fermi level. The carrier concentration at any potential $\emptyset$ with respect to the Fermi level is given by

$$\frac{n}{n_0} = \exp\left(\frac{q\emptyset}{kT_C}\right) \qquad 4.16$$

Point *A* and *B* in Fig.4.7 can be explained in terms of Eq. (4.16).The carrier concentration at *A* must be equal to the carrier concentration at *B* as the carrier concentration at the Fermi level remains unchanged due to an assumption of a flat quasi-Fermi level. A flat quasi-Fermi level is assumed for the density of states to get to an equilibrium point at the barrier. The lower the height of the barrier, the larger is the charge flow to the barrier. The potential barrier seen by the carriers at point *A* and *B* are equal regardless of the position of carrier in the thickness of the organic layer. The carriers at any point in the same energy level have the same thermal energy required to cross over. The movement of charge from its original position is retained and neutralized by the addition of charge through external bias. Thus, at an energy level at any particular point, the number of carriers observed is as before. The conduction mechanism in this case is not considered as conduction due to diffusion is considered unlikely cause of flow of charge across the Schottky barrier. Eq. (4.10) is used indicating that the energetic distribution of charge carriers at the Fermi level determines the current across the top of the barrier.

The carrier concentration *n*, defined in Eq. (4.16), at any point in the grain boundary defines and controls the variation of electrostatic potential in the grains. It is thus important to find a term that defines the potential variation in the grain boundary. For such an analysis, it is essential to define carrier concentration and potential variation in terms of Gauss's law from the Schottky contact to the ohmic contact (z- direction) in terms of a double differential equation.

$$\frac{d^2\emptyset}{dz^2} = \frac{qn}{\varepsilon_0\varepsilon_s} \qquad 4.17$$

where *z* is the thickness of the semiconductor film grain boundary in the z- direction and *n* is the total density at any point $\emptyset$ in the grain boundary.

$$\frac{d^2\emptyset}{dz^2} = \frac{qn_0}{\varepsilon_0\varepsilon_s}\exp\left(\frac{q\emptyset}{kT_C}\right) \quad 4.18$$

Integration of the above equation defines the field,

$$F = \left[\frac{2kT_Cn_0}{\varepsilon_0\varepsilon_s}\right]^{1/2}\exp\left(\frac{q\emptyset}{2kT_C}\right) \quad 4.19$$

Integrating between $\emptyset = \emptyset_B$ at the peak of the barrier at the Schottky contact where *z=0* and $\emptyset = \emptyset_z$ at a point *z=z* in the disordered grain boundary,

$$\int_{\emptyset_z}^{\emptyset_B}\exp\left(-\frac{q\emptyset}{2kT_C}\right)d\emptyset = -\int_z^0\left[\frac{2kT_Cn_0}{\varepsilon_0\varepsilon_s}\right]^{1/2}dz \quad 4.20$$

The Debye length is a material dependent parameter and is defined as the distance over which the exponential distribution of carriers increases towards the neutral region to get to equilibrium or steady state (refer to Chapter 3) [2, 16]. It is given by

$$L_{Dz} = \left(\frac{2kT_C\varepsilon_0\varepsilon_{gb}}{q^2n_0}\right)^{1/2} \quad 4.21$$

and decreases with an increase in the gate voltage. T_C is the characteristic temperature of DOS, n_0 is the density corresponding to the Fermi level, ε_0 is the permittivity of free space and ε_{gb} is dielectric constant of the grain boundary. Therefore, Eq. (4.22) defines $\emptyset_z$ as the first boundary condition at the edge of the grain (Appendix D).

$$\emptyset_z = -\frac{2kT_C}{q}\ln\left[\exp\left(-\frac{q\emptyset_B}{2kT_C}\right) + \frac{z}{L_{Dz}}\right] \quad 4.22$$

As potential $\emptyset_z$ varies exponentially with the distance (from the Schottky contact), the carrier density changes exponentially too. A small change in the potential in the grain boundary, away from the Schottky contact will have little effect on the carrier concentration. The potential can be assumed to be constant after distance z in the organic layer. This distance z in the grain boundary of the organic layer is assumed to be equivalent to the L_{DZ}. The equation above is true for all $\emptyset_z$ less than L_{Dz}. Above this length $z > L_{Dz}$, $\emptyset_z$ is essentially approximated to $\emptyset_0$. The potential barrier seen in the grains is defined by the grain boundaries and only varies as much as the grain boundary. The traps in the grain boundary control the current such that any change in grain boundary confers a similar change in the grain.

II. Second Boundary Condition in the Grain

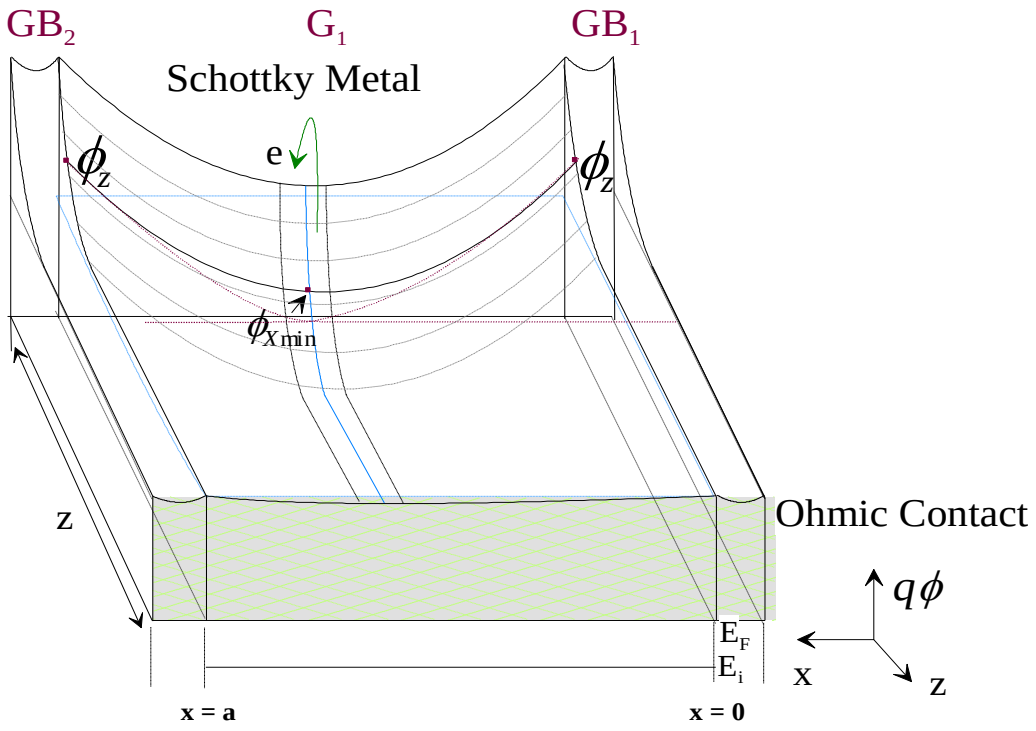

Figure 4.8. A two Dimensional drawing of the band bending in grain due to the potential at the edge of the grain. $q\emptyset_{min}$ is the energy at the centre of the grain w.r.t the neutral region and $q\emptyset_z$ is the energy corresponding to a point z on the grain edge w.r.t to the neutral region.

After developing a term for the change in potential for the grain boundaries in the z-direction, there is a need to develop a term for the variation in potential in the grains in the x-direction. Figure 4.8 illustrates a sketch of an n-type organic polycrystalline semiconductor with a single grain separating two grain boundaries, carried forward from Fig.4.2 It gives an indication of the change in the potential from one grain boundary to the other. The potential seen at the grain edge is demonstrated by the term $\emptyset_z$ obtained from Eq. (4.22) and potential at the centre of the grain is demonstrates by the term $\emptyset_{Xmin}$.The potential $\emptyset_z$ is responsible for the resulting grain illustrated in Fig.4.8.

In the x- direction, the grain is crystalline with the dopant concentration N_D. The variation of the E_T level in the grain is determined by this dopant concentration shown by using Gauss's law as before

$$F_x \frac{dF}{dx} = -\frac{qN_D}{\varepsilon_0 \varepsilon_s} \frac{d\emptyset}{dx} \qquad 4.23$$

The boundary conditions are defined in terms of the field F at the grain boundary $F_{boundary}$ where the potential $\emptyset$ is equal to $\emptyset_z$ at the edge of the grain at $x= 0$. The field F_x corresponding to a potential $\emptyset_x$ in the x-direction is at an arbitrary point $x= x$ on the grain E_T level. These limits are used to define the drop in electric field between two points given by

$$\int_{F_x}^{F_{boundary}} F_x \, dF = -\int_{\emptyset_x}^{\emptyset_z} \frac{qN_D}{\varepsilon_0 \varepsilon_s} d\emptyset \qquad 4.24$$

where the minimum grain condition is $F=0$ at $x=x_D$, $\emptyset = \emptyset_0$ in the neutral region w. r. t the Fermi level ($\emptyset = 0$ at $F=0$). The potential at the point x with regards to the grain edge is then given in terms of the second boundary condition. This is true for any point x on the grain corresponding to the energy level $q\emptyset_z$ on grain edge (Appendix E).

$$\emptyset_x = \left(\emptyset_z{}^{1/2} - \left(\frac{qN_D}{2\varepsilon_0 \varepsilon_s} \right)^{1/2} x \right)^2 \quad 4.25$$

For the model we assume that the two grain boundaries at either side of the grain are equal distance apart from the centre of the grain such that they are symmetric (Fig.4.2). In this case, potential $\emptyset_X$ at the any point x ($x < a$) in the grain for the resultant full curve, $\emptyset_X$, is given by

$$\emptyset_X = \emptyset_{x1} + \emptyset_{x2} \quad 4.26$$

$$\emptyset_X = \left(\emptyset_z{}^{1/2} - \left(\frac{qN_D}{2\varepsilon_0 \varepsilon_s} \right)^{1/2} x \right)^2 + \left(\emptyset_z{}^{1/2} - \left(\frac{qN_D}{2\varepsilon_0 \varepsilon_s} \right)^{1/2} (a - x) \right)^2 \quad 4.27$$

where a is the maximum distance between two adjacent grain boundaries. With this assumption, the minimum potential on the curve $\emptyset_{Xmin}$ at the centre of the grain on the resultant E_T level can be written as (Appendix F)

$$\emptyset_{Xmin} = 2 \left(\emptyset_z{}^{1/2} - \left(\frac{qN_D}{2\varepsilon_0 \varepsilon_s} \right)^{1/2} \left(\frac{a}{2} \right) \right)^2 \quad 4.28$$

The potential variation in the grain boundary in z-direction causes the resulting full curve $\emptyset_X$ in the grain to change. This is because $\emptyset_z$ at the grain edge determines the resulting curve in the grains. As the dopant concentration remains unchanged and $\emptyset_z$ varies in z-direction, the width of an individual grain extending in x-direction from a single grain boundary must be changing with initial $\emptyset_z$ changing along the z-axis. This width x_D is the distance over which field in the x direction due to the grain boundary becomes zero.

Assume that at some potential in the grain boundary, $\emptyset_z$, the field reaches zero at the grain centre ($x_D = a/2$). Consequently at grain boundary potentials of above $\emptyset_z$, the surface potential in grains will not be able to reach a constant value at the grain centre ($x_D > a/2$). The addition of two grains extending from the grain boundaries at either end would, in this case, give a resulting full grain

higher in energy. In this case, the grain would not have reached the neutral level at the centre of the grain. At grain boundary potentials below $\emptyset_z$, the surface potential in the grain would reach a minimum field *F=0* before arriving at the centre of the grain ($x_D < a/2$). The grain extending from the individual grain boundaries is thus smaller. As a result, for any position $x > x_D$, $\emptyset_x$ is assumed constant at $\emptyset = 0$ for *F = 0* in Fig.4.9. This corresponds to $\emptyset_0$, the potential between the neutral region and the Fermi Level. The carrier concentration in the grains is therefore seen constant before the centre of the grain is reached. This happens closer to the ohmic end.

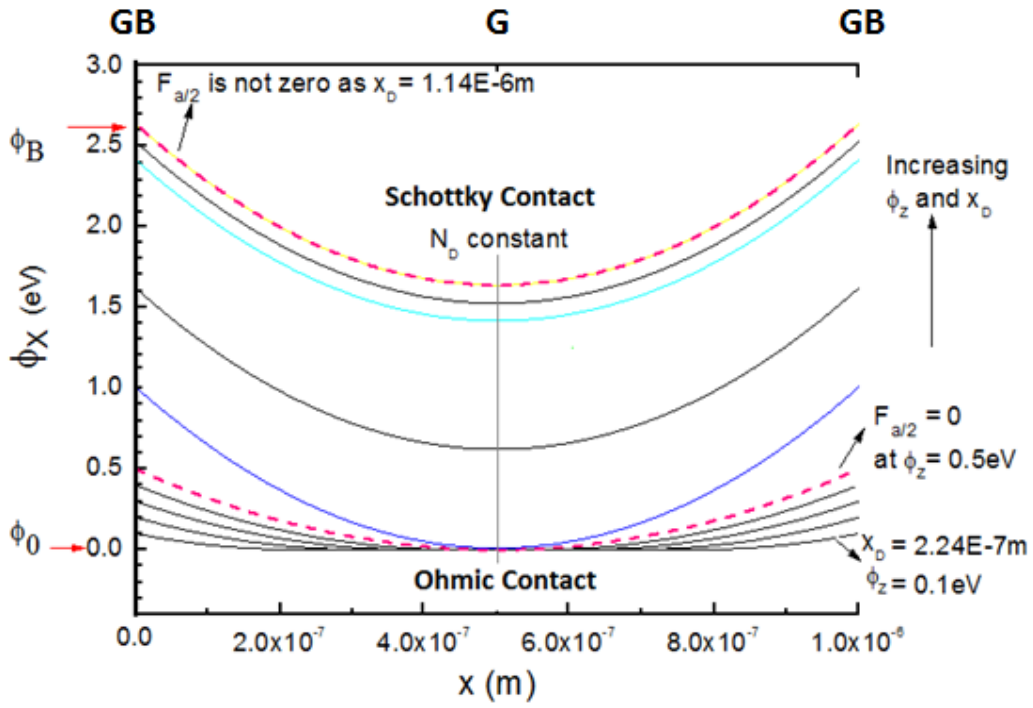

Figure 4.9. The variation of potential in the grain (G) in x-direction defined by the grain boundaries (GB). The example values taken for ϕ_B and a are 2.6eV and 1μm respectively and the grains are fully depleted at the centre of the grain at $\phi_z = 0.5eV$.

4.4 CONDUCTION UNDER FORWARD BIAS

4.4.1 Assuming Gaussian DOS

If a flat quasi Fermi level is considered in the grains and grain boundaries of an n-type semiconductor, the carrier concentration at point A and B should be the same (Fig.4.7), even in steady state conditions. At the energy peak shown in Fig.4.2, the carrier density is also very small and so integrating to infinite energy adds insignificant additional current density. Integration

limits are significant as they identify the amount of carriers that are present enabling current to flow. The current density from the energy level at A to infinity is given by Eq. (4.29) using Eq. (4.9).

$$n(E) = \frac{T_0 N(0)}{T_C} \exp\left(\frac{E_F}{kT}\right) \exp\left(-\frac{E}{kT_0}\right) \qquad 4.29$$

Trap density below the Fermi E_F is considered very small and with relatively few vacant states thus rendering it difficult for the carriers to hop between states and hence producing any significant current.

The barrier to current flow defined by $q\emptyset_B$ in the grain boundary at the Schottky metal and semiconductor interface, at $z=0$, is given by

$$n(q\emptyset_B) = \frac{T_0 N(0)}{T_C} \exp\left(\frac{E_F}{kT}\right) \exp\left(-\frac{q\emptyset_B + q\emptyset_0}{kT_0}\right) \qquad 4.30$$

and with modification by the application of an external voltage ($-V_{app}$),

$$n(q\emptyset_B) = \frac{T_0 N(0)}{T_C} \exp\left(\frac{E_F}{kT}\right) \exp\left(-\frac{q\emptyset_B + q\emptyset_0}{kT_0}\right) \exp\left(\frac{qV_{app}}{kT_0}\right) \qquad 4.31$$

The corresponding carrier density at any point on the full grain curve, given by potential $q\emptyset_{XB}$ at the Schottky metal/semiconductor interface, can thus be written

$$n(q\emptyset_X) = N_T \exp\left(\frac{E_F}{kT}\right) \exp\left(-\frac{q\emptyset_0}{kT}\right) \exp\left(-\frac{q\emptyset_{XB}}{kT}\right) \exp\left(\frac{qV_{app}}{kT_0}\right) \qquad 4.32$$

where N_T is the carrier density at the transport level in the crystalline grains. The maximum current density, J_g , expected at the interface of Schottky metal and the grain centre is defined by

the potential $q\emptyset_{minB}$ as in Eq. (4.28). This corresponds to the energy $q\emptyset_z$ at the edge of the grain from Eq. (4.22)

$$J_g \propto \exp\left(-\frac{q}{kT}\emptyset_{XminB}\right)\exp\left(\frac{qV_{app}}{kT_0}\right). \qquad 4.33$$

4.4.2 Assuming Laplace DOS

Laplace DOS is said to be more suitable to characterize charge conduction in the grain boundaries of a polycrystalline semiconductor, predominantly when explaining conduction in terms of diode current. This is because it is easier to study the density of states with energy in a diode as a large number of energy levels are inspected. The application of voltage at the metal in forward bias causes almost all of the voltage to drop across the semiconductor. The higher the application of voltage, the deeper the investigation of energy levels is carried out. Through the ohmic contact large voltages may be applied thereby allowing a free flow of carriers into the semiconducting material. This consequently allows the study of a much wider distribution of carriers within the semiconductor, which is unlike in MOS capacitors and OTFTs, where only a small voltage is used to vary the carriers on the surface as most of the voltage is across the oxide layer.

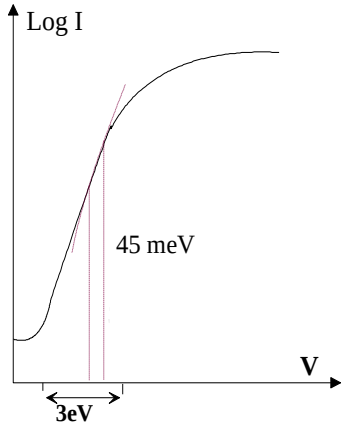

Figure 4.10. A sketch of the log-linear Current-Voltage characteristics of a Schottky diode in forward bias. The voltage drop across the exponential region is much more than the Meyer Neldel Energy of approximately 45meV for polycrystalline materials.

When a small forward bias is applied to the ohmic metal, the current rises exponentially across the barrier into the Schottky metal as indicated in Fig.4.10. Although thinning of the neutral

region can cause the expansion of the depletion region due to the expansion of the exponential voltage range, the conduction is limited by the contraction of the depletion region and the expansion of the neutral region. At higher voltages, the current is limited by the resistivity of the neutral region and therefore it becomes harder for carriers to pass through to the metal. This is shown in Fig.4.10 as the decrease in current at higher voltages from exponential to SCL currents. The difference between Gaussian and Laplace distribution as in Fig.2.5 is that the prediction of current density for a higher range of energy levels is possible with Laplace than the Gaussian distribution to correspond to the rise of the Fermi level with applied bias in the depletion region.

The carrier concentration at the peak of the barrier can be explained by the product of both the carrier density defined by the Laplace DOS and the Maxwell Boltzmann approximation from the tail of Fermi Dirac statistics as in Eq. (4.9). These are both exponential functions and can be used to define the exponential rise of carrier concentration at the peak of the barrier. The Maxwell Boltzmann statistics above the Fermi level is defined in Section 2.3, Eq. (2.3).

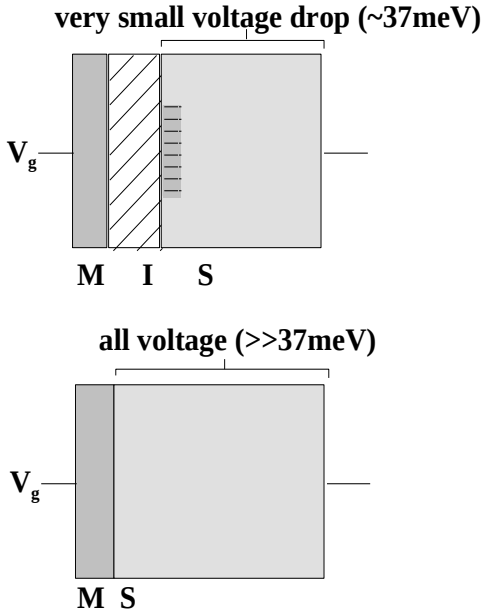

Figure 4.11. Metal Insulator Semiconductor and Schottky diode structure describing the amount of voltage drop across the semiconductor.

Detailed analysis on the Meyer Neldel energy is conducted in Chapter 3. The Meyer Neldel rule is defined in terms of the width of the carrier distribution. The Meyer Neldel energy in the range of

30-40meV is produced in the exponential region of a Schottky diode, representing the density of DOS with energy [6, 17]. Polycrystalline semiconductor based Schottky diodes provide a high MN energy of approximately 45meV from Fig.3.8. But this is only a small portion of the exponential region when compared to the experimental data obtained. In ideal diodes, the applied bias at the metal is completely dropped across the semiconductor (Fig.4.11). The applied bias can scan a wider range of energy levels (>> 37meV) unlike when there exists a dielectric layer between the metal and the semiconductor like in MIS capacitors and TFTs (Fig.4.11) (as in Chapter 5). Gaussian DOS gives a good fit for the energy range measured in TFTs (37meV) but becomes a doubtful distribution when scanning a larger number of states (around 3eV) as in diodes.

Section 2.4.3, Eq. (2.7), gives the carrier density $N_{L1}(E)$ characterised in terms of L1 distribution. The carrier density at *E=0* is $N_{L1}(0)$ and can be written as

$$N_{L1}(0) = N_{peak} \exp\left(\frac{E_\mu}{E_\sigma}\right) \qquad 4.34$$

where

$$N_{peak} = \frac{1}{2\left(\frac{E_\sigma}{E_0}\right)} = \frac{q}{2kT_\sigma} \qquad 4.35$$

and $E_\sigma = {}^{kT_\sigma}/_{q}$ where T_σ is defined as the characteristic temperature corresponding to the Laplace DOS.

$$N_{L1}(E) = N_{L1}(0) \exp\left(-\frac{E}{E_\sigma}\right) \qquad 4.36$$

To define the whole distribution,

$$N_{L1}(E) = N_{L1}(0) \exp\left(\frac{|E|}{E_\sigma}\right) \qquad 4.37$$

The rate of change of energy $N_{L1}'(E)$ becomes

$$N_{L1}'(E) = \frac{N_{L1}(0)}{kT_\sigma} \exp\left(\frac{|E|}{kT_\sigma}\right) \qquad 4.38$$

where T_σ is similar to T_C defined in terms of exponential DOS. Using Eq. (4.9), the carrier concentration in terms of Laplace DOS is written as

$$n = \int \frac{N_{L1}(0)}{kT_\sigma} \exp\left(\frac{|E|}{kT_\sigma}\right) \exp\left(-\frac{E - E_F}{kT}\right) dE \qquad 4.39$$

Assuming that trap density is significantly less below the Fermi level and are almost completely full such that the hopping rate is significantly reduced, the trap density can be ignored. The carrier density is also very small at the peak of the distribution and therefore can be used as an integration limit.

$$n = \frac{N_{L1}(0)}{kT_\sigma} \exp\left(\frac{E_F}{kT}\right) \int_{E_F}^{\infty} \exp\left(-\frac{E}{kT_0}\right) dE \qquad 4.40$$

where T_0 incorporates both absolute temperature T and characteristic temperature due to structural disorder in the Laplace distribution, T_σ, given by $\frac{1}{T_0} = \frac{1}{T} - \frac{1}{T_\sigma}$.

$$n = \frac{T_0 N_{L1}(0)}{T_\sigma} \exp\left(\frac{E_F}{kT_\sigma}\right) \qquad 4.41$$

The current density above the Fermi level, not considering the conduction mechanisms involved, is proportional to the carrier concentration

$$J \propto \exp\left(\frac{E_F}{kT_\sigma}\right) \qquad 4.42$$

If the current is limited by the grain boundaries, the above mentioned phenomenon is true. However, if the current is limited by the conduction in grains, the neutral region has a higher mobility and the curve defining the current turns on much more quickly. The ideality factor obtained in such a case, if high, is due to the poor back contact. This causes a voltage drop at the back metal contact which is visible at lower voltages (such as in the exponential region) and at higher voltages, this voltage drop becomes insignificant. The current in the ordered grains is expected to be much higher than the total disordered grain boundaries and thus higher mobility values can be expected. The Laplace can be compared against the Gaussian distribution if the variance is kept constant and is known as the standardised classical Laplace distribution (Fig.2.5).

The distributions show good similarity, except that Laplace has a thicker tail than the Gaussian distribution and has a higher pointed peak at the centre [18].

4.5 CONCLUSION

The conduction in polycrystalline organic material is represented laterally and vertically. Lateral conduction is expected in between two electrodes, such as the source and the drain electrodes in an organic thin-film transistor (OTFT), consisting of a number of grains and grain boundaries. Considering the effects of an external voltage applied laterally, the formation of grains and grain boundaries depend mainly on two conduction mechanisms, namely drift and diffusion. In the case of organic semiconductors, these terms are developed as quasi- drift and quasi- diffusion. It is said that the exponential distribution of states in the grain boundary defines a potential in the grains. The further the grain boundaries are from each other, the lower the potential barrier exists at the centre of the grain. The difference in energy between the grain centre and the Fermi level is therefore reduced and conduction at the centre of the grain dominates.

From one grain boundary to another, the potential barrier progressively drops till the centre of the grain. The concentration gradient observed in this case is similar to the diffusion mechanism. In the case of drift mechanism, the difference between the energy of Fermi level and the transport level stays the same. Combination of both these mechanisms provides a good idea of the flux across the grain boundaries. The derivation of flux is therefore used to model a polycrystalline organic material for devices such as organic lateral diodes or TFT devices.

Vertical conduction is expected in vertical Schottky diodes between the ohmic and Schottky contacts. A vertical representation is important to determine the grains and grain boundaries across the thickness of the organic layer. The polycrystalline organic layer in this case is thin. Thinner organic layers lead to an extension of the depletion region across the thickness of the organic layer. Assuming that only a single layer of grain and grain boundaries exist, a 2-Dimensional model based on the potential variation in grains due to exponential distribution of traps is proposed in this thesis. The charge conduction is thus dependent on the exponential DOS in the grain boundaries and the conduction mechanisms are not considered. The disordered grain boundaries form a potential barrier to current flow due to the distribution of traps.

To solve this two dimensional problem, the grains and the grain boundaries are considered as two one-dimensional issues that at right angle to each other. In the vertical direction, Poisson's equation is used to define the variation of potential in the grain boundary. A term in the z-direction is thus developed. Accordingly, this causes the grains to see a variation in potential at the grain edge such that the grains can be constructed. The potential variation in grains is developed by the use of Poisson's equation applied at the grain edge. A few assumptions are made to construct the grain and consequently, the variation of potential in the whole of the grain is defined in the x-direction. A novel term for the potential at grain centre is established which provides the maximum number of carriers for charge conduction. Ultimately using drift currents, a new expression corresponding to the current density at the grain centre in the forward characteristics is established.

Laplace L1 DOS is a new approach used to describe the density of states in the grain boundaries of an organic polycrystalline material. Laplace DOS is considered a suitable representation for the distribution of states in a polycrystalline material as prediction of current density for a higher range of energy levels is possible with Laplace DOS. A number of reasons are provided to back the claim made in this thesis. In the case of devices such as a Schottky diode, the drop across the exponential region in the forward electrical characteristics is much more than the Meyer Neldel energy. Consequently, Laplace distribution is believed to be a better representation of the DOS instead of the vastly followed Gaussian DOS. Finally, by taking the exponential L1 distribution and the Maxwell-Boltzmann statistics into account, an expression to identify the carrier concentration is finally developed.

4.6 REFERENCES

[1] W. Eccleston, IEEE Trans. Electron Devices 53, (2006) 474.

[2] S. M. Sze, *Physics of Semiconductor Devices*, Second Ed., John Wiley and Sons, New York, 1981.

[3] S. K. Park, T.N. Jackson, J.E. Anthony, D.A. Mourey, Appl. Phys. Lett. 91, (2007) 63514.

[4] D. H. Kim, Y. D. Park, Y. Jang, H. Yang, Y. H. Kim, J. I. Han, D. G. Moon, S. Park, T. Chang, M. Joo, C. Y. Ryu, K. Cho, Adv. Mater.15, (2005) 77.

[5] H. Sirringhaus, P. J. Brown, R. H. Friend, M. M. Nielsen, K. Bechgaard, B. M. W. Langeveld Voss, A. J. H. Spiering, A. J. Janssen, E. W. Meijer, P. Herwig, D. M. de Leeuw, Nature, London 401 (1999) 685.

[6] W. Eccleston, *Private Communication*, 2011.

[7] J.Z. Wang, Z.H. Zheng, H. W. Li, W.T.S Huck, H. Sirringhaus, Nature Mater. 3, (2004) 171.

[8] H. Klauk, *Organic Electronics: materials, manufacturing and applications*, Wiley-VCH, Germany, 2006.

[9] S. Verlaak, V. Arkhipov, P. Heremans, Appl. Phys. Letts., 82 (2003) 745.

[10] V. Kalihari, E. B. Tadmor, G. Haugstad, C. D. Frisbie, Adv. Mater. 20 (2008) 1.

[11] N. Karl, Synthetic Metals, 133-134 (2003) 649.

[12] G. Horowitz, Adv. Func. Mater. 13, (2003) 53.

[13] D. Natelson, Nature Materials 9, (2010) 703.

[14] C. H. Newman, C. D. Frisbie, D. A. da Silva Filho, J-L Bredas, P. C. Ewbank, K. R. Mann, Chem. Mater. 16 (2004) 4436.

[15] J. Tilman, *Fabrication and characterization of thin-film transistors with organic heterostructure of pentacene and PTCDI-C13*, MSc Thesis, 2010.

[16] M. Raja, W. Eccleston, J. Appl. Phys. 110, (2011) 114524.

[17] M. Mahadhavan, PhD Thesis, University of Liverpool, 2008.

[18] R. Stockute, P. Johnson, website: *www.pj.freefaculty.org/stat/Distributions/Laplace-03.pdf*, viewed: 11/02/2011, 2006.

CHAPTER 5- ANALYSIS OF POLYCRYSTALLINE ORGANIC METAL-OXIDE-SEMICONDUCTOR (MOS) CAPACITORS

Detailed analysis is carried out on the capacitance voltage (C-V) characteristics on an organic MOS capacitor. An RC equivalent circuit to model frequency-dependent capacitance of MOS capacitor is examined. An equivalent circuit model is also considered to find the bulk components. Finally, the temperature dependence of the C-V characteristics is observed to recognize the variation in charge transport, for polycrystalline organic MOS capacitors.

5.1 INTRODUCTION

Metal-Oxide-Semiconductor (MOS) capacitors are essential devices for in depth analysis of semiconductor surfaces. They are also useful in the study of properties at the interface between the oxide and semiconductor, semiconductor bulk and oxide bulk. It is also a fundamental approach to understanding complicated devices such as the MOS transistors. An important factor to consider when designing any semiconductor device is the knowledge of distribution of carriers in the structure of the semiconductor. This is because it offers the fundamental relations between different device parameters dictating their device characteristics. Structural properties are important for the development and improvement of semiconductor devices. For this purpose, a technique for accurate profiling is required. Most commonly, the differential capacitance method with depletion approximation is used [1]. With this, the semiconductor can be separated into distinct regions namely the accumulation, the depletion and the neutral region.

High and low frequencies Capacitance-Voltage (C-V) responses can be obtained from an MOS capacitor and used to measure gate oxide charges, oxide thicknesses, doping concentration of semiconductor, the interface charge density and flat band voltages [2-4]. Recent publications indicate that organic circuits are limited to operation at only a few kilohertz because of their limited carrier mobilities in the organic active materials [5, 6]. Capacitance-Voltage characterisation of pentacene based TFTs have reported a cut-off frequency of tens of kilohertz [5]. Such quantitative characterization is crucial for device performance evaluation and an easy approach to get insight into structures such as organic TFTs (OTFTs) for commercial applications in flexible flat panel TVs, and digital cameras etc [7]. In essence, the workings of a thin-film transistor are similar to that of a capacitor. Application of a gate bias induces an equidistant, equal and opposite charge on both sides of an insulator. A conducting channel is formed in the semiconductor if charge carriers can be injected into it. The conductance of the semiconductor channel in a transistor is proportional to the amount of charge present and hence proportional to the gate voltage. Thus a transistor can effectively be seen to operate as a capacitor.

Detailed study of the frequency and temperature variations on the capacitance voltage (C-V) characteristics of an organic Metal-Oxide-Semiconductor (MOS) capacitor provides information on the defects present in an organic material and the interfacial properties between the gate dielectric and organic semiconductor. Many studies have been reported on the dc characterisation and modelling of polycrystalline organic based structures but little exists on the ac characteristics

of such devices. Non-equilibrium properties of the semiconductor structure in MOS capacitors can also be measured using the transient capacitance response (C-t). These include the generation and recombination lifetimes, and the surface generation and recombination velocities. Speed at which the initial deep depletion changes to the minimum capacitance by the formation of an inversion layer with the generation of minority carriers can be shown by the C-t response, both in the bulk and at the surface of the organic semiconductor. The performance of a device can be considerably affected by these processes especially if it is a charge coupled device.

5.2 CONVENTIONAL MOS CAPACITORS

A MOS capacitor consists of a metallic gate electrode, an oxide (insulator) and a semiconducting electrode. The capacitor is in equilibrium when the Fermi levels, of each of the materials, align themselves such that there is no gradient. The conduction band of the oxide is at a higher level than the conduction band of the Semiconductor. Figure 5.1 a, b shows the band profiles before and after equilibrium.

5.2.1 Accumulation Region

The band profiles for the devices can be changed with the application of an external bias. For a p-type semiconductor, application of a negative bias to the metal with respect to the semiconductor causes a negative charge to build up at the metal. This creates an accumulation of equal positive charge consisting of holes at the oxide-semiconductor interface [8, 9].

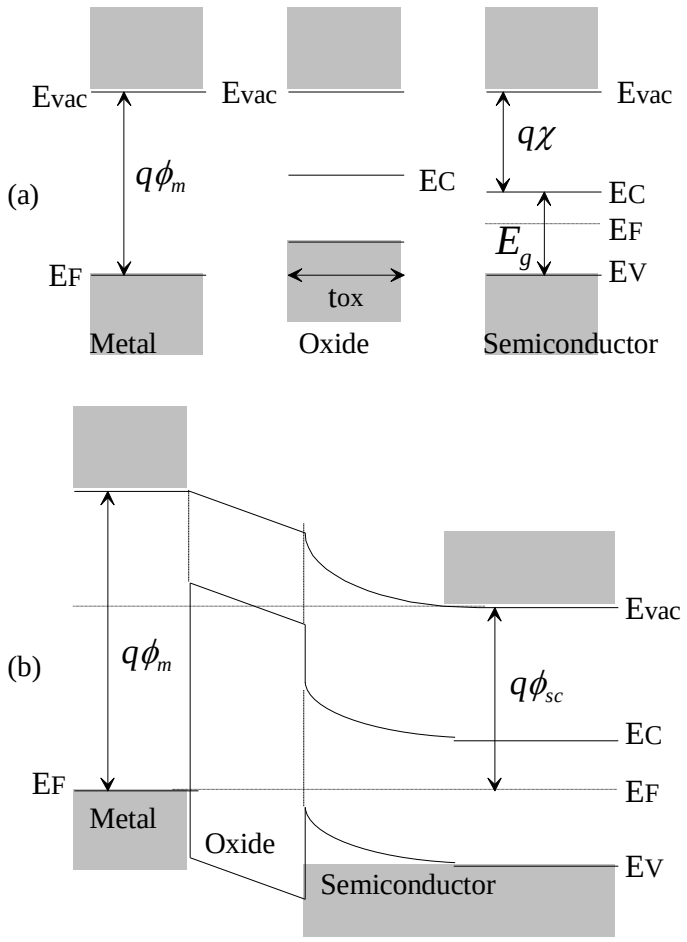

Figure 5.1. (a) Band diagram of the metal, oxide and a p-type semiconductor before contact. (b) Band diagram of a MOS capacitor in equilibrium. $q\emptyset_m$ is the work function of the metal, $q\emptyset_{sc}$ is the work function of the semiconductor, E_g is the energy difference between the valence and conduction band and $q\chi$ is the electron affinity [8, 9].

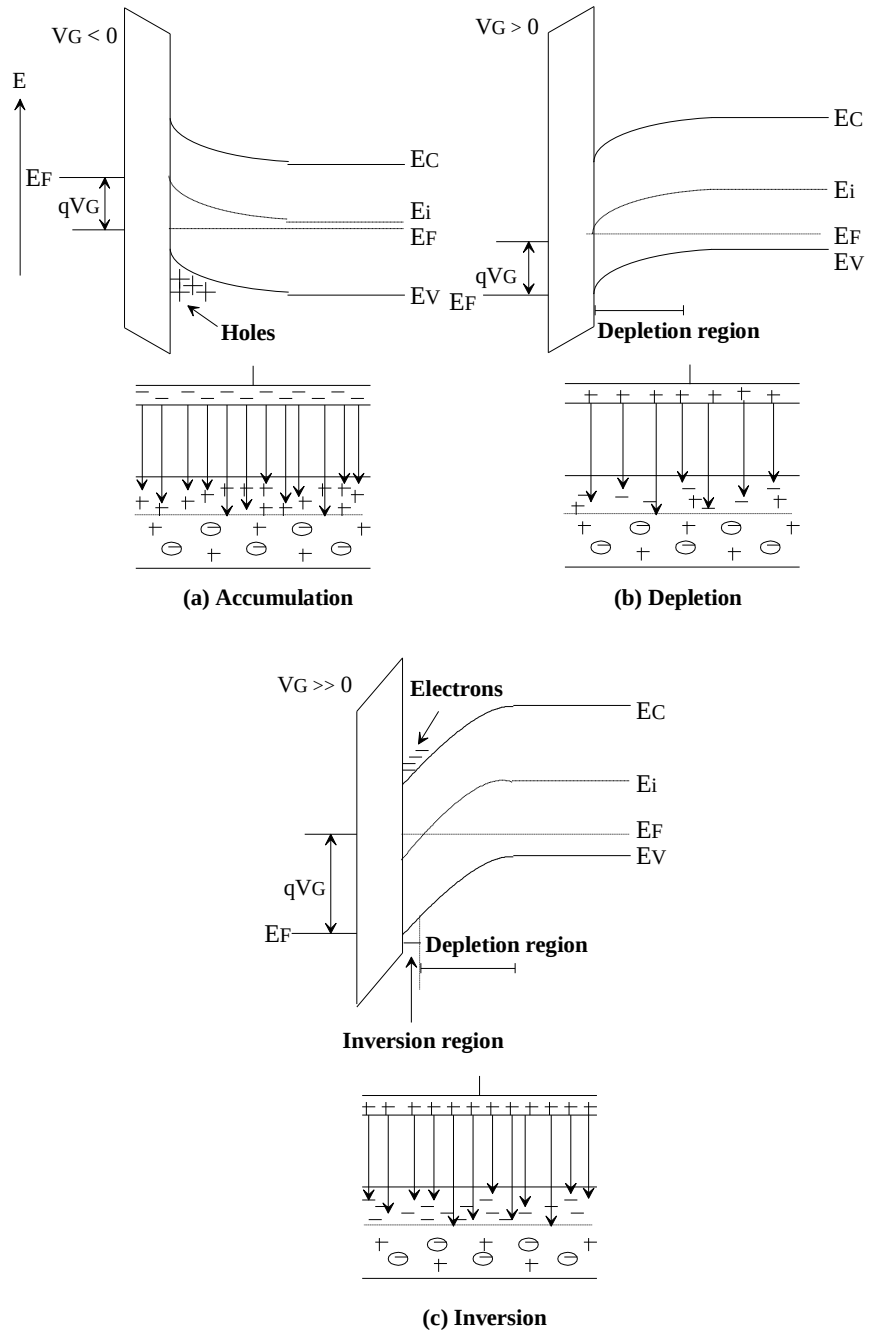

Figure 5.2. Band diagrams and charge distribution in (a) accumulation ($V_G<V_{fb}$), (b) depletion ($V_{fb}<V_G<V_T$) and (c) inversion ($V_T<<V_G$). V_{fb} is the flat band voltage, V_G is the gate voltage and V_T is the threshold voltage [8].

In the accumulation region, increasing the negative potential causes the valence band to bend closer to the Fermi level (Fig.5.2a). A small change in the gate voltage provides an amplification of the accumulation charge so that approximately all the potential falls across the oxide. The capacitance due to the accumulation of holes (C_{acc}) is much more than the capacitance of the oxide (C_{ox}). As C_{acc} is in series with the C_{ox}, the total capacitance C_{MOS} is approximated to C_{ox}. The total MOS capacitance C_{MOS} per unit area is

$$C_{MOS} \cong C_{ox} = \frac{\varepsilon_0 \varepsilon_{ox}}{t_{ox}} \qquad 5.1$$

where C_{ox} is the oxide capacitance per unit area, ε_0 is the permittivity of free space, ε_{ox} is the dielectric constant associated with the oxide and t_{ox} is the thickness of the oxide.

The oxide has an electric field that terminates immediately in a perfect conducting metal but covers a finite distance in the semiconductor due to its finite resistivity. Hence, almost all the potential variation is within the oxide as only a small amount of band bending is required to amplify the accumulation charge. As no charge exists in the oxide, Poisson's Equation gives

$$\frac{dF_{ox}}{dx} = 0 \qquad 5.2$$

Field across the oxide, F_{ox} is constant throughout the oxide referring to linear variation of potential with distance.

5.2.2 Flat Band Condition

When no charge exists in the semiconductor, a flat energy band is assumed at zero bias in ideal conditions called the flat band. Flat band condition exists when the applied gate voltage is equal to the work function difference between the gate metal and the semiconductor and changes with the existence of fixed charge in the oxide and/or at the oxide-semiconductor interface (Fig.5.3).

In an ideal situation where the flat band is at $V_{app}=0$, the depletion region is given by

$$C_{dep}(flat\ band) = \frac{\varepsilon_s \varepsilon_0}{L_D} \qquad 5.3$$

and the total flat band capacitance is given by

$$C_{fb} = \frac{\varepsilon_0 \varepsilon_{ox}}{t_{ox} + \left(\varepsilon_{ox}/\varepsilon_s\right) L_D} \qquad 5.4$$

where ε_{ox} is the dielectric constant of the oxide, ε_s is the dielectric constant of the semiconductor, L_D is the Debye length and t_{ox} is the thickness of the oxide.

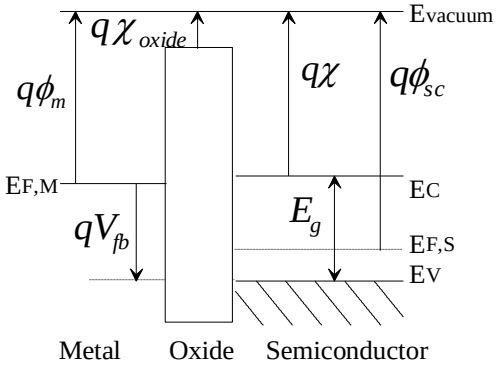

Figure 5.3. Energy diagram in flat band condition. E_g is the energy difference between the conduction and valence band, χ is the electron affinity of the semiconductor, χ_{oxide} is electron affinity of the oxide and V_{fb} is the flat band voltage.

5.2.3 Depletion Region

Increase in the positive voltage on the metal side causes the conduction band edge to bend closer to the Fermi level and in turn increase the negative ionised dopant atoms at the oxide-semiconductor interface forming a depletion layer whose width increases with increasing gate voltage [8, 9]. The positive charge on the gate depletes the mobile carriers at the interface. This causes a negative charge to be left in the space charge region due to the ionized acceptor atoms. In reality, a naturally built in region exists (at V_{fb}) due to the work function difference between the semiconductor and the dielectric layer providing the charge.

The capacitance of a MOS structure C_{MOS} is the series combination of the depletion capacitance in the semiconductor C_{dep} and the oxide capacitance C_{ox}.

$$C_{MOS} = \frac{C_{ox} C_{dep}}{C_{ox} + C_{dep}} \qquad 5.5$$

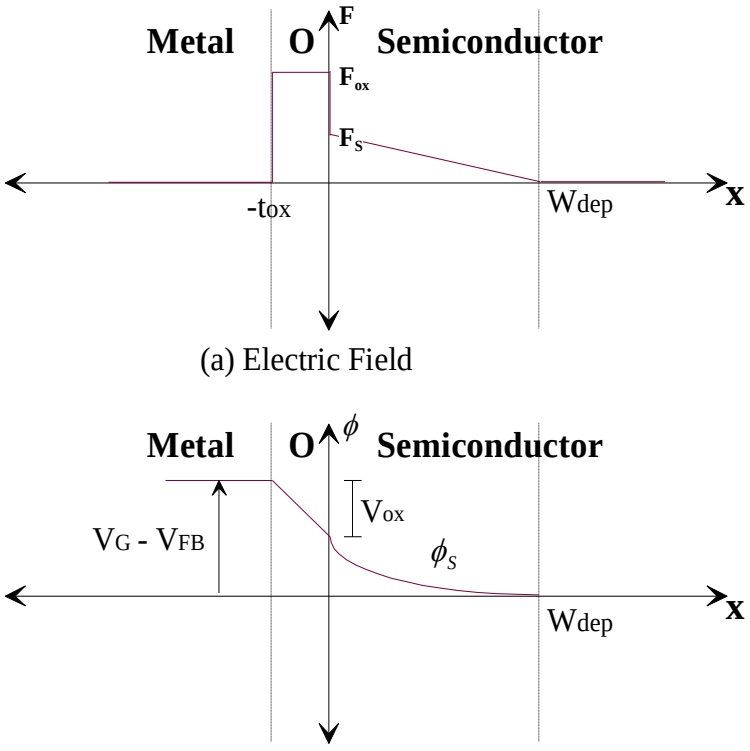

Figure 5.4. The (a) Electric Field and (b) Potential are plotted against distance x for a MOS capacitor. The electric field and the potential are obtained by first and second integrations of Poisson's equation, respectively [8].

The capacitance of the depletion region is seen to dominate with the increase of positive voltage at the gate as the channel is depleted of holes. The depletion capacitance is given by

$$C_{dep} = \frac{\varepsilon_s \varepsilon_0}{W_{dep}} \qquad 5.6$$

ε_s is the relative permittivity of the semiconductor and W_{dep} is the width of the depletion region. And hence,

$$C_{MOS} = \frac{\varepsilon_0 \varepsilon_{ox}}{t_{ox} + \left({}^{\varepsilon_{ox}}/_{\varepsilon_s}\right) W_{dep}} \quad 5.7$$

For a full depletion analysis to be carried out in convention semiconductors, a full depletion approximation and zero inversion layer charge below the threshold voltage is considered. The charge per unit area, Q_{dep}, in deletion region can therefore be given as

$$Q_{dep} = -qN_a W_{dep} \quad 5.8$$

where W_{dep} is the depletion region width and N_a is the acceptor density in the active layer. Integrating the charge density gives the electric field distribution. The electric field in the semiconductor, considering full depletion approximation, changes linearly due to the constant doping density and approaches zero at the edge of the depletion region (Fig.5.4a). The electric field at the oxide-semiconductor interface, F_S and in the oxide, F_{ox} is defined in terms of Gauss's law as

$$\varepsilon_{ox} F_{ox} = \varepsilon_S F_S \quad 5.9$$

$$F_S = \frac{qN_a W_{dep}}{\varepsilon_0 \varepsilon_s} \quad 5.10$$

and

$$F_{ox} = \frac{qN_a W_{dep}}{\varepsilon_0 \varepsilon_{ox}} \quad 5.11$$

respectively. The carrier concentration is more than zero in depletion region as the states below the Fermi level are full. Thus the field, ignoring the exponential component is given by

$$F = \left(\frac{2qN_a \phi}{\varepsilon_0 \varepsilon_S}\right)^{1/2} \quad 5.12$$

Figure 5.4a shows the electric field changing abruptly at the oxide/semiconductor interface. This is because of the change in dielectric constants in both the oxide and the semiconductor. Further integration of the electric field gives the potential ϕ_s at the surface (Fig.5.4b).

$$\phi_s = \frac{qN_a{W_{dep}}^2}{2\varepsilon_s\varepsilon_0} \qquad 5.13$$

5.2.4 Inversion Region

In conventional semiconductors, if the positive bias is increased so much that the conduction band edge gets very close to the Fermi level, the electron concentration increases and the semiconductor shows properties of an n-type semiconductor (Fig.5.2c) [8, 9]. This happens at voltages beyond the threshold voltage V_T which is generally twice the bulk potential, ϕ_0. A negatively charged inversion layer exists at the oxide semiconductor interface with the depletion layer and contains the minority carriers (electrons) that are attracted to the interface by a positive voltage. Unlike in depletion region where the electrostatics of the interface is dominated by the ionised dopant atoms, the electrostatics in inversion is dominated by the concentration of the minority carriers. Increasing gate voltage any further does not change the depletion region width. However, the minority charge in the inversion layer increases exponentially with surface potential. The semiconductor remains in thermal equilibrium even when a voltage is applied at the gate. Applying an electric field does not necessarily mean the semiconductor is in a non-equilibrium state.

When the electron density at the surface exceeds the hole density in the semiconductor, strong inversion takes place. An additional charge Q_{inv} is present in the inversion region and is zero at and below the threshold voltage. The total potential across the surface of the semiconductor, ϕ_s, equals twice the bulk potential, $\phi_s = 2\phi_0$.

The depletion region does not change once the inversion condition is satisfied as the free carriers induced after inversion start to prevent further depletion. The depletion region is therefore restricted to the potential range

$$W_{max} = \left(\frac{2\varepsilon_s \varepsilon_0 \phi_s}{qN_a}\right)^{1/2} \quad 5.14$$

for $0 \leq \phi_s \leq 2\phi_0$.

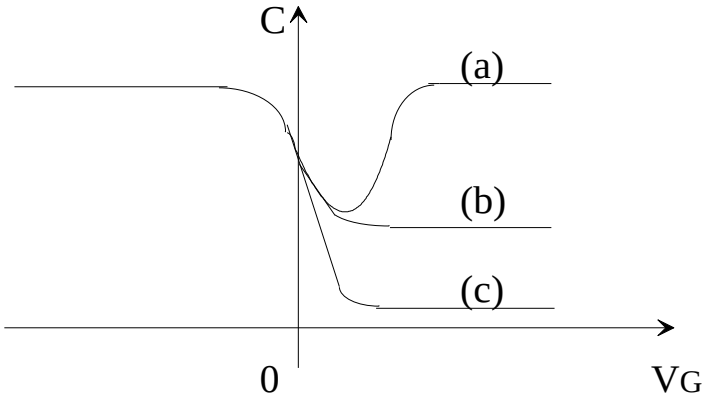

Figure 5.5. A typical C-V plot of a conventional p-type MOS capacitor at various frequencies in inversion; (a) The capacitance due to minority carriers is more than the capacitance due to the oxide and hence the oxide capacitance dominates. (b) At high frequency, the minority carriers (electrons) are unable to keep up with the change in ac signal and (c) at low frequency.

For a conventional semiconductor, the capacitance measured at inversion is dependent on the frequency of the ac signal. Figure 5.5 explains three different inversion conditions at various frequencies. The minority carriers, electrons in a p-type semiconductor, are able to keep up with the dc ramp and the ac signal at low frequencies in the inversion region. This causes an accumulation of minority carriers in the inversion region and hence gives rise to the inversion capacitance. The dominion of the accumulated minority charge causes the device to act as a capacitor C_{inv}, which becomes larger than C_{ox} . The equivalent circuit defined in terms of series combination of C_{inv} and C_{ox} provides a total capacitance thus dominated by C_{ox}, C_{max}= C_{ox} (Fig.5.5a). The dominion of C_{ox} in accumulation is due to the presence of majority carriers, holes but the dominion of C_{ox} in inversion is due to the minority carriers. These minority carriers are able to follow both the ac signal and the dc ramp at low frequencies.

At high frequencies in inversion, the electrons are unable to keep up with the change in ac signal causing a split in the Fermi level. The electrons cannot accumulate at the interface causing the capacitance to stay constant at C_{min} due to the depletion region of ionised dopant atoms. The minimum capacitance in the C-V characteristics is thus given by

$$C_{min} = \frac{\varepsilon_0 \varepsilon_{ox}}{t_{ox} + \left(\varepsilon_{ox}/\varepsilon_s\right) W_{max}} \qquad 5.15$$

W_{max} is the maximum width of the depletion region and does not change. When W_{dep} is less than thickness of the semiconductor, an inversion layer is formed. Any extra gate voltage applied causes electrons to be added to the inversion layer. This produces C-V characteristics as in Fig.5.5b.

Unlike conventional semiconductors, inversion in the case of a polycrystalline organic semiconductor may not be possible. Instead, it is possible for deep depletion to take place across the full thickness of the semiconductor layer (Fig.5.5c). The extension of the depletion width to the back of the semiconductor layer then results in a drop in the depletion capacitance (Fig.5.7). These effects are explained in the following text from the results obtained for a polycrystalline MOS capacitor.

5.3 FABRICATION OF POLYCRYSTALLINE ORGANIC MOS CAPACITORS

For polycrystalline organic semiconductor based capacitors, Aluminium is evaporated as the bottom contact followed by the annodisation of the dielectric layer. Self-assembled-monolayers (SAMs) can be used as dielectric layers in various devices such as TFTs. SAMs with defined deposition process and proper molecular design, are used to decrease the thickness of a dielectric layer and thus enhance device properties and consequently the performance of integrated circuits [10, 11]. Moreover, solution processed polymer gate dielectrics are of vast interest due to their low-cost fabrication processes of the organic devices [12-17]. These solution-processable dielectrics have an advantage of being able to be deposited by methods such as printing, spin-coating and spray-coating instead of expensive techniques as vacuum deposition. Although the solubility of organic layers is an advantage in terms of low cost, it makes the deposited layers in a

top gate configuration more susceptible to intermixing and swelling when preparing an all-organic multilayer structure. Another huge advantage is the ease of dielectric synthesis to suit the application type especially in terms of organic electronics. In a bottom gate configuration, the insulator is able to change the morphology of the semiconductor. The surface energy of the insulator affects the nucleation and growth mechanism of deposited films. A decrease in the grain size with an increase in surface energy is expected when the nucleation rate is increased. Nucleation rate is expected to be different for different insulating layers [18].

Insulators can also affect the chemical and electrical characteristics. High- *k* insulators boost the formation of local states which in turn induces carrier localization and reduces charge-carrier mobility. High- *k* dielectrics have high capacitance which is of interest from the dependence of charge density (or gate voltage) on mobility [19]. For high capacitance insulators at low gate voltages, the increase in mobility is expected with the increase in carrier concentration. Nevertheless, benefits have also resulted from the use of low- *k* insulators [20] and further research is required to understand this.

A large number of inorganic dielectrics have been investigated over the years with a range from bulk materials like inorganic oxides [21-24] and nitrides [12, 25, 26] and their deposition methods, to multi layers and blends consisting of inorganic dielectrics and polymer dielectrics [30-32]. Most high- *k* dielectrics are expensive to process with expensive deposition methods and result in poor film quality unless they are made thick to reduce leakage currents.

Aluminium oxide, a high- *k* dielectric, has shown good progress over the years [27, 30]. For the fabrication of a polycrystalline MOS capacitor, aluminium is converted directly to aluminium oxide (Al_2O_3) by anodisation at 35V. The oxide is annealed under nitrogen gas for two hours at 100°C followed by treatment with either plasma or hexamethyldisilazane (HMDS). HMDS is soluble in organic solvents and is an excellent adhesion promoter deposited prior to the deposition of the organic semiconductor layer [31]. The silanes in HMDS, due to their non-functional nature, react with only one site on the surface making the surface inert. This means unbound polymers are restricted to move freely and elute from the column as polymerization is not viable. Also, HMDS causes elimination of surface moisture by surface dehydration due to mono-functional reagents [32]. Surface treatment is followed by spinning of the organic semiconductors.

Experiments on two kinds of pentacene derivatives are carried out, namely S1150 and TIPS-pentacene [33, 34]. The S1150 solution is spun once at high speeds and re-spun to ensure that a film of S1150 is formed on the oxide. It must be noted that no prior surface treatment is carried out on the S1150 sample. However, surface treatments are carried out with TIPS-pentacene samples. Alternatively, TIPS solution is prepared by dissolving approximately 10mg of TIPS in 1ml of Toluene. The solution is heated to enhance the solubility and increase the concentration of the solution. Increasing the concentration of the organic solution can cause the solution spun film to become too thick and peel off. The solution is spun at different speeds to obtain the best organic film. The organic film is re-spun if the layer formed is visibly unsatisfying. The thickness of both the organic films is in the range of 50 to 100nm.

The effect of grain size is of much importance in organic TFTs and under continuous scrutiny. For conventional polycrystalline semiconductors, the mobility increase with an increase in grain size as the charge transport in polycrystalline materials is limited by the grain boundaries but controlled by the highly conducting ordered grains. An increase in the grain size automatically means that the grain boundaries decrease leading to enhancement in transport. Although this is assumed for oligothiophenes like sexithiophenes [35], the opposite is observed in many of pentacene experiments [36, 37].

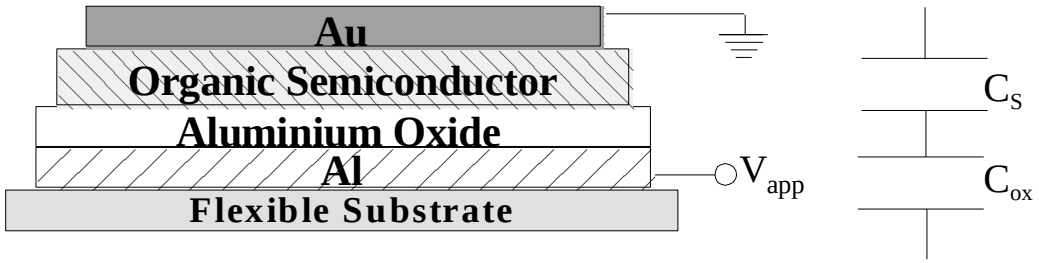

Figure 5.6. Schematics of a MOS capacitor and a simple equivalent circuit consisting of capacitance due to space charge and the oxide in series.

After the samples have dried, gold contact is evaporated through a shadow mask. The ohmic contact is necessary for an unhindered supply of carriers. The structure diagram of the organic MOS capacitor used in our study is given in Fig.5.6 and looks like that of a conventional MOS capacitor. A list of steps, to fabricate the MOS capacitors, is presented in Table 5.1. Because of the different physical and chemical nature of the insulator and the semiconductor, their

association may lead to highly disordered interfaces and hence to poor performance. Heating the substrate during drying of the active layer [38-40] and deposition of the active layer a low rate [39, 41] have shown to lead to better performance. Alternatively, introducing an organic monolayer such as octadecyltrichlorosilane (OTS) on the oxide, prior to the deposition of the active layer has been demonstrated to be effective by Lin et al. [42]. Another way to improve characteristics is to use polystyrene (PS) as an ultra thin film [43] or self-aligned monolayers (SAMs) [44, 45].

Table 5.1. A list of steps involved in producing organic MOS capacitors used in this chapter.

Fabrication Steps	1	2
Substrate	Glass	Glass
Gate Electrode	Aluminium	Aluminium
Insulator	Aluminium Oxide	Aluminium Oxide
Treatment	Annealing	Annealing
Surface Treatment	HMDS Oxygen Plasma	None
Organic Layer	TIPS-Pentacene -Spun	S1150 (Pentacene derivative) -Spun
Binder	None	None
Ohmic Electrode	Gold	Gold

The ac and dc characterisations are carried out using the Hewlett-Packard 4192A Impedance Analyser. The Capacitance-Voltage characteristics were obtained using PC controlled Keithley Voltage Source and Electrometer. Most of the measurements were performed using a step size of 0.1V with a sweep time of 1 second.

5.4 CAPACITANCE VOLTAGE CHARACTERISTICS

The electrical behaviour of the grain boundaries in a polycrystalline organic semiconductor, in essence, is a topic of interest due to their charge conduction properties and hence their link to device performance. In a MOS capacitor structure, the grain boundaries are assumed to be in parallel to the charge transport. This is thought to be because of a minimum number of grain and grain boundaries across the thickness of the thin organic layer. C-V measurements are conducted for polycrystalline S1150 based MOS capacitor to measure changes to the carrier kinetics with applied bias and frequency as they are also parallel to the grain boundaries.

For C-V measurements, a dc voltage is applied in the range of -10V to 5V and a small ac voltage of about 5-10mV is superimposed (Fig.5.8). The dc voltage provides the charge carriers whereas the ac voltage depends on the mobility of the charge carriers. The C-V characteristics shown in Fig.5.8 clearly indicate the behaviour of S1150, as a p-type semiconductor. In accumulation region, the dielectric thickness of the gate dielectric is much larger than the effective Debye length such that the capacitance of the accumulation region is much greater than the oxide capacitance. However as the two capacitances are in series, the smaller oxide capacitance dominates such that $C_{max} \cong C_{ox}$. C_{ox} is approximately 1800pF from Fig.5.8 and gives the oxide thickness of approximately 38nm using Eq. (5.1) at a frequency of 1 kHz. The calculated oxide thickness might not be accurate due to the dependence of accumulation capacitance on the frequency of the ac signal. The capacitance in the accumulation region is determined by the effective Debye length of the semiconductor as in Eq. (4.1). As effective Debye length increases, the capacitance of the accumulation region decreases resulting in the Debye length effect.

The carriers drift within the organic layer depending on the applied bias. After an initial reverse sweep (deep depletion- depletion- accumulation), a thin uniform layer of charge is accumulated at the surface. However, sudden reversal of voltage as in Fig.5.8 shows that the carriers go into instantaneous depletion with the application of forward sweep (accumulation- depletion- deep depletion). The flat band in Fig.5.8 is seen to shift to higher negative voltages as the sweep is reversed. This anti-clockwise effect is most likely due to the combined effect of the fixed oxide charge, work function difference between the metal and the semiconductor and mobile ionic charge. The flat band voltage is thus higher than expected. The presence of fixed oxide charge creates a fixed voltage drop across the oxide which can be seen on the C-V curve.

When both ac and dc signals are applied together, the depletion region moves back and forth due to the ac term such that the depletion region is seen to be constant while increasing dc voltage provides the flow of electrons. In the depletion region, the depletion capacitance falls and therefore dominates as the depletion width increases. The slope obtained from the C-V method gives a good approximate of the dopant concentration, N_D (or N_a), which is independent of the interface trap effects.

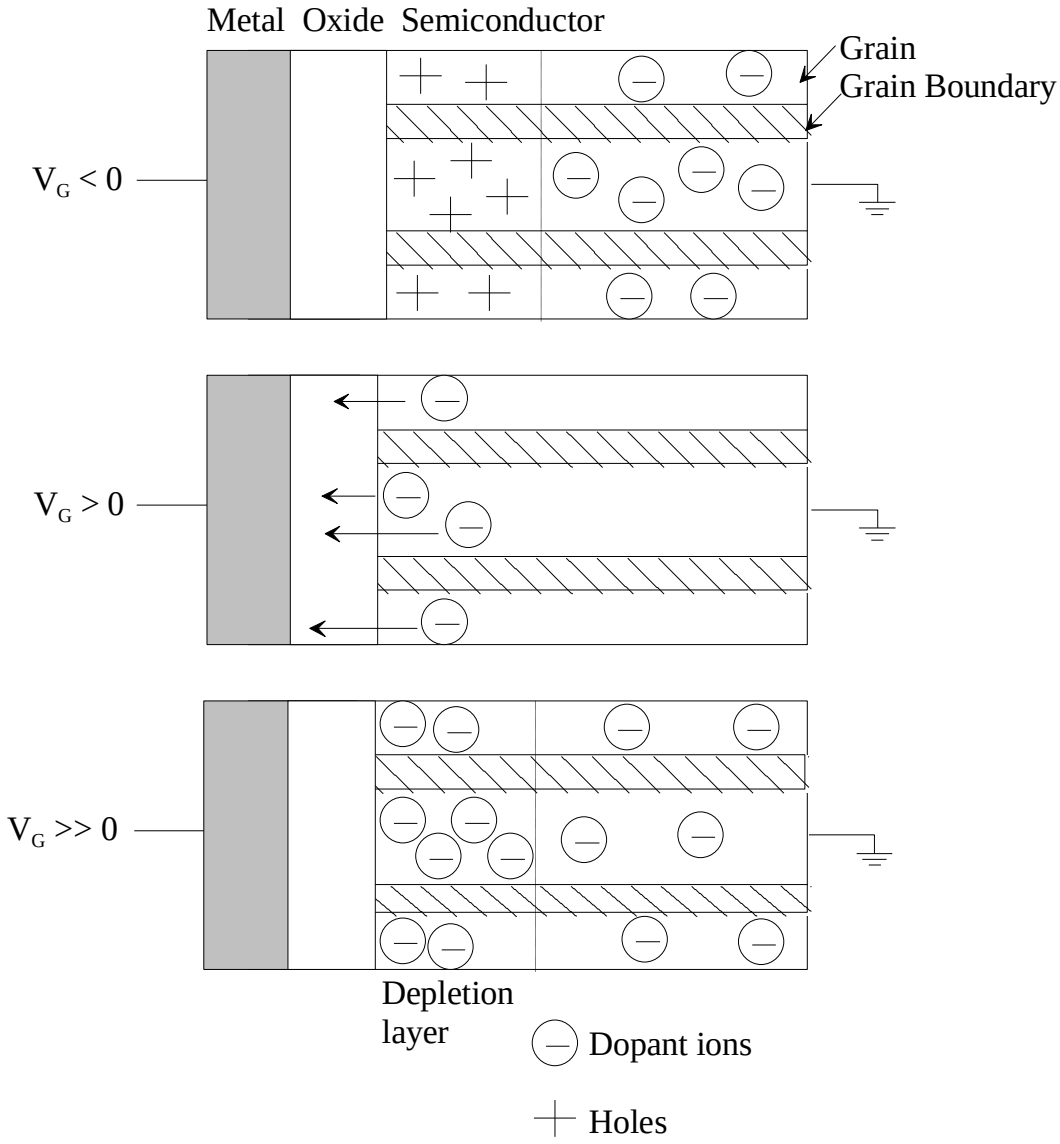

Figure 5.7. The change in organic MOS capacitor with application of an external bias at the gate electrode. The polycrystalline active layer shows both the grains and the grain boundaries. A negative potential $V_G<0$ causes an accumulation of holes at the interface. Application of a positive voltage $V_G>0$ causes the dopant ions to drift to the interface and the depletion of holes. Increasing the positive bias $V_G>>0$ causes the extension of the depletion region into deep depletion where depletion region falls across the thickness of the organic layer.

In the inversion region for high frequency C-V plots (V_G >>0, Fig.5.7), the interface trap effect does not contribute to the total capacitance directly. The capacitance in inversion is given by C_{min} as discussed before. This is because the response time is longer than the period of the ac signal and therefore they cannot respond to the ac excitation. They do, however, stretch out of the C-V curve. As C_{min} has a value, there is assumed to be some accumulation of minority carriers. Nevertheless, the depletion condition in organic materials is stronger than in the inorganic counterparts and there may not be a supply of minority carriers causing inversion. The electron-hole pairs exist in organic materials. However, the separation of these charge pairs is improbable due to their low relative permittivity values [46, 47]. A high percentage of these charge pairs recombine quickly before the separation. The charge carrier movement is also considered to be one dimensional and thus may cause the charge pairs to recombine without separation.

A constant C_{min} is observed due to Fermi level pinning of traps in grain boundaries of the polycrystalline layer so any further application of bias makes little difference to the capacitance [47, 48].The Fermi level is pinned because of a large surface state density at an energy level such that any further increase in applied bias prevents any reduction in capacitance. The C_{min} is seen to be constant when trap filling causes little or no effect with change in voltage [48]. It is also believed that a constant C_{min} is observed once the depletion region extends across the whole thickness of the active layer as discussed earlier [47].

The contact of gold with S1150 does not provide an unhindered injection of electrons since the electrons have to overcome a large barrier at the gold/S1150 interface. The contact treatments carried out for barrier reduction at the gold/TIPS-pentacene interface, for Schottky diodes in Chapter 3, are not application in such a situation. The treatments cannot be attempted on top of the organic layer as they greatly affect the device characteristics. Also, even if electrons were introduced into the organic film, they would not be able to invert the surface at low frequencies due to their low mobility values.

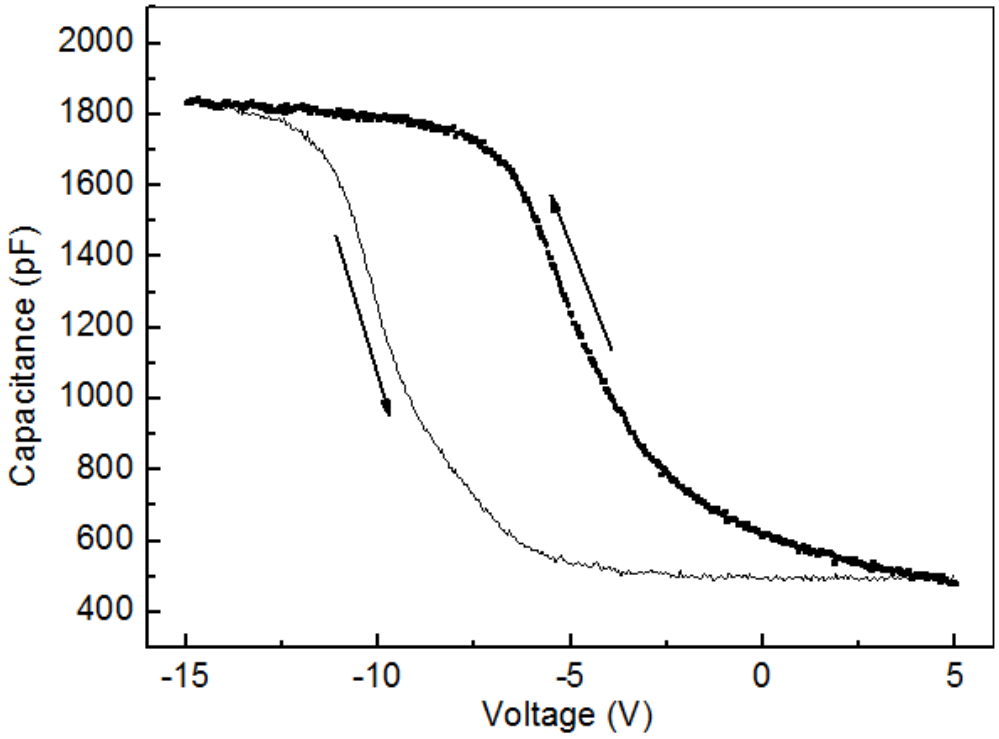

Figure 5.8. The best obtained capacitance voltage (CV) characteristics of a S1150 based MOS capacitor at 1kHz with device area of 7.85x10^{-7}m^2. The oxide capacitance is approximated to be 1800pF. A constant C_{min} is observed at higher positive biasing conditions. An anti-clockwise hysteresis is thought to be due to the oxide charges, charge at the metal/semiconductor interface, mobile ionic charges and the metal/semiconductor work function difference.

Using the conventional method, the dopant density from C_{max} and C_{min} ratio provides enough information to find the approximate maximum depletion width by,

$$\frac{1}{C_{dep}} = \frac{1}{C_{min}} - \frac{1}{C_{max}} \qquad 5.16$$

$$W_{dep} = \varepsilon_0 \varepsilon_S \left(\frac{1}{C_{min}} - \frac{1}{C_{max}} \right) \qquad 5.17$$

For an MOS capacitor made with a polycrystalline organic material, equating Eq. (5.17) in Eq. (5.14) gives the dopant concentration for ordered grains and the surface concentration (equivalent to dopant concentration) for disordered grain boundaries respectively.

$$N_a = \frac{2{C_{max}}^2 \emptyset_S}{q\varepsilon_0\varepsilon_S\left(\frac{C_{max}}{C_{min}} - 1\right)^2} \qquad 5.18$$

The dopant concentrations obtained, from the C-V plots of an MOS capacitor are only an approximation. N_a obtained at the frequency of 1 kHz is approximately $3.6\text{x}10^{17}\text{cm}^{-3}$ with the conventional method. This value cannot be treated as an accurate value for N_a as C_{min} changes with frequency. The true value of C_{min} is thought to occur at a lower frequency than 1 kHz. However, N_a obtained at 1 kHz can be considered a good approximation as C_{max} is equivalent to the C_{ox} at this frequency and C_{min} is flat such that a maximum depletion width is reached. This is discussed further in Section 5.5.

5.4.1 Effects of Oxide and Interface charge on C-V Characteristics

Hysteresis is due to charge trapping in the oxides. Two basic types of charges can exist in the oxide layer, the trap charges Q_{ot} and the fixed oxide charges Q_{fixed}. These types of charges can either shift or stretch the characteristics along the axes (Fig.5.9a). The direction of the shift relative to an ideal C-V curve can be used to determine the magnitudes of the oxide. A positive oxide charge tends to move the characteristics towards the negative side of the plot whereas a negative charge does the opposite and shifts the characteristics in the positive voltage direction. The anticlockwise movement of characteristics can be due to the interface trapped charges, Q_{it}. A positive interface charge exists at the interface, causing the plot to shift towards more negative voltages. Interface charge stretches the CV and may give an overestimation of N_a. Both interface trapped charge and the oxide charge must be present to shift the CV to negative voltages in Fig.5.8.

Figure 5.9b explains the change in the C-V characteristics if the fixed oxide charge is responsible for the voltage shift. The fixed charge displayed in Fig.5.9b is assumed to be close to the oxide-organic semiconductor interface and cannot be charged or discharged over a wide variation of surface potential. Thus fixed oxide charge is position dependent. The fixed charge is usually

thought to be positive and depends on oxidation and annealing processes. It does not depend on the type or concentration of impurities in the semiconductor and/or the thickness of the oxide [2, 8]. Existence of a fixed oxide charge leads to an increase in the capacitance for all values of the gate bias in the depletion and weak inversion region. However, depletion capacitance is less in the presence of fixed charge. When no fixed charge is present, the depletion capacitance increases and total charge comprise of the ionized donors at a given bias.

Oxide trapped charge Q_{ot} exists due to imperfections in the oxide. Interface state charge Q_{it}, arises at the interface between oxide and semiconductor, due the sudden break in the semiconductor lattice at the oxide interface and depends on the lattice structure of the semiconductor itself. At the interface, adding all the components of charges gives the effective positive charge Q_i. This induces an equivalent negative charge in the semiconductor. The flat band voltage then becomes

$$V_{fb} = \phi_{ms} - \frac{Q_i}{C_{ox}} \qquad 5.19$$

Band bending at the semiconductor surface thus occurs due to both the combined positive charge due to work function difference ϕ_{ms} and the effective interface charge Q_i. This charge causes the semiconductor to become negative as a negative charge is induced in it. A less positive voltage is thus applied to the metal to achieve the flat band conditions.

For S1150 MOS capacitor, an anti-clockwise hysteresis is obtained when the voltage is swept in both directions (Fig.5.8), as discussed earlier. The anti-clockwise hysteresis is thought to be due to oxide charges and the work function difference between the TIPS-pentacene and oxide layer. It is also likely that hysteresis is dependent on the thickness of the semiconducting layer, increasing with decreasing thickness. Slow trapping of electrons is also a possible reason for the anti-clockwise hysteresis but as this is a slow process, it is unlikely to cause such a large effect as seen in Fig.5.8. A possible effect for this large hysteresis can be the presence of mobile residual impurities and dopant ions within the bulk of the organic semiconductor film. Mobile residual doping and impurities can be introduced into the structure unintentionally during fabrication processes. Therefore, it is essential to use clean chemicals, water, gases and processing environment to minimise the effects of contamination. Increasing the temperature makes the

impurities much more mobile so they can drift closer to the interface due to an applied electric field and have a bigger effect on the semiconductor.

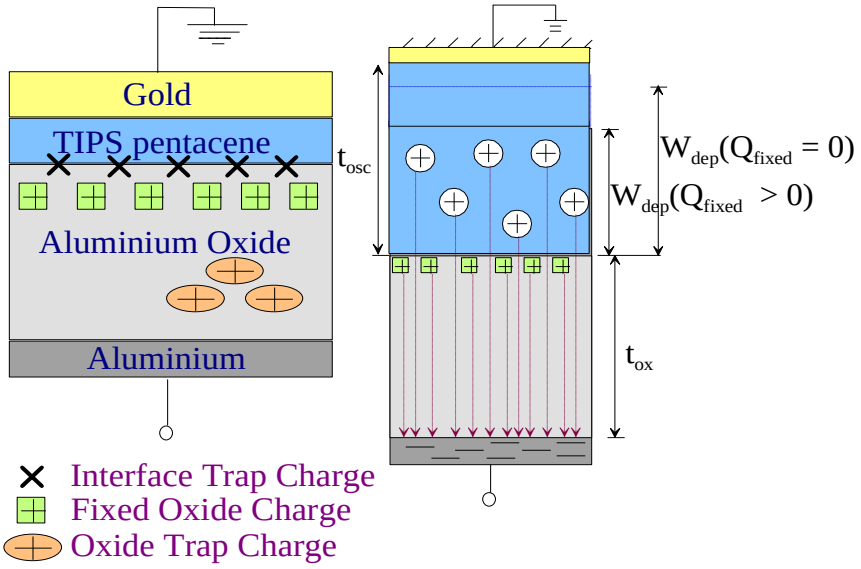

Figure 5.9. A MOS capacitor (a) with various oxide and interface charges, (b) with a negative bias and fixed oxide charge [49]

5.4.2 Effect of Air Exposure

Upon exposure to air, an interesting phenomenon is observed in the accumulation region of the C-V plot of a TIPS-pentacene based MOS capacitor as in Fig 5.10. As the capacitor is exposed in air, an improvement in C_{max} is observed with increase number of days, reaching a value close to that of the oxide capacitance. The high measured C_{max} is thought to be due to the improvement in charge transport. The exposure to air and light, an effect known as photo-oxidation facilitates the charge transport in the organic layer. Photo-oxidation causes doping of the semiconductor implying that the lowest trap states are filled and the carriers introduced by applied bias occupy higher closer states thus allowing for an ease in hopping. Enhanced transport means that the carriers are much more active to hop around in the available states present along with the dopant

ions such that the charge mobility improves and the maximum capacitance increases. In addition, an increase in hysteresis is observed with photo-oxidation.

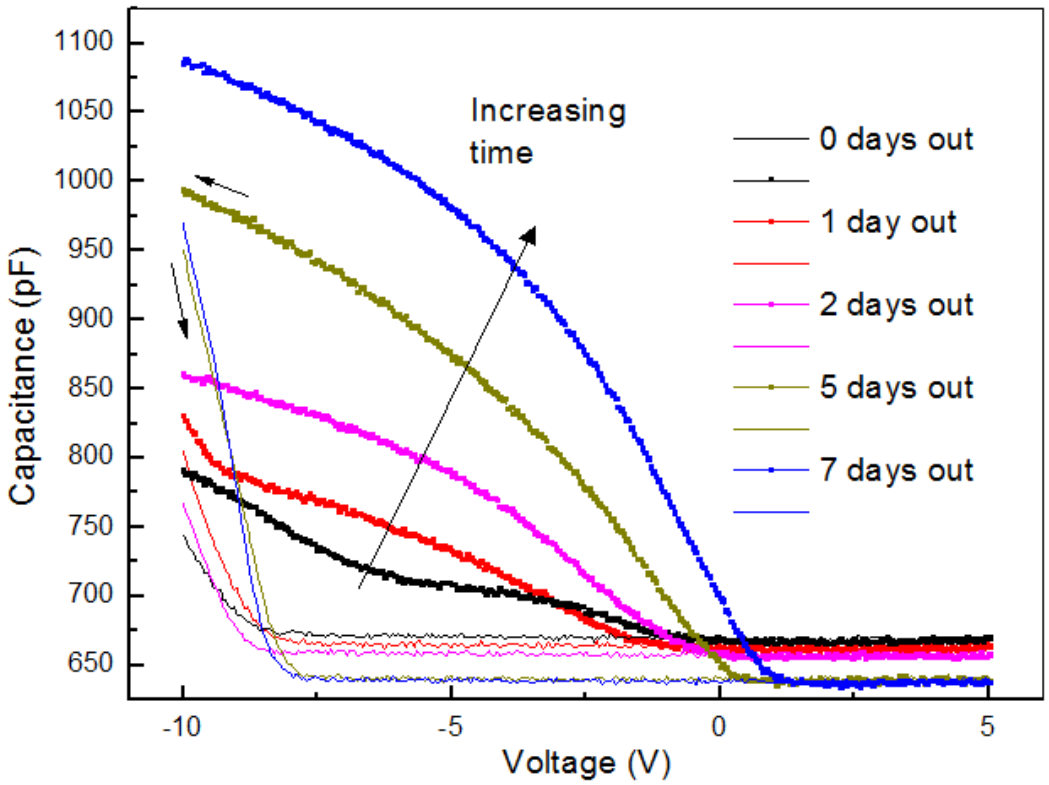

Figure 5.10. The effects on Capacitance Voltage Characteristics on plasma treated undoped TIPS pentacene based MOS capacitor from Table 5.1 with days left in air. The active material is spun at 1000 rpm for 30s and left to dry in air before further fabrication and the device area is $7.85x10^{-7}m^2$.

Furthermore, oxygen is expected to increase the acceptor-like traps in organic materials to promote surface oxidation of the semiconductor. In pentacene OTFTs, these oxygen- induced traps are thought to be the basis of the generation of extra hole current in the sub-threshold region [50, 51]. Impurities, improving the C-V characteristics with time, also include positive trap charge due to moisture or mobile charges [51, 52]. These impurities increase the charge collected at the interface such that the accumulation charge at the interface improves and resulting accumulation capacitance increases.

5.5 CAPACITANCE-VOLTAGE FREQUENCY CHARACTERISTICS

The capacitance voltage (C-V) behaviour of an organic S1150 based MOS capacitor is different from an ideal case as a result of the presence of the interface states between the S1150 and Al_2O_3 or other non-uniformities mentioned earlier in Section 5.4. These interface states can be due to the various fabrication processes involved, surface morphology, formation of an insulating layer and impurities added to the organic semiconductor during synthesis. A bias shift and frequency dispersion on a C-V characteristics denotes existence of these interface states as seen in Fig.5.8. C-V analysis is also useful to find parameters such as the flat and the mid band-gap voltages and the oxide thickness. This has been done in the previous sections.

Recently, Kim et al. [53] used an RC equivalent circuit to model frequency-dependent capacitance of pentacene transistors. They also suggested that a charge control model based on Meyer [54] may be effective in explaining the voltage dependent intrinsic capacitance of a pentacene TFT. This section deals with the variation of frequency of an organic polycrystalline based MOS capacitor from the lowest to the highest measurable frequency. This is to extract parameters such as the mobility, conductivity, cut-off frequency and the bulk components. An equivalent circuit model is also proposed to find the bulk resistance and the bulk capacitance of the organic semiconductor. For these reasons, it is important to consider the effect of frequency and applied bias voltage in the examination of electrical characteristics of MOS devices. The C-V measurements have been carried out in the frequency range of 500 Hz–1 MHz, in air and at room temperature (Fig.5.11).

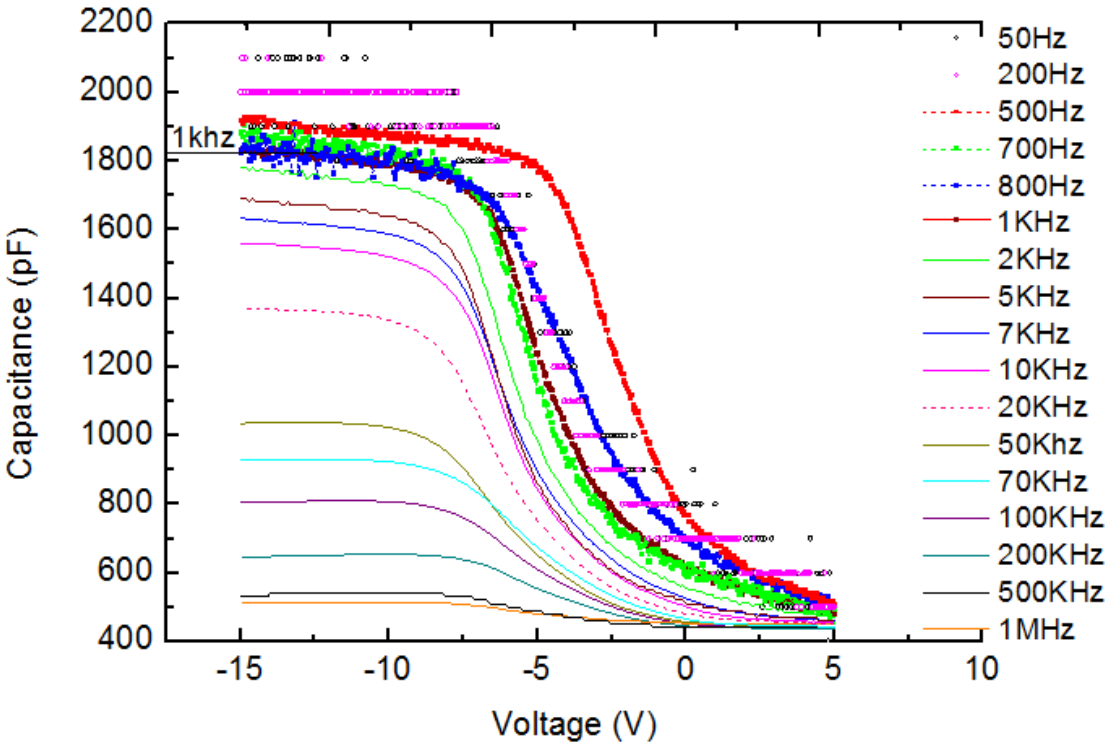

Figure 5.11. Variation of Capacitance Voltage characteristics with change in frequency for the $Al/Al_2O_3/S1150$ MOS structure from Table 5.1. The increase in frequency causes a decrease in both the accumulation capacitance and C_{min}.

Change in frequency causes a change in the accumulation capacitance. The capacitance frequency (C-f) plot is obtained by plotting the capacitance in strong accumulation against frequency (Fig.5.12). As the frequency increases, the accumulation capacitance decreases due to a reduction in the concentration of holes at the surface associated to the relaxation time attributed to the conductivity of the S1150 layer. At lower frequencies, a constant capacitance is expected however not evident as in Fig.5.12. Factors such as the fringe effect at the sides of the contact electrodes or a rough oxide layer can cause the capacitance to vary at lower frequencies. Fringe effect is caused due to the field lines spreading outside the active device area resulting in a larger effective area. However, a rough oxide layer is mainly associated with the fabrication process.

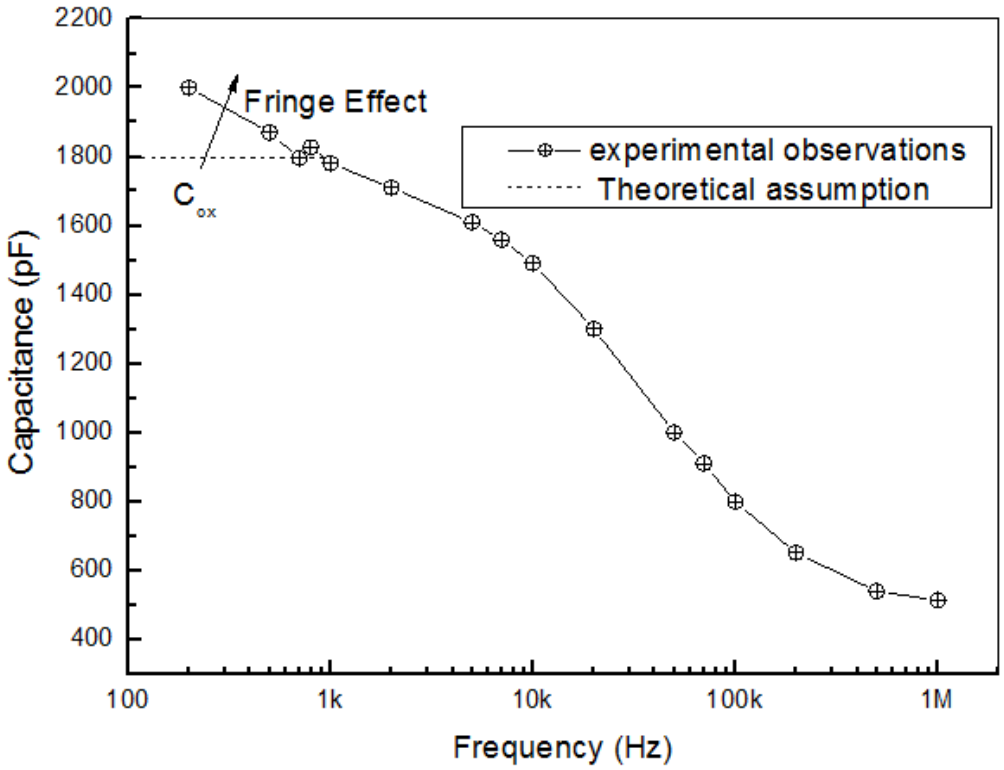

Figure 5.12. Accumulation capacitance against frequency for a S1150 based MOS capacitor (at -15V). The small deviation at lower frequencies is thought to be owing to fringe effects.

In accumulation at high frequencies, the ac signal is too fast for the carriers to follow. The mobility of the carriers is low for organic materials to respond to the ac signal at higher frequencies and accordingly the contribution to the overall capacitance is reduced. At lower frequencies, the oxide capacitance dominates $C_{max} \sim C_{ox}$ and therefore, C_{acc} must be larger than C_{ox}. However as the resultant capacitance decreases with increasing frequency and the oxide capacitance is fixed, the accumulation capacitance must be decreasing as in Fig.5.12.

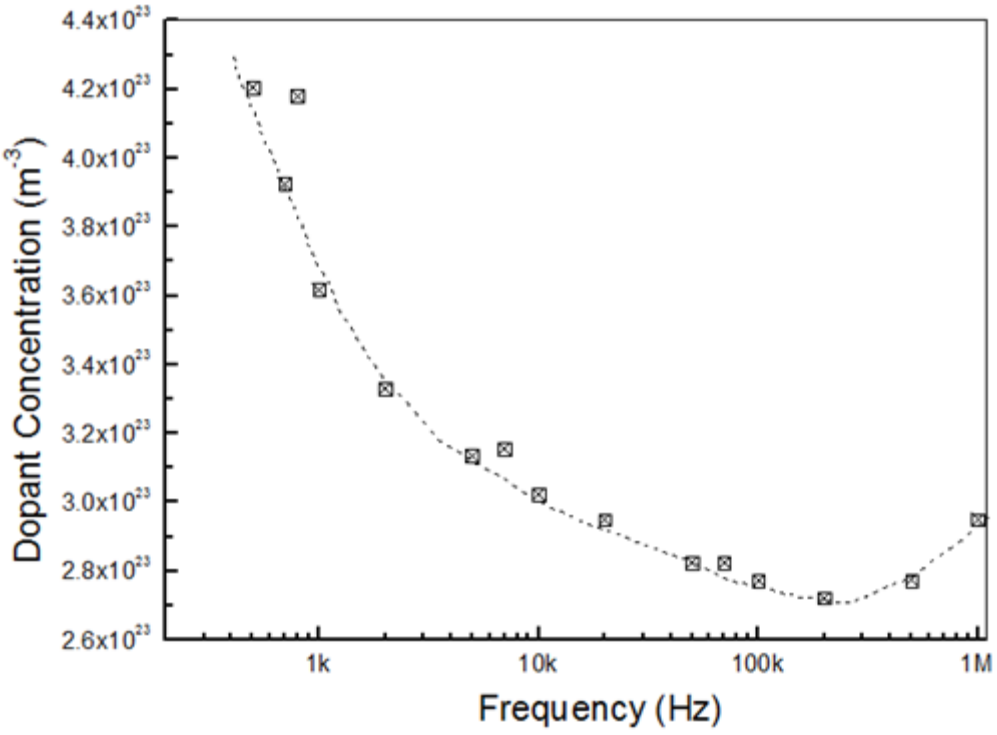

Figure 5.13. Plot of dopant concentration against frequency for the Al/Al2O3/S1150 MOS capacitor. The dopant concentration is seen to decrease with an increase in frequency.

For polycrystalline organic based MOS capacitor, the dopant concentration is found to decrease with increase frequency as in Fig. 5.13, particularly due to changes in C_{max}. At lower frequencies, the charge is able to follow both ac and dc voltage and holes are able to deplete easily. At higher frequencies, however, the carriers cannot accumulate sufficiently and thus C_{max} decreases. The carriers are only able to follow the dc voltage and cannot contribute to the capacitance. Also, inversion is considered unlikely in organic semiconductors, especially at higher frequencies as the width of the depletion region is assumed to extend to the back of the organic layer, causing deep depletion. This causes the semiconductor to deplete at the back contact. The thickness of the organic layer in this case is assumed less than the width of the depletion region. Ideally the dopant concentration for a given semiconductor must remain constant with the change in frequency. Thus, the decrease in dopant concentration with frequency is unlikely, therefore, making the method to obtain N_a not very accurate but only estimation.

The maximum capacitance is equivalent to the oxide capacitance at 1 kHz where C_{ox}~ 1800pF corresponding to the thickness of the oxide layer of 38nm in Fig.5.11. The thickness of approximately 40nm is expected from the annodisation process to form Al_2O_3. C_{max} for the purpose of obtaining the dopant concentration is kept constant at C_{max}~ C_{ox}. At 1 kHz the dopant concentration from the C-V plot in Fig.5.11 is approximately $3.6x10^{17}cm^{-3}$. This is much higher than the dopant concentration of approximately $5.2x10^{14}cm^{-3}$ obtained at 1 kHz using Eq. (3.45) from the C-V analysis of polycrystalline TIPS/PAMS diodes in Section 3.5. However, Eq. (5.18) is still limited by the frequency for a polycrystalline organic based MOS capacitor. C_{min} is also seen to fall with the increase in frequency. The reasons for a constant C_{min} have been discussed earlier in Section 5.4.

5.5.1 Small Signal Behaviour of an Ideal Organic MOS Capacitor

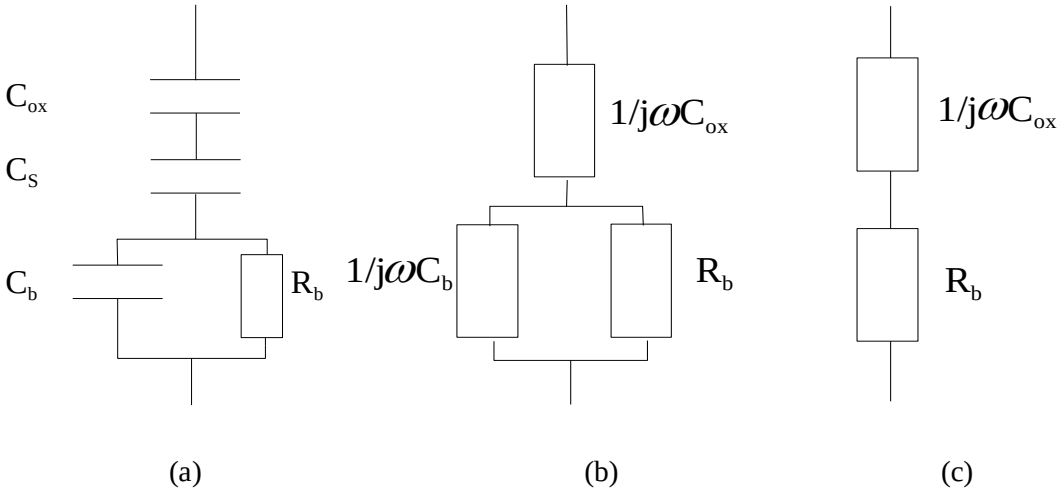

Figure 5.14. Proposed model for an equivalent circuit of a polycrystalline organic MOS capacitor (a) at accumulation of space charge C_S, (b) simplified model assuming C_S>> C_{ox} so that C_{ox} dominates and (c) a further simplified circuit ignoring the effects of bulk capacitance C_b.

A simple model of an MOS capacitor based in accumulation can be obtained by assuming the space charge capacitance, C_S and the oxide capacitance, C_{ox} to be in series. Addition of the bulk properties of an organic semiconductor includes the capacitance C_b and resistance R_b to the existent model. The circuit consists of the bulk resistor and bulk capacitor in parallel to each other

with a space charge capacitor and oxide capacitor in series as in Fig.5.14a. The interface properties have been ignored at either side of the semiconducting layer for a simplified analysis.

Total admittance of the bulk circuit is given by

$$Y_b = \frac{1}{R_b} + j\omega C_b \qquad 5.20$$

where ω is the angular frequency and $j = \sqrt{-1}$. When the device is in accumulation, the space charge capacitance can be ignored as in Fig.5.14b and total admittance Y_{MOS} of the circuit is given by

$$Y_{MOS} = G_{MOS} + j\omega C_{MOS} \qquad 5.21$$

$$C_{MOS} = C_c + \frac{C_{ox} - C_C}{1 + (\omega\tau)^2} \qquad 5.22$$

where C_C is the series equivalent of C_{ox} and C_b and τ is the relaxation time, $\tau = R_b(C_{ox} + C_b)$

$$\frac{G_{MOS}}{\omega} = \frac{\omega R_b {C_{ox}}^2}{1 + (\omega\tau)^2} \qquad 5.23$$

If space charge capacitance is considered as in fig.5.14a, the series equivalent capacitance for C_{ox} and C_s is given by C_1. The total impedance, Z_t, for the circuit is then given by Eq.(5.17).

$$Z_t = \frac{R_b}{1 + j\omega R_b C_b} + \frac{1}{j\omega C_1} \qquad 5.24$$

As the depletion region changes with application of an external field, R_b and C_b both are adapted to explain the decline in the effective thickness of the bulk semiconductor.

$$R_b = \frac{(t_{OSC} - W_{dep})}{AN_a q\mu_b} \qquad 5.25$$

$$C_b = \frac{A\varepsilon_S\varepsilon_0}{(t_{OSC} - W_{dep})} \qquad 5.26$$

μ_b is the bulk mobility of carriers in the semiconductor [55].

For frequencies of $\omega \ll 1/R_b C_b$, the impedance in accumulation region can ignore the bulk capacitance and the space charge capacitance such that the circuit looks like Fig.5.14c

$$Z_t = \frac{1}{j\omega C_{ox}} + R_b \qquad 5.27$$

The space charge capacitance, in accumulation, is much bigger than the oxide capacitance resulting in $C_{max} \sim C_{ox}$. The bulk capacitance, at very low frequencies, has no effect as it is thought to be dependent on the dielectric constant and the thickness of the organic layer. The measured capacitance, thus, does not vary with frequency. Below a low frequency of about 5 kHz, the measured capacitance is constant and given by the oxide capacitance. The angular frequency at 5 kHz corresponds to $1/R_bC_b \approx 3.14\text{x}10^4\ \text{rads}^{-1}$. $1/R_bC_b$ is the higher limit of the relaxation frequency discussed later in the section. Above this frequency, the capacitance falls rapidly with frequency.

The frequency at which the bulk capacitance starts having an effect on the circuit is also dependant on the bulk resistance. For instance, a resistance connected in series with the MOS capacitor would confirm that the frequency at which C_b starts to fall decreases with increasing resistance.

At high frequencies of $\omega \gg 1/R_b C_b$, the bulk resistor is shorted out by the bulk capacitance such that both the R_b and C_b can be ignored and the equivalent circuit can be simplified to Fig.5.15. The measured capacitance then varies with frequency as observed in Fig.5.11. Impedance Z_t is therefore the series combination of the space charge and the oxide capacitance.

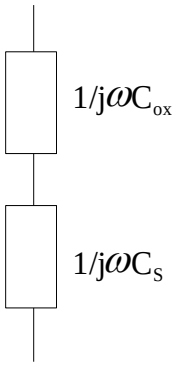

Figure 5.15. Simplified circuit for a MOS capacitor consisting of the oxide and space charge capacitance.

$$Z_t = \frac{1}{j\omega C_{ox}} + \frac{1}{j\omega C_S} \qquad 5.28$$

The small signal behaviour of an ideal MOS capacitor can be explained in terms of the equivalent circuit given in Fig.5.14a. The frequency response in inversion is indicative that the minority carriers are completely inactive. Only the majority carriers at the depletion layer edge contribute to the capacitance which becomes almost independent of the applied voltage. The model proposed in Fig.5.14 is explored further. Expanding Eq. (5.24) gives the total impedance,

$$Z_t = \frac{1 + j\omega R_b(C_1 + C_b)}{j\omega C_1(1 + j\omega R_b C_b)} \qquad 5.29$$

The total admittance from Eq. (5.29) is then

$$Y_t = \frac{j\omega C_1(1 + j\omega R_b C_b)}{1 + j\omega R_b(C_1 + C_b)} \qquad 5.30$$

The equivalent circuit, as a function of frequency, can thus be written in terms of an equivalent capacitor C_t , resistor R_t and conductance G_t.

$$Y_t = G_t + j\omega C_t = \frac{1}{R_t} + j\omega C_t \qquad 5.31$$

$$C_t(j\omega) = C_1 \frac{1 + \omega^2 {R_b}^2 C_b(C_1 + C_b)}{1 + \omega^2 {R_b}^2 (C_1 + C_b)^2} \quad 5.32$$

$$R_t = \frac{1 + \omega^2 {R_b}^2 (C_1 + C_b)^2}{\omega^2 {C_1}^2 R_b} \quad 5.33$$

In accumulation and at very low frequencies, C_t is C_1 and hence given by C_{ox}. C_{ox} gives the thickness of the oxide which is 42nm like the one from the oxide C-V measurements with dielectric constant of Al_2O_3, $\varepsilon_{ox} \approx 10$. Eq. (5.32) and (5.33) can be simplified at lower frequencies as

$$C_t = C_1 \quad 5.34$$

$$R_t = \infty \quad 5.35$$

and at higher frequencies as

$$C_t(j\omega) = \frac{C_1 C_b}{(C_1 + C_b)} \quad 5.36$$

$$R_t = \frac{R_b(C_1 + C_b)^2}{{C_1}^2} \quad 5.37$$

The imaginary part of Y_t gives C_t with two poles and two zeros at

$$\omega = \pm 1/R_b(C_1 + C_b) \quad 5.38$$

$$\omega = \pm 1/R_b\sqrt{C_b(C_1 + C_b)} \quad 5.39$$

At very high frequencies, C_b can be found from Eq. (5.36) as C_1 is already known and C_t is 514pF at 1MHz from the plot. C_b, found is approximately 760pF from Fig.5.16. This provides enough information to give the spun film thickness which is approximately 27nm. C_1 and C_b then give the bulk resistance R_b if R_t is known. With N_a from the slope of C-V plot, bulk mobility can also be

found from Eq. (5.40). Although, the poles and zeros provide crucial information, if they are close enough to each other, the error is critical providing a poor estimate for the bulk mobility.

The bulk capacitance has a value similar to the depletion capacitance such that the frequency dependent term of total capacitance C_t is nearly constant and is approximately equal to the depletion capacitance. Consequently, C_t does not change significantly with frequency. However, the frequency dependence of C_{min} can be significant in such a case.

The dielectric constant of the oxide is approximately 10 and is bigger than the dielectric constant associated with the semiconductor (~3) by a factor of more than 3. Hence, the depletion capacitance is less than the oxide capacitance by at least a factor of 3 and so C_1 is smaller but very close to C_s. The reduction in the capacitance above the frequency of 5 kHz may be explained by Maxwell–Wagner dispersion. The depletion region in this case is dependent on the frequency [53]. It is described as a momentary delay in the polarization of molecules at the boundary between two materials of different dielectric constants such as the oxide and the semiconductor, with respect to the change in electric field.

The bulk resistance can be found from the cut-off frequency f_C of the maximum capacitance in accumulation C_{max} versus frequency (Fig.5.16). The maximum slope of capacitance versus frequency is -6.2dB/decade which is much less than the slope of the ideal curve of -40dB/decade for large frequencies [56]. Hence the poles and zeros are not far from each other. However, if the low cut-off frequency is assumed to be around 5 kHz, the bulk resistance R_b found using Eq. (5.38) is approximately 13kΩ. If the concentration of holes is equivalent to the doping density ($N_a \approx 3.6 \times 10^{17} cm^{-3}$ at 1 kHz), the hole mobility from Eq. (5.40) of approximately 4.6×10^{-7} $cm^2V^{-1}s^{-1}$ can be estimated assuming the neutral region has ohmic conduction. At room temperature, the hole mobility μ_b obtained from TIPS/PTAA Schottky diodes in Fig.3.24 and TIPS/PAMS Schottky diodes in Fig.3.32 is in the range of 10^{-7} $cm^2V^{-1}s^{-1}$ approximately. The hole mobilities obtained from either of the devices are low but nearly equivalent.

$$\mu_b = \frac{t_{OSC}}{qAN_aR_b} \qquad 5.40$$

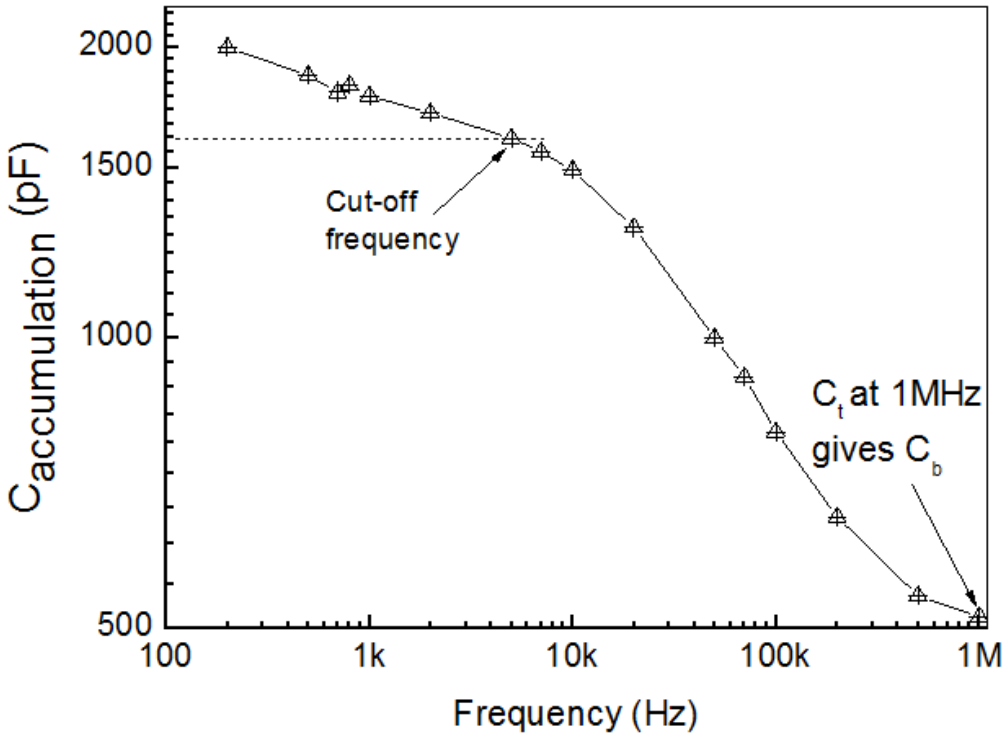

Figure 5.16. Cut-off Frequency and bulk capacitance from plot of accumulation capacitance and frequency at -15V.

N_a stays the same throughout the frequency range and therefore some other parameter must be changing for the change in hole mobility. The bulk resistance and thickness of the organic layer are both extracted values and must be approximates for a change in the mobility to occur. The bulk resistance is dependent on the frequency response and the t_{OSC} dependent on the spun film. Moreover, at lower frequencies the area of the device is an approximate if fringe effects are considered. A low value of bulk mobility obtained can be accounted by the frequency dependence of the C-V characteristics, the approximated constant value for the dopant concentration obtained from Eq. (5.18) at 1kHz or trapping effects at the semiconductor/oxide interface. The cut-off frequency f_C is dependent on the hole mobility in the organic layer. As the cut-off frequency increases indicating a decline in bulk resistance, the hole mobility increases. f_C is greatly dependent on the slope of the C-f curve. In essence, f_C is defined by the hole mobility and the active area of the device. Kim et al. [53] studied mobility effects on the cut-off frequency in pentacene transistors with the application of gate bias. The cut-off frequency was seen to improve

with an increase in gate voltage as it provided carriers to fill in the traps inside of pentacene and thus improved the mobility values [54].

Effects of Contact Resistance

The previous analysis comprises of an equivalent circuit without the effects of a contact resistance R_C (Fig.5.14a). However, it is now included in series with other components for a better understanding of the contact between the organic layer and the ohmic contact. Relaxation frequency for a circuit is the frequency over which the system comes into equilibrium with the surrounding. In such a circuit, two relaxation frequencies are visible; lower frequency due to bulk effects and a higher frequency due to the presence of the contact resistance. The circuit admittance, without the frequency effects of the series resistance, is given by Eq. (5.30) and is characterised as the typical Maxwell-Wagner effect [58, 59]. Maxwell- Wagner effect for two dielectric layers, namely the oxide and the semiconducting layer in our case, is defined in terms of the frequency response whose relaxation frequency f_{R1} (using the poles from Eq. (5.32) given in Eq. (5.38)) is

$$f_{R1} = \frac{1}{2\pi R_b(C_1 + C_b)} = \frac{1}{2\pi\tau} \qquad 5.41$$

where τ is the device relaxation time. The relaxation frequency $f_{R1}$is approximately equivalent to 5.19 kHz and τ is thus estimated to about 30µs.

As described above, the depletion region width is not constant in a MOS capacitor with constantly changing bulk resistance and bulk capacitance. Hence, the depletion capacitance is constantly changing with applied bias as well. For the device moving from accumulation to maximum depletion or back of the semiconductor thickness, the relaxation frequency f_{R1} is taken to stay within the limits of [58, 59]

$$\frac{qN_a\mu_b}{2\pi\varepsilon_0\varepsilon_s} > f_{R1} > \frac{1}{2\pi R_{b0}(C_1 + C_{b0})} \qquad 5.42$$

where μ_b is the bulk mobility, N_a is the dopant concentration, R_{b0} is the bulk resistance when the $W_{dep} = 0$ and C_{b0} is the bulk capacitance when $W_{dep} = 0$. The higher limit is independent of the geometric parameter of the MOS capacitor and can be obtained even without the knowledge of the thickness of the device or the area in contact with the electrode. Thus, f_{R1} limits are defined

between the frequencies of 5.2 kHz and 15.9 kHz approximately. The second relaxation frequency f_{R2}, observed due to the contact resistance, is at a higher frequency given by

$$f_{R2} = \frac{1}{2\pi R_C C_C} \qquad 5.43$$

where C_C is the series combination of C_{ox}, C_S and C_b. If the second relaxation frequency is very high (> 1MHz), the contact resistance is calculated to be < 309Ω.

5.6 CAPACITANCE-VOLTAGE TEMPERATURE CHARACTER-ISTICS

5.6.1 Experimental Procedure

Measurements on the capacitance-voltage (C-V) characteristics of polycrystalline organic S1150 based MOS capacitors are conducted for a range of temperatures to understand the variation in charge transport due to the presence of grains and grain boundaries. The C-V measurements were carried out using the method defined previously in Section 5.3. For the temperature measurements, the device was connected onto a liquid nitrogen cryostat under 0.1 mbar vacuum and the temperature was lowered from room temperature to 228K. Detailed analysis of the capacitance dependency on temperature with bias voltage is conducted and discussed further. The samples were attached to a metal holder using silver paint. The holder was then connected inside the cryostat with crocodile clips. Measurements following the connections show a large drop in accumulation capacitance associated with silver paint. It is thus very vital to establish a good connection between the metal and the metal holder to achieve better C-V characteristics.

5.6.2 Effects of Temperature Variance

Detailed analysis of surface states in a polycrystalline organic semiconductor based MOS capacitor requires temperature variation of capacitance with applied voltage. A method to find interface state density near the HOMO level can be explained in terms of a technique defined by Gray and Brown for inorganic semiconductors [60]. This technique measures interface density close to the majority carrier band edge. The change in flat band voltage is measured with change in temperature. The Fermi level, in this case, determines the small length of band gap available as the temperature changes. At high temperature it is likely for the oxide stability to control the Fermi level. The results obtained for temperature variation on C-V plots (Fig.5.17) are seen to be noisy due to the connections.

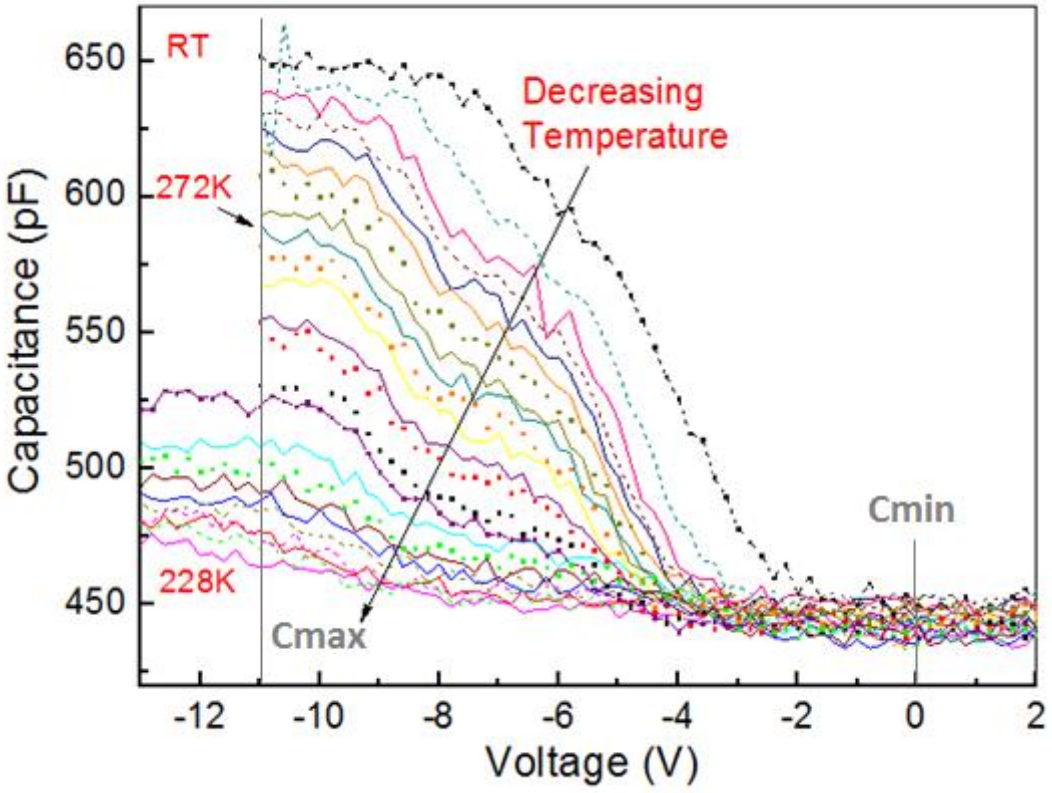

Figure 5.17. Change in the plot of capacitance voltage characteristics as the temperature decreases from room temperature to 228K for a polycrystalline S1150 based MOS capacitor. Typical area of the device is $7.85 \times 10^{-7} m^2$.

In disordered materials, the C-V measurements are used to define the conduction as a function of temperature. The change in applied bias and hence the surface charge is used as a measurement process. To maintain a flat quasi Fermi level, the change in surface charge is measured with a change in temperature. A flat band condition is maintained but the flat band voltage becomes more negative with a decrease in temperature hence indicating a change in Debye length. Using Poisson's equation for the change in electric field with distance gives

$$\frac{dF}{dx} = -\frac{d^2\emptyset}{dx^2} = \frac{dF}{d\emptyset}.\frac{d\emptyset}{dx}$$

The electric field in terms of effective Debye length, L_{De},

$$F_S = \frac{kT_C}{qL_{De}} \exp\left(\frac{q\emptyset_S}{2kT_C}\right) \quad 5.44$$

Space Charge, Q_S, is given in terms of the surface field

$$Q_S = -\varepsilon_0 \varepsilon_S F_S \quad 5.45$$

$$Q_S = \frac{kT_C \varepsilon_0 \varepsilon_S}{qL_{De}} \exp\left(\frac{q\emptyset_S}{2kT_C}\right) \quad 5.46$$

Assuming that the device is in accumulation at ~-11V, the space charge capacitance C_S can be explained in terms of the Debye length (Eq. (3.37)) in flat band condition due to the accumulated charge layer.

$$C_S = \frac{dQ_S}{d\emptyset_S} = \frac{\varepsilon_0 \varepsilon_S}{L_D} = \frac{\varepsilon_0 \varepsilon_S}{\sqrt{2}\, L_{De}} \quad 5.47$$

where L_{De} is defined in Eq. (5.3). However, this analysis may be flawed as the max-min capacitance ratio certainly decreases with a decrease in temperature and is seen to move to a more negative voltage. The thickness of the oxide layer is not changing with temperature hence the capacitor is assumed to be in depletion even at a very high negative applied bias in the temperature range of 228 K- 300K.

$$C_S = \frac{\varepsilon_0 \varepsilon_S}{\left(\frac{2kT_C \varepsilon_0 \varepsilon_S}{q^2 p_s}\right)^{1/2}} \quad 5.48$$

The max-min capacitance ratio change with temperature is indicative of the movement of Fermi level. Hence, considering the concentration of traps at the surface, p_S, is given by

$$p_S = p_0 \exp\left(\frac{q\emptyset_S}{kT_C}\right) \quad 5.49$$

where $\emptyset_S$ is the surface potential and T_C is the characteristic temperature of the exponential function and p_0 is the total intrinsic hole concentration above and below the Fermi Level is given by, p_0 (Appendix G)

$$p_0 = N_i\left(1 + \frac{T_0}{T_C}\right)\exp\left(\frac{E_F - E_i}{kT_C}\right) \quad 5.50$$

N_i is the number of states per unit volume at energy level E_i, the intrinsic level, and E_F is the energy at Fermi level. Thus, the relationship between the space charge capacitance and temperature can be derived as in Eq. (5.52) (Appendix H).

$$1/_{C_S{}^2} = \left(\frac{2kT_C}{q^2\varepsilon_0\varepsilon_S p_0}\exp\left(-\frac{q\emptyset_S}{kT_C}\right)\right) \quad 5.51$$

$$1/_{C_S{}^2} = \left(\frac{2k}{q^2\varepsilon_0\varepsilon_S N_i}\exp\left(\frac{E_i - E_F}{kT_C}\right)\exp\left(-\frac{q\emptyset_S}{kT_C}\right)\right)(T_C - T) \quad 5.52$$

In ordered grains, the space charge capacitance in the accumulation region is defined in terms of Debye length

$$C_S = \frac{\varepsilon_0\varepsilon_S}{L_D} = \frac{\varepsilon_0\varepsilon_S}{\left(\frac{2kT\varepsilon_0\varepsilon_S}{q^2 p}\right)^{1/2}} \quad 5.53$$

where $p = p_0\exp\left(\frac{q\emptyset}{kT}\right)$, ε_0 is the permittivity of free space and ε_S is the dielectric constant. $1/C_S{}^2$ and temperature can thus be defined in terms of surface potential as follows

$$\frac{1}{C_S{}^2} = \frac{2k}{q^2 p_0\varepsilon_0\varepsilon_S}\exp\left(-\frac{q\emptyset_S}{kT}\right)T \quad 5.54$$

and in terms of intrinsic carrier density as (Appendix I)

$$\frac{1}{{C_S}^2} = \frac{k}{q^2 N_i \varepsilon_0 \varepsilon_S} \exp\left(-\frac{q\emptyset_S}{kT}\right) \exp\left(\frac{E_i - E_F}{kT}\right) T \qquad 5.55$$

Recalling the equivalent circuit in Fig.5.15, the total capacitance C_{MOS} can then be defined by Eq. (5.5). For a p-type disordered organic semiconductor based MOS capacitor, the voltage required on the gate metal to reach the flat band condition becomes more negative with decreasing temperature. At high temperatures, the Fermi level is in the band tail of the Gaussian distribution. Application of a positive voltage thus causes flat band conditions and partial depletion of hole concentration at the surface.

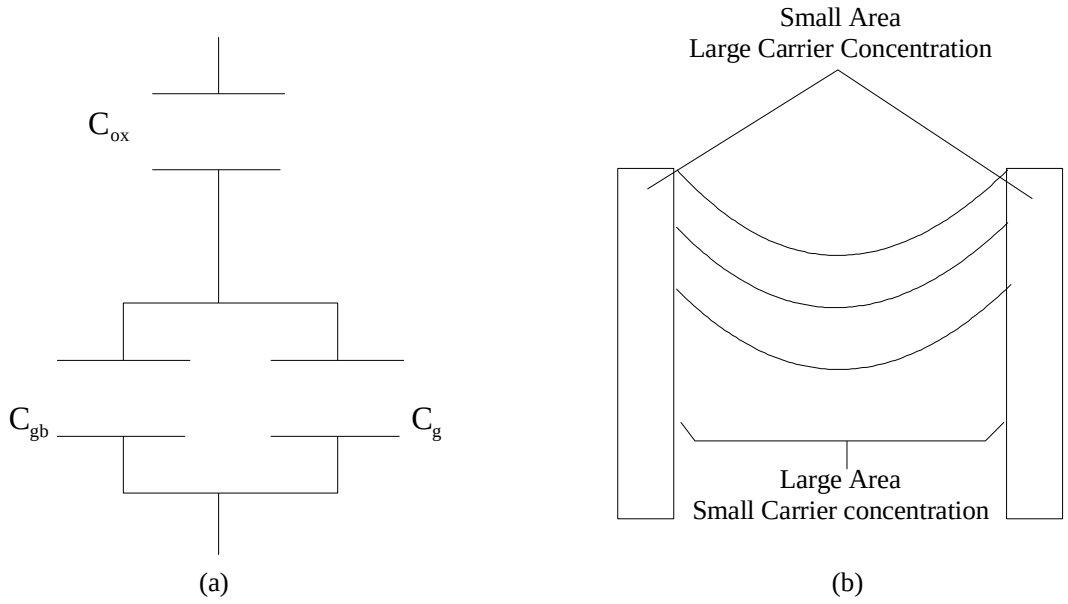

Figure 5.18. (a) Equivalent circuit for a polycrystalline material in contact with an oxide. The capacitance associated with the grain boundary C_{gb} or the grain C_g dominates the overall capacitance. (b) A simple model showing both the small area grain boundaries with large carrier concentration and large area grains with smaller carrier concentration.

For polycrystalline organic MOS capacitor, an equivalent circuit such as shown in Fig.5.18a can be assumed. The capacitance measured is associated with the charge in the grain or the grain boundary. The grains are ordered and conducting with low hole concentration and have a much larger area than the grain boundaries. Conversely, the grain boundaries are very thin compared to

the grains with a much larger concentration of trapped holes due to their disordered nature [61]. For this reason, either the grain capacitance or the grain boundary capacitance can dominate at any point. If the grain boundary dominates, a plot from Eq. (5.52) will provide x-intercept indicative of characteristic temperature of exponential DOS, T_C. If the x-intercept is not T_C but much lower, the grains are most likely to be dominating the capacitance. Figure 5.18b shows a resultant grain formed between two grain boundaries for a polycrystalline semiconductor.

In disordered MOS structures, decrease in temperature does not change the minimum capacitance or the T_C value and hence dopant concentration is not affected. However, as the temperature decreases the Fermi level moves closer to the HOMO level of an organic semiconductor. Rise in the positive voltage thus causes more holes to leave the surface of the semiconductor and a larger insulating, depletion region with no mobile holes remains. The number of holes leaving the surface is directly proportional to the number of empty traps available and defines the dopant concentration. Although an increase in positive voltage causes such an increase, the width of the depletion region in disordered materials cannot be defined as the depletion region may expand across the whole organic film. It is, therefore, considered impossible to achieve inversion in organics. The minimum capacitance C_{min} observed, although considered constant, is not the true value of capacitance in inversion as has been discussed in Section 5.4. The organic film is not totally depleted of holes at C_{min}.

The dopant concentration is not expected to change in the range of temperature measured. However, the experimental results in Fig.5.19 indicate otherwise. This effect is similar but not identical to the fall in dopant concentration with temperature in organic polycrystalline based Schottky diodes (chapter 3). The dopant concentration in this case is obtained from Eq. (5.18) keeping the value of C_{max} constant at the oxide capacitance (~1800pF). From the plot of inverse square of depletion capacitance $1/C_S^2$ against temperature (Fig.5.20), it is visible that $1/C_S^2$ rises with decreasing temperature at different applied bias in accumulation and depletion. The depletion capacitance must therefore be falling with decreasing temperature. The depletion region width extends across the whole thickness of the organic layer, hence, causing the capacitor to go into deep deletion.

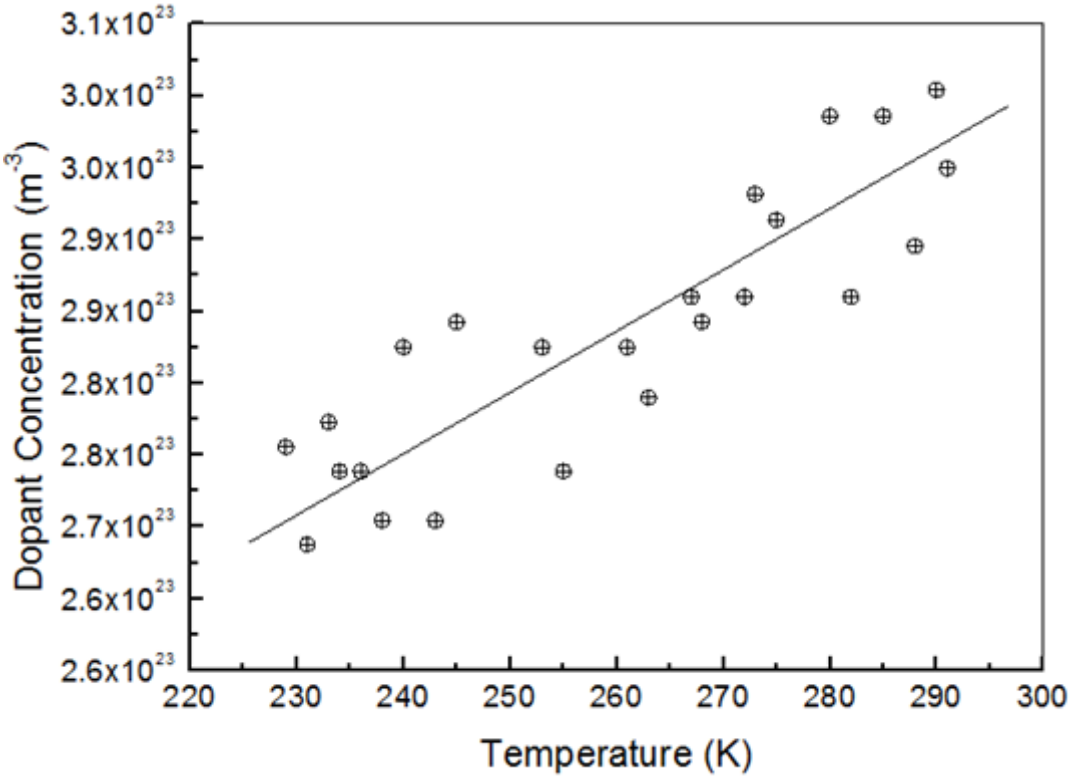

Figure 5.19. The variation of dopant concentration with temperature. The dopant concentration is seen to decrease with temperature.

The characteristic temperature of exponential distribution of traps, T_C, is expected to stay constant because the exponential DOS has no observed mechanism by which they might vary with temperature. Sedghi et al. [62] experiment on disordered material for MOS capacitor produced T_C of 425 K from $1/C^2$ against temperature plot using Eq. (5.52). The capacitance was measured in accumulation at flat band assuming that the flat band was constant with changing temperature. As the flat band is not constant in our case and the C-V plot moves towards negative voltages with temperature, a range of applied bias were taken in both accumulation and early depletion region. Early depletion is referred to the start of depletion of carriers in the semiconductor with an application of a small positive voltage, more than the flat band voltage. Using Eq. (5.52), the intercept of Fig.5.20 gives T_C in the range of 320–336K for bias in range of -11.4 V (accumulation) and -6 V (early depletion). This is lower than to the values of T_C obtained from Schottky diodes at room temperature in Chapter 3. The values for T_C found at room temperature

are almost 365K and 400K from TIPS/PTAA and doped TIPS/PAMS Schottky diodes respectively.

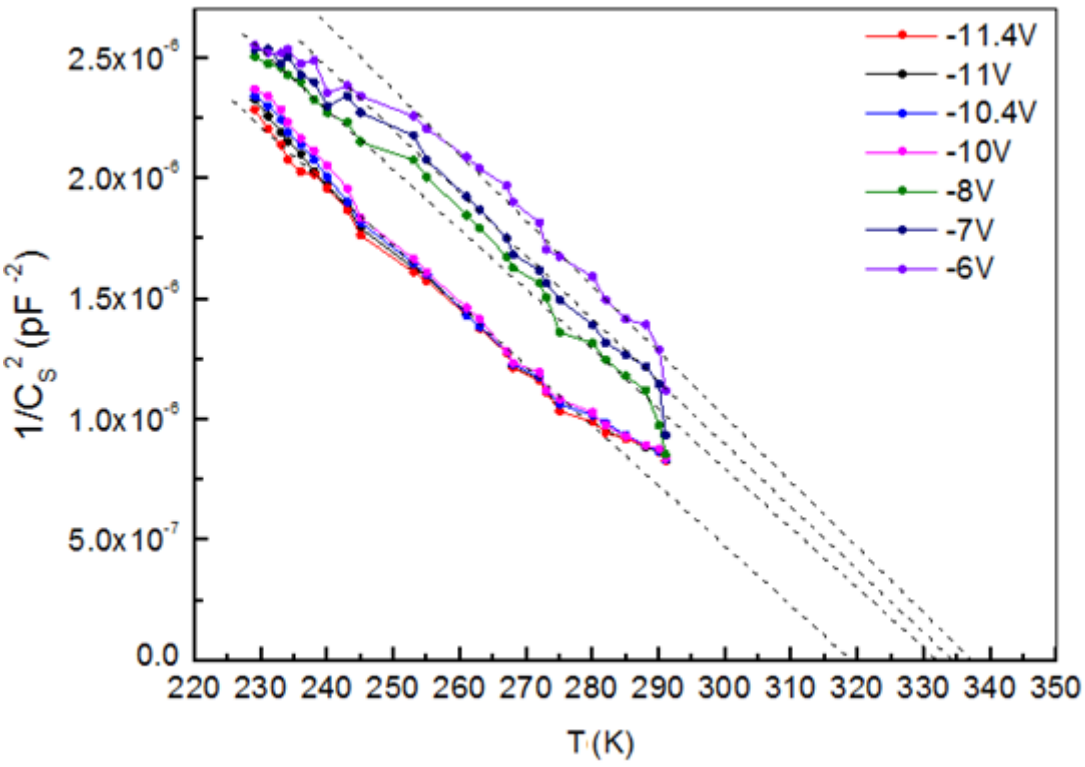

Figure 5.20. The inverse square of space charge capacitance against temperature for different applied bias conditions from accumulation to early depletion to find T_C at the x-intercept.T_C obtained is lower than expected for disordered organic semiconductors (425K [62]).

Furthermore, the low value of T_C obtained from Fig.5.20 indicates the absence of disorder in the polycrystalline material. It is maybe that the measurements obtained are from a grain instead of a grain boundary and Eq. (5.55) applies. If T_C is approximately 300K, Eq. (5.52) does not apply. That is to say that the change is Fermi level due to change in temperature is not sufficient to cause any increase or decrease in surface state concentration. Another explanation for a low value of T_C is the movement of grains and grain boundaries with change in voltage. If the number of carriers at grain minimum (where most conduction takes place) is proportional to the number of carriers at the grain boundary, the relation gives the Meyer Neldel Energy (MNE) where MNE gives

information on the disorder in the grain boundaries. It is well known that although the conduction is maximized at the grain centre, the grain boundary controls the surface potential in the grains and defines the energy barrier due to Fermi level pinning. A low T_C of approximately the same value as T indicates that the movement of grain centre with voltage does not follow the grain boundary potential and hence are not proportional. A small change in the grain boundary with an applied gate potential, thus, causes a great change in the grains such that the value of T_C obtained is lower than expected for disordered organic semiconductors (425 K [62]). A small value of T_C obtained from the intercept signifies the dominion of grains.

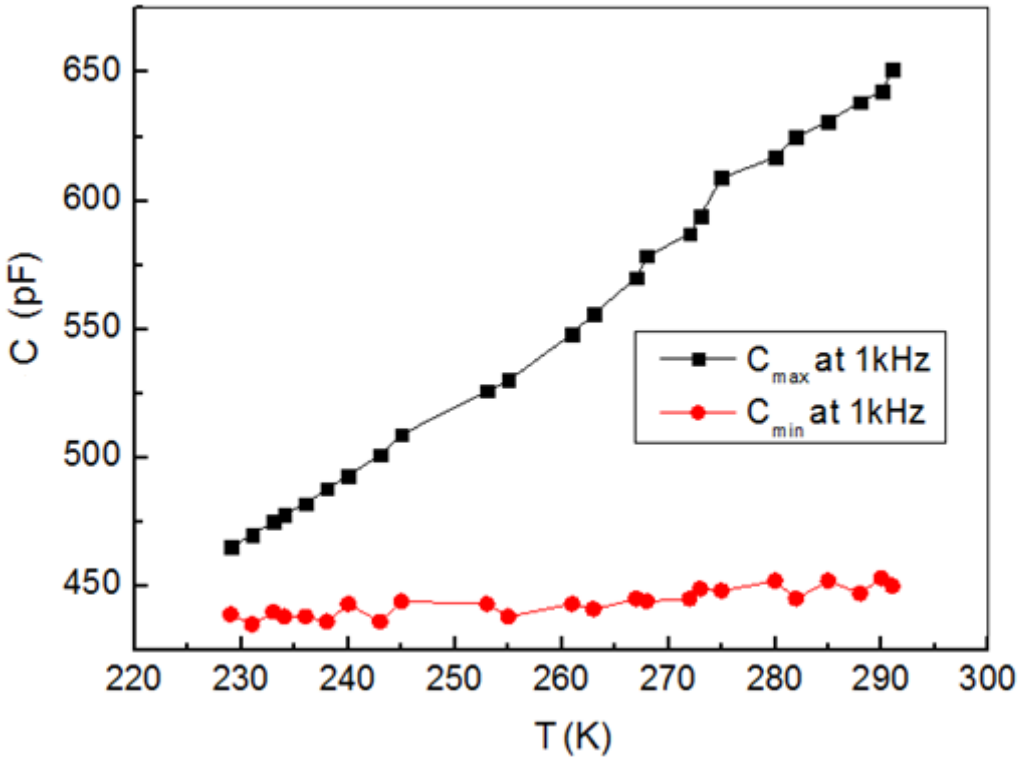

Figure 5.21. The maximum capacitance (at -11V) and minimum capacitance (at 0V) are plotted against temperature at the frequency of 1kHz. C_{max} falls linearly with decreasing temperature

Last but not the least, from chapter 3, the current voltage plots show dc characteristics. The capacitance voltage characteristics however show the ac characteristics. As discussed before, the characteristics indicate that the boundary traps are filling so that the grain boundary controls the

barrier seen by the carriers and hence the capacitance. However, that is not the case seen from the results obtained. A small value of T_C comparable with T indicates that the boundary traps are not filling and that the capacitance is being controlled by the grains instead of the grain boundaries.

The effective mobility values lowers in organic MOS capacitor with decreasing temperature. This phenomenon is also seen in polycrystalline pentacene TFTs as the temperature decreases [63]. In the temperature range observed, the change in effective mobility is due to the thermally activated behaviour of carriers in disordered grain boundaries. Reasons for a decline in mobility with temperature include the disorder-promoted trap states near the edge of the grain and the Fermi level being unable to reach the mobile trap states [64]. This effect can be better understood by plotting the maximum and minimum capacitance values against temperature (Fig.5.21). As seen, the ratio between the C_{max} and C_{min} falls linearly with temperature indicating that at lower temperatures, the Fermi level indeed has difficulty reaching the mobile trap states.

As the temperature falls, the thermal energy of the holes is significantly reduced and the hopping rate declines suggesting that the carriers may only be capable of accurately obeying the Fermi-Dirac distribution function and not Maxwell-Boltzmann approximation further into the organic film. The Fermi level is thought to move closer to the HOMO level. At lower temperatures, outside the range measured, the Fermi level may not lie in the band tail of the Fermi-Dirac distribution anymore and therefore it may be unlikely that a quasi level exists at much lower temperatures. A decrease in temperature may also have an effect on the plot of capacitance against frequency. As the temperature falls, it is expected that the resistivity in the bulk of the semiconductor increases and thus the plot moves towards lower frequencies. An increase in resistivity is indicative of decrease in conductivity of an organic film if the conduction is controlled by the bulk of the semiconductor.

5.7 CONCLUSION

The effect of frequency and temperature in the examination of electrical characteristics of MOS devices are important to consider. Parameters such as the doping concentration, insulator thickness and threshold voltage can be found by analysing the C-V characteristics. A high frequency C-V plot for a p-type semiconductor based MOS capacitor shows higher and lower capacitance values at negative and positive gate biases respectively. Maximum capacitance is as a result of the accumulation of holes at the semiconductor surface whilst the minimum capacitance

corresponds to the maximum depletion layer width. The deviation from ideal C-V characteristics is attributable to various oxide charges and interface charges. Effects of duration of exposure to air are discussed for TIPS-pentacene based MOS capacitors and an attempt is made to explain the results obtained.

The variation of C-V characteristics with frequency is examined for the case of a polycrystalline organic S1150 MOS capacitor. In theory, C_{max} and C_{min} can be used to estimate the doping concentration N_a, which is found to be approximately $3.6x10^{17}cm^{-3}$ at 1 kHz. An RC equivalent circuit to model frequency-dependent capacitance of MOS capacitor is considered and examined in detail. The frequency is altered from lowest to the highest measurable value so as to characterize parameters such as the mobility, conductivity, thickness of the organic semiconducting layer t_{OSC} and cut-off frequency. Furthermore, an equivalent circuit model is also proposed to find the bulk components, namely the bulk resistance R_b and the bulk capacitance C_b of the organic semiconductor. Terms for conductance and impedance for the equivalent circuits are derived for a number of equivalent circuit cases. The cut-off frequency, the poles and the zeros of the device are also defined. R_b, C_b and t_{OSC} found are 13 kΩ, 760pF and 27nm respectively. The maximum depletion width obtained from the C-V plot at 1 kHz is approximately 30nm. This indicates that the minimum capacitance is not due to inversion but due to the extension of the depletion width across the thickness of the semiconducting layer.

The value of doping density obtained from Eq. (5.18) is very sensitive to the ratio of C_{max}/C_{min} such that any decrease in C_{min} will also change the mobility value. From the equivalent circuit proposed, it is assumed that C_{min} is in series with the oxide capacitance C_{ox} and that in 'so- called' inversion, the space charge capacitance C_s and the bulk capacitance C_b can be ignored. Nevertheless, the bulk capacitance in high mobility semiconductors may as well be ignored as the bulk resistance compensates by being huge but in organic lower mobility semiconductors, this approximation provides unexpected results. This is because the bulk resistance is not large enough to overlook the effects of the bulk capacitance.

Furthermore, a contact resistance owing to the existence of barrier between the semiconductor and ohmic contact is considered. Two relaxation frequencies are visible due to the Maxwell Wagner effect for two connecting dielectric layers. The lower relaxation frequency is because of the bulk effects whereas the higher relaxation frequency gives the contact resistance. In the case

considered in this thesis, R_C is lower than expected especially because no contact treatment is performed between the semiconductor and ohmic contact layer.

Finally, the temperature dependence of the capacitance-voltage characteristics is observed to recognize the variation in charge transport, for polycrystalline organic S1150 based MOS capacitors. A low value of T_C (approximately 330 K) obtained from temperature measurements indicates a decrease in disorder in the polycrystalline material compared to disordered materials (~450K). A number of reasons are provided for this low value. Eventually, the capacitance measurements obtained are assumed to be from a grain instead of a grain boundary. The grain dominates the capacitance observed and therefore the dopant concentration, in theory, does not vary with temperature. The change in Fermi level due to change in temperature is not enough to cause any increase or decrease in surface state concentration.

5.8 REFERENCES

[1] M. Nishida, IEEE Trans. Elec. Dev. 26 (1979) 71.

[2] E. H Nicollian, J. R Brews, *MOS (metal oxide semiconductor) Physics and Technology,* John Wiley and Sons, New York, 2003.

[3] G.B. Barbottin, A. Vapaille, *Instabilities in Silicon Devices*, 1- 2, North-Holland, New York, 1989.

[4] D. K. Schroder, *Semiconductor Materials and Device characterization*, John Wiley and sons, New York, 1990.

[5] T. Miyadera, T. Minari, K. Tsukagoshi, H. Ito, Y. Aoyagi, Appl. Phys. Lett., 91,1, 013 (2007) 512.

[6] K. D. Jung, C. H. Lee, D.W. Park, B. G. Park, and J. D. Lee, IEEE Electron Device Lett., vol. 28, no. 3 (2007) 204.

[7] T. P. Nguyen, P. Destruel, *Handbook of luminescence display materials and devices*, American Scientific Publishers, 2003.

[8] S. M. Sze, *Physics of Semiconductor devices*, Second Edition, Wiley, New York, 1981.

[9] B. G. Streetman, S. Banerjee, *Solid state electronic devices*, Prentice Hall, fifth edition, New Jersey, 2000.

[10] M. Halik, H. Klauk, U. Zschieschang, G. Schmid, C. Dehm, M. Schütz, S. Maisch, F. Effenberger, M. Brunnbauer**,** F. Stellacci**,** Nature, 431, (2004) 963.

[11] H. Klauk, M. Halik, F. Eder, G. Schmid, and C. Dehm, IEDM- Techn. Dig. (2004) 369.

[12] D. Knipp, R. A. Street, B.S. Krusor, R. B. Apte, MRS symp. Proc., Pittsburg (2001) 553.

[13] J.A Rogers, Z. Bao, K. Baldwin, A. Dodabalapur, B. Crone, V. R. Raju, V. Kuck, H. Katz, K. Aumdson, J. Ewing, P. Drzaic, Proc. Natl. Acad. Sci. USA, 98, (2001) 4835.

[14] G. H. Gelinck, T.C.T Geuns, D.M. de Leeuw, Appl. Phys. Lett., 77, (2000) 1487.

[15] H. Sirringhaus, T. Kawase, R. H. Friend, T. Shimoda, M. Inbasekaran, W. Wu, E. P. Woo, Science, 290, (2000) 2123.

[16] T. Kawase, H. Sirringhaus, R. H Friend, T. Shimoda, Adv. Mater., 13, (2001) 1601.

[17] H. Klauk, M. Halik, U. Zschieschang, G. Schmid, W. Radlik, W. Weber, J. Appl. Phys., 92, 9, (2002) 5259.

[18] H. Klauk, *Organic Electronics: materials, manufacturing and applications*, Wiley-VCH, Germany, 2006.

[19] J.Veres, S. D. Ogier, S. W. Leeming, D. C. Cupertino, S. M. Khaffaf, Adv. Funct. Mater., 13, (2003) 199.

[20] C. D. Dimitrakopoulos, I. Kymissis, S. Purushothaman, D. A. Neumayer, P. R. Duncombe, R. B. Laibowitz, Adv. Mater., 11, (1999) 1372.

[21] C. D. Sheraw, L. Zhou, J. R. Huang, D. J. Gundlach, T. N. Jackson, M. G. Kane, I. G. Hill, M. S. Hammond, J. Campi, B. K. Greening, J. Francl, J. West, Appl. Phys. Lett., 80, (2002) 1088.

[22] C. D. Sheraw, J. A. Nicols, D. J. Gundlach, J. R. Huang, C. C. Kuo, H. Klauk, T. N. Jackson, M. G. Kane, J. Campi, F. P. Cuomo, B. K. Greening, IEDM Tech. Dig. (2000) 619.

[23] H. Klauk, D. J. Gundlach, J. A. Nichols, T. N. Jackson, EEE Transactions on Electron Devices, 46, (1999) 1258.

[24] T. W. Kelly, D.V. Muyres, P.F. Baude, T.P. Smith, T.D. Jones. MRS Symp. Proc.,771, (2003) 169.

[25] B. K. Crone, A. Dodabalapur, R. Sarpeshkar, R. W. Filas, Y. Y. Lin, Z. Bao, J. H. O'Neill, W. Li, H. E. Katz, J. Appl. Phys., 89, (2001) 5125.

[26] H. E. A. Huitema, G. H. Gelinck, J. B. P. H. Van der Putten, K. E. Kuijk, K. M. Hart, E. Cantatore, D. M. Dr Leeuw, Adv. Mater., 14, (2002) 1201.

[27] S. W. Huang, J- G. Hwu, IEEE Trans. on Electron. Dev. 50, 7, (2003), 1658.

[28] F. C. Chen et al., Appl. Phys. Lett., 85, (2004) 3295.

[29] L. A. Majewski, R. Schroeder, M. Grell, Adv. Mater., 17, (2005) 192.

[30] L. A. Majewski, R. Schroeder, M. Grell, J. of Phys. D: Appl. Phys., 37, (2004) 21.

[31] *HMDS, SPI Chem Hexamethyldisilazane,* website: *www.2spi.com* , viewed: 03/03/2010.

[32] *HMDS, Thermo scientific*, website: *www.piercenet.com*, viewed: 03/03/2010.

[33] P. Sung Kyu, K. Chung Chen, J. E. Anthony, T. N. Jackson, Elec. Dev. Meet., IEDM Tech. Digest, IEEE Inter. (2005) 4.

[34] P. Sung Kyu, J. E. Anthony, T. N. Jackson, Elec. Dev. Lett., IEEE, 28, (2007) 877.

[35] G. Horowitz, M .E. Hajlaoui, Adv. Mater., 12, 14, (2000) 1046

[36] D. Knipp, R. A Street, A. Vlkel, J. Ho, J. Appl. Phys., 93, (2003) 347.

[37] M. Shtein, J. Mapel, J. B. Benziger, S. R. Forrest, Appl. Phys. Lett., 81, (2002) 268.

[38] B. Servet, G. Horowitz, S. Ries, O. Lagorsse, P. Alnot, A. Yassar, F. Deloffre, P. Srivastava, R. Hajlaoui, P. Lang, F. Garnier, Chem. Mater. 6, (1994) 1809.

[39] D. J. Gundlach, Y. Y. Lin, T. N. Jackson, S. F. Nelson, D. G. Schlom, IEEE Electron. Device Lett., 18, (1997) 87.

[40] W. A. Schoonveld, R. W. Stok, J. W. Weijtman, J. Vrijmoeth, J. Wildeman, T. M. Klapwijk, Synth. Metal., 84, (1997) 583.

[41] C. D. Dimitrakopoulos, A. R. Brown, A. Pomp, J. Appl. Phys., 80, (1996) 2501.

[42] Y. Y. Lin, D. J. Gundlach, T. N. Jackson, S. F. Nelson, IEEE Trans. Electron. Dev., 44, (1997) 1325.

[43] T. W. Kelley, D. V. Muyres, P. F. Baude, T. P. Smith, T. D. Jones, MRS symp. Proc., 771, (2003) 169.

[44] M. Halik, H. Klauk, U. Zschieschang, G. Schmid, S. Ponomarenko, S. Kirchmeyer, W. Weber, Adv. Mater., 15, (2003) 917.

[45] J. Collet, O. Tharaud, A. Chapoton, D. Vuillaume, Appl. Phys. Lett. 76, (2000) 1941.

[46] N. C. Greenham, R. H. Friend, Sol. Stat. Phys. 49, (1995) 85.

[47] M. Raja, PhD Thesis, University of Liverpool, 2004.

[48] G.C. Lloyd, PhD Thesis, University of Liverpool, 1999.

[49] E. H. Nicollian, A. Goetzberger, Appl. Phys. Lett. 7, (1965) 216.

[50] M. A. Alam, A. Dodabalapur, M. R. Pinto, IEEE Trans. Elec. Dev. 44 (1997) 1332.

[51] [S. Scheinert, G. Paasch, Phys. Status Solidi. A 201, (2004) 1263.

[52] A. Bolognesi, A.D. Carlo, P. Lugli, Appl. Phys. Lett. 81, (2008) 4646.

[53] K. Kim, Y. Kim, IEEE Trans. on Elec. Dev. 57, 9 (2010), 2344.

[54] J. E. Meyer, RCA Rev. 32, (1971) 42.

[55] D. M. Taylor, N. Alves, J. Appl. Phys. 103, (2008), 054509.

[56] *Bode Plots, Exploring Classical Control Systems*, website: *www.facstaff.bucknell.edu /mastascu/econtrolhtml/Freq/Freq5.html*, viewed: 10/10/2011.

[57] D. Greve and V. Hay, J. Appl. Phys., 61, 3 (1987) 1176.

[58] A. R. von Hippel, *Dielectrics and Waves* , Wiley, New York, 1954.

[59] I. Torres, D. M. Taylor, J. Appl. Phys. 98, (2005) 073710.

[60] P. V. Gray, D. M. Brown, Appl. Phys. Letts. , 8, (1966) 2.

[61] W. Eccleston, IEEE Trans. Electron Devices 53, (2006) 474.

[62] N. Sedghi, D. Donaghy, M. Raja, S. Badriya, S.J. Higgins, W. Eccleston, J. Non-Crys. Solids 352 (2006) 1641.

[63] R. A. Street, D. Knipp, A. R. Volkel, Appl. Phys. Lett. 82 (2003) 3907.

[64]R. A. Street, D. Knipp, A. Volkel, Appl. Phys. Lett. 80, (2002) 1658.

CHAPTER 6- CONCLUSION AND FURTHER RESEARCH PROSPECTS

This chapter provides the conclusion to the work presented in this thesis. Further research recommendations are also discussed.

6.1 DISCUSSION AND CONCLUSION

Organic polymeric semiconductors are potentially simpler to process and can be used for printable electronics due to their ease of solubility in organic solvents [1]. Material such as P3HT is considered more suitable for organic thin film transistors (OTFTs) whereas disordered PTAA can be used in the formation of organic light-emitting diodes (OLEDs) [2]. The charge transport and processing of amorphous [3] and liquid crystalline [4] is quite similar to the polymeric semiconductors.

A detailed review of the various charge transport models for organic materials is presented. Such models include the Miller Abraham model, percolation theory, variable range hopping mechanism, and multiple trap and release model. The density of states (DOS) particularly in disordered organic semiconductors is commonly defined by the Gaussian distribution and the associated exponential approximate at the band tail. The Meyer-Neldel Energy (MNE) is related to the width of such Gaussian distribution, which is associated with the degree of disorder in the semiconductor. It can also be explained in terms of shift in the quasi-Fermi level with temperature. Previous models proposed for Meyer Neldel Energy (MNE) go back decades. Detailed review of MNE is provided in Section 2.4.4.

The existence of T_C, the characteristic temperature of the DOS, indicates that although the concept of MNE is purely for disordered materials, it is also obtained in polycrystalline organic semiconductors. Thus, the equations already developed on a disorder model seem to be valid for polycrystalline organic materials. The universal mobility law is discussed and reformed to fit in terms of polycrystalline materials where the disordered grain boundary is in contact with the grain. The disordered organic grain boundary has mobility values depending on the energetic distribution of states and the hopping characteristics instead of a single mobility value like in a crystalline grain. The crystalline grain is akin to inorganic crystalline semiconductors. A term to define mobility in polycrystalline semiconductor can therefore be explained as the effective mobility.

The charge mobility obtained for organic materials is to a large extent lower than the inorganic counterparts (eg. silicon). For TFTs, the minimum acceptable mobility for the use in circuits is $1 cm^2 s^{-1} V^{-1}$ but organic materials are unable to produce mobilities of that order. The best results obtained with polymeric materials are an order lower than inorganic materials [3]. For a highly

pure polycrystalline pentacene crystal [5], the mobilities obtained are more than $10cm^2s^{-1}V^{-1}$. Rubrene has shown similar mobility values [6]. TIPS- pentacene, a derivative of pentacene, is another promising polycrystalline material with expected mobilities more than that of pentacene. Therefore, it has been tested in the thesis.

The charge transport in crystalline organic materials is said to be due to weak Van der Waal forces rendering the material soft whereas polymeric materials show a high level of ordering indicating that they offer better mobility values [7-9]. Small molecule structures (polycrystalline material) consist of crystalline domains separated by amorphous sections. It is seen that it is easier to form better ordered crystals from molecules in lower molecular weight films than high molecular films [10]. Contrary to Cheung and Troisi [10], films formed with high molecular weight P3HT films have seen to give superior charge mobility values [11]. This has been believed to be due to the link between small molecules and different crystalline domains [12]. To research it further, mobility values in organic semiconductors are obtainable experimentally in this thesis. However, reproduction of mobility values in synthesised materials is hard experimentally and even harder computationally. This is because the mobility values highly depend on the quality of the material and their fabrication processes.

Inadequacy in explaining the charge transport methods in organic material has led to an interest in researching this topic at the University of Liverpool. The theories and methods used are similar to the ones existent for the inorganic counterparts with variation to fit the organic semiconductor. This is seen as an uncomplicated way to define parameters such as the mobility of the material. However, the charge transport in a polycrystalline organic material such as TIPS-pentacene cannot be defined simply by a band like model or as hopping between localised states without disagreeing with the results obtained from experiments. Using theories, a simple model for charge transport for polycrystalline organic semiconductor is defined in terms of current, voltage, frequency and temperature in this thesis. This leads to the derivation of properties like the mobility and the ideality factors. DOS models like the Gaussian model for disordered materials [13] and derivatives of Gaussian model [14-16] are a few such theoretical models for charge distribution in existence.

Polycrystalline organic Schottky diodes are fabricated using organic TIPS- Pentacene in chapter 3. TIPS-pentacene is a particularly interesting material as it can be deposited easily from solution. A relatively thicker drop cast active layer produced continuous films but showed less uniformity

than the spin coated layer. The former also produces better overall results. Space charge limited currents (SCLC) are defined in the saturation region of the forward characteristics of the Schottky diode where the current is dominated by the bulk effects. The theory of SCLC is reviewed for trap free dielectric material and eventually for a disordered material with exponential distribution of traps. Furthermore, a model demonstrating the universal dependency of mobility on carrier density is presented for space charge limited currents. Disordered materials are compared with the conventional crystalline solids to define the universal mobility law (UML) in disordered materials. Hence, space charge limited current expression including UML is developed for disordered organic semiconductors. Moreover, the importance of UML in polycrystalline organic semiconductor is also established. In SCLC, the current density is therefore dependent on voltage by a power law given in terms of *m*, also temperature dependent.

Following the discussion on space charge limited currents the analysis of the DC characteristics of polycrystalline organic Schottky diodes is carried out with change in temperature. Temperature effects on the electrical characteristics of two different blends of polycrystalline organic Schottky diodes is conducted, namely TIPS/PTAA and doped TIPS/PAMS. The characteristic temperature of the intrinsic distribution of carriers T_0 is obtained from the exponential region of these diodes. This is equivalent to the ideality factor multiplied by the absolute temperature where the ideality factor is the measure of defects and the presence of traps in the organic semiconductor.

Various other parameters such as characteristic temperature of DOS (T_C), the ratio of free charge carriers to the total charge carriers in the intrinsic DOS (θ) and MNE are also extracted. For a TIPS/PTAA Schottky diode at room temperature, the respective values for N_a, μ_{eff}, W_{dep}, L_{De}, *MNE* and the characteristic temperature describing the width of the carrier distribution, T_0,are found to be approximately $1x10^{17}\,cm^{-3}$, $1.8x10^{-2}\,cm^2V^{-1}s^{-1}$, 185nm, 11nm, 31.5meV and 780K. For a doped TIPS/PAMS Schottky diode at room temperature, these parameters correspond with $2x10^{17}cm^{-3}$, $1x10^{-2}cm^2V^{-1}s^{-1}$, 100nm, 5nm, 35meV and 1200K respectively. A large value for ideality factor obtained in both samples, TIPS/PAMS and TIPS/PTAA, is consistent with previous experiments on disordered materials. The high value in the range of 3-5 proves that the material suffers from some trapping effects. High values of T_C and hence MNE are indicative of both the extrinsic and intrinsic traps at room temperature. The nature of the forward saturation current is thought to be dependent on the back metal/organic junction. Considering the change of parameters over the temperature range measured, the fall in temperature does not change for most of the parameters until a critical temperature for TIPS/PTAA Schottky diode. After this critical

temperature, most parameters are observed to decrease. For the case of doped TIPS/PAMS Schottky diode, parameters such as effective mobility, carrier concentration, MNE decrease with decreasing temperature.

In order to further understand the transport properties and the effect of temperature on the transport energy the activation energy E_a of the organic material at high temperatures is determined, from the Arrhenius plot of current density J_s against *1000/T* in saturation. For TIPS/PTAA Schottky diode, the activation energy remains constant at approximately 0.3eV for various applied voltages in saturation. However, for doped TIPS/PAMS Schottky diode, two different activation energies are obtained in the range of temperatures observed. In higher temperature range, the activation energy obtained from the Arrhenius plot of current density is seen to be twice (~63meV) that of the one obtained in the lower temperature range (31meV). Difference in activation energies is assumed to be due to two different mechanisms governing two separate temperature ranges. It is thought to be due to the movement of quasi-Fermi level in the energy domain. Furthermore, the two activation energies may be an evidence of both intrinsic and extrinsic DOS with two different transport energy levels. As this sample is doped, the extrinsic DOS may be owing to the DDQ dopant ions. More experimental and analytical work is required to fully comprehend this theory.

Small signal capacitance analysis is conducted on Schottky diodes at ac voltages of as low as 5mV. The dopant concentration are found from the slope of the inverse square of the depletion capacitance against voltage plot with a corresponding value of 5.2×10^{14} cm^{-3} at 1 kHz. This method for obtaining the dopant concentration is frequency dependent and can only be used as estimation as a large difference in N_D is observed between C-V and I-V analysis.

Charge conduction in polycrystalline organic semiconductor is determined in the vertical Schottky structure. A straightforward method is to define a polycrystalline material such as pentacene to be made up of ordered and disordered sections. A 2D model is therefore proposed to define the charge transport model in terms of both ordered grains and disordered grain boundaries (in Chapter 4). The potential variation at the grain edge is used to define the variation of potential in the grains. The grains are constructed by making a number of assumptions. Thus, the variation of potential in the whole of the grain is defined in the x-direction. A new term for the potential at grain centre is recognized such that the maximum number of carriers for charge conduction is found. Finally with the use of drift currents, the current density at the grain centre in the forward

characteristics is established. Although this is a simple method to define the experimentally obtained results, the charge transport in organic materials is still not anywhere close to be thoroughly understood.

Two different directions of current flow are considered in this thesis. Firstly, lateral conduction is introduced between a number of grains and grain boundaries. The carrier conduction is dominated by diffusion and drift at low and high applied biases respectively. A term for the flux between the grain and the grain boundary is established. Assuming that the thickness of the semiconductor is significantly smaller than the lateral length, vertical conduction in terms of a single layer of grain and grain boundary can be established. Subsequently, a two dimensional model for a polycrystalline organic semiconductor based Schottky diode is proposed based on simple two one dimensional cases using Gauss's law. The model assumes that the carrier density in the grain boundaries determines the electrostatics in the grains. The exponential distribution controls the potential barrier seen at the grain boundaries. This potential barrier in the grain boundary noticed over the top of the Schottky barrier limits the flow of charge due to trapping effects. The grains, on the other hand, dominate the charge transport from the ohmic contact to the Schottky interface with the application of an external bias due to the lower energy barrier seen at the grain centre compared to the grain boundary. Boundary conditions for the edge of the grain and grains are determined. Thus, the grains and the grain boundaries are identified in terms of simple equations and the current density classified for both in the forward bias. These are new terms to define the charge conduction in the grain boundaries and at the centre of the grain where the charge transport dominates. Furthermore, a new model is proposed for the DOS to define conduction in the grain boundaries of a polycrystalline semiconductors based on Laplace's first law- L1. It is thought to be a better suited distribution then the Gaussian DOS. This is because it gives the MNE for a wider range of voltage values than the Gaussian DOS (~37meV). Finally, a term for the carrier concentration using L1 DOS is also derived.

Organic polycrystalline based MOS capacitors are fabricated for oxide/semiconductor interface analysis. The electrical behaviour of the grain boundaries, in essence, is a topic of interest due to their charge conduction properties and hence their link to device performance. Also, the presence of an oxide layer between the metal and the organic semiconductor strongly affects the device characteristics. MOS capacitors with two different pentacene derivatives, S1150 and TIPS-pentacene are fabricated in a bottom gate configuration. Capacitance Voltage (C-V) analysis is carried on both samples and the best obtained results discussed. TIPS-pentacene based MOS

capacitors are used for experiment involving effects of air exposure on device characteristics. However, S1150 based MOS capacitors are used to explain both the effects of temperature and frequency on device characteristics.

The C-V characteristics obtained from the S1150 MOS capacitor demonstrated a decrease in the maximum capacitance with the change in frequency of the ac signal and temperature, unlike the conventional inorganic MOS capacitors. This indicated that the surface charge is very important in the case of organics, especially polycrystalline semiconductors with ordered grains and disordered grain boundaries. The grain boundaries control the trapping effects, Fermi level pinning and hence the conduction in the grains. Interface states, in such an instance, do not matter.

In accumulation region, the oxide capacitance is assumed to dominate. When both ac and dc signals are applied together, the depletion region moves back and forth due to the ac term such that the depletion region is seen to be constant while increasing dc voltage provides the flow of electrons. In so-called inversion region, the capacitance does not drop to zero but has a value. The dopant density is provided from the slope obtained from the C-V method but may only be an approximation due to the nature of the material where the dopant ions are not typically uniformly distributed. The thickness of the oxide obtained is 40nm at C_{ox} of 1800pF and the dopant concentration is approximately $3.6x10^{17}cm^{-3}$ at 1 kHz.

Interface states and other non-uniformities at the metal/semiconductor cause the C-V behaviour of an organic semiconductor based MOS capacitor to be different from an ideal case. These interface states can be as a result of the various fabrication processes involved, lattice structure at the surface, development of an insulating layer and owing to impurities added to the organic semiconductor during synthesis. A bias shift and frequency dispersion on a C-V characteristics obtained from MOS capacitors signify the presence of these interface states.

From accumulation-depletion-deep depletion (forward sweep), the flat band is more negative than from deep depletion-depletion-accumulation (reverse sweep). This anti-clockwise hysteresis is thought to be owing to oxide charges, the interface charges, the mobile ions and also the slow trapping of electrons. The presence of mobile dopant ions in the organic film, introduced during fabrication, is expected to increase the instability. Especially when the temperature is raised making the mobile ions more mobile.

The C-V characteristics of the TIPS-pentacene based MOS capacitor are seen to improve with time in air. This is associated with the accumulation of charge at the metal semiconductor interface. Impurities, improving the C-V characteristics with time, include positive trap charge due to moisture, oxygen or mobile charges. Also, exposure to air assists the charge transport in the organic layer. The carriers are able to hop around into and out of the available states such that the transport properties improve and the maximum capacitance increases.

Effects of changing the frequency are analysed on S1150 based MOS capacitors. The accumulation capacitance decreases with increasing frequency because of a decline in the surface hole concentration. The conductivity of the S1150 layer decreases, causing the relaxation times to increase. Plotting accumulation capacitance against frequency demonstrates this effect more clearly. Various equivalent circuits are proposed for understanding the small signal behaviour for an ideal MOS capacitor to consider the device characteristics. A simple model of an MOS capacitor is obtained by assuming the space charge capacitance, C_S and the oxide capacitance, C_{ox} to be in series. Addition of the bulk properties of an organic semiconductor includes the capacitance C_b and the resistance R_b of the bulk region of the S1150 film to the existent model. C_b and R_b are in parallel to each other and in series with C_S and C_{ox}. Parameters such as the thickness of the oxide layer, thickness of the organic semiconducting layer, bulk capacitance and bulk resistance are found from the C-f analysis. These are approximated to 40nm, 27nm, 760pF, 13 kHz respectively. The hole mobility obtained at 1 kHz is low (4.6×10^{-7} $cm^2V^{-1}s^{-1}$) but can be compared to bulk hole mobilities obtained from the TIPS/PTAA and TIPS/PAMS Schottky diodes at room temperature. The bulk hole mobilities are considered approximately two orders of magnitude lower than the mobilities obtained in OTFTs. The mobility of the carriers is low for organic materials to respond to the ac signal at higher frequencies and accordingly the contribution to the overall capacitance is reduced. Finally, a contact resistor is also considered to be in series to all the above mentioned components, denoting the existence of a barrier between the semiconductor and the (not so) ohmic metal. Terms for conductance and impedance for the equivalent circuits are derived for a number of equivalent circuit cases. The cut-off frequency, the poles and the zeros of the device are also defined.

This leads to the derivation of two relaxation frequencies indicating the existence of Maxwell Wagner effect for two dielectrics in contact with each other. In this is case, the semiconductor and oxide layer both acts as dielectric layers in contact with each other. For the device moving from accumulation to maximum depletion or back of the semiconductor thickness, the relaxation

frequency f_{R1} is taken to stay within the limits of 5.19 kHz and 15.9 kHz. Considering that the second relaxation frequency f_{R2} is > 1 MHz, the contact resistance of < 309 Ω is calculated. A low value obtained for the contact resistance is an indication of a good ohmic contact between the ohmic metal and semiconductor. It shows that a low barrier to carrier flow exists and there is an unhindered flow of carriers into the semiconductor.

Temperature dependence of the C-V characteristics is also observed for organic S1150 MOS capacitors to distinguish the charge transport variation. Either the grain or the grain boundary of the polycrystalline material is expected to dominate the charge transport depending on the device structure and the morphology of the organic semiconductor. In the case that disordered grain boundaries control the charge, detailed study of surface states involve temperature variation of capacitance with applied voltage. The change in temperature causes the Fermi level of S1150 to vary. Thus to maintain a flat quasi Fermi level, the modification in surface charge is calculated with change in temperature. The movement of the Fermi level is examined with the change in the ratio of max-min capacitance temperature.

For a polycrystalline organic MOS capacitor, the grain boundaries are very thin compared to the ordered and conducting grains nevertheless with a much larger concentration of holes. Consequently, either the grain capacitance or the grain boundary capacitance is thought to dominate at any one point. In the case where the grain boundary dominates, a plot of $1/C_S^2$ against temperature will provide x-intercept indicative of characteristic temperature of exponential DOS, T_C. If the x-intercept is not T_C but much lower, the grains are most likely to be dominating the capacitance of the system. This is contrary to what is expected according to the theory. Experimental results provide a temperature very close to the absolute temperature T in the range of 320 – 336K, instead of the T_C of around 450K expected of organic disordered materials. Thus, opposing the expected, the ordered grains may dictate the capacitance. Nevertheless, a lower T_C may be indicative of less disorder in the grain boundaries of the polycrystalline semiconductor due to a narrower distribution of density of states.

6.2 FURTHER RESEARCH PROSPECTS

Organic materials such as polycrystalline materials can show poorer mobility values when compared to inorganic materials such as silicon. These organic materials are flexible or easy to process so the charge transport is highly dependent on the processing technique. The disorder

induced in the small molecule backbone and the chemical defects introduced during processing can highly affect the mobility of the material. Morphology, both at a molecular level and over larger scales, can strongly affect the charge mobility in the semiconductor. Apart from these considerations, the molecular packing of the small molecule is also important as a better packed molecular structure can strongly affect the mobility values. Improved organic structures are thus the key to producing better mobility devices. The ability to tweak the organic structures according to user-preference provides better organic materials with better outcomes.

The ease of processing of organic semiconductors, such as TIPS-pentacene, is a route to produce low cost organic circuits and for other product development opportunities. Unlike its parent molecule, pentacene, TIPS-pentacene is soluble in various organic solvents and can therefore be spun or drop cast. The use of semi-crystalline binders and other organic semiconductors seem to help the morphology but requires considerable amount of more work. Solvents with rapid drying times seem to produce much better performance in Schottky diodes unlike materials such as P3HT where the solvent with higher boiling point and thus longer drying time is ideal. Research into the different drying times for various number of solvents must also be considered to understand the characteristic temperature of the DOS, T_C. The T_C is considered independent of the temperature variation and dependent on the nucleation rate of the solution processed layer. Further experimental work is required to confirm the magnitude of T_C with the change in drying temperature which effects the rate of nucleation and hence the morphology of the organic layer. In terms of organic MOS capacitors with spun thin films, the rate of spinning can affect the active layer morphology and hence the structure. Carrying out these experiments will lead to a better understanding of the effect of drying temperature on the intrinsic distribution of states and thus the Meyer Neldel energy. This can then be checked for TIPS with various organic binder or insulator combinations.

The contact between the ohmic metal and the organic semiconductor is another area that requires optimization. Especially with polycrystalline organic semiconductors, the so-called ohmic metal forms a barrier to carrier flow. Thus some of applied external bias must be used to overcome this barrier. One way to improve the contact between the ohmic metal and the organic material is through surface treatments. Oxygen plasma, HMDS and PFBT are some of the surface materials that have been successfully used in the past. Most of these treatments are also used in Schottky diodes. The use of PFBT showed no significant improvements to the device characteristics (refer

to chapter 3). Testing these treatments on oxide/semiconductor interfaces is also essential and must be looked into.

Furthermore, the use of chemical treatments on the organic semiconductor before the deposition of an ohmic contact in a bottom-gate MOS structure degrades the morphology of the organic layer. However, deposition of ohmic contact without carrying out these treatments leads to an energy barrier at the contact such that it cannot be considered ohmic. Therefore, chemical treatments that do not affect the semiconductor morphology need to be considered in the future.

Another topic of interest is the dielectrics in MOS capacitors in either a top-gate or a bottom-gate approach. The use of organic dielectric layers and double dielectrics for the use in organic devices is of significant interest to produce high mobility low voltage organic devices. A number of complications are faced with the deposition of soluble organic semiconductor on a solution processes organic dielectric or vice versa. One example is a chance of intermixing of the solution processed organic dielectric and the organic semiconductor. This process affects the device morphology and provides lower mobilities than expected. There is a vital need for the separation of these steps without affecting the layers involved.

Small signal analysis is performed using equivalent circuits to represent a MOS capacitor. This provides information about the conductance and the resistance of the device. In the model considered in Chapter 5, the resistance at both the semiconductor/ohmic and oxide/semiconductor contact are considered at the interface, respectively. However, a more accurate representation is to consider these individual interface effects as equivalent circuits consisting of both a resistor and a capacitor in parallel, at either end of the semiconductor. In addition, it is also of interest to consider the effects at the metal/oxide interface as an equivalent circuit. Future work on this includes considering these additional equivalent circuits for a more precise analysis of a MOS capacitor.

The degradation of organic devices with time is of crucial concern especially in the use of commercial applications. This effect is owing to instabilities commonly observed in terms of hysteresis in the electrical characteristics. Degradation of organic materials is thought to be by the photo-oxidation of organic material upon exposure to air or light, drifting of mobile atoms or the absorption of ozone in the organic materials. These instabilities require the need to develop an effective method for encapsulation designed for the construction of more stable organic devices.

The use of Schottky theory in the reverse characteristics to obtain the dopant concentration for inorganic semiconductors has been used for the polycrystalline organic semiconductors in this thesis. The experimental plots show good fits to the $ln\ J_R$ against $V^{0.25}$ plots. However, a major disadvantage of this method is the unaccountability of the conduction processes involved in reverse bias. The conduction in the disordered grain boundaries of a polycrystalline organic material is thought to be by charge hopping between exponentially varying localised states. Therefore, injection of charge carriers in the exponential distribution of states must be considered along with the Schottky theory in the reverse bias.

The structure, morphology and charge mobility have already been investigated by a number of techniques. Techniques for morphology measurements are namely atomic force microscopy (AFM) for the surface of the sample, X-Ray diffraction or scattering. However, it is still difficult to link the structure with the mobility to comprehend the relation between the transport mechanism and structure. Consequently, a sensible way forward is the development of computational methods.

The lateral fabrication of Schottky diodes is another topic for further inspection as it would be extremely beneficial in printed circuitry. Lateral Schottky diodes are akin to transistor based diodes that are appealing due to their ease of integration within a circuit, with the transistors, logic gates and other electrical components for the use of low cost printable circuits. However, the lateral diodes have significantly higher area consumption, a high load capacitance and a lower frequency than a vertical Schottky diode. A noticeable downside in lateral diodes that requires further research is the long channel length between the ohmic metal and the Schottky metal compared to the thin film organic semiconductor layers in vertical Schottky diodes. This is a major shortcoming in terms of the speed and hence the frequency of the device. The fabrication processes employed to produce lateral diodes in a laboratory based environment expect the channel lengths to reduce to around 1μm which is much better than what would be expected when these lateral diodes are produced by means of cheap printing techniques for mass production (>10μm) . Moreover, isolation of these lateral diodes is another topic of great interest. Moreover, there is a need for the development of a computational method to analyse the experimental results for transient analysis of both lateral and vertical Schottky diodes.

The use of organics in applications such as radio frequency identification tags (RFIDs) is much anticipated. RFIDs are at present defined by silicon chips and can hold information that can be

communicated to a reader at a distance. Applications for RFIDs incorporate the automated toll booth systems, items at a supermarket and ID badges that can be converted to organic integrated circuits to advance the control and security and to lower the cost. This will introduce RFID applications such as stock tagging at stores instead of using barcodes. A range of applications where organic electronics can play an important role from reducing cost, improving flexibility and improving functionality is in the use of sensors, displays for handheld devices, gauges and other gadgets. Another area of relevance is photo-voltaics developed for organic electronics. The energy market is on a lookout for low cost solutions for energy generation, construction and other applications brought by the cheap development of organic solar cells.

The concept of (down) scaling defined by Moore's law, based on transistors made out of silicon, can be used to fit high number of components, improve yield and to create large area systems. This requires a reduction of area, channel length, dopant levels, gate dielectric thickness and cross over capacitance. The detailed understanding of modelling in organic electronics will open up considerable opportunities for the future of organics. Once scaling in organic electronic circuitry has been tackled, a road map can be produced to predict the speed at which the organic electronics market will grow, especially in places such as Europe, China and India.

The potential for growth in organic electronics is immense and the learning curve is steep. The advancement of organics requires the collaboration of diverse groups such as the engineers, chemists, material scientists, manufacturing specialists, fabrication experts and other expertise. Ultimately, the aim is for organic electronics to complement the inorganic counterparts. The ability for organics to merge with inorganic electronics will lead to an improvement in areas either is deficient at. The possibilities for both the fields to work in parallel will unlock doors for research in the device structures, circuitry, commercial applications and much more. Combining forces will create research opportunities that are endless.

6.3 REFERENCES

[1] W. Clemens, I. Fix, J. Ficker, A. Knobloch and A. Ullmann, J. Mater. Res. 19, (2004) 1963.

[2] R. J. Kline and M. D. McGehee, Polym. Rev., 46, (2006) 27.

[3] J. Zaumseil and H. Sirringhaus, Chem. Rev. 107, (2007) 1296.

[4] M. O'Neill and S. M. Kelly, Adv. Mater.15, (2003) 1135.

[5] O. D. Jurchescu, J. Baas, T. T. M. Palstra, Appl. Phys. Lett. 84, (2004) 3061.

[6] V. Podzorov, E. Menard, A. Borissov, V. Kiryukhin, J. A. Rogers, M. E. Gershenson, Phys. Rev. Lett. 93,(2004) 086602.

[7] H. Sirringhaus, P. J. Brown, R. H. Friend, M. M. Nielsen, K. Bechgaard, B. M. W. Langeveld-Voss, A. J. H. Spiering, R. A. J. Janssen, E. W. Meijer, P. Herwig, D. M. de Leeuw, Nature 401, (1999) 685.

[8] G. M. Wang, J. Swensen, D. Moses, A. J. Heeger, J. Appl. Phys. 93, (2003) 6137.

[9] R. J. Kline, M. D. McGehee and M. F. Toney, Nat. Mater. 5, (2006) 222.

[10] D. L. Cheung, A. Troisi, Phys. Chem. Chem. Phys. 10, (2008) 5941.

[11] R. J. Kline, M. D. McGehee, E. N. Kadnikova, J. Liu and J. M. J. Frechet, Adv. Mater. 15, (2003) 1519.

[12] R. J. Kline, M. D. McGehee, E. N. Kadnikova, J. Liu, J. M. J. Frechet, M. F. Toney, Macromolecules 38, (2005) 3312.

[13] H. Bassler, Phys. Stat. Sol. (b), 175, (1993) 15.

[14] S. V. Novikov, D. H. Dunlap, V. M. Kenkre, P. E. Parris, A. V. Vannikov, Phys. Rev. Lett. 81 (1998) 4472.

[15] M. Vissenberg and M. Matters, Phys. Rev. B 57, (1998) 12964.

[16] W. F. Pasveer, J. Cottaar, C. Tanase, R. Coehoorn, P. A. Bobbert, P. W. M. Blom, D. M. de Leeuw, M. A. J. Michels, Phys. Rev. Lett. 94, (2005) 206601.

APPENDICES

APPENDIX A: *Carrier concentration in an n-type and a p-type semiconductor*

Carrier concentration in an n-type semiconductor

Carriers lying below the Fermi level are considered as trapped where as carriers located at higher energies are thought to be free due to the much larger density of barely populated localized states. The likelihood of occupancy of the energy states are estimated by the Fermi Dirac equation given by

$$f(E) = \frac{1}{1 + \exp\left(\frac{E - E_F}{kT}\right)}$$

when E-E_F >>kT

$$f(E) = \begin{cases} \exp\left(-\frac{E - E_F}{kT}\right) & E > E_F \\ 1 & E \leq E_F \end{cases} \qquad \text{A.1}$$

where E is the energy of localized states, E_F is the Fermi Level, k is the Boltzmann constant and T is the absolute temperature.

Rate of change of density of traps with energy is given by

$$N'(E) = \frac{N(0)}{kT_C} \exp\left(\frac{E}{kT_C}\right)$$

where $\frac{kT_C}{q}$ is the Meyer Neldel Energy.

Electron Density in a disordered organic material is given by integrating Maxwell Boltzmann's approximation above Fermi level (from E=E_F to E= ∞) and the exponential density of states as shown below.

$$n(E) = \int_{E_F}^{\infty} \frac{N(0)}{kT_C} \exp\left(\frac{E}{kT_C}\right) \exp\left[-\left(\frac{E - E_F}{kT}\right)\right] dE$$

The lower limit for integration is not ideal and is the nearest available approximation. It is made valid because the carriers with the highest energies contribute most to the currents. This is because the traps through which the carriers hop are much closely spaced than at the higher energies.

$$n(E) = \int_{E_F}^{\infty} \frac{N(0)}{kT_C} \exp\left(\frac{E_F}{kT_C}\right) \exp\left[-E\left(\frac{1}{kT} - \frac{1}{kT_C}\right)\right] dE$$

$$\frac{1}{T_0} = \frac{1}{T} - \frac{1}{T_C}$$

where T_0 is the characteristic temperature of a carrier distribution in a disordered material, T_C is characteristic temperature of a trap distribution in a disordered material and T is the absolute temperature.

$$n(E) = \frac{N(0)}{kT_C}\int_{E_F}^{\infty} \exp\left(\frac{E_F}{kT}\right)\exp\left(-\frac{E}{kT_0}\right)dE$$

$$n(E) = \frac{N(0)T_0}{T_C}\exp\left(\frac{E_F}{kT}\right)\exp\left[-\left(\frac{E_F}{kT_0}\right)\right]$$

The electron concentration for a disordered organic semiconductor is thus given by

$$n(E) = \frac{N(0)T_0}{T_C}\exp\left(\frac{E_F}{kT_C}\right)$$

Also written as

$$n(E) = N'(0)kT_0\exp\left(\frac{E_F}{kT_C}\right)$$

where *N'(0)* is the rate of change of density of traps at *E=0*.

Carrier concentration in a p-type semiconductor

Following the same method as above, the rate of change of density of traps with energy can be written as

$$N'(E) = \frac{N(0)}{kT_C}\exp\left(-\frac{E}{kT_C}\right)$$

The Fermi Dirac equation when $E < E_F$ is given by

$$f(E) = \exp\left(-\frac{E_F - E}{kT}\right)$$

And therefore, the total hole concentration below the Fermi level can be written as

$$\int p'(E)\,dE = \frac{N(0)}{kT_C}\int_{-\infty}^{E_F}\exp\left(-\frac{E}{kT_C}\right)\exp\left(-\frac{E_F - E}{kT}\right)dE$$

$$p(E) = \frac{N(0)}{kT_C}\exp\left(-\frac{E_F}{kT}\right)\int_{-\infty}^{E_F}\exp\left(\frac{E}{kT_0}\right)dE$$

$$p(E) = \frac{T_0 N(0)}{T_C}\exp\left(-\frac{E_F}{kT_C}\right)$$

APPENDIX B: *Space charge limited currents (SCLC) in saturation in terms of universal mobility law (UML)*

The current density due to drift currents in a disordered organic semiconductor is given as

$$J = qn\mu_{eff}F$$

The effective mobility is written as

$$\mu_{eff} = \mu_0 n^{\left({}^{T_C}/_{T}-1\right)} = Kn^m$$

and refers to as the universal mobility law (UML) where $m = \left({}^{T_C}/_{T} - 1\right)$.

In disordered materials, both the trapped and free carriers are expected to belong to the intrinsic DOS. In a simple model, the carriers below the Fermi level are regarded as trapped whereas the ones above the Fermi level are free due to a large number of density of states with a small population. The ratio of free carriers to the total number of injected carriers is given by the term θ

$$\theta = \frac{n_f}{n_f + n_t}$$

where n_f is the free carrier concentration and n_t is the trapped carrier concentration.

The free carriers causing the current transport above the Fermi level and change with the amount of carriers determines the field across the semiconductor. Poisson's equation to understand the change in electric field with thickness of the active layer is given by

$$\frac{dF}{dx} = -\frac{q}{\theta\varepsilon_0\varepsilon_S}n$$

$$\frac{dF}{dx} = -\frac{q}{\theta\varepsilon_0\varepsilon_S}\left(\frac{J}{qKF}\right)^{\frac{1}{m+1}}$$

Integrating the electric field with respect to the thickness of the active layer is given by

$$\int_F^0 (F)^{\frac{1}{m+1}}\, dF = \int_0^x -\frac{q}{\theta\varepsilon_0\varepsilon_S}\left(\frac{J}{qK}\right)^{\frac{1}{m+1}} dx$$

$$\frac{F^{\frac{1}{m+1}+1}}{\frac{1}{m+1}+1} = \frac{q}{\theta\varepsilon_0\varepsilon_S}\left(\frac{J}{qK}\right)^{\frac{1}{m+1}} x$$

$$\frac{(m+1)}{(m+2)}F^{\frac{m+2}{m+1}} = \frac{q}{\theta\varepsilon_0\varepsilon_S}\left(\frac{J}{qK}\right)^{\frac{1}{m+1}} x$$

$$F = \left(\left(\frac{m+2}{m+1}\right) \frac{q}{\theta \varepsilon_0 \varepsilon_S} \left(\frac{J}{qK}\right)^{\frac{1}{m+1}} x \right)^{\frac{m+1}{m+2}}$$

$$F = \left(\left(\frac{m+2}{m+1}\right) \frac{q}{\theta \varepsilon_0 \varepsilon_S} \right)^{\frac{m+1}{m+2}} \left(\frac{J}{qK}\right)^{\frac{1}{m+2}} x^{\frac{m+1}{m+2}}$$

Integrating the applied voltage with respect to the thickness of the semiconductor can be written as

$$F = -\frac{dV}{dx}$$

$$-\frac{dV}{dx} = \left(\left(\frac{m+2}{m+1}\right) \frac{q}{\theta \varepsilon_0 \varepsilon_S} \right)^{\frac{m+1}{m+2}} \left(\frac{J}{qK}\right)^{\frac{1}{m+2}} x^{\frac{m+1}{m+2}}$$

$$\int_{V_{app}}^{0} dV = -\left(\left(\frac{m+2}{m+1}\right) \frac{q}{\theta \varepsilon_0 \varepsilon_S} \right)^{\frac{m+1}{m+2}} \left(\frac{J}{qK}\right)^{\frac{1}{m+2}} \int_0^x x^{\frac{m+1}{m+2}}\, dx$$

$$V_{app} = \left(\left(\frac{m+2}{m+1}\right) \frac{q}{\theta \varepsilon_0 \varepsilon_S} \right)^{\frac{m+1}{m+2}} \left(\frac{J}{qK}\right)^{\frac{1}{m+2}} \frac{x^{\frac{2m+3}{m+2}}}{\left(\frac{2m+3}{m+2}\right)}$$

The space charge limited current for a disordered organic semiconductor is then said to be

$$J = \frac{K}{q^m} \left(\frac{\theta \varepsilon_0 \varepsilon_S (m+1)}{m+2}\right)^{m+1} \left(\frac{2m+3}{m+2}\right)^{m+2} \frac{{V_{app}}^{m+2}}{x^{2m+3}}$$

where $m>0$ for any disordered material and K is a constant. For an insulator with no disorder, $m=0$ and Mott-Gurney Law is followed.

$$m = \frac{T_C}{T} - 1$$

$$\theta = \frac{T_0}{T_0 + T_C}$$

On a double logarithmic scale, the current density continues to vary linearly with V_{app}.

$$J \propto \left(\frac{1}{q^m} \left(\frac{\varepsilon_0 \varepsilon_s (m+1)}{m+2}\right)^{m+1} \left(\frac{2m+3}{m+2}\right)^{m+2} \frac{1}{x^{2m+3}} \right) {V_{app}}^{2+m}$$

The gradient in the saturation region determines if the currents dominant are either ohmic, if the slope is unity or space charge limited where the slope is ≥ 2.

APPENDIX C: *Current continuity equation*

The charge transport in a p-type semiconductor is assumed to occur due to drift and diffusion mechanisms. Drift occurs due to the influence of external field on the carrier motion and diffusion is caused due to concentration gradient. The current density considering these both mechanisms can then be written as

$$J = qp\mu F - qD\frac{dp}{dx}$$

where q is the electronic charge, D is the diffusion coefficient, $\frac{dp}{dx}$ is the change in hole density with distance, p is the hole density and μ and F are the hole mobility and applied field respectively.

Both drift and diffusion components of the current at equilibrium are equivalent and written as

$$qp\mu F = qD\frac{dp}{dx}$$

Substituting $F = -\frac{d\emptyset}{dx}$ in the equation above gives

$$qp\mu\left(-\frac{d\emptyset}{dx}\right) = qD\frac{dp}{d\emptyset}\left(\frac{d\emptyset}{dx}\right)$$

Also, it is known that

$$p = p_i \exp -\frac{q\emptyset}{kT_C}$$

Substituting the derivative of this equation and placing it in the equilibrium equation yields

$$p\mu = D\frac{qp}{kT_C}$$

Rearranging this equation gives

$$D = \frac{\mu kT_C}{q}$$

This is known as the Einstein's Relationship for organic semiconductors. The relationship is dependent on the characteristic temperature T_C instead of absolute temperature, T, used for crystalline materials like silicon. The mobility term in the equation above is considered to be dependent on temperature.

If $F = -\frac{d\emptyset_F}{dx}$ is the change in potential with distance associated with drift and $F = -\frac{d\emptyset_D}{dx}$ is the change in potential with distance associated with diffusion, the current density equation can then be written as

$$J = -qp\mu\frac{d\emptyset_F}{dx} - \mu kT_C\frac{dp}{d\emptyset_D}\frac{d\emptyset_D}{dx}$$

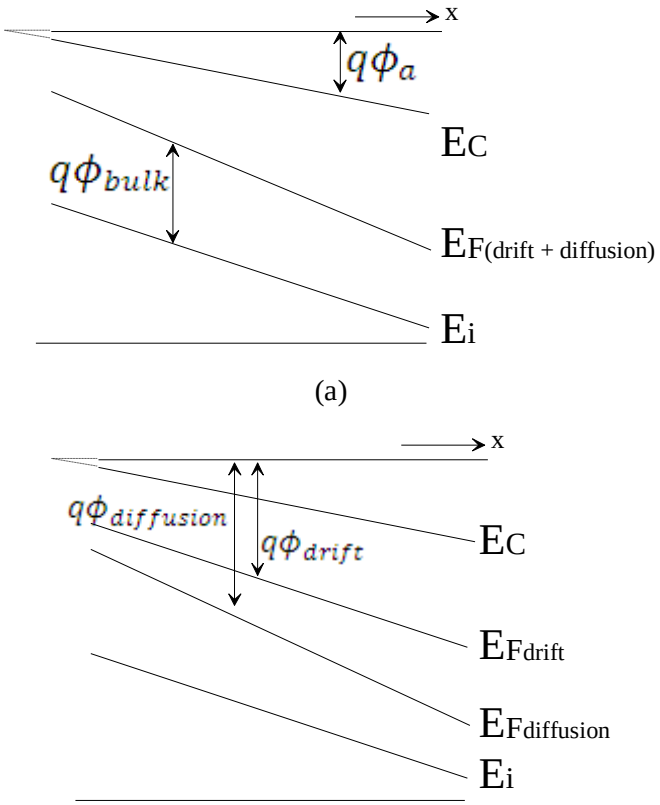

Figure C.1. Energy diagram for Fermi level gradient (a) in non equilibrium state. (b) Change in Fermi level gradients due to drift and diffusion separately. $q\phi_a$ is the potential energy at point a on the conduction band, E_C in the x direction. The value of this energy varies with distance in the x direction. For an n type semiconductor, $q\phi_a$ increases with increasing distance between the Fermi level and the conduction band E_C.

Substituting the derivative of $p = p_i \exp\left(-\frac{q\emptyset}{kT_C}\right)$ and placing it into the new current density equation gives

$$J = -qp\mu\frac{d\emptyset_F}{dx} - \mu kT_C\frac{qp}{kT_C}\frac{d\emptyset_D}{dx}$$

$$J = -qp\mu\left(\frac{d\emptyset_F}{dx} + \frac{d\emptyset_D}{dx}\right)$$

Also written as

$$J = -qp\mu\left(\frac{d\xi}{dx}\right)$$

where $\frac{d\xi}{dx}$ is the gradient of the Fermi level. It can be seen from the equation above that the Fermi level will be flat in the absence of current flow. The new Fermi level is proportional to the current. Higher the electron concentration, the lower is the slope of the Fermi level. The quasi Fermi level can be assumed flat if the current entering the Semiconductor and all through the Semiconductor is constant.

APPENDIX D: *First boundary condition*

According to Gauss's Law applied in the grain boundary,

$$\frac{d^2\emptyset}{dz^2} = \frac{qn}{\varepsilon_0\varepsilon_s}$$

where *z* is the thickness of the semiconductor film grain boundary and *n* is the total density at any point $\emptyset$ in the depletion region.

$$\frac{d^2\emptyset}{dz^2} = \frac{qn_0}{\varepsilon_0\varepsilon_s}\exp\left(\frac{q\emptyset}{kT_C}\right)$$

Integrating by a factor, $\frac{d\emptyset}{dz}$

$$\frac{d\emptyset}{dz}\frac{d^2\emptyset}{dz^2} = \frac{qn_0}{\varepsilon_0\varepsilon_s}\exp\left(\frac{q\emptyset}{kT_C}\right)\frac{d\emptyset}{dz}$$

$$\int F\,dF = \frac{qn_0}{\varepsilon_0\varepsilon_s}\int \exp\left(\frac{q\emptyset}{kT_C}\right)d\emptyset$$

where electric field, *F*, is zero in the neutral region and is defined as

$$F = \left[\frac{2kT_Cn_0}{\varepsilon_0\varepsilon_s}\left(\exp\left(\frac{q\emptyset}{kT_C}\right)-1\right)\right]^{1/2}$$

in the depletion region (z-direction).

Since $\exp\left(\frac{q\emptyset}{kT_C}\right) \gg 1$, simplified F is

$$F = \left[\frac{2kT_Cn_0}{\varepsilon_0\varepsilon_s}\right]^{1/2}\exp\left(\frac{q\emptyset}{2kT_C}\right)$$

$$\frac{d\emptyset}{dz} = -\left[\frac{2kT_Cn_0}{\varepsilon_0\varepsilon_s}\right]^{1/2}\exp\left(\frac{q\emptyset}{2kT_C}\right)$$

Integrating between $\emptyset = \emptyset_B$ at the Schottky contact, *z=0* and $\emptyset = \emptyset_z$ at a point *z=z* in the depletion region of the disordered grain boundary,

$$\int_{\emptyset_z}^{\emptyset_B}\exp\left(-\frac{q\emptyset}{2kT_C}\right)d\emptyset = -\int_{\mathrm{z}}^{0}\left[\frac{2kT_Cn_0}{\varepsilon_0\varepsilon_s}\right]^{1/2}dz$$

$$-\frac{2kT_C}{q}\left(\exp\left(-\frac{q\emptyset_B}{2kT_C}\right)-\exp\left(-\frac{q\emptyset_z}{2kT_C}\right)\right) = \left[\frac{2kT_Cn_0}{\varepsilon_0\varepsilon_s}\right]^{1/2}(0-z)$$

$$\exp\left(-\frac{q\emptyset_B}{2kT_C}\right)-\exp\left(-\frac{q\emptyset_z}{2kT_C}\right) = -\left[\frac{q^2n_0}{2kT_C\varepsilon_0\varepsilon_s}\right]^{1/2}z \qquad \text{D.1}$$

As the Debye length can be explained as

$$L_{Dz} = \left(\frac{2kT_C \varepsilon_0 \varepsilon_{gb}}{q^2 n_0} \right)^{1/2}$$

T_C is the characteristic temperature of DOS, n_0 is the density corresponding to the Fermi level, ε_0 is the permittivity of free space and ε_{gb} is dielectric constant of the grain boundary.

Therefore, Eq. (D.1) can be rewritten as

$$\exp\left(-\frac{q\emptyset_B}{2kT_C}\right) - \exp\left(-\frac{q\emptyset_z}{2kT_C}\right) = -\frac{z}{L_{Dz}}$$

giving $\emptyset_z$ which is the first boundary condition at the edge of the grain.

$$\emptyset_z = -\frac{2kT_C}{q} \ln\left[\exp\left(-\frac{q\emptyset_B}{2kT_C}\right) + \frac{z}{L_{Dz}}\right]$$

APPENDIX E: *Defining the curve in grains*

The variation of the LUMO level is determined by this dopant concentration shown by using Gauss's law as before and assuming that the grain is fully depleted of carriers due to grain boundary

$$F_x \frac{dF}{dx} = -\frac{qN_D}{\varepsilon_0 \varepsilon_s} \frac{d\emptyset}{dx}$$

Considering the boundary conditions $F = F_{boundary}$ at $x = 0$, $\emptyset = \emptyset_z$ at the edge of the grain and $F = F_x$ at $x = x$, $\emptyset = \emptyset_x$ at any point x on the grain LUMO level.

$$\int_{\mathrm{F_x}}^{\mathrm{F_{boundary}}} F_x \, dF = -\int_{\emptyset_x}^{\emptyset_z} \frac{qN_D}{\varepsilon_0 \varepsilon_s} d\emptyset$$

where the minimum grain condition is $F = 0$ at $x = x_D$, $\emptyset = \emptyset_0$ at the edge of the depletion region and in the neutral region w.r.t the Fermi level ($\emptyset = 0$ *at F=0*).

$$\mathrm{F_{boundary}}^2 - \mathrm{F_x}^2 = -\frac{2qN_D}{\varepsilon_0 \varepsilon_s}(\emptyset_z - \emptyset_x)$$

$F_{boundary} = \left(\frac{2qN_D\emptyset_z}{\varepsilon_0\varepsilon_s}\right)^{1/2}$, $F_x = \left(\frac{2qN_D\emptyset_x}{\varepsilon_0\varepsilon_s}\right)^{1/2}$ and $F_0 = \left(\frac{2qN_D\emptyset_0}{\varepsilon_0\varepsilon_s}\right)^{1/2}$

The potential at the point *x* with regards to the grain edge is then

$$-\frac{\mathrm{d}\emptyset}{\mathrm{dx}} = \left(\frac{2qN_D\emptyset}{\varepsilon_0\varepsilon_s}\right)^{1/2}$$

$$\int_{\emptyset_x}^{\emptyset_z} \frac{1}{\emptyset^{1/2}} \mathrm{d}\emptyset = -\left(\frac{2qN_D}{\varepsilon_0\varepsilon_s}\right)^{1/2} \int_x^0 dx$$

$$\left[2\emptyset^{1/2}\right]_{\emptyset_x}^{\emptyset_z} = -\left(\frac{2qN_D}{\varepsilon_0\varepsilon_s}\right)^{1/2} (0 - x)$$

$$\emptyset_z{}^{1/2} - \emptyset_x{}^{1/2} = \left(\frac{qN_D}{2\varepsilon_0\varepsilon_s}\right)^{1/2} x$$

This gives the second boundary condition for any point *x* on the grain corresponding to the energy level $q\emptyset_z$ on grain edge.

$$\emptyset_x = \left(\emptyset_z{}^{1/2} - \left(\frac{qN_D}{2\varepsilon_0\varepsilon_s}\right)^{1/2} x\right)^2 \qquad \text{E.1}$$

APPENDIX F: *Second boundary condition in grain*

The minimum potential on the curve $\emptyset_{min}$ at the centre of the grain can be explained using Eq. (E.1)

$$\emptyset_X = \left(\emptyset_z{}^{1/2} - \left(\frac{qN_D}{2\varepsilon_0\varepsilon_s}\right)^{1/2} x\right)^2 + \left(\emptyset_z{}^{1/2} - \left(\frac{qN_D}{2\varepsilon_0\varepsilon_s}\right)^{1/2} (a-x)\right)^2$$

$$\emptyset_X = 2\emptyset_z - 2\left(\frac{qN_D}{2\varepsilon_0\varepsilon_s}\right)^{1/2} a\emptyset_z{}^{1/2} + 2\left(\frac{qN_D}{2\varepsilon_0\varepsilon_s}\right)x^2 - 2\left(\frac{qN_D}{2\varepsilon_0\varepsilon_s}\right)ax + \left(\frac{qN_D}{2\varepsilon_0\varepsilon_s}\right)a^2$$

Rewritten as

$$\emptyset_X = 2\emptyset_z - 2S^{1/2}a\emptyset_z{}^{1/2} + 2Sx^2 - 2Sax + Sa^2$$

where $S = \frac{qN_D}{2\varepsilon_0\varepsilon_s}$

$$\frac{d}{d\emptyset}\emptyset = \frac{d}{d\emptyset}\left(2\emptyset_z - 2S^{1/2}a\emptyset_z{}^{1/2} + 2Sx^2 - 2Sax + Sa^2\right)$$

$$1 = 4Sx\,\frac{dx}{d\emptyset} - 2Sa\frac{dx}{d\emptyset}$$

$$\frac{d\emptyset}{dx} = 4Sx - 2Sa$$

At the minimum of the curve $\frac{d\emptyset}{dx} = 0$ and therefore,

$$x = \frac{1}{2}a$$

Therefore, Eq. (G.1) can be rewritten as

$$\emptyset_x = \left(\emptyset_z{}^{1/2} - \left(\frac{qN_D}{2\varepsilon_0\varepsilon_s}\right)^{1/2}\left(\frac{a}{2}\right)\right)^2 \qquad \text{F.1}$$

APPENDIX G: *Total intrinsic concentration in a disordered material*

The total hole concentration can be found by integrating above and the Fermi level. Above the Fermi Level p_+ and below, p_-

$$p_0 = p_+ + p_-$$

The tail of the Gaussian function, for any particular energy range, can be approximated to an exponential function

$$N_g{}'(E) = \frac{N_i}{kT_C} \exp\left(\frac{E - E_i}{kT_C}\right)$$

where N_i is the number of states per unit volume at energy level E_i, the intrinsic level, k is the Boltzmann constant, and T_C is the characteristic temperature. Fermi–Dirac statistics to Maxwell-Boltzmann relationship can be approximated as Eq. (A.1). The hole concentrations above and below the Fermi level can be defined by integrating the product of the approximated exponential function and the Maxwell-Boltzmann approximation

$$p_+ = \frac{N_i}{kT_C} \exp\left(\frac{E - E_i}{kT_C}\right) \int_{E_F}^{\infty} \exp\left(-\frac{E - E_F}{kT}\right) dE$$

$$p_- = \int_{-\infty}^{E_F} \frac{N_i}{kT_C} \exp\left(\frac{E - E_i}{kT_C}\right) dE$$

Therefore,

$$p_0 = N_i \left(1 + \frac{T_0}{T_C}\right) \exp\left(\frac{E_F - E_i}{kT_C}\right)$$

APPENDIX H: *Relationship of capacitance and temperature in disordered grain boundaries*

Poisson equation for the change in electric field with distance is

$$\frac{dF}{dx} = -\frac{d^2\emptyset}{dx^2} = \frac{dF}{d\emptyset}.\frac{d\emptyset}{dx}$$

The electric field due to the accumulation of charge at the surface, F_S, can be written in terms of effective Debye length, L_{De},

$$F_S = \frac{kT_C}{qL_{De}} \exp\left(\frac{q\emptyset_S}{2kT_C}\right)$$

where the effective Debye Length, $L_{De} = \left(\frac{kT_C\varepsilon_0\varepsilon_S}{q^2p_s}\right)^{1/2}$. Charge, Q_S, is given in terms of the surface field

$$Q_S = -\varepsilon_0\varepsilon_S F_S$$

$$Q_S = \frac{kT_C\varepsilon_0\varepsilon_S}{qL_{De}} \exp\left(\frac{q\emptyset_S}{2kT_C}\right)$$

Space charge capacitance at flat band, C_S, due to the accumulated charge layer is given by

$$C_S = \frac{dQ_S}{d\emptyset_S} = \frac{\varepsilon_0\varepsilon_S}{L_D} = \frac{\varepsilon_0\varepsilon_S}{\sqrt{2}\,L_{De}}$$

$$C_S = \frac{\varepsilon_0\varepsilon_S}{\left(\frac{2kT_C\varepsilon_0\varepsilon_S}{q^2p_s}\right)^{1/2}}$$

$$C_S = \left(\frac{q^2p_s\varepsilon_0\varepsilon_S}{2kT_C}\right)^{1/2}$$

$$1/{C_S}^2 = \left(\frac{2kT_C}{q^2p_s\varepsilon_0\varepsilon_S}\right)$$

$$1/{C_S}^2 = \left(\frac{2kT_C}{q^2\varepsilon_0\varepsilon_S p_0} \exp\left(-\frac{q\emptyset_S}{kT_C}\right)\right)$$

The total intrinsic hole concentration above and below the Fermi Level is given by p_0

$$p_0 = N_i\left(1 + \frac{T_0}{T_C}\right) \exp\left(\frac{E_F - E_i}{kT_C}\right)$$

where N_i is the number of states per unit volume at energy level E_i, the intrinsic level, and E_F is the energy at Fermi level. The variation of Inverse Square of space charge capacitance against temperature can thus be defined as

$$1/C_S{}^2 = \left(\frac{2kT_C}{q^2\varepsilon_0\varepsilon_S N_i\left(1+\frac{T_0}{T_C}\right)}\exp\left(\frac{E_i-E_F}{kT_C}\right)\exp\left(-\frac{q\emptyset_S}{kT_C}\right)\right)$$

$$1/C_S{}^2 = \left(\frac{2kT_C{}^2}{q^2\varepsilon_0\varepsilon_S N_i(T_C+T_0)}\exp\left(\frac{E_i-E_F}{kT_C}\right)\exp\left(-\frac{q\emptyset_S}{kT_C}\right)\right)$$

In terms of characteristic temperature of density of states, T_C

$$1/C_S{}^2 = \left(\frac{2k}{q^2\varepsilon_0\varepsilon_S N_i}\exp\left(\frac{E_i-E_F}{kT_C}\right)\exp\left(-\frac{q\emptyset_S}{kT_C}\right)\right)(T_C-T)$$

where T_C is the x-intercept obtained.

APPENDIX I: *1/C_S^2 variation with temperature in ordered grains*

Debye length for ordered material is defined as

$$L_D = \left(\frac{2kT\varepsilon_0\varepsilon_S}{q^2N_a}\right)^{1/2}$$

where N_a is the acceptor ion concentration, T is the absolute temperature, ε_0 is the permittivity of free space and ε_S is the dielectric constant. The dopant concentration is assumed to equivalent to the carrier concentration such that it varies exponentially.

Above and below the Fermi level, the total carrier concentration is defined as

$$p_0 = 2N_i \exp\left(\frac{E_F - E_i}{kT}\right)$$

The space charge capacitance can be defined as

$$C_S = \frac{\varepsilon_0\varepsilon_S}{\left(\frac{2kT\varepsilon_0\varepsilon_S}{q^2p}\right)^{1/2}}$$

$$1/_{C_S{}^2} = \left(\frac{2kT}{q^2\varepsilon_0\varepsilon_S p_0}\exp\left(-\frac{q\emptyset_S}{kT}\right)\right)$$

Substituting the total intrinsic concentration into the inverse square capacitance equation gives

$$1/_{C_S{}^2} = \left(\frac{k}{q^2\varepsilon_0\varepsilon_S N_i}\exp\left(\frac{E_i - E_F}{kT}\right)\exp\left(-\frac{q\emptyset_S}{kT}\right)\right)T$$

where N_i is the number of states per unit volume at energy level E_i, the intrinsic level, k is the Boltzmann constant, and T is the absolute temperature and $\emptyset_S$ is the total barrier seen by the carrier.

APPENDIX J: *Conferences and journal papers*

Journal Papers

[1] S. Afzal, M. Raja, W. Eccleston, "*Temperature effects on TIPS-based Schottky diodes,"* (In preparation for submission to IEEE Transactions on Electron Devices).

[2] S. Afzal, M. Raja, W. Eccleston, *"Temperature and frequency effects on TIPS-based MOS Capacitors,"* (In preparation for submission).

[3] S. Afzal, M. Raja, W. Eccleston, *"A 2-Dimensional representation to model an organic Polycrystalline material based Schottky diode,"* (In preparation for submission).

Conferences

[1] S. Afzal, M. Raja, W. Eccleston, *"Temperature measurements on TIPS-pentacene based Organic Schottky diodes,"* The 7th International Conference on Organic Electronics, Paris, France, June 2010.

[2] S. Afzal, M. Raja, W. Eccleston, *"Analysis of Polycrystalline Organic TIPS-pentacene Schottky diodes,"* Salford Postgraduate Association Research Conference, Manchester, UK, June 2010.

[3] S. Afzal, M. Madec, M. Raja, S. Yeates, W. Eccleston, "*Transient Behaviour in Doped Polycrystalline TIPS diodes,*" The 6th International Conference on Organic Electronics, Liverpool, UK, June 2009.